National Library of Canada
Canadian Theses Service
Ottawa, Canada
K1A 0N4

Bibliothèque nationale du Canada
Services des thèses canadiennes

CANADIAN THESES

THÈSES CANADIENNES

NOTICE

The quality of this microfiche is heavily dependent upon the quality of the original thesis submitted for microfilming. Every effort has been made to ensure the highest quality of reproduction possible.

If pages are missing, contact the university which granted the degree.

Some pages may have indistinct print especially if the original pages were typed with a poor typewriter ribbon or if the university sent us an inferior photocopy.

Previously copyrighted materials (journal articles, published tests, etc.) are not filmed.

Reproduction in full or in part of this film is governed by the Canadian Copyright Act, R.S.C. 1970, c. C-30. Please read the authorization forms which accompany this thesis.

AVIS

La qualité de cette microfiche dépend grandement de la qualité de la thèse soumise au microfilmage. Nous avons tout fait pour assurer une qualité supérieure de reproduction.

S'il manque des pages, veuillez communiquer avec l'université qui a conféré le grade.

La qualité d'impression de certaines pages peut laisser à désirer, surtout si les pages originales ont été dactylographiées à l'aide d'un ruban usé ou si l'université nous a fait parvenir une photocopie de qualité inférieure.

Les documents qui font déjà l'objet d'un droit d'auteur (articles de revue, examens publiés, etc.) ne sont pas microfilmés.

La reproduction, même partielle, de ce microfilm est soumise à la Loi canadienne sur le droit d'auteur, SRC 1970, c. C-30. Veuillez prendre connaissance des formules d'autorisation qui accompagnent cette thèse.

THIS DISSERTATION
HAS BEEN MICROFILMED
EXACTLY AS RECEIVED

LA THÈSE A ÉTÉ
MICROFILMÉE TELLE QUE
NOUS L'AVONS REÇUE

NL 339 (r. 86/01)

Canada

113

0-315-23309-5

National Library of Canada
Bibliothèque nationale du Canada

Canadian Theses Division
Division des thèses canadiennes

Ottawa, Canada
K1A 0N4

PERMISSION TO MICROFILM — AUTORISATION DE MICROFILMER

• Please print or type — Écrire en lettres moulées ou dactylographier

Full Name of Author — Nom complet de l'auteur

HAROLD ANDREW CHRISTIAN

Date of Birth — Date de naissance	Country of Birth — Lieu de naissance
DECEMBER 31, 1959	CANADA

Permanent Address — Résidence fixe

2183 WINDSOR ST.
HALIFAX, NOVA SCOTIA,
B3K-5B7

Title of Thesis — Titre de la thèse

STRESS HISTORY OF SURFICIAL BEAUFORT SEA SEDIMENTS

University — Université

UNIVERSITY OF ALBERTA

Degree for which thesis was presented — Grade pour lequel cette thèse fut présentée

MASTER OF SCIENCE

Year this degree conferred — Année d'obtention de ce grade	Name of Supervisor — Nom du directeur de thèse
1985	NORBERT R. MORGENSTERN

Permission is hereby granted to the NATIONAL LIBRARY OF CANADA to microfilm this thesis and to lend or sell copies of the film.

The author reserves other publication rights, and neither the thesis nor extensive extracts from it may be printed or otherwise reproduced without the author's written permission.

L'autorisation est, par la présente, accordée à la BIBLIOTHÈQUE NATIONALE DU CANADA de microfilmer cette thèse et de prêter ou de vendre des exemplaires du film.

L'auteur se réserve les autres droits de publication; ni la thèse ni de longs extraits de celle-ci ne doivent être imprimés ou autrement reproduits sans l'autorisation écrite de l'auteur.

Date	Signature
SEPT. 27, 1985	H Christian

THE UNIVERSITY OF ALBERTA

Stress History of Surficial Beaufort Sea Sediments

by

Harold Christian

A THESIS

SUBMITTED TO THE FACULTY OF GRADUATE STUDIES AND RESEARCH

IN PARTIAL FULFILMENT OF THE REQUIREMENTS FOR THE DEGREE

OF Master of Science

IN

Civil Engineering

EDMONTON, ALBERTA

Fall 1985

THE UNIVERSITY OF ALBERTA

RELEASE FORM

NAME OF AUTHOR Harold Christian

TITLE OF THESIS Stress History of Surficial Beaufort Sea Sediments

DEGREE FOR WHICH THESIS WAS PRESENTED Master of Science

YEAR THIS DEGREE GRANTED Fall 1985

Permission is hereby granted to THE UNIVERSITY OF ALBERTA LIBRARY to reproduce single copies of this thesis and to lend or sell such copies for private, scholarly or scientific research purposes only.

The author reserves other publication rights, and neither the thesis nor extensive extracts from it may be printed or otherwise reproduced without the author's written permission.

(SIGNED) ...H. Christian.....

PERMANENT ADDRESS:

2183 Windsor St.....
Halifax, Nova Scotia....
B3K 5B7.....

DATED September 24...1985

THE UNIVERSITY OF ALBERTA

FACULTY OF GRADUATE STUDIES AND RESEARCH

The undersigned certify that they have read, and recommend to the Faculty of Graduate Studies and Research, for acceptance, a thesis entitled Stress History of Surficial Beaufort Sea Sediments submitted by Harold Christian in partial fulfilment of the requirements for the degree of Master of Science in Geotechnical Engineering.

.....

Supervisor

.....

.....

Date..September..24,..1985.....

Abstract

The phenomenon of apparent overconsolidation is shown to occur within the upper 6 to 10 meters of recent marine sediments in the Beaufort Sea. This thesis produces stress history data from back pressured consolidation tests that follows the trend of very high overconsolidation ratios near the mudline found in marine sediments worldwide by many different investigators.

The underlying mechanism is concluded to be ageing associated with a numerical inconsistency in the present definition of overconsolidation ratio. A solution to the paradox is presented in this study.

The stress history of the surficial sediments in the Beaufort Sea is shown to be entirely consistent with present understanding of sea level movements during the Holocene period, and overconsolidation occurs at erosional surfaces developed during that period of exposure. The recent marine sediments are shown to be normally to slightly overconsolidated, a conclusion supported by the occurrence of a finite effective cohesion existing at zero normal effective stress.

Permeability data is collected from the consolidation samples between stress increments using modifications made to the existing apparatus. The sediment permeability is shown to be extremely low and compares well with other illitic marine clays from the deep-sea.

Effective shear strength parameters are obtained from undrained triaxial compression tests performed on undisturbed samples.

Acknowledgements

This thesis was undertaken under the guidance of Professor N.R. Morgenstern of the Department of Geotechnical Engineering at the University of Alberta. Funding for the programme was generously provided by the Geological Survey of Canada and also by Prof. Morgenstern, which the author gratefully acknowledges. Thanks are extended to Prof. Morgenstern for his keen interest in this topic and the author is grateful for his exceptional patience and guidance throughout. Special thanks are due Ms. Kathryn Moran of the Atlantic Geoscience Centre, Geological Survey of Canada for her suggesting the topic, her invaluable comments, and for making possible the thesis through her funding in the first place. Ms. Moran kindly provided undisturbed samples for testing along with a wealth of proprietory data. The author is indebted to Dr. P.R. Hill, also of the Atlantic Geoscience Centre for his assistance in developing an understanding of the regional surficial geology in relation to past sea level movements.

Sincere thanks are expressed to Dr. M.J. Jefferies of Frontier Gulf Canada Resources, Inc. for supplying proprietory data from the Sauvrak and East Amauligak sites. Thanks are also extended to Dr. S. Shinde of Esso Resources Ltd. for his helpful comments on the first draft. Appreciation is acknowledged to Dr. J-M. Konrad of the National Research Council for the use of his triaxial data.

I wish to further thank Mr. G. Cyre and Mr. S. Gamble for their helpful assistance and to Prof. Morgenstern for financing the upgrading and modification of the consolidation apparatus. Thanks are extended again to Ms. Moran for reviewing the first draft and for her constructive criticism.

Finally, I wish to thank my parents for their support in times of crisis, but most of all, Patricia for her moral support and understanding nature.

Table of Contents

Chapter — Page

1. Introduction 1

2. Regional Surficial Geology of the Beaufort Sea 6

   2.1 Early Development of a Geological Model 6

   2.2 A Sea Level Curve for the Canadian Beaufort Sea 10

   2.3 A Three-Unit Geologic Model for the Beaufort Sea 13

   2.4 Occurrence of Acoustic Permafrost 16

   2.5 Classification of APF Types 16

      2.5.1 Marginally or Partially Ice-Bonded APF 16

      2.5.2 Stratigraphically Controlled APF 17

      2.5.3 Hummocky APF 17

   2.6 The Physiographic Regions of the Continental Shelf 18

      2.6.1 The Natsek Plain 18

      2.6.2 The Mackenzie Trough 18

      2.6.3 The Kringalik Plateau 21

      2.6.4 The Ikit Trough 22

      2.6.5 The Akpak Plateau 24

      2.6.6 The Kugmallit Channel 25

      2.6.7 The Tingmiark Plain 25

      2.6.8 The Niglik Channels 26

      2.6.9 The Kaglulik Plain 27

3. Consolidation Characteristics of Surficial Sediments 28

   3.1 Testing Apparatus 28

      3.1.1 Sample Extruder 28

3.1.2 The Back Pressured Consolidometer/Permeameter 28

3.2 The Phenomenon of Apparent Overconsolidation ...33

3.2.1 Definition 33

3.2.2 Occurrence of Apparent Overconsolidation 35

3.2.3 Impact of AOC in Foundation Engineering .39

3.2.4 Geological Impact of AOC 44

3.2.5 Estimation of the Preconsolidation Pressure 44

3.3 Possible Causes of Overconsolidation in Marine Soils 50

3.3.1 Compressibility of Soil Particles 50

3.3.2 Sedimentation Rate 54

3.3.3 Removal of Overburden 57

3.3.4 Erroneous Location of the Mudline 61

3.3.5 Stress Relief and Sample Disturbance 72

3.3.6 Thermal Regime 78

3.3.7 Cementation 81

3.3.8 Ice Scouring of the Seabed 82

3.3.9 The Effective Unit Weight 83

3.3.10 Thaw Consolidation 87

3.3.11 Delayed Consolidation and Ageing 88

3.3.12 Cyclic Loading Through Wave-induced Pore Pressures 95

3.4 A Predictive Model for OCR 96

3.5 Sensitivity of Marine Soils 107

3.6 Conclusions 107

4. One-Dimensional Consolidation Testing 110

4.1 Variation in Index Properties 110

4.1.1 Liquidity Index Correlations for Marine Soils 110

4.1.2 Water Contents at the Time of Deposition 116

4.2 Sample Sites 119

4.3 Recent (or Holocene) Marine Sediments 123

4.4 GSC Spring 1984 Borehole Program 137

4.5 Gulf Sauvrak 157

4.6 Mackenzie Trough West 160

4.7 Rates of Secondary Compression 178

4.8 Prediction of OCR from the Critical State Line 184

4.9 Clay Mineralogy 190

4.10 Analysis of Soil Fabric by SEM Techniques 192

5. Constant Head Permeability Testing 195

5.1 The Constant Head Permeability Test 195

5.2 Holocene Sediments in the Beaufort Sea 197

5.3 Transgressive Silts and Clays in the Beaufort Sea 203

5.4 Comparisons with Other Sediments 207

5.5 Comparison with Terrestrial Soils 210

6. Strength of Surficial Sediments 212

6.1 Synopsis 212

6.2 Recent Clayey Sediments (Unit A) 214

6.3 Transgressive Silty Sediments (unit B) 222

Conclusions 230

6.1 General 230

6.2 Consolidation Testing 231

6.3 Permeability Testing 232
6.4 Shear Strength Testing 233
6.5 Recommendations for further study 234
References 237
Appendix A 245
A.1 Operating Procedure 246
A.1.1 Consolidation 246
A.1.1.1 Saturation and Back Pressuring .246
A.1.1.2 Consolidation 250
A.1.2 Permeability 251
A.1.2.1 Constant Head Test 251
A.1.2.2 Falling Head Test 253
Appendix B 260
Appendix C 276
Appendix D 279
Appendix E 282
Appendix F 290
Appendix G 325
Appendix H 330

List of Tables

Table		Page
3.1	Comparison of compressibilities for some marine soils (mod. Carchedi, 1979)	53
3.2	Sedimentation rates for some depositional environments (mod. Skempton, 1970)	56
4.1	Typical soil types encountered offshore (mod. Skempton, 1970)	117
4.2	Summary of sample information for areas in this study	121
4.3	Oedometer data for PC-09	125
4.4	Comparison of techniques of determining stress history for PC-09	130
4.5	Compressibility results for PC-09	131
4.6	Oedometer data for BH 20+00	143
4.7	Comparison of techniques for determining stress history for BH 20+00	148
4.8	Compressibility results for BH 20+00	155
4.9	Oedometer data for Gulf Sauvrak (mod. Jefferies et al, 1984)	161
4.10	Comparison of techniques of determining stress history for Sauvrak	162
4.11	Compressibility results for Gulf Sauvrak (mod. Jefferies, 1984)	163
4.12	Oedometer results for MTWS1	172
4.13	Comparison of techniques of determining stress history for MTWS1	173
4.14	Classification of soil based on secondary compressibility (mod. Mesri, 1973)	179
4.15	Summary of predicted versus observed OCR for BH 20+00	186
4.16	Summary of predicted versus observed OCR for Sauvrak	187

Table		Page
4.17	Summary of clay mineralogy for consolidation samples	191
6.1	Results of isotropic triaxial compression tests performed on piston core samples PC-02 and PC-03	215
6.2	Summary of static triaxial compression tests conducted on Beaufort Sea silts (mod. Konrad, 1985)	224
A.1	Calibration chart showing load pressure settings for Systems A and B	254
C.1	Index property data for PC-09 (1 of 2)	277
C.2	Index property data for PC-09 (2 of 2)	278
D.1	Index property data for BH 20+00 (1 of 2)	280
D.2	Index property data for BH 20+00 (2 of 2)	281
E.1	Index property data for BH MTWS1 (1 of 7)	283
E.2	Index property data for BH MTWS1 (2 of 7)	284
E.3	Index property data for BH MTWS1 (3 of 7)	285
E.4	Index property data for BH MTWS1 (4 of 7)	286
E.5	Index property data for BH MTWS1 (5 of 7)	287
E.6	Index property data for BH MTWS1 (6 of 7)	288
E.7	Index property data for BH MTWS1 (7 of 7)	289
G.1	Consolidation summary for PC-09, back pressure = 250 kpa	326
G.2	Consolidation summary for BH 20+00, back pressure = 250 kpa	327
G.3	Consolidation summary for BH MTWS1, back pressure = 250 kpa	329
H.1	Permeability data for PC-09, Z = 1.16 m bsb	331
H.2	Permeability data for PC-09, Z = 2.08 m bsb	332

Table

Page

H.3 Permeability data for BH 20+00, Z = 4.85 m bsb.....333

H.4 Permeability data for BH 20+00, Z = 13.74 m bsb.....334

List of Figures

Figure		Page
2.1	Physiographic provinces for the Canadian Beaufort Sea (mod. O'Connor, 1982a)	7
2.2	A relative sea level curve for tha Canadian Beaufort Sea (mod. Hill et al, 1985)	11
2.3	Geological model for the Beaufort Sea (mod. O'Connor, 1982a)	14
2.4	Industry borehole locations in the Beaufort Sea (mod. O'Connor, 1982a)	19
2.5	East-west cross-section of the shelf summarizing the surficial geology (vertical scale exaggerated), (Hill, pers. comm., 1985)	23
3.1	Layout of back-pressured consolidometer/permeameter.	31
3.2	OCR versus depth below seabed for two sites in the North Atlantic and the North Pacific Oceans (mod. Carchedi, 1979)	40
3.3	Overconsolidation ratio versus depth below seabed for the Alaskan and Canadian Beaufort Sea (mod. Hivon, 1983)	41
3.4	Profile of OCR versus depth in Bermuda Rise sediments displaying apparent overconsolidation (OCR > 1) in upper 3 to 4 m and underconsolidation (OCR < 1) below 6 to 8 m (mod. Silva and Jordan, 1984).	42
3.5	Load versus compression curve for strain energy derivation	49
3.6	(a) Effective overburden stresses within a marine sediment; (b) Effect of erosion on the effective overburden pressure.	59
3.7	Overconsolidation caused by removal of overburden (mod. Skempton, 1970)	60
3.8	Effective overburden and preconsolidation pressure profiles for the AOC zone	63

Figure Page

3.9 Possible profiles showing OCR before and after application of the correction to redefine the location of the mudline.....70

3.10 Variation of the a-parameter for the cases shown in Figure 3.9.....71

3.11 Back pressure required to saturate a specimen with an initial degree of saturation S_i (mod. Black and Lee, 1973).....75

3.12 Standard piston corer at three stages of operation: (a) lowering, (b) free fall, and (c) penetration (mod. Hunt, 1984).....77

3.13 Compressibility of Harrison Bay silts at room temperature versus in situ temperature (mod. Ladd et al, 1985).....80

3.14 Variation in the profile of effective overburden pressure resulting from non-linearity of the unit weight.....85

3.15 Effect of ageing on the compressibility of normally consolidated clays (mod. Bjerrum, 1967).....90

3.16 Critical state line and yield envelope (mod. Wroth, 1979).....99

3.17 (i) Relationship between consolidation pressure and liquidity index; (ii) Idealized relationship between liquidity index and remoulded strength (mod. Wroth, 1979). 99

3.18 Idealized relationship between vertical effective stress and liquidity index (mod. Wroth, 1979).....102

3.19 Relationship between κ the rebound coefficient, and plasticity index (mod. Wroth, 1979.....103

4.1 Sedimentation curves for normally consolidated argillaceous sediments (mod. Skempton, 1970).....112

Figure Page

4.2 Relation between liquidity index and effective overburden pressure for the sediments in Figure 4.1 (mod. Skempton, 1970). 113

4.3 Plasticity chart for the sediments designated in Figures 4.1 and 4.4 (mod. Skempton, 1970).....114

4.4 Depositional water contents of clays below the seabed and intertidal flats (mod. Skempton, 1970).....118

4.5 Map of the Canadian Beaufort Sea showing some sample locations.....122

4.6 Profile for PC-09, Kugmallit Channel.....126

4.7 Consolidation curve for PC-09 at 1.16 m bsb.....127

4.8 Consolidation curve for PC-09 at 2.08 m bsb.....128

4.9 Strain energy versus effective stress for PC-09; 1.16 m bsb.....132

4.10 Strain energy versus effective stress for PC-09; 2.08 m bsb.....133

4.11 Normalized undrained strength versus overburden pressure for PC-09.....135

4.12 Normalized undrained strength versus overburden pressure for PC-28.....136

4.13 Map of sample sites for the GSC 1984 Spring Drilling Program (mod. Hill et al, 1985)....138

4.14 Profile for BH 20+00; nearshore environment.....139

4.15 Consolidation curve for BH 20+00 at 4.85 m bsb.....144

4.16 Consolidation curve for BH 20+00 at 10.95 m bsb.....145

4.17 Consolidation curve for BH 20+00 at 13.74 m bsb.....146

4.18 Strain energy versus effective stress for BH 20+00; 4.85 m bsb.....149

Figure Page

4.19 Strain energy versus effective stress for BH 20+00; 10.95 m bsb.....150

4.20 Strain energy versus effective stress for BH 20+00; 13.74 m bsb.....151

4.21 Normalized undrained strength for BH 20+00.....156

4.22 Idealized profile for Gulf Sauvrak, Kringalik Plateau.....158

4.23 Profile for MTWS1, Mackenzie Trough.....166

4.24 Peizometric Cone Penetrometer trace for MTWC01.....167

4.25 MTWC01 continued.....168

4.26 Peizometric Cone Penetrometer trace for MTWC02.....169

4.27 Consolidation curve for MTWS1 at 6.16 m bsb.....174

4.28 Strain energy versus effective stress for MTWS1; 6.16 m bsb.....175

4.29 Normalized undrained shear strength for MTWS1.....177

4.30 Normalized coefficient of secondary compression versus effective stress for all consolidation samples.....181

4.31 Coefficient of secondary compression for natural soil deposits (mod. Mesri, 1973).....182

4.32 Compression index for Beaufort Sea soils.....183

4.33 OCR for BH 20+00 showing measured values versus predicted.....188

4.34 OCR for Sauvrak showing measured values versus predicted.....189

5.1 Flow velocity data from PC-09 versus hydraulic gradient showing the validity of the assumption of laminar flow.....200

5.2 Measured and predicted values of the coefficient of permeability versus void ratio for PC-09; Z=1.16 m.....201

Figure Page

5.3 Measured and predicted values of the coefficient of permeability versus void ratio for PC-09; Z=2.08 m.....202

5.4 Flow velocity data from BH 20+00 verifying the assumption of laminar flow during the permeability test.....204

5.5 Measured and predicted values of the coefficient of permeability versus void ratio for BH 20+00; Z=4.85 m.....205

5.6 Measured and predicted values of the coefficient of permeability versus void ratio for BH 20+00; Z=13.74 m.....206

5.7 Void ratio vs. coefficient of permeability plots showing range of measurements made to date for five marine sediment types (mod. Silva et al, 1981).....209

5.8 Comparison of permeabilities for various soil types (mod. Lambe and Whitman, 1969).....211

6.1 Stress-strain curves for the triaxial tests of soft recent marine clays (PC-02 and PC-03).....218

6.2 Modified Mohr plot showing the effective stress paths followed during undrained shear for the tests shown in Figure 6.1.....219

6.3 Mohr failure envelope for the tests in Figures 6.1 and 6.2.....220

6.4 Stress-strain curves for isotropically consolidated triaxial compression tests on Beaufort Sea silt (mod. Konrad, 1985).....225

6.5 Stress-strain curves for an anisotropically consolidated triaxial compression test on Beaufort Sea silt (mod. Konrad, 1985).....226

6.6 Effective stress paths for the triaxial tests in Figure 6.4 and 6.5 (mod. Konrad, 1985)....227

6.7 Failure envelope for triaxial compression tests performed on Beaufort Sea silt (mod. Konrad, 1985).....229

Figure		Page
A.1	Schematic of Modified Anteus Back Pressured Consolidometer/Permeameter	255
A.2	Calibration of loading system of System A (low range)	256
A.3	Calibration of loading system of System A (high range)	257
A.4	Calibration of loading system of System B (low range)	258
A.5	Calibration of loading system of System B (high range)	259
B.1	Borehole log for PC-09 (1 of 2)	261
B.2	Borehole log for PC-09 (2 of 2)	262
B.3	Borehole log for BH 20+00 (1 of 5)	263
B.4	Borehole log for BH 20+00 (2 of 5)	264
B.5	Borehole log for BH 20+00 (3 of 5)	265
B.6	Borehole log for BH 20+00 (4 of 5)	266
B.7	Borehole log for BH 20+00 (5 of 5)	267
B.8	Borehole log for BH MTWS1 (1 of 8)	268
B.9	Borehole log for BH MTWS1 (2 of 8)	269
B.10	Borehole log for BH MTWS1 (3 of 8)	270
B.11	Borehole log for BH MTWS1 (4 of 8)	271
B.12	Borehole log for BH MTWS1 (5 of 8)	272
B.13	Borehole log for BH MTWS1 (6 of 8)	273
B.14	Borehole log for BH MTWS1 (7 of 8)	274
B.15	Borehole log for BH MTWS1 (8 of 8)	275
F.1	Void ratio versus log effective vertical stress for BH SK 82S14; Z=1.13 m bsb. (Jefferies, pers. comm., 1985)	291

Figure Page

F.2 Strain energy versus effective vertical stress for BH SK 82S14; Z=1.13 m bsb.....292

F.3 Void ratio versus log effective vertical stress for BH SK 82S13 1B; Z=1.90 m bsb. (Jefferies, pers. comm., 1985).....293

F.4 Strain energy versus effective vertical stress for BH SK 82S13 1B; Z=1.90 m bsb.....294

F.5 Void ratio versus log effective vertical stress for BH SK 82S03 5B; Z=3.75 m bsb. (Jefferies, pers. comm., 1985).....295

F.6 Strain energy versus effective vertical stress for BH SK 82S03 5B; Z=3.75 m bsb.....296

F.7 Void ratio versus log effective vertical stress for BH SK 82S13; Z=4.04 m bsb. (Jefferies, pers. comm., 1985).....297

F.8 Strain energy versus effective vertical stress for BH SK 82S13; Z=4.04 m bsb.....298

F.9 Void ratio versus log effective vertical stress for BH 1-5; Z=6.40 m bsb. (Jefferies, pers. comm., 1985).....299

F.10 Strain energy versus effective vertical stress for BH 1-5; Z=6.40 m bsb.....300

F.11 Void ratio versus log effective vertical stress for BH SK 82S03 9B; Z=7.60 m bsb. (Jefferies, pers. comm., 1985).....301

F.12 Strain energy versus effective vertical stress for BH SK 82S03 9B; Z=7.60 m bsb.....302

F.13 Void ratio versus log effective vertical stress for BH SK 82S14 4B; Z=9.56 m bsb. (Jefferies, pers. comm., 1985).....303

F.14 Strain energy versus effective vertical stress for BH SK 82S14 4B; Z=9.56 m bsb.....304

F.15 Void ratio versus log effective vertical stress for BH SK 82S13 5B; Z=10.40 m bsb. (Jefferies, pers. comm., 1985).....305

Figure Page

F.16 Strain energy versus effective vertical stress for BH SK 82S13 5B; Z=10.40 m bsb.....306

F.17 Void ratio versus log effective vertical stress for BH 1-8; Z=11.00 m bsb. (Jefferies, pers. comm., 1985).....307

F.18 Strain energy versus effective vertical stress for BH 1-8; Z=11.00 m bsb.....308

F.19 Void ratio versus log effective vertical stress for BH SK 82S13 7B; Z=14.10 m bsb. (Jefferies, pers. comm., 1985).....309

F.20 Strain energy versus effective vertical stress for BH SK 82S13 7B; Z=14.10 m bsb.....310

F.21 Void ratio versus log effective vertical stress for BH SK 82S13 11B; Z=21.70 m bsb. (Jefferies, pers. comm., 1985).....311

F.22 Strain energy versus effective vertical stress for BH SK 82S13 11B; Z=21.70 m bsb.....312

F.23 Void ratio versus log effective vertical stress for BH SK 82S13 12B; Z=23.23 m bsb. (Jefferies, pers. comm., 1985).....313

F.24 Strain energy versus effective vertical stress for BH SK 82S13 12B; Z=23.23 m bsb.....314

F.25 Void ratio versus log effective vertical stress for BH SK 82S13 13B; Z=24.67 m bsb. (Jefferies, pers. comm., 1985).....315

F.26 Strain energy versus effective vertical stress for BH SK 82S13 13B; Z=24.67 m bsb.....316

F.27 Void ratio versus log effective vertical stress for BH SK 82S13; Z=33.70 m bsb. (Jefferies, pers. comm., 1985).....317

F.28 Strain energy versus effective vertical stress for BH SK 82S13; Z=33.70 m bsb.....318

F.29 Void ratio versus log effective vertical stress for BH 1-24; Z=34.00 m bsb. (Jefferies, pers. comm., 1985).....319

Figure

Page

F.30 Strain energy versus effective vertical stress for BH 1-2; Z=34.00 m bsb.....320

F.31 Void ratio versus log effective vertical stress for BH 1-27; Z=38.40 m bsb. (Jefferies, pers. comm., 1985).....321

F.32 Strain energy versus effective vertical stress for BH 1-2; Z=38.40 m bsb.....322

F.33 Void ratio versus log effective vertical stress for BH 1-32; Z=46.80 m bsb. (Jefferies, pers. comm., 1985).....323

F.34 Strain energy versus effective vertical stress for BH 1-32; Z=46.80 m bsb.....324

List of Plates

Plate		Page
3.1	Two modified Anteus back-pressured consolidometer/permeameters used in the testing of Beaufort Sea sediments	32
4.1	Scanning Electron Micrograph of marine bioturbated silty clay from 1 m bsb. in PC-09	193
4.2	Scanning Electron Micrograph of marine silty clay that has begun the process of consolidation; 13.7 m bsb. in BH 20+00	194

1.0 Introduction

The stress history of the surficial sediments in the Canadian Beaufort Sea appears to show some very perplexing trends. The parameter referred to as the overconsolidation ratio is usually thought to be a reliable indicator of the stress history of a soil deposit, since it relates the presently existing yield strength of the soil to the effective stress the soil is currently experiencing. However, over the past two decades, researchers compiling consolidation data from the marine environment have remarked on a seemingly inexpicable behaviour occurring the closer one gets to the mudline. Marine soils are generally believed to be in a state of normal consolidation. That is to say that the present effective stress is similar in magnitude to the preconsolidation or yield stress. But this is not always the case in marine soils.

The overconsolidation ratio has been measured as being over 50 a few centimeters below the mudline in deep-sea sediments, which would seem to invalidate the assumption of normal consolidation. This behaviour is termed "apparent overconsolidation" and is found throughout the world's oceans at depths below seabed between 0 and 10 meters. One aim of this study is to define this phenomenon and determine whether it occurs in the Beaufort Sea. Preliminary industry data would seem to show that it does occur on a widespread basis. An attempt will be made to isolate the factors contributing to apparent overconsolidation. If possible, the

effect will be quantified in terms of identifiable factors that can be separated and used to predict the phenomenon. Should this prove possible, the data from the zone of apparent overconsolidation can be used to interpret the stress history as it pertains to the depositional environment.

This study will undertake high quality consolidation testing using a system that is capable of back-pressuring the soil sample in order to determine accurate values of the preconsolidation pressure. Another series of tests will be run on similar soil samples from the same areas under conditions of undrained triaxial shear, reconsolidated to the in situ effective stress in order to determine the existence of overconsolidation in the form of a measureable cohesion intercept. This would support the occurrence of a certain amount of overconsolidation in the soil.

Only the highest quality samples can be used for this testing since the determination of the preconsolidation pressure is very sensitive to the amount of soil disturbance. Samples of such quality are difficult to obtain in the marine environment because of the softness of the sediments at such shallow burial depths. However the use of the standard piston corer has been shown to be an effective solution to the problem.

Since the consolidation samples are to be back pressured to the in situ hydrostatic pressure, it is a simple matter to adapt the testing apparatus so that

constant or falling head permeability tests can be run at the end of each load increment. This will allow the void ratio versus permeability relationship to be determined. These values of permeability should be in closer agreement with in situ permeabilities than predictions derived from oedometer time-compression curves.

Shear strength testing will be conducted on undisturbed, reconsolidated samples from selected sites in the Beaufort Sea to determine undisturbed values of the effective stress parameters, c' and ϕ'. These samples will be sheared in undrained triaxial compression after being consolidated to different stress levels. An attempt will be made to test samples from the problematic soft zone immediately below the mudline.

In summary, it is of prime importance to deduce a useable relationship between OCR and the depth below seabed, since the interpretation of stress history often relies solely on results from one-dimensional testing. Stress-controlled triaxial testing would be a very desirable addition to the analysis for stress history, however its useage is limited to research institutions and remains a specialized tool for in depth, expensive analysis of yield behaviour. What is needed is a simple, straightforward understanding of the large body of data that already exists for the Beaufort Sea sediments. This body of data follows the trend of apparent overconsolidation within the upper 6 to 10 meters of sediment.

Chapter One of this thesis is a statement of the geology of the surficial sediments in the Beaufort Sea. The occurrence and distribution of acoustic permafrost, as noted on high resolution seismic profiles is discussed along with the characteristic features of each of the nine physiographic regions.

Chapter Two discusses the phenomenon of apparent overconsolidation and reviews its possible causes. A method of redefining the way stress history is interpreted from oedometer tests is proposed to avoid the boundary problem of apparent overconsolidation. A technique for predicting preconsolidation pressure (Wroth, 1979) is discussed.

Chapter Three presents the results of the consolidation testing programme as they relate to the geology at each sample site. The trend of apparent overconsolidation is supported by the test data. Predictions of preconsolidation pressure from use of the Casagrande technique are compared with predictions using the method of strain energy (Crooks and Graham, 1976).

Chapter Four presents the results of the permeability testing programme. Constant head test results agree very well with predictions based on oedometer time-compression data.

Chapter Five reviews the results of the static triaxial testing programme and presents basic effective stress parameters for both the soft surficial marine clay and the underlying transgressive variable sequence of interbedded

silts and clays found in the Beaufort Sea.

The conclusions are summarized in Chapter Six, followed by appendices containing all of the test data from which the conclusions were drawn.

2.0 Regional Surficial Geology of the Beaufort Sea

2.1 Early Development of a Geological Model

Much work has been undertaken by M.J. O'Connor and Associates over the past ten years in the interpretation of the surficial geology over the Canadian continental shelf in the Beaufort Sea. The development of a preliminary three-unit geological model arose from numerous high-resolution seismic records and a large amount of geotechnical borehole data made available to the Geological Survey of Canada in association with M.J. O'Connor by the various petroleum operators in the area. Using the three unit model along with bathymetric data, O'Connor (1982a) was able to divide the continental shelf into nine physiographic regions (Figure 2.1).

The presence of submarine acoustic permafrost visible as strong reflectors on the seismic records was verified in the first few boreholes drilled by industry. Acoustic permafrost occurs only on seismic records where the compression wave velocity is increased within ice-filled voids in the sediments. This decreases the return time for reflected sound waves and thus ice-bonded or gassy zones appear as strong reflectors or anomalies on the seismic profile. These voids are not necessary full of ice; they may contain gas which then results in a decrease in compression wave velocity and so gassy zones appear as bright spots on the acoustic record. The sediments may be well-bonded or

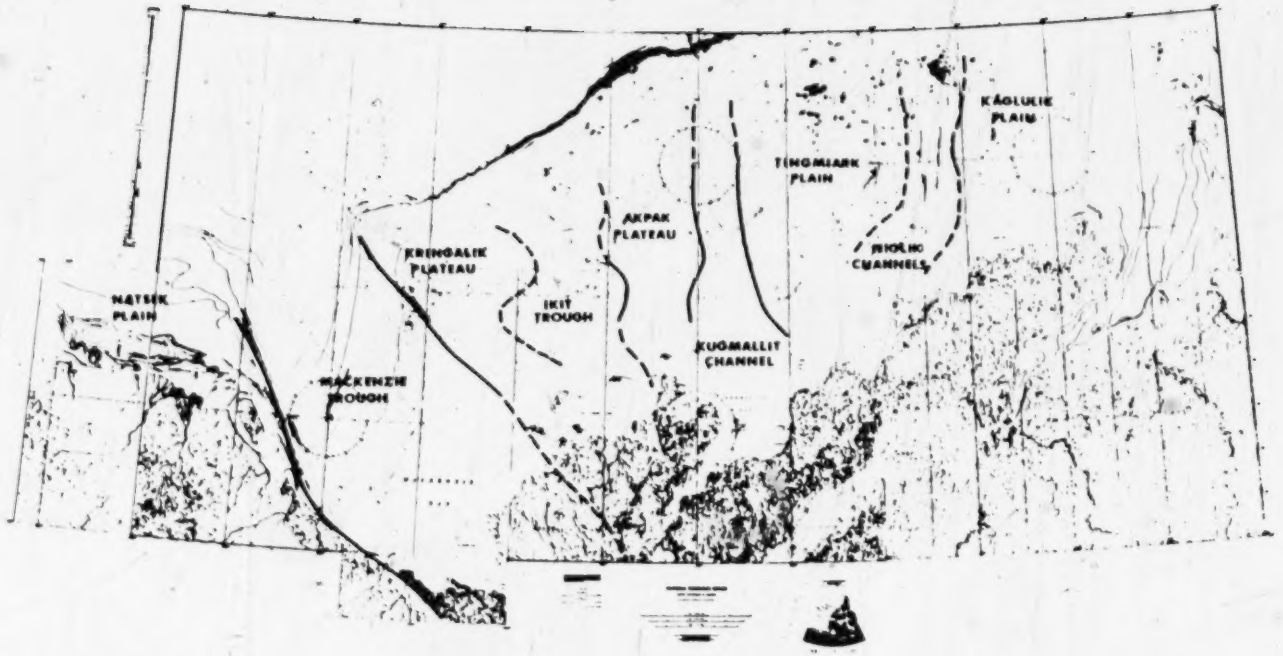

Figure 2.1 Physiographic provinces for the Canadian Beaufort Sea (mod. O'Connor, 1982a).

only partially bonded by ice, the relative abundance being evident in the brightness of the reflector on the seismic profile.

A distinction exists between acoustic permafrost (APF) and permafrost since by definition permafrost represents any material possessing sub-zero temperatures for more than one year. Clayey sediments often possess sub-zero temperatures in the Beaufort Sea, and are therefore termed permafrost, but because of the salinity of the pore fluid and activity of the clay mineralogy they remain largely unfrozen or at best, poorly bonded.

The distribution of APF has been mapped by O'Connor (1982b) and was used to assist in delineating the physiographic provinces shown in Figure 2.1. However, the presence of ice-bonding and gas-charged sediments complicates the interpretation of stratigraphy underlying the uppermost reflector. Reflected sound waves from strata beneath the reflector are accelerated through the ice-bonded layers which may result in a "pull-up" of deeper strata. Depths on the vertical scale are difficult to determine below strong reflectors, because distances are derived from the travel times of the reflected sound waves and one must assume a constant compression wave velocity of 1500 meters per second in the sediments. Consequently, boreholes were drilled to confirm the stratigraphy and the extent of ice-bonding below the topmost reflectors.

The major geologic control in the Beaufort Sea lies in the existence of a regional unconformity separating the recent marine sediments deposited during and subsequent to the last sea level rise, from the pre-unconformity coarse-grained sediments deposited during the last sea level minimum (O'Connor, 1982a). The development of extensive permafrost within the outwash sands and deltaic silts occurred during this period of reduced sea level as the sediments were exposed to a periglacial climate.

2.2 A Sea Level Curve for the Canadian Beaufort Sea

Hill et al (1985) have proposed a relative sea level curve for the Canadian Beaufort Sea that represents the transgression beginning after the last major sea level minmum, about 30,000 years ago (Figure 2.2). This curve is based on Quinlan and Beaumont's (1981) visco-elastic crustal model which was used to deduce the amount of isostatic rebound following the retreat of the last continental ice sheet. A minor stillstand or recession during transgression is inferred from the consistent depth of the shelf break at 70 meters below present sea level along with numerous truncated fluvial channel levees on the outer shelf present on seismic records (Hill et al, 1985). There is further evidence to support the concept of a minor recession. On the outer continental shelf there appears a more recent unconformity existing in apparently marine sediments that overlie the major unconformity. This upper unconformity is also found at a similar depth in the Mackenzie Trough, there also overlying the major unconformity. Therefore, the evidence is compelling for a period of exposure within the marine sequence wherever it exists 50 meters or more below the present sea level. The minor recession is believed to have commenced about 17,000 years ago in response to a re-advance of the ice sheet into the area and reached a minimum about 12,000 years ago.

A number of radiocarbon dates have been determined from in situ organic samples recovered in boreholes from many

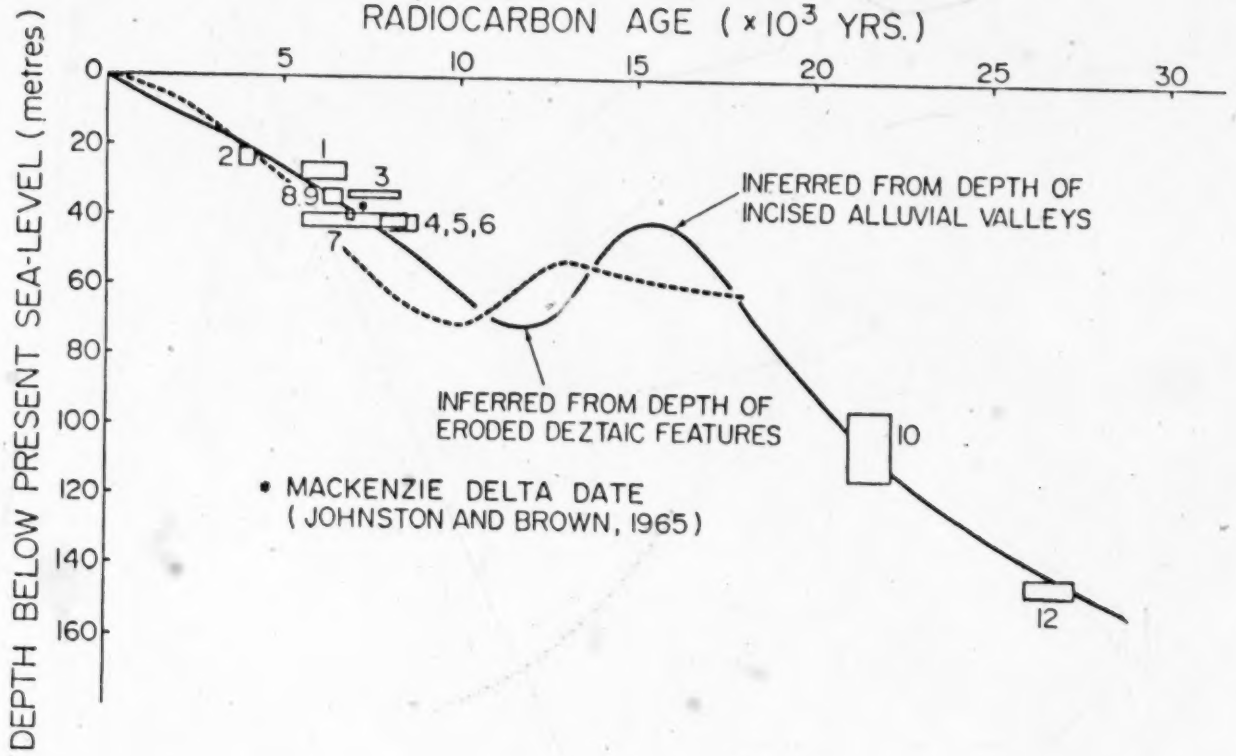

Figure 2.2 A relative sea level curve for tha Canadian Beaufort Sea (mod. Hill et al, 1985).

different areas and have been placed on the curve of relative sea level to improve on the results from Quinlan's visco-elastic model. The dates are constrained by palynological analyses and are believed to represent the oldest dates possible. The identification of foraminifera and dinoflagellates was used to verify the origin of the fine-grained soils comprising the most recent marine sediments (Hill et al, 1985).

2.3 A Three-Unit Geologic Model for the Beaufort Sea

O'Connor (1982a) proposed a simple geologic model comprised of three distinct stratigraphic units. A schematic of the model is shown in Figure 2.3. The three units are denoted by capital letters A, B, and C. Unit C consists of dense pre-unconformity sands, silts, and in some cases gravels. The top of this unit marks the location of the major unconformity developed during the last major sea level recession. This unit is composed of well-sorted aeolian sands at the eastern end of the continental shelf, and becomes more silty to the west, where it exists as prodeltaic deposits. A number of river valleys were cut down into this unit to the east of the Mackenzie Trough, which created a series of plateaus and linear depressions. These depressions have since been largely infilled with marine sediments. The veneer of marine sediments is much thinner over the plateaus, being only several meters thick. The buried valleys still appear as minor bathymetric depressions, as can be seen in Figure 2.1.

A transgressive or reworked unit (B) overlies the major unconformity but is in some areas, equivalent to pre-unconformity strata (O'Connor, 1982a). This is especially true of the eastern margins of the buried valleys where sequences of well-laminated transgressive sediments (unit B) are equivalent with prodeltaic sand and silt deposits. Unit B is highly variable in geotechnical properties and often serves as a trap for subterranean gas

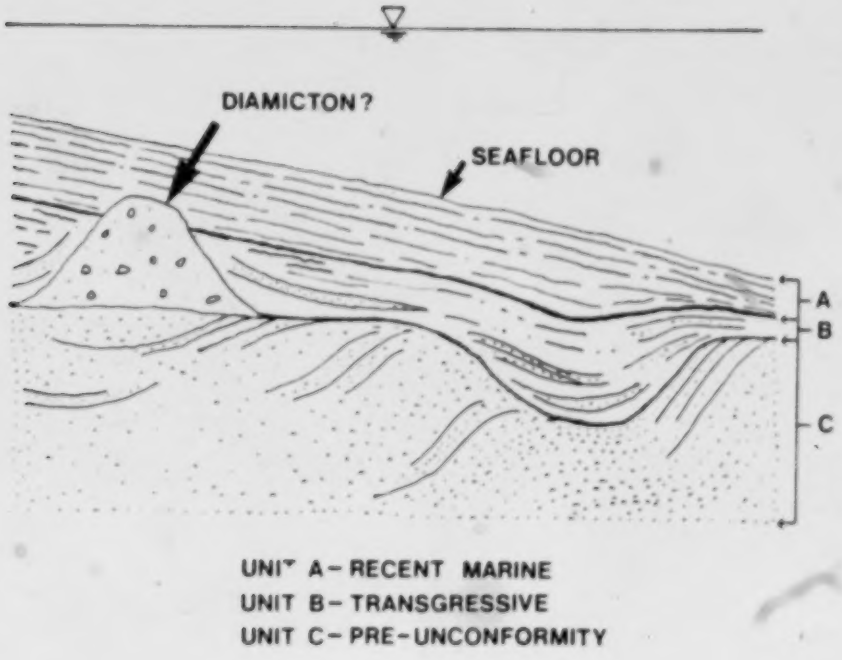

Figure 2.3 Geological model for the Beaufort Sea (mod. O'Connor, 1982a).

percolating up through the sediments, as well as marking the top of the permafrost table in some areas (e.g. in the buried river valleys).

Overlying unit B is an accumulation several meters thick on average of young bioturbated marine clays and silty clays having a very soft to soft consistency. This soil is predominantly a weak unit as it has not been subjected to the high energy environments that units B and C have experienced. It has been further weakened by the effects of ice scouring. Ice scours are found throughout units A and B and there exists in the Mackenzie Trough a zone of almost complete remoulding, termed the Saturated Scour Zone. The texture of unit A becomes finer as distance from the Mackenzie Delta increases, with the majority of the silts settling out in the Mackenzie Trough. Littoral drift accounts for the widespread distribution of marine sediments occurring at present.

2.4 Occurrence of Acoustic Permafrost

Most APF reflectors occur between 10 and 65 m below seabed (bsb.) and are limited to the pre-unconformity strata (O'Connor, 1982b). The overlying fine-grained sediments are in some cases, permafrost affected but are generally unfrozen. APF is thought to be aggrading near the shelf edge in the coarse pre-unconformity sediments where present water temperatures are lower than the seabed temperature (O'Connor, 1982b).

2.5 Classification of APF Types

2.5.1 Marginally or Partially Ice-Bonded APF

This class of APF is found in permafrost-affected fine-grained marine and transgressive sediments. The pore water salinity and the colloidal activity of the clays depresses the freezing point to the point where these sediments can remain unfrozen to temperatures of 1 to 2 degrees below zero. A minor amount of ice-bonding does take place in the pore water surrounding the coarser particles in the clay matrix, hence the sediments are said to be partially ice-bonded. These sediments remain acoustically transparent whereas other types of APF tend to impede the transmission of reflected sound waves from underlying strata (O'Connor, 1982b).

2.5.2 Stratigraphically Controlled APF

This class of APF produces a strong reflector at the point where a marked change in lithology occurs and a fine-grained soil overlies a coarse-grained soil. The reflector disappears where lithology changes are less pronounced. It is for this reason that stratigraphically controlled APF is found predominantly below the unconformity in the buried fluvial valleys. It is sometimes referred to as an APF table because it tends to follow the horizontal stratifications. The zero degree isotherm commonly overlies the reflector by a short distance (Brown and Kupsch, 1974).

2.5.3 Hummocky APF

Hummocky APF is thought to be a degrading relic of more widespread ice-bonding. Reflectors are strong in amplitude where lithology changes are well-defined and are missing where changes are gradational (O'Connor, 1982b). Hummocky APF usually occurs in association with stratigraphically controlled APF at greater depth and represents a hiatus in the downward progression of the thaw front. Hummocky APF is not relatable to stratigraphy on a continuous basis and is of variable thickness and lateral extent. Wide hummocks may be connected directly to stratigraphically controlled APF where it occurs below (O'Connor, 1982b).

2.6 The Physiographic Regions of the Continental Shelf

2.6.1 The Natsek Plain

Little geotechnical data is available from this region, since only one borehole has been drilled in this area to date; at Natsek (Figure 2.4). The stratigraphy consists of 2 m of very soft marine sediments (unit A) directly overlying the unconformity and 63 m of stiff to hard clay, which probably is of pre-Wisconsinan age (Hill, pers. comm., 1985). Sedimentation is extremely slow in this area, as littoral drift sweeps all of the discharge from the Mackenzie River eastward.

Segregated massive ice was found between the 4 and 17 m depths, with lenses oriented both vertically and horizontally. The ifi clay was in general ice-poor, possessing ice contents less than 10 percent. This supports the assumption that the unconformity exists at the 2 m level; the horizon that was exposed to a periglacial climate during a time of lower sea level.

2.6.2 The Mackenzie Trough

This area exists as a deep bathymetric depression, bounded on the west by the Yukon coast and a submerged ice-thrust feature known as the Herschel Sill, and on the east by the Kringalik Plateau. The western margin is a steep slope and is known to be an area of very slow sedimentation. It is likely that beds end abruptly against the slope. The

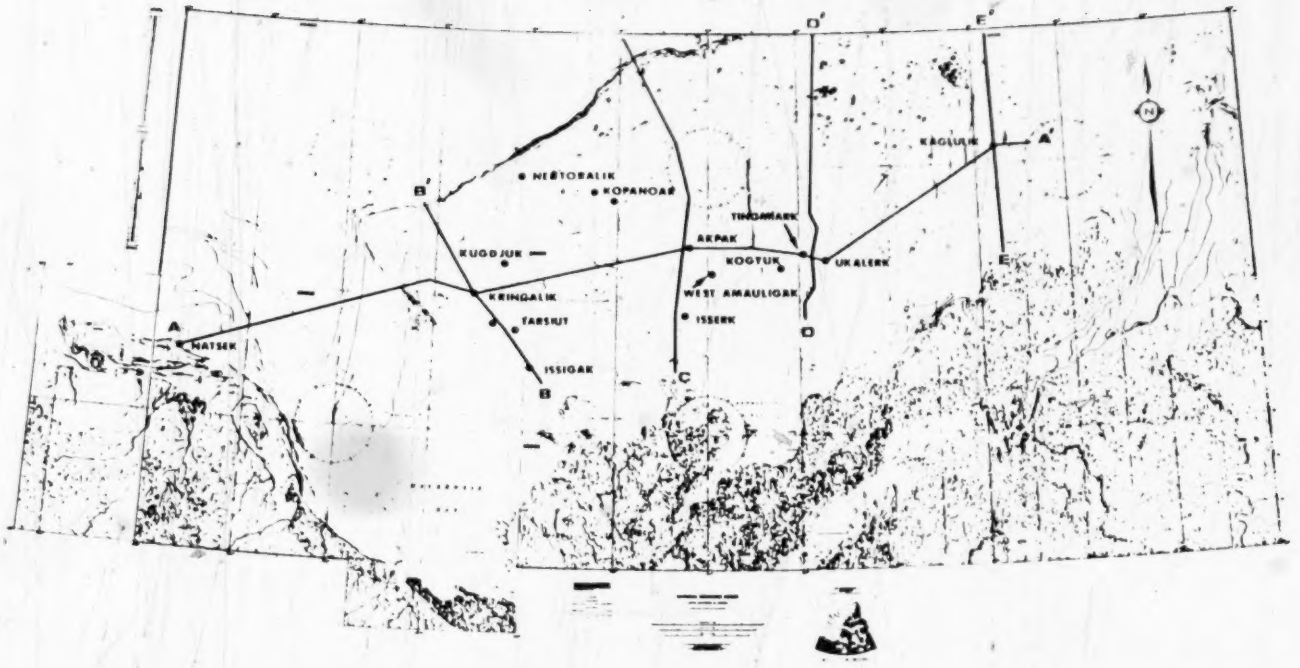

Figure 2.4 Industry borehole locations in the Beaufort Sea (mod. O'Connor, 1982a).

eastern boundary of the region is not well defined and may be contiguous with sequences on the Kringalik Plateau. A prominent seafloor lineation exists on the eastern boundary beyond the 30 m isobath, which may be related to tectonic faulting during the Cretaceous. The Trough is being infilled by silts being discharged from the Mackenzie River at present and the sedimentation rate at the mouth of the delta is very high.

The depth at which older marine sediments are encountered is unknown at present; it is thought that they may interlap with the prograding deltaic beds at some depth (Hill, pers. comm., 1985). Relic ice scours have been observed on seismic records at depths ranging between 16 and 24 m below the mudline (O'Connor, 1980; Blasco and O'Connor, 1982). The occurrence of this saturated scour zone tends to support the idea of a minor regression or a stillstand in sea level during the overall transgression. This feature thins seaward and is entirely absent in deep water.

Seabed temperatures are known to be less than zero in the Trough (Appendix E) and at significant depth they appear to increase, consistent with a certain amount of crustal warming from below. However, the sediments are unfrozen to the depth of exploration.

A number of theories have been proposed to account for the formation of the Trough. Shearer (1972) suggested that the Trough was gouged out by a tongue of the continental ice sheet during a previous glaciation. Mackay (1959) proposed

that Herschel Island was created by ice-thrusting within the Herschel Basin, a thesis that is supported by the occurrence of ice-thrust features recently discovered by the Geological Survey of Canada. Yorath (1973) contends that the Mackenzie Delta occupies a glacially scoured structural graben created during the Cretaceous period.

2.6.3 The Kringalik Plateau

More than one unconformity is found near the shelf edge in this region (O'Connor, 1982a); further evidence to support a minor recession in sea level. The major unconconformity is exposed at the seafloor nearshore and again at the shelf break. Deltaic sediments are thereby believed to have reached the shelf edge during the last major recession in sea level (Hill, pers. comm., 1985). There is little lithology change across the unconformity, and beds are severely disrupted where ice scouring has been extensive.

The recent (Holocene) marine sediments possess very low undrained shear strengths at the mudline (0 to 10 kpa), after which there is an increase of about 10 kpa per meter of burial. The undrained strength increases dramatically across the unconformity, indicating that the fine-grained sediments at the unconformity are overconsolidated.

The major unconformity is placed some 14 m bsb. in the Tarsiut-Sauvrak area (Figure 1.5), based on a change in the number of foraminifera and the pollen profile. Radiocarbon

dates also place the unconformity at this level (Hill, pers. comm., 1985). At the level of the unconformity, the numbers of foraminifera decrease, then increase again; which suggests a period of sub-aerial erosion. The erosion at the unconformity is not thought to have removed more than one to two meters of deltaic sediment as the sea transgressed over the area about 6500 years ago (Hill, pers. comm., 1985).

Extensive gas was noted by O'Connor (1982a) near the unconformity. There is a wide variation in the value of the preconsolidation pressure between 15 and 150 m bsb. in the Tarsiut area (Hivon, 1983). It is not known whether this variation is related to gas disturbance or ice scouring; or solely to variations in the geology. Jefferies et al (1984) report very high values of lateral effective stress occurring at the 15 m bsb. level. The reason for this is not known at present.

O'Connor (1982b) states that the sediments below the unconformity are marginally ice-bonded. Samples recovered from boreholes did not show any ice crystals. Small patches of hummocky APF exist below the unconformity, as observed on seismic records (O'Connor, 1982b).

2.6.4 The Ikit Trough

The Ikit Trough appears in Figure 2.1 as a lesser bathymetric depression. This region is a relic fluvial river valley that has been infilled initially by transgressive sediments (unit B), then more recently by marine sequences

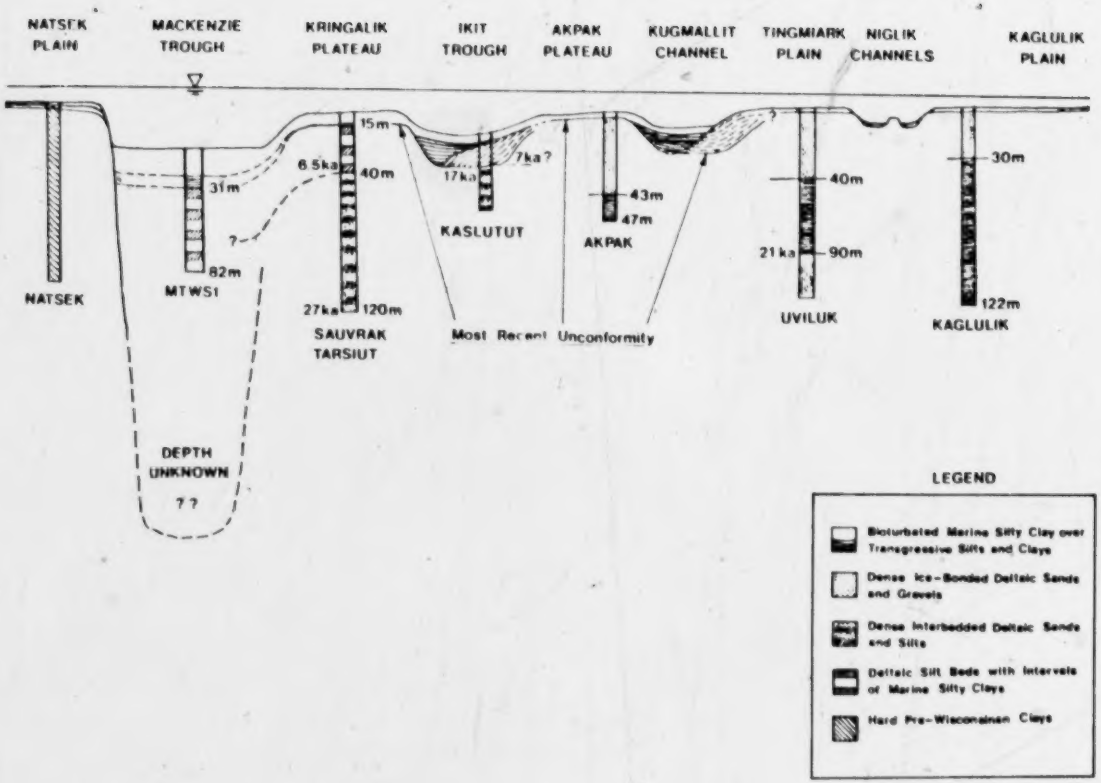

Figure 2.5 East-west cross-section of the shelf summarizing the surficial geology (vertical scale exaggerated), (Hill, pers. comm., 1985).

(unit A), as can be seen in Figure 2.5. Seismic records show prograding beds at the eastern margin, which are interbedded with the well-laminated sequence (unit B). The major unconformity lies at the base of the buried channel over well-sorted deltaic sands (Hill, pers. comm., 1984).

2.6.5 The Akpak Plateau

The boundaries of this region were deduced from morphological changes in the major unconformity as well as bathymetry (O'Connor, 1982a). The unconformity is elevated with respect to the adjacent buried channels. A second, more recent unconformity appears on seismic records in deep water in association with a great number of buried truncated channel margins, supporting the concept of a minor recession in sea level (Hill et al, 1985). Geotechnical boreholes show the recent sediment veneer to be thin, averaging 3 m in thickness, thickening to 8 m along the edges of the plateau.

Near Isserk (Figure 2.4), the soils at the seabed are stiff and ice-bonded, suggesting a glacial origin (O'Connor, 1982a). Between the 15 and the 60 m isobath there exists a predominance of hummocky APF. Stratigraphically controlled APF is evident at greater burial depths and exists to a large extent beyond the 60 m isobath (O'Connor, 1982b).

The depth of ice scouring over the plateau does not penetrate below the unconformity. This is a direct result of the density of the sands underlying the unconformity.

2.6.6 The Kugmallit Channel

The Kugmallit Channel is a partially infilled flat-bottomed fluvial valley extending from Kugmallit Bay to the shelf edge. It is very similar in characteristics to the Ikit Trough, as is shown on Figure 2.5. Like the Ikit Trough, a lobe of deltaic sands has prograded into the paleo-channel from the plateau to the east. Complex reflectors at the base of the channel conform with the underlying strata, which consist of a sequence of dense outwash sands 30 m thick. A stratum of stiff clay and silt underlies the sand, a unit that O'Connor (1982a) suggests outcrops at the shelf edge.

On the western edge of the channel, sediments have been washed off the adjacent Akpak Plateau during transgression (O'Connor, 1982a). The thickness of recent marine sediments varies from 20 m inshore of the 30 m isobath to being non-existent beyond the 50 m water depth. These sediments have been heavily ice-scoured and therefore exhibit no structure (Blasco and O'Connor, 1982).

Seismic records show extensive amounts of gas to be trapped below the unconformity by the fine-grained sediments (O'Connor, 1977 and 1980).

2.6.7 The Tingmiark Plain

The geology of this area is practically identical to the Akpak Plateau. Littoral drift has deposited 3 m of clayey sediment over the pre-unconformity aeolian sands.

This sand sequence is 40 m thick and overlies a 30 m thick deposit of marine silts and clays, which is in turn underlain by a further sand sequence.

Hummocky APF is extensive along the western margin of the region and occurs with stratigraphically controlled APF nearshore and beyond the 60 m isobath (O'Connor, 1982b). O'Connor observes that pingo-like features (PLF's) are abundant beyond the 40 m isobath; occurring in shallow saebed depressions. These may be relic thermokarst features formed during the last sea level minimum, or they may be mud lumps or diapirs (Poley,1982). Moran (pers. comm., 1985) mentions that they may even be gas-related.

2.6.8 The Niglik Channels

Two more elongated depressions about 5 km wide are found beyond the 25 m isobath in this area. O'Connor (1982a) indicates that they may have once been connected to the Kugmallit Channel. Like other relic fluvial channels in the Beaufort Sea, they have been infilled by marine sediments, in this case being only 3 m thick. The pre-unconformity sands and silty sands are found at the base of the relic channels, below which exist the same stiff sequence of marine silts and clays. The APF is primarily stratigraphically controlled (O'Connor, 1982b) below the unconformity.

2.6.9 The Kaglulik Plain

No seismic or bathymetric data has been collected north of 71 degrees latitude, but the profile encountered in the Kaglulik Borehole is thought to be representative of the entire region (Figures 2.4 and 2.5).

The recent sediments are 2 m thick, consisting of silty to sandy clays directly overlying the unconformity (O'Connor, 1982a); below which is found a 28 m thickness of sands with thin clay and silt interbeds. Below that exists 44 m of stiff to hard laminated silts and clays followed by 20 m of fine sand.

All strata below 22.5 m bsb. are frozen and stratigraphically controlled APF was observed on a nearby seismic profile. Isolated islands of hummocky APF also occur (O'Connor, 1982b).

3.0 Consolidation Characteristics of Surficial Sediments

3.1 Testing Apparatus

3.1.1 Sample Extruder

A prime requirement in subsampling shelby tubes containing especially soft marine sediments is that they should be kept in a vertical position as much as possible. Therefore, a system was devised that maintained a vertical position for index tests such as miniature vane shear, NGI fall cone, and bulk density; but that also permitted the tube to be rotated through 90 degrees into a horizontal position for extrusion and further subsampling. This would include subsamples for specific gravity, grain size distribution, and Atterberg Limit determinations. The extruded core could then be examined visually for structure and logged for lithology.

Core can be extruded in either the horizontal or the vertical direction using this extruder. Testing for undrained shear strength was performed using a miniature vane shear apparatus with the soil still in the tube, with the tube in a vertical position.

3.1.2 The Back Pressured Consolidometer/Permeameter

When a soil sample is recovered from the seabottom, the hydrostatic pressure is removed, and as a result dissolved pore gases come out of solution, creating minute gas bubbles

within the soil fabric. This entrapped air can lead to erroneous calculations of void ratio, causing problems of excessive compressibility of the soil fabric during the first few load increments of the consolidation test. The presence of air bubbles within the pore space is also undesirable because it may inhibit the passage of pore fluid from the soil skeleton.

It is desirable to recreate the in situ stress state as closely as possible within the test specimen; so a system is required that possesses the capability of resaturating the specimen under a back pressure, in order to redissolve any exsolved pore gases. This is achieved with the Modified Anteus Back Pressured Consolidometer/Permeameter. Application of a back pressure for 72 hours before beginning the consolidation test is considered adequate to fully resaturate the specimen (Black and Lee, 1973).

Constant and falling head permeability testing was incorporated into the program. A test could be performed at the end of any desired load increment. Modifications were made to the standard Anteus equipment in order to allow this testing. These modifications included the addition of a pressure system capable of delivering very low to very high hydraulic gradients across the sample. A 5 ml burette (+ or - 0.01 ml) was added to facilitate the accurate measurement of very small flows through the sample.

The head difference across the specimen in the consolidation ring is applied by raising a variable height

permeability reservoir above the level of the water in the saturation reservoir for hydraulic gradients less than 20. (Figure 3.1 is a schematic of the modified apparatus.) Plate 3.1 is a photograph of two identical consolidometer/permeameters that were rebuilt and modified for this study. For hydraulic gradients in excess of 20, the permeability reservoir is set at the same elevation as the back pressure reservoir, and a pressure in excess of the back pressure is applied with a pressure regulator system to the permeability reservoir and hence also to one side of the sample. Water is then allowed to drain through the sample into the back pressure reservoir. The quantities of flow involved are small so that no appreciable change in the height of the water level in the back pressure reservoir takes place and the hydraulic gradient remains constant throughout the duration of the period of flow measurement. This apparatus allows permeability tests to be run either as falling head or as constant head, with flow either upward or downward through the sample. All tests were of the constant head type for this study, with upward flow through the sample.

The introduction of saturation water (in this case, salt water) into the system is very simply accomplished through a series of connections with a Nold Deairaetor placed some two meters above the level of the sample chamber. Water is then introduced to the system under the influence of gravity.

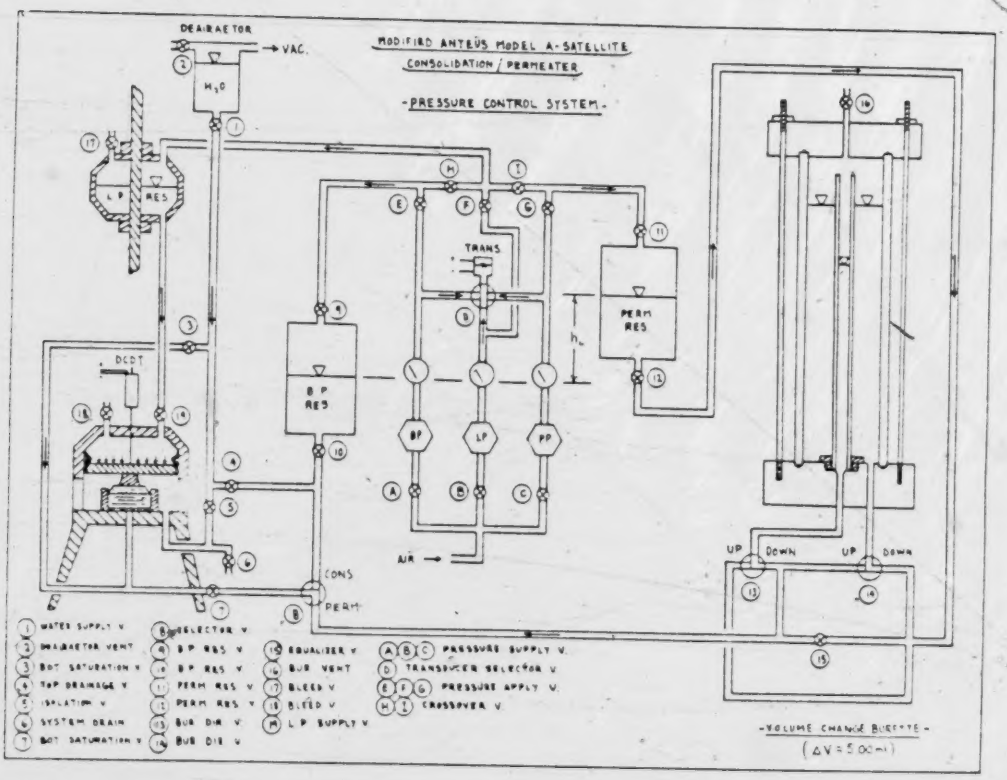

Figure 3.1 Layout of back-pressured consolidometer/permeameter.

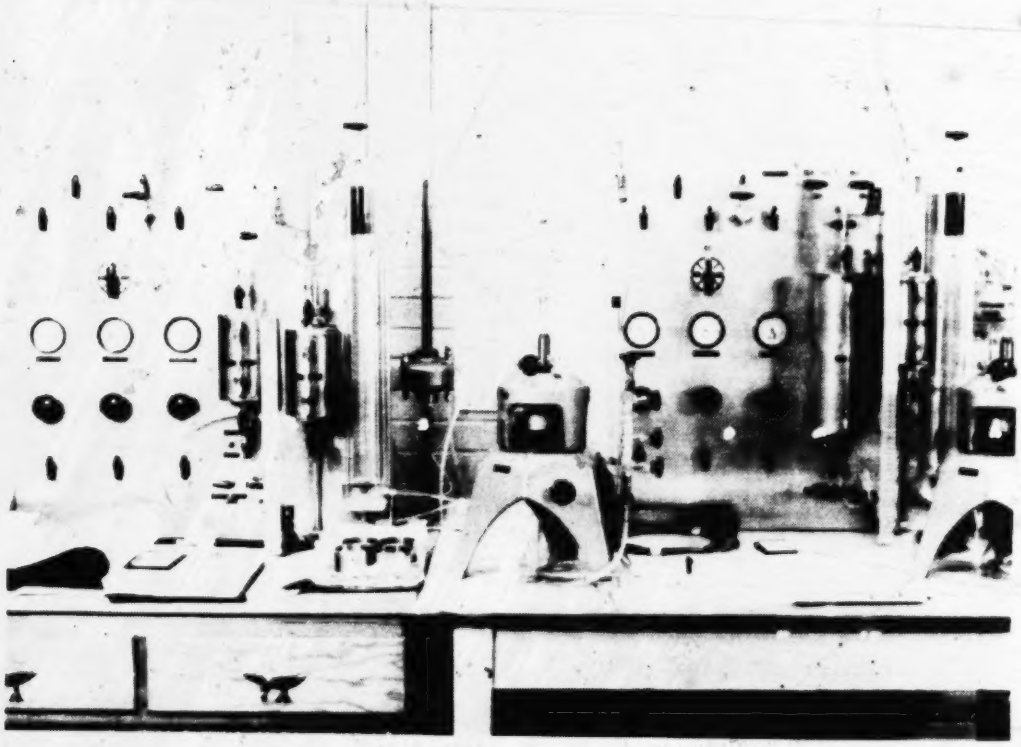

Plate 3.1 Two modified Anteus back-pressured consolidometer/permeameters used in the testing of Beaufort Sea sediments.

3.2 The Phenomenon of Apparent Overconsolidation

3.2.1 Definition

ASTM (1983) defines some basic terms as follows:

A normally consolidated soil deposit is one that has never been subjected to an effective stress greater than the present effective overburden pressure (P_o').

An overconsolidated soil deposit is one that has been subjected to an effective stress greater than the existing effective overburden pressure.

An underconsolidated soil deposit is one that is not fully consolidated under the existing effective overburden pressure. (In the case of marine sediments, excess pore pressures created by the addition of sediment have not been allowed to dissipate for one reason or another.)

A useful means of relating the existing effective overburden pressure to the preconsolidation pressure is by way of the overconsolidation ratio where OCR is given by:

$$OCR = P_c / P_o' \qquad 3.1$$

The effective overburden pressure in the vertical direction is calculated on the the basis of specific gravity, water content, and unit weight data for the depth interval in question.

Noorany (1984) has derived a series of phase relationships for use with marine soils that account for the amount of dissolved salt in the pore water, and these have been adopted in this study to calculate in situ void ratios. They have not been generally applied to correct water contents, since this requires knowledge of the salinity of the pore water, which is not available for the study areas in question at this time.

In general, water contents calculated solely on the basis of dry solids weight invariably neglect the weight of salt in the water content calculation. This results in water contents that are underestimated by about two percent for soils having salinities similar to that of sea water. Subsequent calculations of in situ void ratio are thereby also too low. For marine soils, it is perhaps more important

to use the unit weight for salt water in the calculation of effective overburden pressure.

$$P_o' = (\gamma_s - \gamma_{sw}) * Z \qquad 3.2$$

where γ_s and γ_{sw} denote the unit weights of saturated soil and sea water, respectively. The depth below seabed is termed Z.

The preconsolidation pressure is determined from the void ratio versus logarithm effective stress curve using one or more of the graphical constructions (Casagrande, 1936; Schmertmann, 1955; Burmister, 1951). A new method that appears to offer promise is the technique of strain energy for determination of the level of the preconsolidation pressure (Tavenas et al, 1979; Crooks and Graham, 1976).

3.2.2 Occurrence of Apparent Overconsolidation

Almost all subaqueous cohesive soil deposits exhibit the phenomenon of apparent overconsolidation (AOC) to a greater or lesser degree. Typically the overconsolidation ratio (OCR) is found to be greatly in excess of unity immediately below the mudline, and decreases rapidly to unity at a depth between six and ten meters below seabed. Thereafter, OCR is observed to vary very little; ranging anywhere from 0.4 to values slightly greater than 1.0. OCR

is generally considered to be a reliable indicator of the previous stress history, however the occurrence of OCR's in excess of 50 at the mudline would seem to present a problem.

According to Terzaghi (1941), a clay is normally consolidated if it has never been under a pressure greater than the existing effective overburden pressure. Therefore, sediments that reside in situ under their maximum overburden pressure should in theory be normally consolidated. This is generally considered to be the case with most marine sediments; that is to say, they have not become overconsolidated by means of any observable mechanism.

There does appear to be a certain confidence in the values of preconsolidation pressure measured in the vicinity of the mudline, which would seem to indicate that a certain amount of overconsolidation does in fact exist. Here lies the fundamental error many researchers seem to make when dealing with AOC; the relative magnitude of the difference between P_c and P_o' tends to be magnified in this zone because of the low stresses involved. In this sense, AOC can be very misleading. Attempts have been made to reduce AOC to a linear function on a semi-logarithmic plot, but have not yielded satisfactory results to date (Silva and Jordan, 1984).

It is proposed that the measured values of OCR are realistic and hence can be used to assist in interpreting the stress history. However this degree of overconsolidation is of secondary importance when compared to the rest of the

soil profile. It remains a significant effect within the upper 6 to 10 meters of sediment where the effective stresses imposed by the weight of the overlying sediment are small.

The occurrence of P_c values somewhat in excess of P_o' within the upper several meters of sediment leads to AOC. That is to say that the sediments are considered to be "apparently overconsolidated". AOC is widespread and would appear to be independent of water depth, since it is found in the ocean basins as well as over the world's continental shelves (Hamilton, 1964; Richards and Hamilton, 1967).

The depth at which the OCR decreases to unity may merely indicate a transition from AOC (or perhaps normal consolidation) to underconsolidation and may not be characteristic (Richards, 1984). Richards states that the transition from overconsolidation to underconsolidation between the 5 and 15 meter depths is real; however he does not rule out the possibility that this may just be an artifact of the consolidation test or the computation of the effective overburden and preconsolidation pressures.

Richards goes on to indicate that there generally exists a depth in the profile where OCR increases to unity. Presumably this would indicate a change in the depositional environment or change in the drainage conditions at that depth, or an insensitivity to secondary compression. A statistical approach may reveal significant trends, especially in the case of thick deposits of deep-sea

sediments where influences such as erosion, dessication, ice scouring, rapid deposition, et cetera can effectively be ruled out.

An OCR of less than unity can be generally interpreted as representing real underconsolidation and therefore is a reliable indicator of the presence of excess pore pressures in situ.

The presence of OCR's greatly in excess of unity near the mudline in a geologically-interpreted normally consolidated sediment clearly violates the accepted definition of overconsolidation. Sediments showing AOC or underconsolidation cannot be termed normally consolidated in the usual sense. It is thereby partly the object of this study to investigate the phenomenon of AOC in detail, and if possible, reduce it to an appropriate level of significance. Such a solution to AOC would then permit the interpretation of actual overconsolidation (or underconsolidation) in the soil profile, and will allow researchers to draw conclusions regarding the contribution of secondary consolidation. Oedometer data could be used as an interpretive agent to define the stress history in this very troublesome shallow zone.

Figure 3.2 is a summary of OCR data plotted versus depth below seabed for two deep-sea sites; the North Atlantic and the North Pacific Ocean (after Carchedi, 1979). Figure 3.3 shows the variation in OCR versus depth over the Beaufort Sea; the data plotted has been derived from

industry vertical oedometer tests. The OCR's are high (greater than 2) in the upper 25 m and decrease to the normally consolidated range at depths below seabed in excess of 50 meters. The upper 10 meters of the profile could be considered to possess AOC.

AOC is known to occur in the upper 4 meters of pelagic sediments within the world's oceans (Richards and Hamilton, 1967; Bryant et al, 1974; Richards, 1976; Silva et al, 1976; Silva, 1979). Figure 3.4 shows a typical OCR profile showing AOC in a deposit of deep-sea sediments, which illustrates the fact that AOC is not limited to the relatively shallow waters overlying continental shelves (after Silva and Jordan, 1984). Thus, AOC is generally believed to be independent of water depth. It may then be concluded that AOC is not produced by ice scouring or cyclic loading, since these processes are not generally found in the deep sea. This is not to say, however, that these processes do not create some overconsolidation in continental shelf sediments; simply that there must exist another primary mechanism for AOC.

3.2.3 Impact of AOC in Foundation Engineering

It is of importance to determine the causes of apparent overconsolidation. Is the phenomenon related to the sampling and testing process? Or is it actually a realistic representation of the state of stress within the soil? It is of interest to evaluate the amount of disturbance inherent

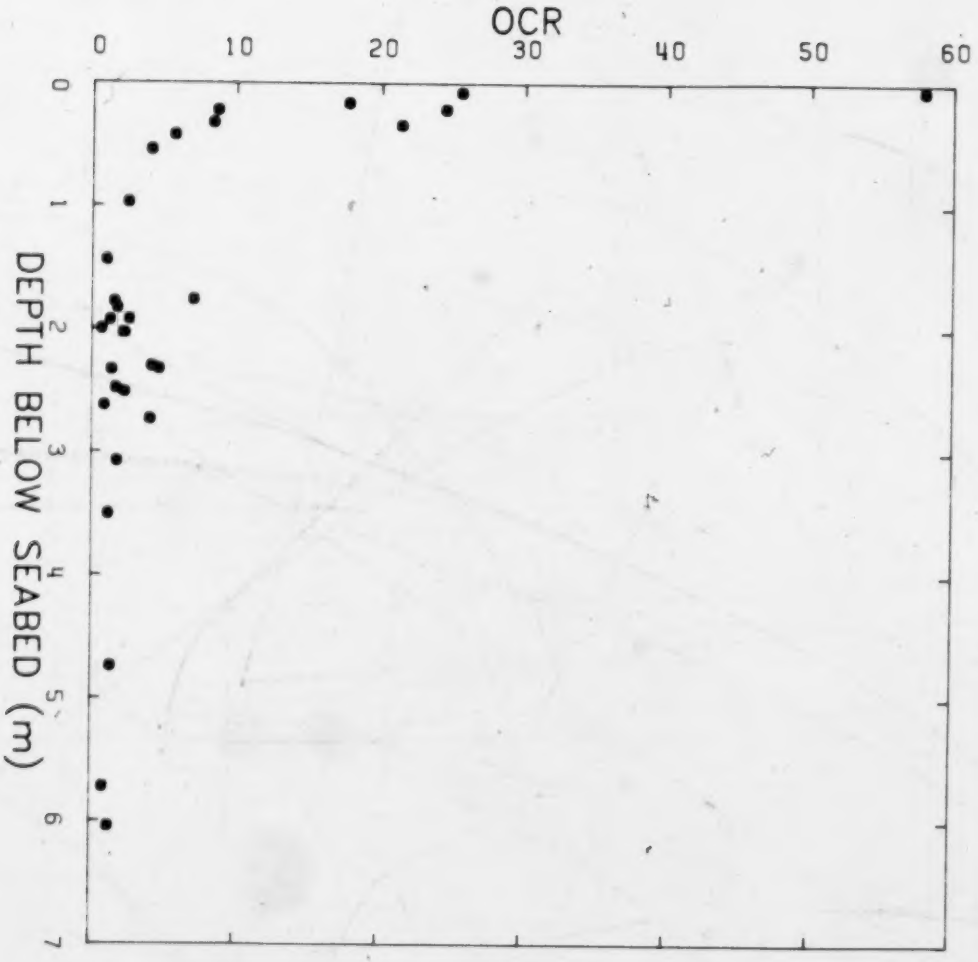

Figure 3.2 OCR versus depth below seabed for two sites in the North Atlantic and the North Pacific Oceans (mod. Carchedi, 1979).

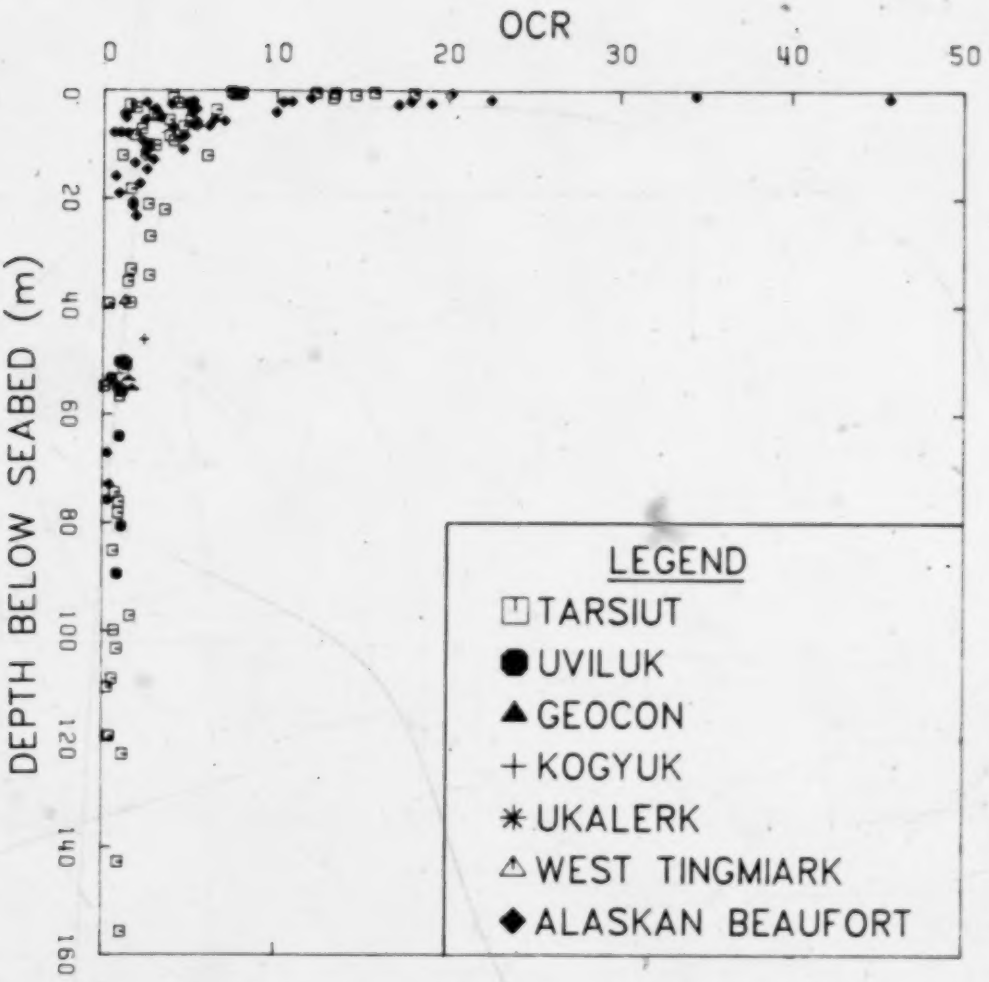

Figure 3.3 Overconsolidation ratio versus depth below seabed for the Alaskan and Canadian Beaufort Sea (mod. Hivon, 1983).

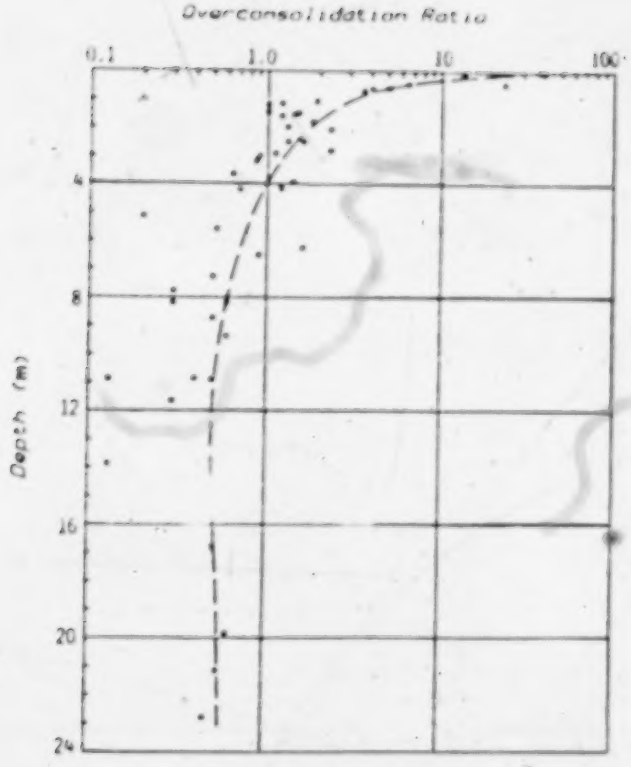

Figure 3.4 Profile of OCR versus depth in Bermuda Rise sediments displaying apparent overconsolidation (OCR > 1) in upper 3 to 4 m and underconsolidation (OCR < 1) below 6 to 8 m (mod. Silva and Jordan, 1984).

in obtaining quality samples for geotechnical testing in order to have some assurance that accurate values of P_c can be obtained.

Some factors can perhaps be ignored as being inconsequential; others may be definable and hence, predictable. It may prove impossible to entirely separate the various influences and come up with a reliable prediction for OCR in certain marine sediments. In those cases a statistical approach may yield a correlation between the amount of AOC and factors such as the sediment type (or the clay mineralogy), the rate of sedimentation, the depositional environment, or other factors.

The significance of AOC is perhaps over-emphasized since the actual yield strengths are still insignificant compared o the stresses induced in the foundation soils by the setdown or construction of an offshore structure. In most cases, standard practice when dealing with these soils is either to avoid them or remove them. The existence of modest amounts of overconsolidation to depths of six to ten meters below the mudline does however have a important effect upon the shear strength selected for design, and may significantly increase the stability of a structure built on these soils.

However, it is noteworthy that sampling methods now exist which can obtain essentially undisturbed samples for geotechnical testing from this very soft zone. Soil disturbance is minimized with the use of a standard piston

corer with a split piston, which was initially developed to handle the difficult sampling problems in the deep sea. This method provides a cost-effective way to obtain samples, and for this soft zone, a most effective tool. Good quality samples ensure accurate estimates of soil compressibility.

3.2.4 Geological Impact of AOC

A soil profile showing overconsolidated strata at depth may indicate periods of subaerial exposure and dessication in their geologic past. If AOC can be explained on the basis of simple influences, it should then prove possible to relate the actual consolidation data to the geologic history of the deposit. This requires a larger and higher quality database than presently exists, particularly on a site specific basis where accurate dates are available to ground truth the stratigraphy as it pertains to the depositional environment.

3.2.5 Estimation of the Preconsolidation Pressure

As defined above, a normally consolidated soil will possess an effective overburden pressure P_o' close or equal to its preconsolidation pressure P_c. The minimum possible value of P_c can be determined graphically by extrapolating the linear portion of the void ratio versus log effective stress back until it intersects a horizontal line drawn at e_o, the in situ void ratio, which is determined from the natural water content and the specific gravity. This

intersection establishes a minimum value for P_c (Schmertmann, 1955).

The upper limit for P_c is easily determined using one or more of the graphical constructions (Casagrande, 1936; Schmertmann, 1955; Burmister, 1951). As a rule, these methods only yield accurate values of P_c when the soil is tested in a relatively undisturbed state. The techniques of Schmertmann and Burmister can cope with slightly more sample disturbance than the Casagrande method, however the interpretation is still largely subjective. As sample disturbance increases, the soil skeleton is gradually disrupted, until little memory of the yield strength remains and the break in the void ratio versus log effective stress curve is very gradual. As the overall change in slope decreases from the reloading to virgin loading portions of the curve, the break at P_c becomes much less pronounced.

According to the present definition, normally consolidated soils will have a value of P_o' somewhere between $P_{c,min}$ and $P_{c,max}$. Another way of checking the state of consolidation involves plotting the undrained shear strength C_u on the x-axis versus the effective overburden pressure on the y-axis. The data should then result in a straight line with a slope between 0.2 and 0.5 for normally consolidated soils (Skempton, 1954), often with a cohesion intercept at the mudline on the order of 10 kpa, referred to as the 'original cohesion' (Jakobson, 1953). Conversely, the relationship is distinctly non-linear in the case of

overconsolidated soils. Where sediment has been disturbed in situ and then allowed to reconsolidate, the undrained shear strength is relatively high but the liquidity index is low (Skempton, 1970).

The use of strain energy (Tavenas et al, 1979; Crooks and Graham, 1976) appears to offer promise in better defining the point where a maximum change in slope occurs on the consolidation curve. The method involves plotting the total strain energy stored in the sample during the consolidation test versus the effective principal stress, both on arithmetic scales. This method relegates data scatter occurring during the low stress increments to a lesser level of significance. The strain energy versus effective stress curve can be approximated by three lines of increasing slope. The first break in slope on the strain energy plot is said to occur at σ_o' , the second at σ_y' ; which then correspond to P_o' and P_c (Crooks and Graham, 1976).

The strain energy is the amount of work done in recompressing the sample. The total strain energy is equal to the area beneath the stress-strain curve and can be computed incrementally by multiplying the average effective stress for each load increment by the vertical strain that occurred over that stress change. Strain energy is calculated as follows:

$$SE = \int \sigma_1' * d\epsilon_1 + \int \sigma_2' * d\epsilon_2 + \int \sigma_3' * d\epsilon_3 \qquad 3.3$$

where the subscripts 1, 2, and 3 refer to the major, minor, and intermediate principal stresses. Since in a consolidation test no straining is permitted in the lateral direction, the following is true:

$$d\epsilon_2 = d\epsilon_3 = 0$$

and 3.3 reduces to:

$$SE = \int \sigma_1' * d\epsilon_1 \qquad 3.4$$

From Figure 3.5, the total strain energy is given by:

$$\Sigma\ SE = \sum_{i=1}^{n} (0.5 * (\sigma'_{i+1} + \sigma'_i) * (\epsilon_{i+1} - \epsilon_i)) \qquad 3.5$$

So over any stress increment from σ_1' to σ_2' the strain energy can be simply stated as:

$$SE = 0.5 * (\sigma_1' + \sigma_2') * (\epsilon_2 - \epsilon_1) \qquad 3.6$$

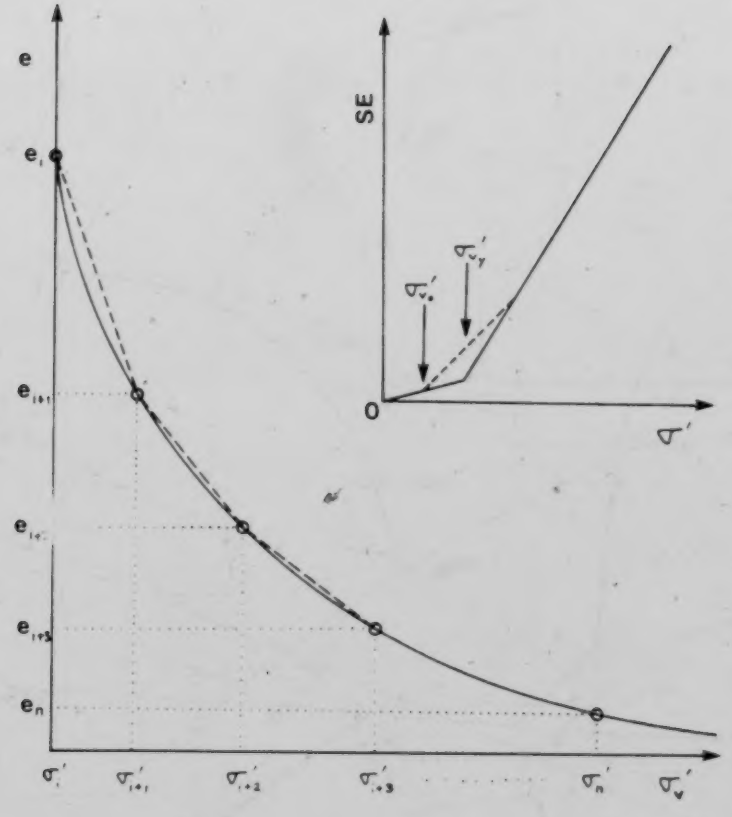

Figure 3.5 Load versus compression curve for strain energy derivation.

3.3 Possible Causes of Overconsolidation in Marine Soils

3.3.1 Compressibility of Soil Particles

The effect of fluid compressibility can be significant in water depths of several thousands of meters but would not be a significant source of error in the calculation of the effective vertical stress within the water depths encountered on the continental shelf.

In great water depths (exceeding 50 m), the effect of particle compressibility can become significant in bringing about a denser soil skeleton and an increased shear strength, as compared to a similar soil at a similar stress state in shallower water. It is of interest to investigate the extent of the increase in overall compressibility if one includes the amount of individual particle compressibility, and also determine the water depth at which it might become significant in increasing the shear strength.

Referring to Figure 3.6, the effective overburden stress P' is usually expressed as a function of the effective unit weight γ' and the depth below seabed, Z.

$$P_o' = \sigma_v - u \qquad 3.7$$

where u denotes the water pressure at depth Z. Equation 3.7

can be rewritten as:

$$P_o' = \gamma' * Z \qquad 3.8$$

But if the soil particles are themselves compressible, 3.7 must be formulated in the form of the following equation (Skempton, 1960):

$$P_o' = \sigma_v - (1 - C_s/C_c) * u \qquad 3.9$$

where C_s and C_c denote the compressibilities of the soil particles and the soil skeleton, respectively. Equation 3.9 can be rewritten as:

$$P_o' = (\gamma_w * H) + (\gamma_s * Z) - (1 - C_s/C_c) * u \qquad 3.10$$

Equation 3.10 reduces to 3.8 if the soil particle compressibility is taken to be insignificant compared to the

overall soil compressibility due to compression of the void spaces.

Carchedi (1979) presents some values of particle compressibility for some typical materials (Table 3.1). In general compressibility does not significantly influence the calculation of P_o' in water depths shallower than 50 meters. (Neglecting the individual particle compressibility in water depths in the order of 50 meters results in an error of approximately 1 kpa on the high side.)

Table 3.1 Comparison of compressibilities for some marine soils (mod. Carchedi, 1979).

MATERIAL	Skempton C_s/C*	C_t/C_c
Vermont Marble	0.08	
Clay (high effective stress)#	0.02	
Calcerous ooze (high eff. stress)#	0.01	
Core G6 (calcerous sandy silt)		0.0038
Core H20 (sandy clayey silt)		0.0022
Dense sand (clayey silt)	0.0015	
Core H6 (clayey silt)		0.00093
Core H4 (clayey silt)		0.00045
Core M3 (highly plastic silty clay)		0.00036
Loose sand		
Overconsolidated clay	0.00025	
Core M7 (highly plastic silty clay)		0.00007
Normally consolidated clay	0.00003	

* Data from Skempton (1961). All values of C_s/C except # represent computations for water at atmospheric conditions.

C_s is the compressibility of the solid particles. (C_t)

C_c is the compressibility of the material.

3.3.2 Sedimentation Rate

Because of the long drainage path imposed on fine-grained sediments existing at depth in the seabed, an interplay is set up between the rate of addition of sediment which results in excess pore pressures in the soil at depth, and the length of time required for excess pore pressures to dissipate. For a sediment deposit rapidly increasing in thickness (e.g. 5 cm/year), there will exist a cutoff depth below the mudline below which excess pore pressures will be unable to dissipate fast enough to keep pace with the growth of the total stress. For a sediment deposit increasing in thickness very slowly (e.g. 0.0005 cm/year), excess pore pressures at depth may be dissipating at the same time as the total stress increases, depending on the total depth of the consolidating yer or layers For this situation, underconsolidation may not exist within the soil profile and the soil would behave in a normally consolidated manner. However, few profiles exist that show no apparent underconsolidation at some depth below seabed, even in areas of very slow deposition. This is true of the Gulf Sauvrak site in the Beaufort Sea. Underconsolidation may be proven to be an erroneous conclusion once peizometric data becomes available from areas like these.

An example of underconsolidation is reported to occur at the North Bermuda Rise (Silva and Jordan, 1984). The sedimentation rate in this area is of the order of 0.3 to 0.4 mm per year. Sedimentation rates in the pelagic 'red

clays' of the North Central Pacific are even lower (0.004 mm per year), yet consolidation tests show the existence of underconsolidation at depth (Silva and Jordan, 1984).

An important control on the time needed for the dissipation of excess pore pressures is the coefficient of permeability, especially when coupled with a larger drainage path. Thus the sedimentation rate controls the depth at which excess pore pressures are found in a given fine-grained sediment.

Portions of the Mississippi Delta show next to no consolidation down to depths below seabed of 50 and 60 meters (McClelland, 1967). This area has the highest known sedimentation rate in the world. Table 3.2 illustrates the variation in sedimentation rate with water depth and deposition environment.

Extremely low rates of deposition have been reported in the deep-sea basins (Rosholt et al, 1961), where all deposition occurs via pelagic settling through the water column. Such sediments are termed 'old' as opposed to 'young' or 'recent'. On average, deltaic environments possess the highest rates of sedimentation, while the lowest rates are found in the ocean abyss far from any terrestrial source of sediment.

Table 3.2 Sedimentation rates for some depositional environments (mod. Skempton, 1970).

Location	Depositional Environment	Deposit Age	Thickness (meters)	Sedimentation Rate (cm/year)	Reference
Mississippi	Deltaic	Holocene	55	12.0	McClelland (1957)
Rhone			65	1.7	Leggett (in litt.)
Orinoco			40	0.8	Kidwell and Hunt (1958)
Mackenzie			105	0.5	Hill et al. (1985)
Avonmouth	Estuarine	Holocene	13	0.25	Skempton (1970)
Tilbury			18	0.20	Skempton (1970)
Pisa			10	0.25	Skempton (1970)
Oslofjord	Sp. Marine	Holocene	--	0.08	Richards (in litt.)
Po valley		Pleistocene	2000	0.12	Skempton (1970)
Po valley		Pliocene	3000	0.10	Skempton (1970)
Kamgara		Pliocene	2600	0.09	Skempton (1970)
Caribbean	Deep Marine	Pleistocene	----	0.003	Reshelt et al. (1980)
N. Bora Rise			200-300	0.0035	Silva and Jordan (1984)
N. Cent. Pac.			15-45	0.0004	Silva and Jordan (1984)

3.3.3 Removal of Overburden

The removal of overburden by erosion or mass sediment wasting results in a decrease in the effective overburden pressure throughout the soil profile. The preconsolidation pressure remains unchanged, creating a state of overconsolidation, with the highest values of OCR near the mudline. This can result in an OCR profile similar in nature to actual profiles exhibiting AOC. However erosion of sediments is not widespread enough to create such a profile on a regular basis and cannot therefore explain the consistent phenomenon of AOC found in all marine areas. Figures 3.6 and 3.7 illustrate how erosion of overburden results in an unloading of the soil deposit, leading to a state of overconsolidation. The amount of AOC created near the mudline resulting solely from a uniform reduction in P_o' throughout the sediment profile is greatest immediately below the soil-water interface. The amount of AOC decreases rapidly with increasing depth below seabed.

Erosion is not generally found in areas of slow deposition rate, and mass wasting processes are normally limited to the continental shelf break and upper slope. In any case, AOC brought about by sediment removal is difficult to distinguish from other ongoing factors affecting OCR.

A simple calculation exists for determining the height of overburden that has been eroded away, given some basic soil parameters, and a suspicion that a certain amount of erosion has occurred. Figure 3.6 (a) shows the case of a

homogeneous sediment deposit that has been partly eroded. The present in situ void ratio is calculated from the natural water content and the specific gravity of the soil solids of an element located at depth Z below the mudline. The problem requires an estimate of the void ratio that existed at the same location prior to erosion. This initial void ratio can be obtained from the void ratio versus log effective stress curve as shown on Figure 3.6 (b). Implied in this procedure is the assumption that the preconsolidation pressure has been created solely from the unloading caused by sediment removal. This does not include other mechanisms of overconsolidation, and so application of this method in the case of a soil that has become overconsolidated by other means will produce an extra amount of overburden removal, which may be misleading. But for a deposit that has experienced sediment removal, Skempton (1970) gives an equation for the height of overburden removed (ΔZ) with all terms defined in Figure 3.6:

$$\Delta Z = \frac{Z * e_i - Z_i * e_o}{(1 + e_o)} \qquad 3.11$$

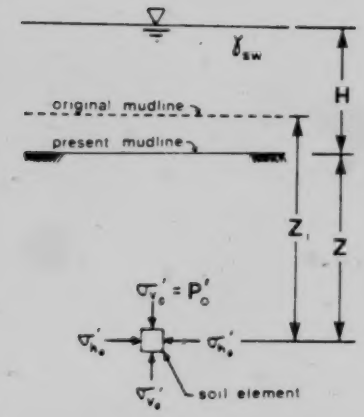

Before Erosion	At present time
e_1	$e_o > e_1$
Z_1	$Z < Z_1$
w_{n1}	$w_n > w_{n1}$
$P_o' = P_c$	$P_o < P_c$

(a)

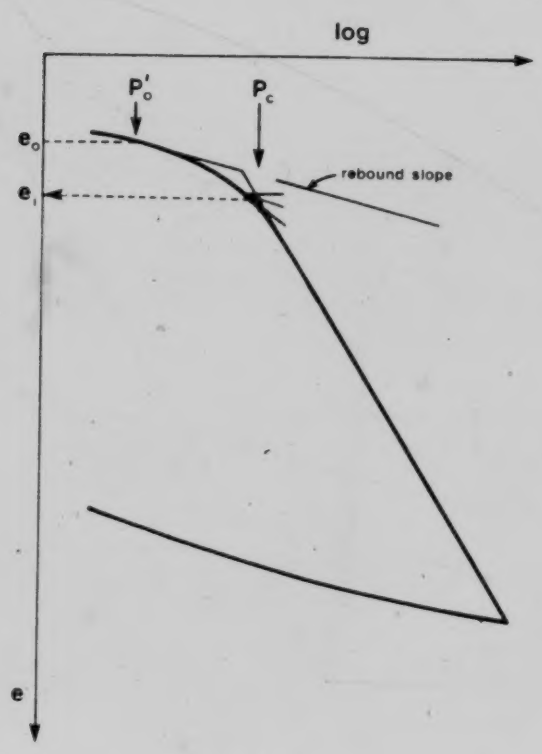

(b)

Figure 3.6 (a) Effective overburden stresses within a marine sediment; (b) Effect of erosion on the effective overburden pressure.

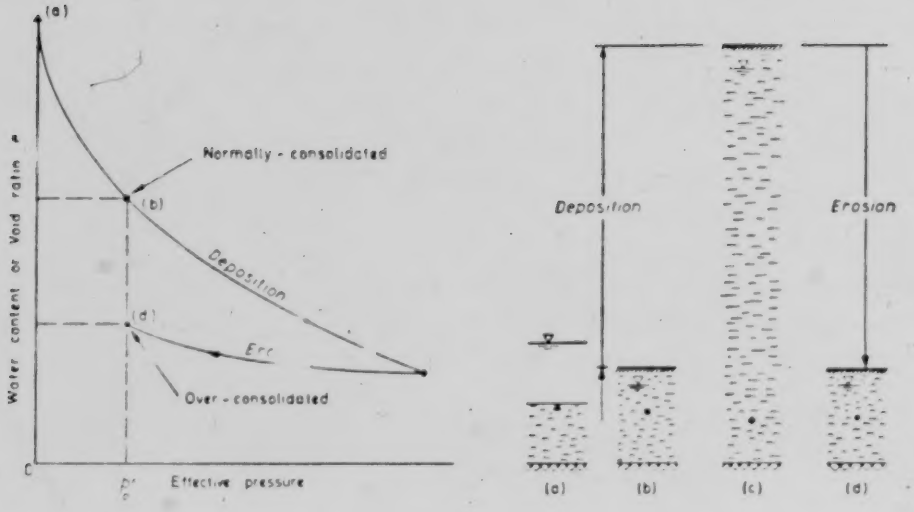

Figure 3.7 Overconsolidation caused by removal of overburden (mod. Skempton, 1970).

3.3.4 Erroneous Location of the Mudline

A significant error in the computation of P_o' can be introduced by underestimating the depth below seabed of a particular soil sample, caused by incorrectly taking the upper level of sediment in the sample tube as the actual location of the soil-water interface.

The real location of the mudline probably existed somewhat above this observed level in the sample tube. Disturbance and settling of this very sensitive ooze during coring could have resulted in a decreased height of soil in the tube. The mudline is defined as the level in the sediment column at which shear stresses begin to be transmitted across particle contacts and the sediment starts to form a metastable, flocculated structure (Silva and Jordan, 1984).

A zone of hindered settling occurs immediately above the mudline, within which no shear stresses are continuously transferred to adjacent soil particles. This zone actually exists in situ as a viscous fluid and soil particles are present in such abundance that Stokesian settling is hindered as the soil particles periodically come into contact with each other.

Figure 3.8 presents an idealized soil profile for a homogeneous marine sediment exhibiting unusually high values of OCR along with a finite preconsolidation pressure at the observed location of the mudline. This boundary presents a problem in the calculation of OCR since by definition, Z is

equal to zero at that level and OCR tends to infinity as a result.

The real location of the mudline can be determined by extrapolating the profile of preconsolidation pressure back until P_c is equal to zero, then using the slope of that line to calculate an equivalent height of missing overburden (Z_{oa}). It should be noted that for sediments that are not normally consolidated for one reason or another, then the preceding technique will give misleading values for Z_{oa}.

For a normally consolidated sediment, OCR approaches unity at point (b) in Figure 3.8 (a), at which depth the difference in P and P' becomes insignificant compared to P_o'. Thus P_o' is essentially equal to P_c at point (b). Given unit weight and preconsolidation data extrapolated to the observable mudline at point (o), it is a simple matter to calculate the equivalent height of overburden that has settled in the sample tube:

$$Z_{oa} = P_{co} / \gamma_o' \qquad 3.12$$

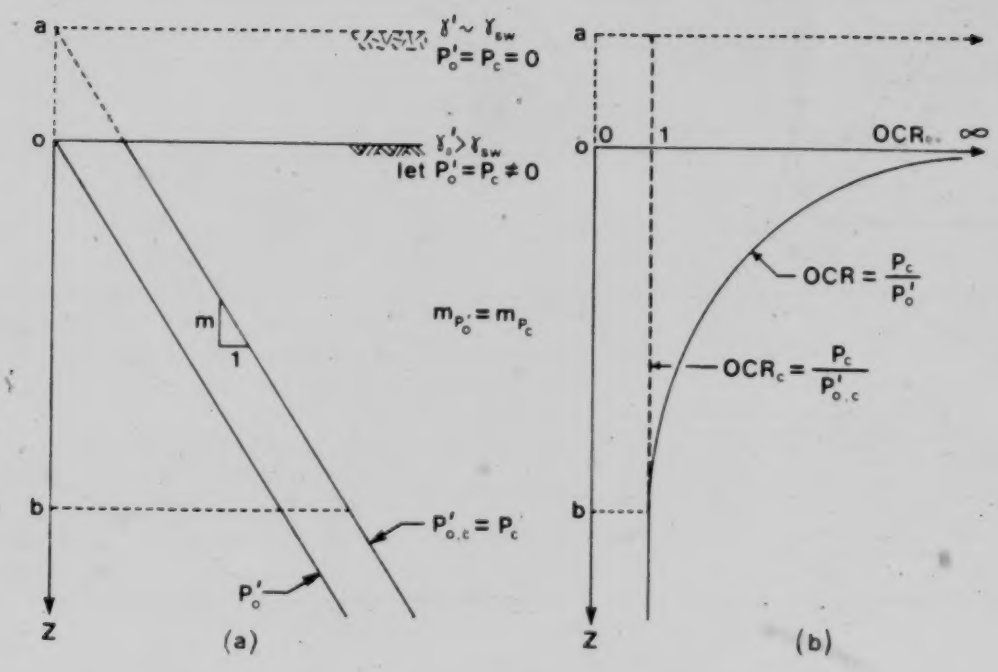

Figure 3.8 Effective overburden and preconsolidation pressure profiles for the AOC zone.

Data from a piston core 2 meters in length taken in 50 meters of water in the Kugmallit Channel (PC-09) yields the following information at point (o):

$\gamma_{.o}$ = 14 kN/m

γ_o' = 3.91 kN/m

$P_{c\,o}$ = 10.5 kN/m

Using this data, the error in the mudline proves to be 2.68 m. This is clearly inconsistent with the amount of settlement one might expect inside a sampling tube as a result of disturbance. This site is unlikely to have experienced erosion at this depth (Hill, pers. comm., 1984). Studies conducted in the North Central Pacific with a remote camera attached to a corehead have shown that in fact, the piston corer retains a level of sediment in the tube closely corresponding to the observed level of the mudline (Moran, 1982).

Therefore it can be concluded that back calculated estimates of the mudline cannot fully account for AOC in cases where the strength of the sediment has been modified by overconsolidation processes. A finite P_c intercept at the mudline invariably leads to unusually high values of OCR;

then as the depth below seabed increases, the OCR decreases as a result of the difference in P_c becoming insignificant compared to P_o'. A new procedure is proposed to avoid the problem incurred by the singularity at the mudline where OCR is undefined.

The depth below seabed where OCR is reduced to unity is denoted in Figure 3.8 (b) as point (b). If an effective unit weight is available at point (b), it is possible to determine a 'corrected' value of OCR. Then at point (b):

$$P_o' = P_c = \gamma_b' * Z \qquad 3.13$$

At depth Z_{ob} the preconsolidation pressure can be expressed in the form:

$$P_c = P_{co} + m * Z_{ob} \qquad 3.14$$

Where:

$$m = \Delta Z / \Delta P_c \qquad 3.15$$

Equating 3.14 and 3.15 results in an expression for the corrected depth Z_{ab} to be used in the calculation of P_o', which can then be used to calculate a value of OCR that is free of the boundary effect at the mudline and is also free of the amount of overconsolidation caused by ageing.

$$Z_{ab} = \frac{P_{c.o} + m * Z_{ob}}{\gamma_b'} \qquad 3.16$$

Equation 3.1 can now be rewritten to yield a back calculated value of OCR:

$$OCR = \frac{P_c}{\gamma_z' * Z_{az}} \qquad 3.17$$

Use of equation 3.16, that is, with the mudline shifted up to point (a) on Figure 3.8 (a), results in an OCR of unity for any profile where the difference in P_c and P_o' is constant with increasing depth. This is shown in Figure 3.9 (b). When the slope of the P_c profile is different than the P_o' profile, application of equation 3.16 to the calculation of P_o' will result in either case (a) or case (c) in Figure 3.9.

The effects of ageing (Bjerrum, 1967) can create a profile where P_c is slightly greater than P_o'. The effect of ageing will be discussed in more detail in section 3.3.11, however it is mentioned here as a possible mechanism for creating a P_c profile that is shifted to the right of the P_o' profile as derived from unit weight data (Bjerrum, 1967). Clearly, the various mechanisms for overconsolidation must be weighed against each other to determine which mechanism dominates in creating overconsolidation for a particular location.

Figure 3.8 illustrates the case where a sediment profile is normally consolidated, yet the preconsolidation pressure plots slightly to the right of the effective overburden pressure. This difference in P_c and P_o' may be a result of ageing. The older a particular soil horizon is, the longer it will have been subjected to secondary compression, and its yield strength will be somewhat higher than that of a younger soil at a similar stress level. It was this increase in shear strength that prompted the author

to investigate whether a shift in the effective overburden pressure profile would be useful in linearizing AOC.

A correction can be applied to the effective overburden pressure in order to remove AOC. The procedure involves shifting the profile of P_o' so that it intersects the P_c line at point (a), where P_c is defined to be equal to zero. This then is the location of the equivalent mudline; the corrected OCR is found to be equal to unity for any depth. The procedure may be useful in denoting levels in the profile where overconsolidation exists, after the correction. However, it does not yield any new information about AOC other than the fact that it is primarily a boundary effect.

Figure 3.9 shows the results of applying this adjustment to the three possible profiles of P_o' and P_c that one may expect to encounter in the field. Note that case (b) has already been discussed. Case (a) may arise either as a result of sampling disturbance or where excess pore pressures occurring in situ have been neglected in the calculation of P_o'. It is unlikely that case (c) will be encountered in situ, but may exist in soil deposits possessing preconsolidation pressures well above P_o', for one reason or another. Sampling disturbance might also lead to an underestimation of P_c here.

Both the uncorrected and the corrected OCR are shown for all three cases. The shaded regions in Figure 3.9 (iii) delineate the possible envelopes of OCR corrected to exclude

the cohesion intercept at the mudline.

A curve-fitting equation can be derived empirically for each of the three cases, given profiles of P_o' and P_c. The profile of (uncorrected) OCR is given by the equations shown on Figure 3.9 (a.ii), (b.ii), and (c.ii).

Figure 3.10 illustrates how the parameter 'a' can be used instead of the corrected OCR to represent the three cases (a), (b), and (c); where the a-parameter is given by:

$$a = (P_c - P_o')/P_o' \qquad 3.18$$

The a-parameter is useful in defining the relative size of the ageing effect. If 'a' is negative (ranging from -1 to 0), then the profile corresponds to case (a). If 'a' is positive (ranging from 0 to infinity), then the profile corresponds to case (c). Case (b) will produce an 'a' equal to zero for any depth. The shaded envelopes illustrate the possible variations in the a-parameter. The a-parameter denotes the amount of increase in P_c over P_o', which is herein attributed to the effects of ageing; all other possible mechanisms of overconsolidation having been discounted. This clearly is only valid on a site specific basis where the geologic history is reasonably well understood.

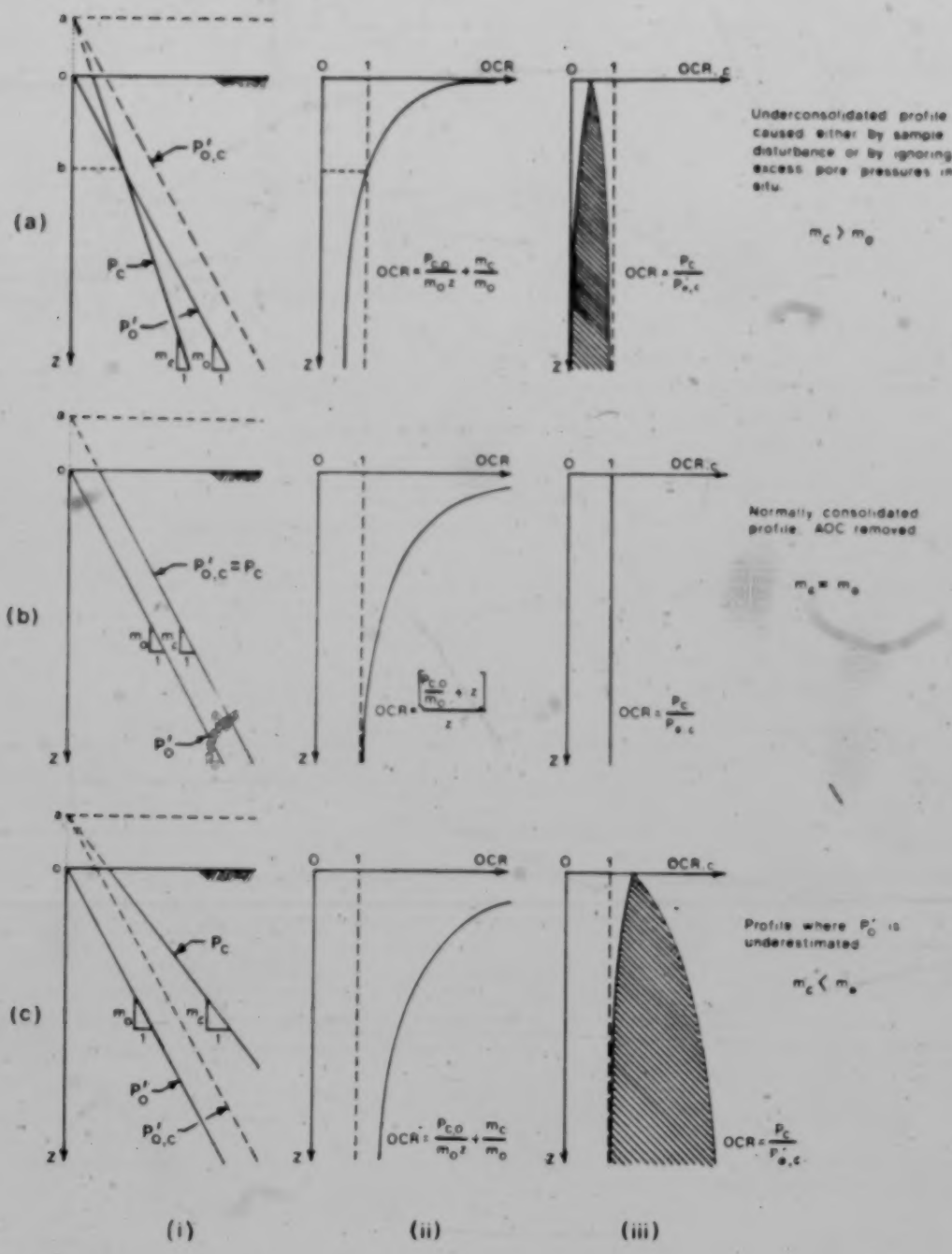

Figure 3.9 Possible profiles showing OCR before and after application of the correction to redefine the location of the mudline.

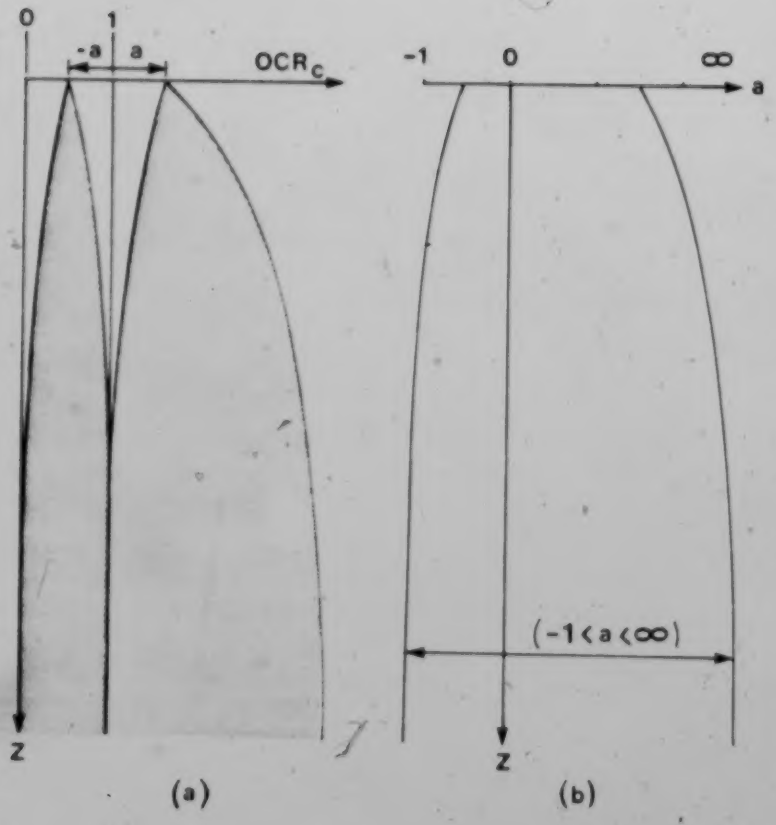

Figure 3.10 Variation of the a-parameter for the cases shown in Figure 3.9.

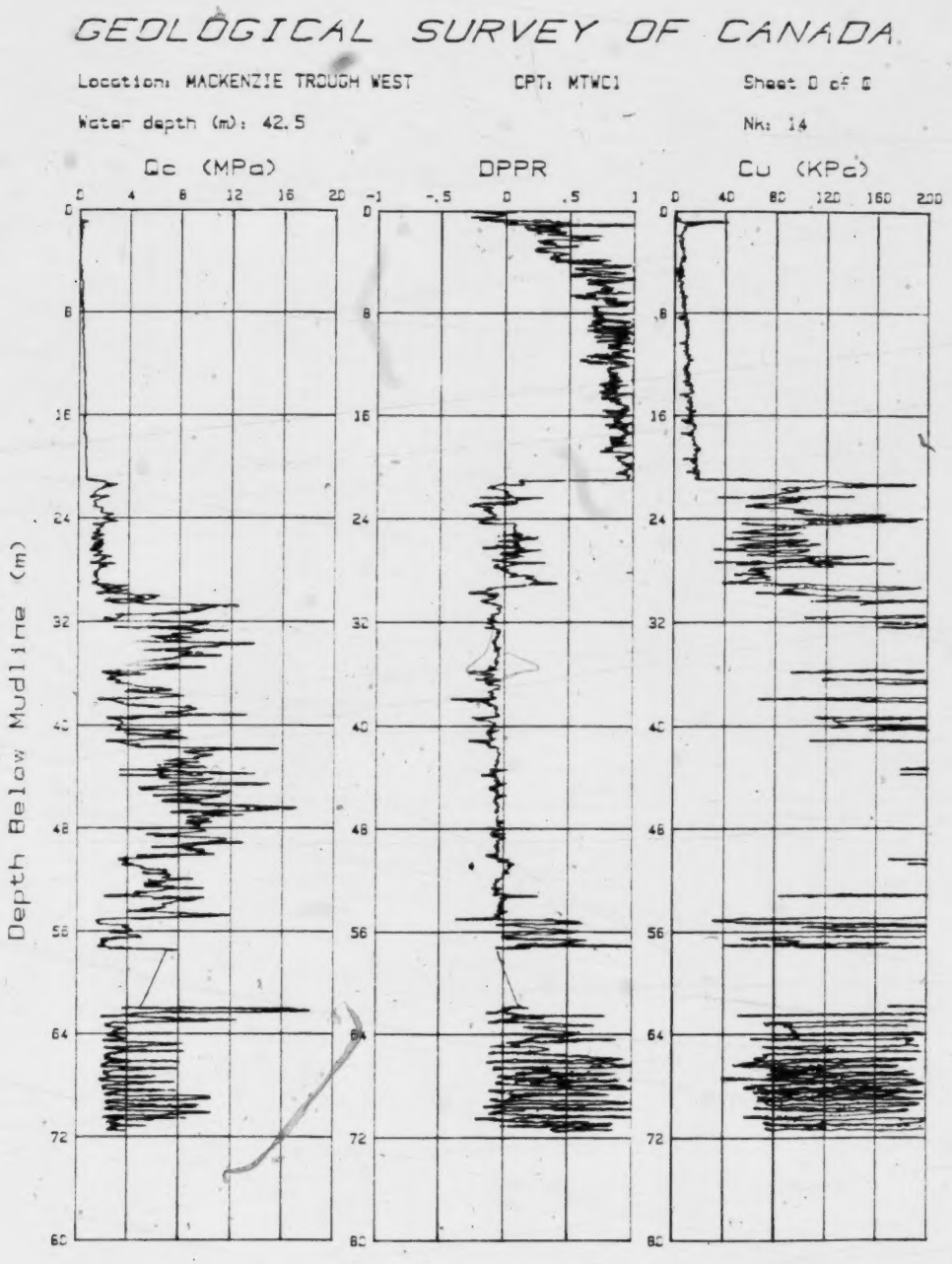

Figure 4.26 Peizometric Cone Penetrometer trace for MTWC02.

grade down into coarse sands and silts at 30 m and become very dense and highly dilatant. The dilatancy was observed on board ship and is evident from the negative dynamic pore pressure ratios in Figures 4.24 to 4.26. This horizon marks the top of the pro-deltaic unit (C). Seismic records show consistent dipping prograding reflectors below the major unconformity, which is typical of the pro-delta sequence (Hill, pers. comm., 1985). No more foraminifera were found below 30 m, which is somewhat surprising because there would appearto be another sequence of marine sediments at the bottom of the borehole (tentatively classified as belonging to unit B in Figure 4.23).

The pore pressure response measured by the piezocone is not consistent with the stiffness and high strengths noted at depth in unit C. This may be due to disturbance around the cone tip, but is more likely attributable to the highly dilatant behaviour of the silts when sheared.

The lobal form of deposition which characterizes pro-deltaic deposits explains the intermittent sequences of silts and clays in unit C. Associated with the changes in lithology are substantial variations in the undrained shear strength, with high strengths measured in the less saline, coarser deltaic silts; and low strengths within the more plastic fine-grained marine interbeds.

The results of the oedometer test conducted at 6.16 meters bsb. are given in Table 4.12. The test revealed that the sample was slightly overconsolidated, which again can be

extrapolated to fit the general trend of overconsolidation ratios increasing toward the mudline.

The void ratio versus log effective stress curve is shown in Figure 4.27. The sample quality is observed to be high since the break in the curve is quite pronounced. This represents the shallowest sample that was recovered in an undisturbed state. The material above the 6 meter depth was too soft to work with as it may have been partially remoulded by sampling.

Figure 4.28 shows the strain energy curve for the sample from the 6.16 meter depth.

The agreement was excellent between the methods of strain energy and the more conventional Casagrande construction. Table 4.13 compares the P_o' and the P_c determined by both methods. The compressibilities were high for this sample, being very comparable to those observed in PC-09, which would suggest that if one measures a low compression index within the upper several meters of recent marine sediment in the Beaufort Sea, then the sample is likely disturbed.

The profile of C_u/P_o' versus P_o' is shown in Figure 4.29. The trend of overconsolidation within the upper zone of sediments is less pronounced in BH MTWS1 than at other sites, suggesting that the age of the sediment may play a key role in the strength-gain process. This is supported by estimates of the rate of sedimentation in this area, which is an order of magnitude higher than the area sampled in the

Table 4.12 Oedometer results for MTWS1.

PARAMETER		MTWS1
WATER DEPTH	H (m)	42
DEPTH BELOW SEABED	Z (m)	6.16
VOID RATIO	e_o	1.835
WATER CONTENT	w_N (%)	65.8
LIQUID LIMIT	w_L (%)	65.2
PLASTIC LIMIT	w_P (%)	27.7
PLASTICITY INDEX	PI (%)	37.5
LIQUIDITY INDEX	LI (%)	1.02
UNIT WEIGHT	γ_s (kN/m^3)	16.04
SPECIFIC GRAVITY	G_s	2.79
SAND FRACTION	%	6
SILT FRACTION	%	7
CLAY FRACTION	%	87
EFF. OVERBURDEN PRESSURE	P_o' (kpa)	36.6
PRECONSOLIDATION PRESSURE	P_c (kpa)	49.0
OVERCONSOLIDATION RATIO	OCR	1.34

Table 4.13 Comparison of techniques of determining stress history for MTWS1.

DEPTH BSB. (m)	PARAMETER	BY CASGRANDE	BY STRAIN ENERGY	$\frac{P_{SE}}{P_{Cas}}$
6.16	P_o'	36.6	31	0.85
	P_c	49.0	42	0.86
	OCR	1.34	1.35	1.01

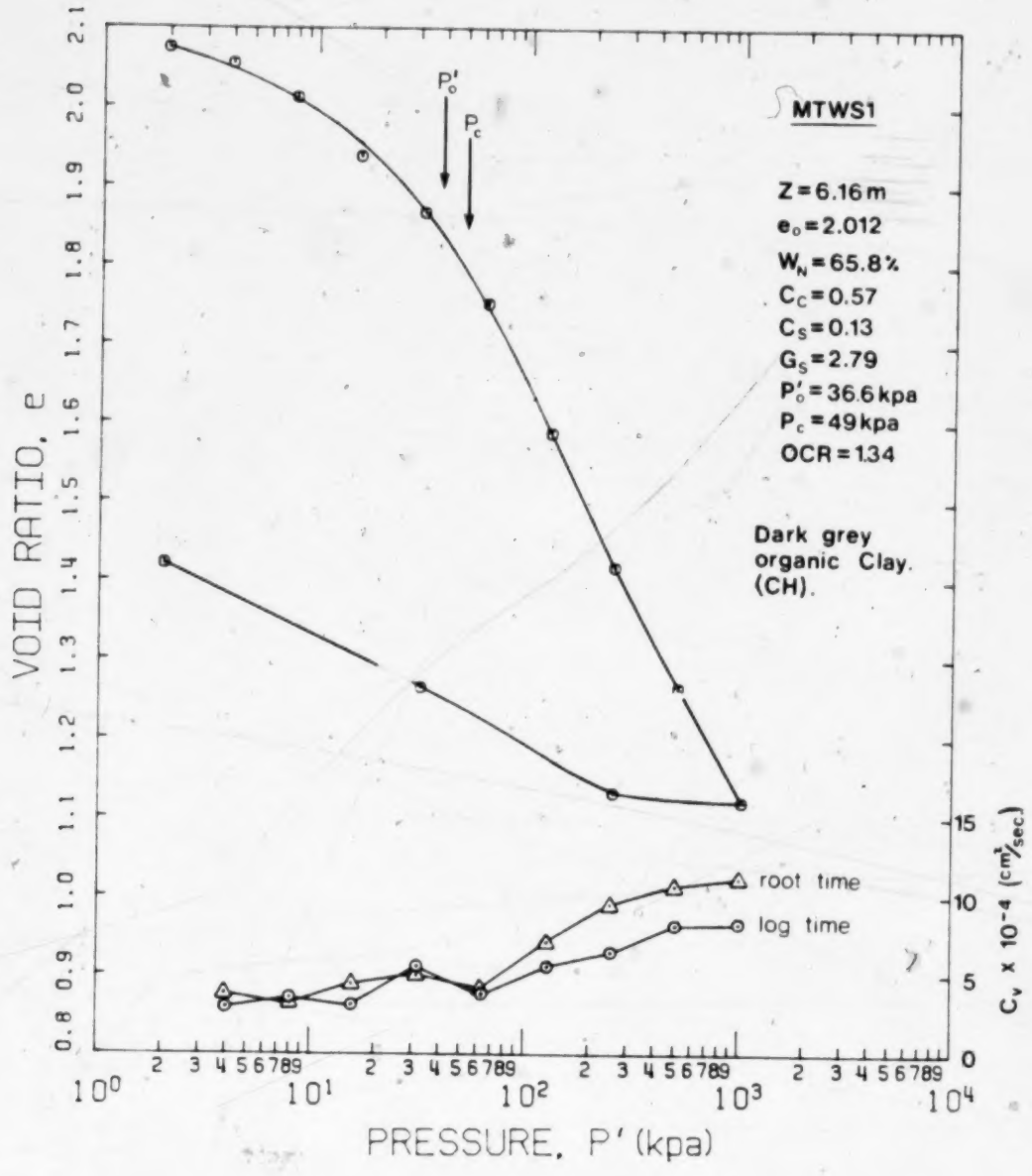

Figure 4.27 Consolidation curve for MTWS1 at 6.16 m bsb.

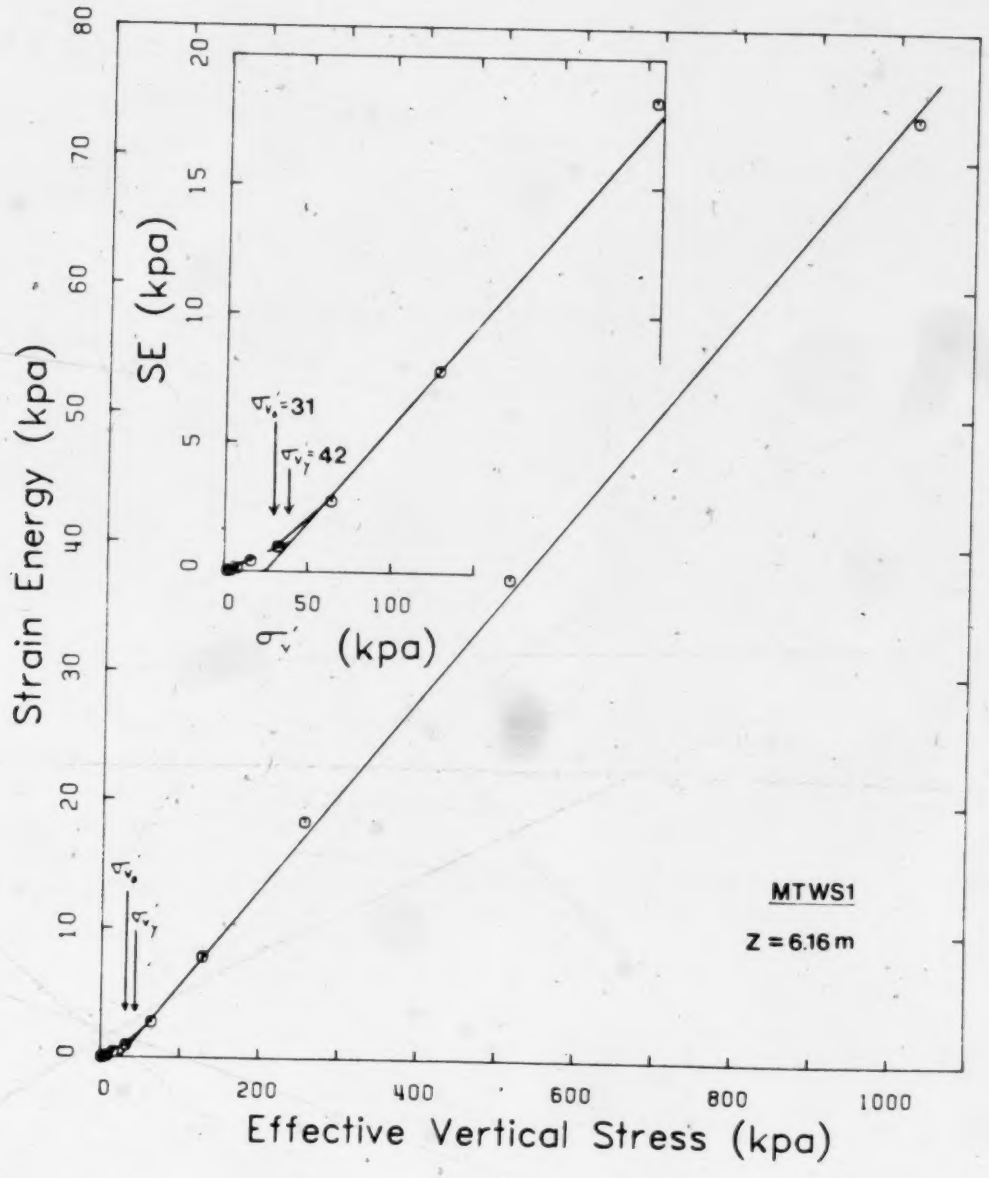

Figure 4.28 Strain energy versus effective stress for MTWS1; 6.16 m bsb.

Kugmallit Channel and also the site designated as BH 20+00. If one assumes the rate of accumulation of sediment within the upper 22 m of BH MTWS1 to have been uniform, one calculates a sedimentation rate on the order of 1.4 cm/year assuming that the age of 16,000 years is correct. The rate of sedimentation for the BH 20+00 area is about 3 to 3.3 mm/year. The rate of sedimentation for the surficial marine sediments over the Sauvrak/Tarsiut area is about 5 mm/year. Figure 4.29 shows the upper (minor) unconformity for MTWS1, occurring as stated at 22 m bsb. Shear strength data was not available at the level of the major unconformity at 30 m bsb., due to the non-plastic nature of the soil.

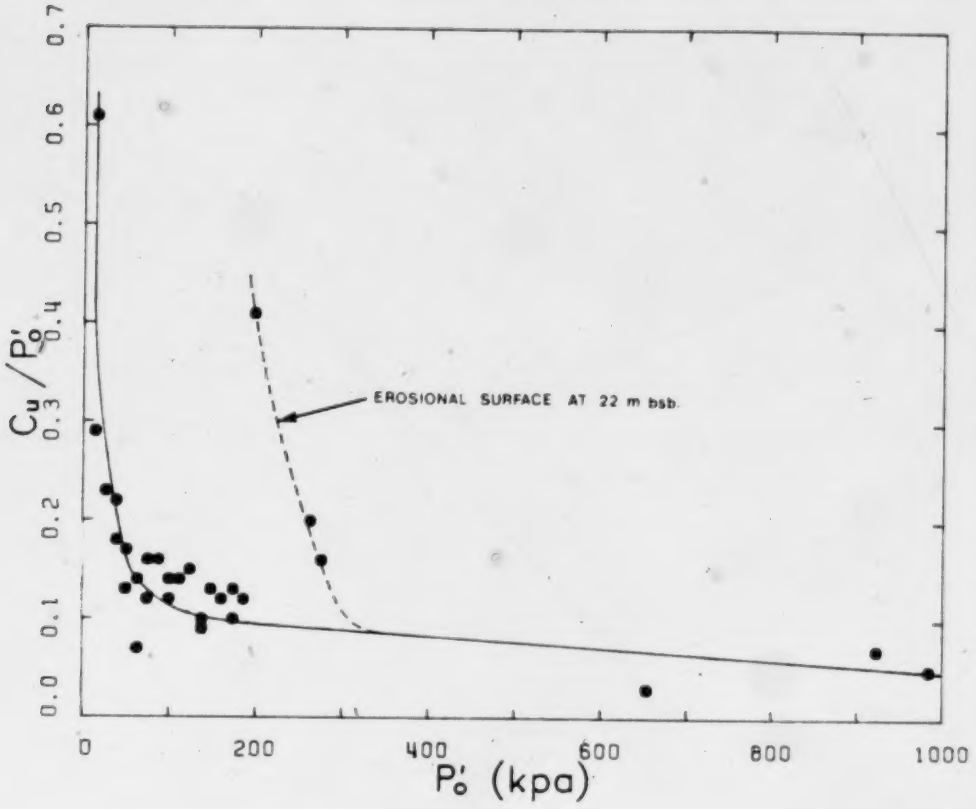

Figure 4.29 Normalized undrained shear strength for MTWS1.

4.7 Rates of Secondary Compression

Mesri (1973) gives a relation for the coefficient of secondary compression as follows:

$$C_\alpha = \frac{\Delta H_t / H_t}{(\log t_2 - \log t_1)} \qquad 4.1$$

Mesri (1973) classified soil type according to coefficient of secondary compresion as shown in Table 4.14. The surficial silty clays had the highest rates of C_α, averaging about 0.01. This puts them in the medium range of secondary compressibility. Figure 4.30 shows all of the C_α/C_c data collected for the six consolidation samples tested by the author for all sample sites plotted versus the logarithm of effective vertical stress. The values of C_α/C_c varied from 0.002 to about 0.02. Mesri and Godlewski (1977) suggest ratios of C_α/C_c of 0.025 to 0.06 for inorganic soils, and values between 0.04 and 0.10 for organic soil. It is the author's contention that the high compression indices measured in this study are not reflected in Mesri and Godlewski's data base. Therefore, comparison to their values of C_α/C_c is of little value.

Figure 4.31 shows the data for C_α plotted versus the log of the natural water content. The data follows the trend

Table 4.14 Classification of soil based on secondary compressibility (mod. Mesri, 1973).

C_α	SECONDARY COMPRESSIBILITY
< 0.002	Very Low
0.004	Low
0.008	Medium
0.016	High
0.032	Very High
0.064	Extremely High

of Mesri's reported data, and the surficial silty clays plot in the same region as for organic silty clay. The silt samples plotted in the same area as for Boston Blue Clay. In other words, the rates of secondary compression were in the medium range as compared to Mesri's C_α data (1973). All of the data for compression index are plotted versus the in situ void ratio for the samples tested as well as the data provided by Gulf (Figure 4.32). It was found that a least squares correlation can be deduced for C_c and e_o as follows, based on data collected from consolidation tests performed in this study (excludes Sauvrak):

$$C_c = 0.38 * (e_o - 0.35) \qquad 4.2$$

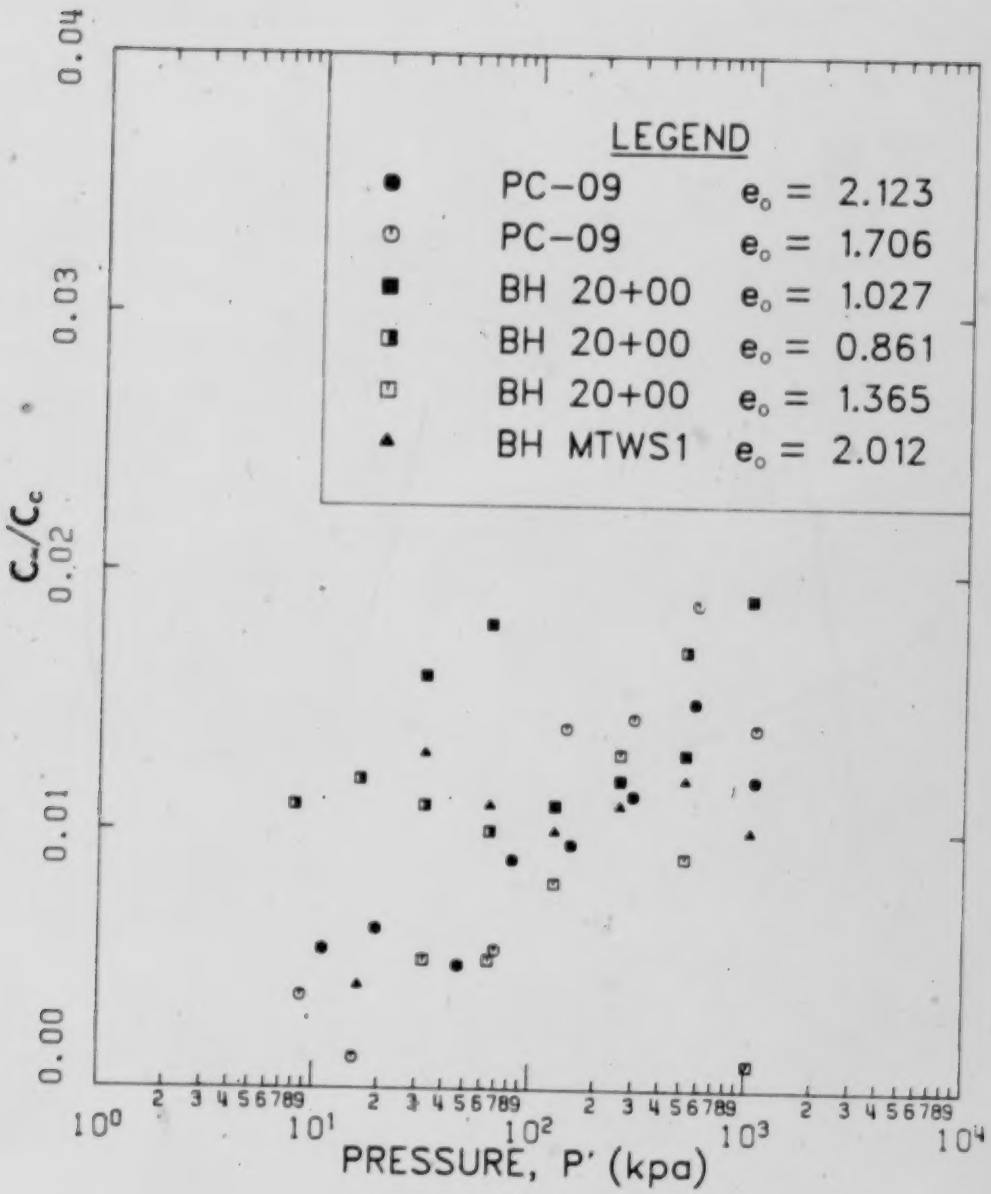

Figure 4.30 Normalized coefficient of secondary compression versus effective stress for all consolidation samples.

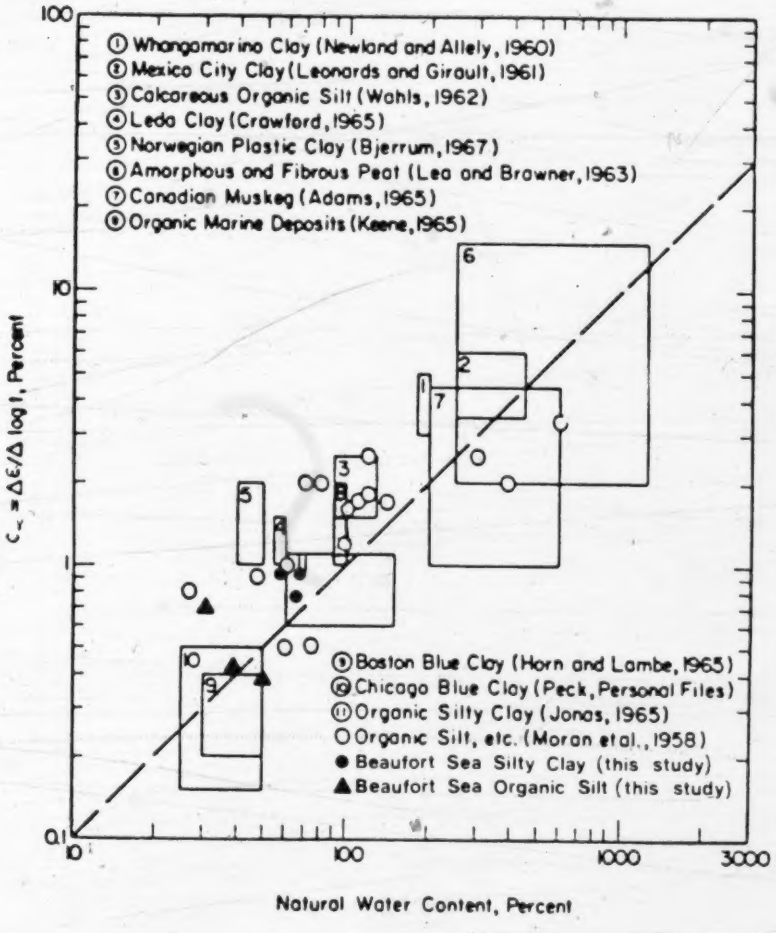
① Whangamarino Clay (Newland and Allely, 1960)
② Mexico City Clay (Leonards and Girault, 1961)
③ Calcareous Organic Silt (Wahls, 1962)
④ Leda Clay (Crawford, 1965)
⑤ Norwegian Plastic Clay (Bjerrum, 1967)
⑥ Amorphous and Fibrous Peat (Lea and Browner, 1963)
⑦ Canadian Muskeg (Adams, 1965)
⑧ Organic Marine Deposits (Keene, 1965)
⑨ Boston Blue Clay (Horn and Lambe, 1965)
⑩ Chicago Blue Clay (Peck, Personal Files)
⑪ Organic Silty Clay (Jonas, 1965)
○ Organic Silt, etc. (Moran et al., 1958)
● Beaufort Sea Silty Clay (this study)
▲ Beaufort Sea Organic Silt (this study)
100
10
1
0.1
10
100
1000
3000
Natural Water Content, Percent

Figure 4.31 Coefficient of secondary compression for natural soil deposits (mod. Mesri, 1973).

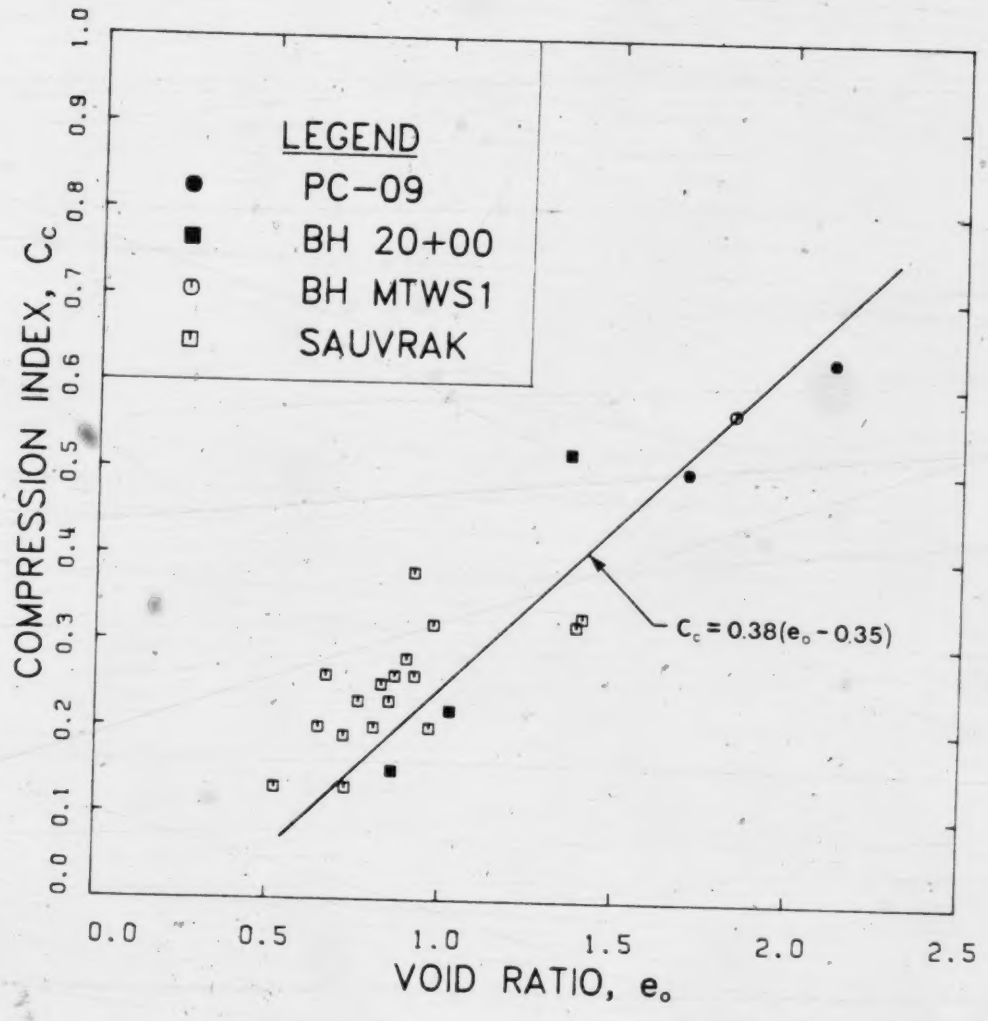

Figure 4.32 Compression index for Beaufort Sea soils.

4.8 Prediction of OCR from the Critical State Line

The Wroth (1979) method of obtaining stress history data from only a few simple index properties was presented in Chapter 2. This section reports the results of the application of those methods to two sites; BH 20+00 and Gulf Sauvrak. The results were truly remarkable; the technique would appear to have captured the essential ingredients of the stress history, namely, the soil plasticity and water content, the slope of the reloading consolidation curve, and makes use of the present effective overburden stress in calculating values of OCR that agree phenomenally well with the test data from two independent studies.

Table 4.15 summarizes the predicted versus the measured values of P_c and OCR for BH 20+00. Table 4.16 makes the same comparison for data collected and made available by Dr. Michael Jefferies of Gulf Canada. Figure 4.33 illustates the same comparison in a graphical form for BH 20+00. Note that the predicted values band the measured values very well, and there is one predicted value for an OCR of 16 at the 1.48 meter depth bsb. This is indeed remarkable, since it validates in principle that the phenomenon of apparent overconsolidation is in fact, real, and also that it is predictable. Furthermore, AOC is concluded to arise from the ill-conditioned nature of the equation of OCR at very shallow burial depths.

The technique has captured the effects of soil disturbance, as can be seen in Figure 4.34; where there

would appear to be two disturbed samples from the 1.18 and 1.90 meter depths bsb. The disturbance has manifested itself in the form of a reduced water content, which the technique of Wroth is very sensitive to. This disturbance is to be expected at this depth, when sampling with open-drive shelby tubes, and is unavoidable in these very soft sediments.

Table 4.15 Summary of predicted versus observed OCR for BH 20+00.

Z (m)	1.48	3.20	4.60	4.68	4.80	6.00	10.78	11.01	13.71
w_N (%)	36.7	32.2	29.7	30.0	30.0	43.6	31.2	27.0	49.1
w_P (%)	28.2	25.6	21.5	22.7	20.8	31.8	25.8	23.1	30.0
w_L (%)	51.7	40.1	39.8	38.5	38.0	51.0	37.9	36.3	54.1
PI (%)	23.5	14.5	18.3	15.8	17.2	19.2	12.1	13.2	24.1
LI (%)	36.2	45.5	44.8	46.2	53.5	61.4	45.0	29.8	37.8
G_s	2.74	2.74	2.74	2.74	2.73	2.73	2.75	2.75	2.72
γ_s (kn/m^3)	16.78	18.08	19.22	19.02	19.31	16.64	19.40	19.65	17.09
P'_o (kpa)	9.9	25.6	42.0	42.5	44.2	39.3	100.4	105.2	96.0
κ	.0335	.0139	.0574	.0168	.0198	.0242	.0087	.0111	.0348
$P_{c\cdot WROTH}$ (kpa)	158.8	84.2	96.9	78.7	54.6	37.1	78.3	164.1	112.4
OCR	16.04	3.29	2.31	1.8	1.23	0.94	0.78	1.56	1.17

Measured Values:

Z (m)	4.85	10.95	13.74
P'_o (kpa)	46.1	104.7	99.3
$P_{c\cdot MEAS}$ (kpa)	90.0	123.0	108.0
OCR	1.94	1.17	1.09

Table 4.16 Summary of predicted versus observed OCR for Sauvrak.

BOREHOLE NO.	82S14 1B	82S13 1B	82S03 5B	82S13	82S03 9B	1-B
Z (m)	1.18	1.90	3.80	4.04	7.60	11.00
w_N (%)	51.2	48.2	35.3	36.3	29.6	28.0
w_L (%)	57	59	56	56	47	43
w_P (%)	35	30	26	26	25	25
PI (%)	22	29	30	30	22	18
LI (%)	0.74	0.63	0.31	0.34	0.21	0.17
G_s	2.72	2.72	2.74	2.68	2.69	2.70
γ_s (KN/m^3)	17.07	17.36	18.64	18.44	19.32	18.81
P'_o (kpa)	8.2	13.9	32.5	34.0	72.3	99.0
	0.0303	0.0455	0.0477	0.0477	0.0303	0.0216
$P_{c\ mech}$ (kpa)	23.6	39.4	184.9	155.5	276.0	324.5
OCR	2.89	2.83	5.69	4.57	3.82	3.28

MEASURED VALUES:

P'_o (kpa)	8.2	13.9	32.5	34.0	72.3	99.0
$P_{c\ Meas}$ (kpa)	28.5	37.0	173.0	233.0	290.0	340.0
OCR	3.47	2.66	5.32	6.85	4.01	3.43

BOREHOLE NO.	82S13 7B	82S13 12B	82S13 13B	82S13	82S13 11B
Z (m)	14.10	23.23	24.67	33.70	21.70
w_N (%)	29	30	25	30	23
w_L (%)	42	47	34	50	40
w_P (%)	20	24	18	26	21
PI (%)	22	23	16	24	22
LI (%)	0.27	0.30	0.44	0.17	0.14
G_s	2.73	2.70	2.70	2.72	2.70
γ_s (KN/m^3)	18.64	18.83	19.82	19.52	19.62
P'_o (kpa)	121.4	203.0	240.0	318.0	194.0
	0.0303	0.0324	0.0172	0.0346	0.0303
$P_{c\ mech}$ (kpa)	187.2	150.6	76.9	289.1	358.6
OCR	1.54	0.74	0.32	0.91	1.85

MEASURED VALUES:

P'_o (kpa)	187.2	203.0	240.0	318.0	194.0
$P_{c\ Meas}$ (kpa)	257.0	175.0	110.0	280.0	340.0
OCR	2.12	0.86	0.46	0.88	1.75

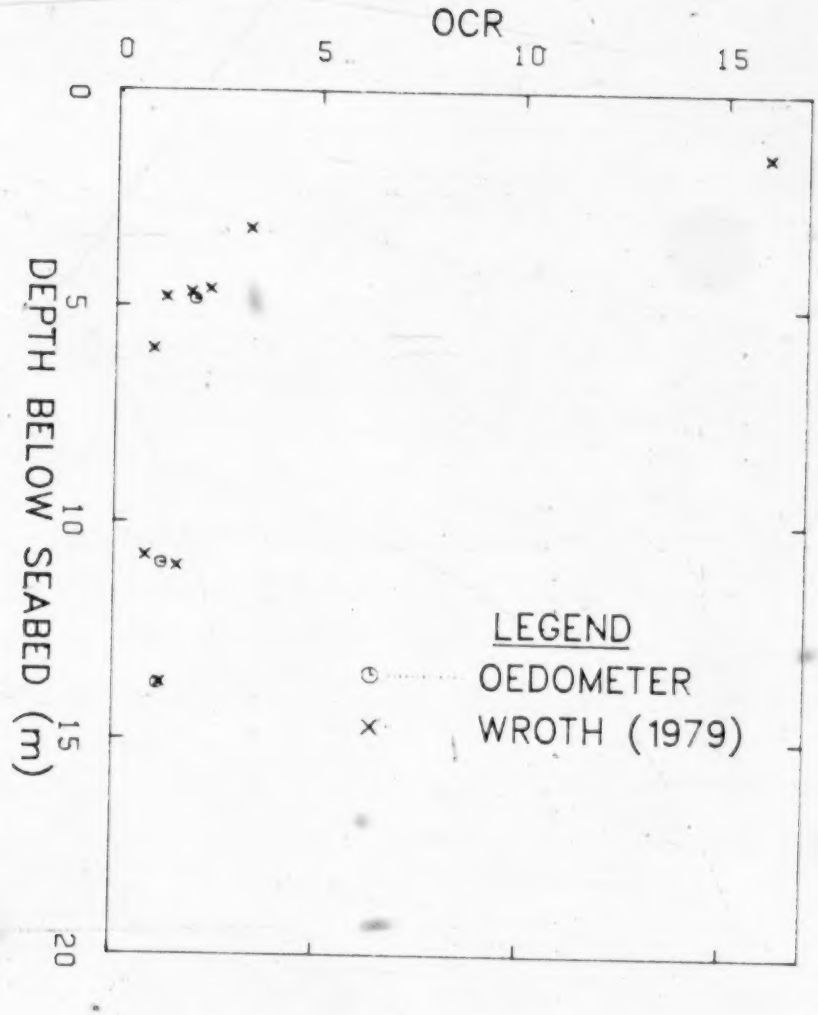

Figure 4.33 OCR for BH 20+00 showing measured values versus predicted.

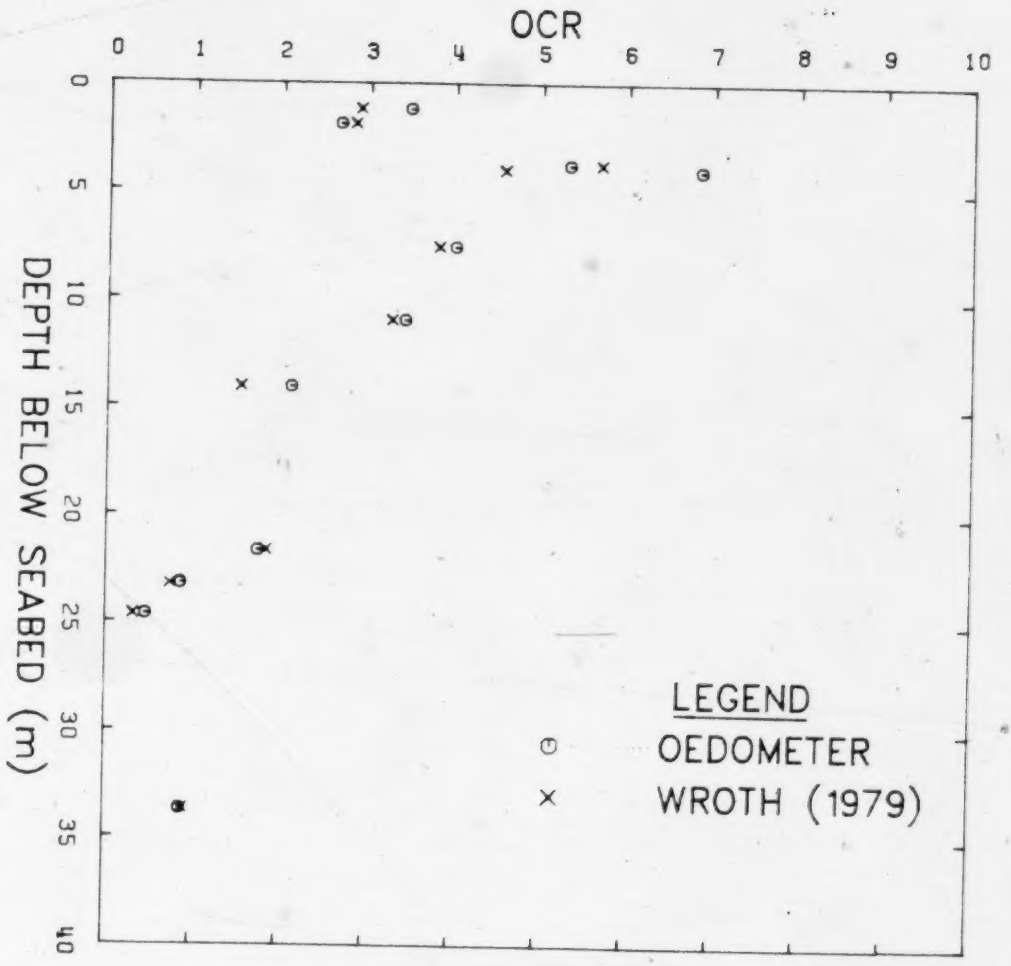

Figure 4.34 OCR for Sauvrak showing measured values versus predicted.

4.9 Clay Mineralogy

The sites sampled for this study were subsampled in order that an analysis could be performed of the mineralogy of the soil particles smaller than 2 microns. This was easily accomplished during the hydrometer test, where the suspension was siphoned off into a drying tray at a time when only clay particles were left in suspension. The dried particles were then pulverized and sent to the Alberta Research Council where X-Ray Diffraction Techniques were used to determine the composition of the clay fraction.

Table 4.17 summarizes the results for all of the samples. It is obvious that the predominant clay mineral at the sample sites in this study is illite, with a small accompanying percentage of kaolinite and an even smaller percentage of chlorite. No smectites at all were observed, so the peculiar swelling characteristics of the consolidation samples is attributed to the illite.

Table 4.17 Summary of clay mineralogy for consolidation samples.

CORE I.D.	DEPTH BSB. (m)	% CLAY	% CHLORITE	% KAOLINITE	%ILLITE	% MONTMORILLONITE
PC-09	1.16	78	5	25	70	0
	2.08	70	5	25	70	0
MTWS1	9.37	87	5	25	70	0
BH 20+00	4.68	23	10	20	70	0
	4.80	15	5	25	70	0
	11.01	34	5	30	65	0
	13.66	11	10	20	70	0

4.10 Analysis of Soil Fabric by SEM Techniques

The Scanning Electron Microscope owned by the Entomnology Department of the University of Alberta was employed to obtain high-resolution detailed pictures of the soil structure. The trend seems to be that the larger pore spaces close with increasing burial, which brings about a more compact soil skeleton. Plate 4.1 shows the very random, open structure existing 1 m below the mudline in PC-09. Plate 4.2 shows how the pore spaces have begun to close up (depth of 13.7 m below seabed in BH 20+00). No preferred orientation of particles has occurred, as can be seen in Plate 4.2. No unusual structures were observed, no slickensides, and no continuous sheared zones which might suggest some sort of metastable soil framework. There was an unusually high amount of organic matter, mainly transported wood particles and detrital remains of marine organisms, particularly within the upper two meters of sediment.

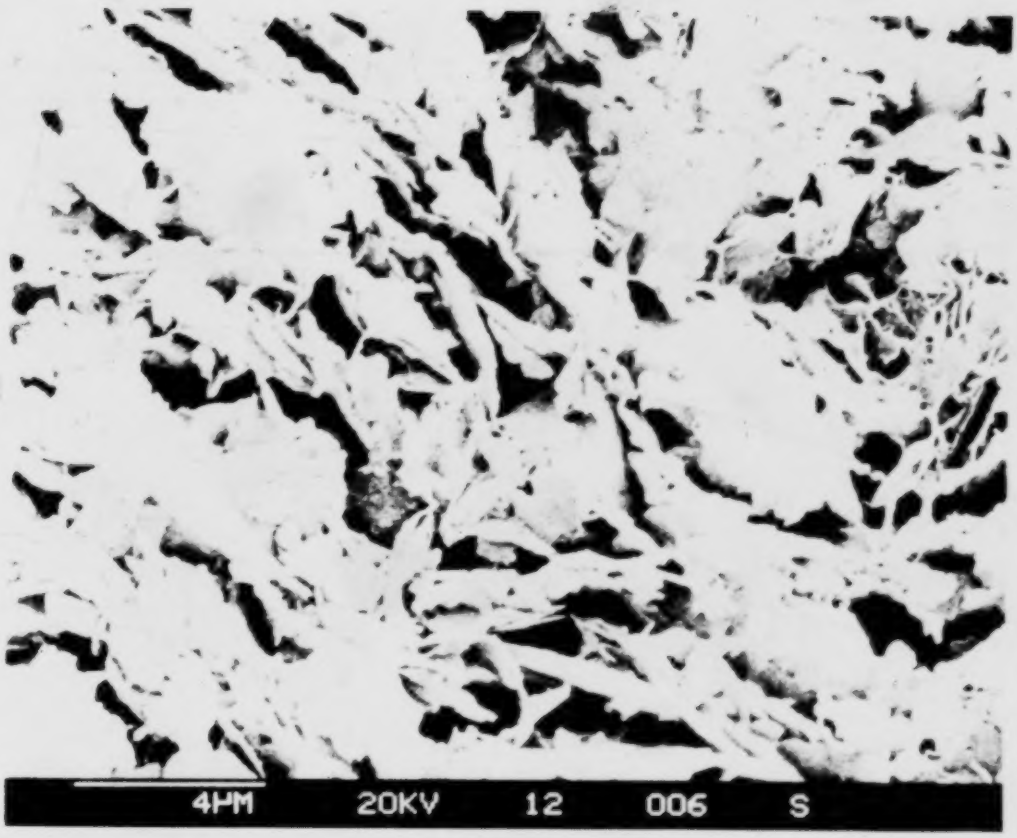

Plate 4.1 Scanning Electron Micrograph of marine bioturbated silty clay from 1 m bsb. in PC-09.

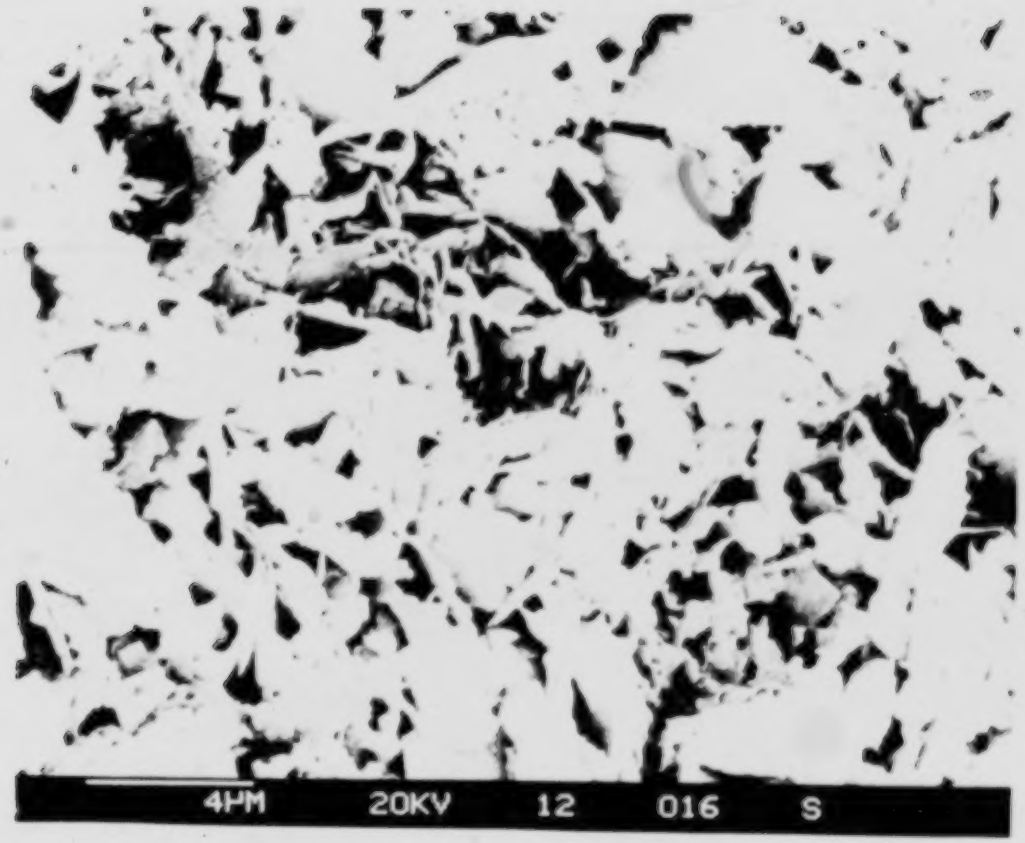

Plate 4.2 Scanning Electron Micrograph of marine silty clay that has begun the process of consolidation; 13.7 m bsb. in BH 20+00.

5.0 Constant Head Permeability Testing

5.1 The Constant Head Permeability Test

The constant head permeability test can be performed with the modified Anteus apparatus at the end of any load increment. The variable head system permits the application of any desired hydraulic gradient across the sample in the ring.

The flow velocity (V) during a constant head test is given by:

$$V = Q/(t * A) \qquad 5.1$$

where Q is the volume of permeant passing through the sample over a measured length of time (t), with (A) being the circular area of the sample in the consolidation ring. The coefficient of permeability can be expressed using Darcy's Law, provided that a condition of laminar flow exists within the sample:

$$k = Q * L / (A * h_i * t) \qquad 5.2$$

The parameters Q, A, and t have the same meanings as in equation 5.1, and L is the distance over which a head loss (h_L) occurs. L must be determined from the compression readings at the end of the load increment in question.

Verification can be made of the existence of laminar flow during the permeability test by plotting the flow velocity versus the hydraulic gradient, both on an arithmetic scale. A linear correlation of observed data indicates that the passage of permeant through the sample follows Darcy's Law and thus the data can be said to be of high quality. The hydraulic gradient is given as:

$$i = h_L / L \qquad 5.3$$

5.2 Holocene Sediments in the Beaufort Sea

Two permeability tests were performed on consolidation samples from PC-09, at 1.16 m and 2.08 m bsb. respectively; each with a vertical effective consolidation stress of 128 kpa.

This stress is significantly greater than the in situ overburden stress for these depths, and was in fact greater than the preconsolidation pressures as determined from the void ratio versus effective stress curves. Hence, the soil had been loaded to a state of normal consolidation in order that comparisons could be made between the void ratio and the coefficient of permeability. These measurements can then be used to predict the consolidation settlement and rate of consolidation of the foundation soils beneath a gravity structure placed on the seabed, as the addition of such a structure would likewise exceed the in situ overburden stresses.

All flow data has been corrected for a decreased viscosity of pore fluid at 0°C, which represents the in situ thermal regime more accurately than the test temperature of 23 C. The flow velocity data for both samples are plotted in Figure 5.1 versus the hydraulic gradient. Figures 5.2 and 5.3 show the measured values of the coefficient of permeability (k), corrected for viscosity, in relation to values of k calculated from oedometer data using the square root of time and the logarithm of time methods of plotting time-compression data. The coefficient of consolidation (C_v)

was calculated for each load increment of the consolidation test as follows:

$$k = C_v * \gamma_s * m_v * \nu_t/\nu_f \qquad 5.4$$

The coefficient of volume change (m_v) is calculated from the amount of strain occurring over a given stress increment where:

$$m_v = \Delta\epsilon_v/\Delta\sigma_v' \qquad 5.5$$

The value of m_v actually represents the instantaneous inverse slope of the stress-strain curve.

The viscosity correction is included in equation 5.4, where ν_t is the viscosity of the pore fluid at the test temperature and ν_f is the viscosity at the in situ temperature.

Figures 5.2 and 5.3 illustrate the point that the methods of log time and root time for plotting time versus compression data generally overpredict the coefficient of permeability when compared to measured values. The measured

data is in closer agreement with the log time predictions than with values based on root time.

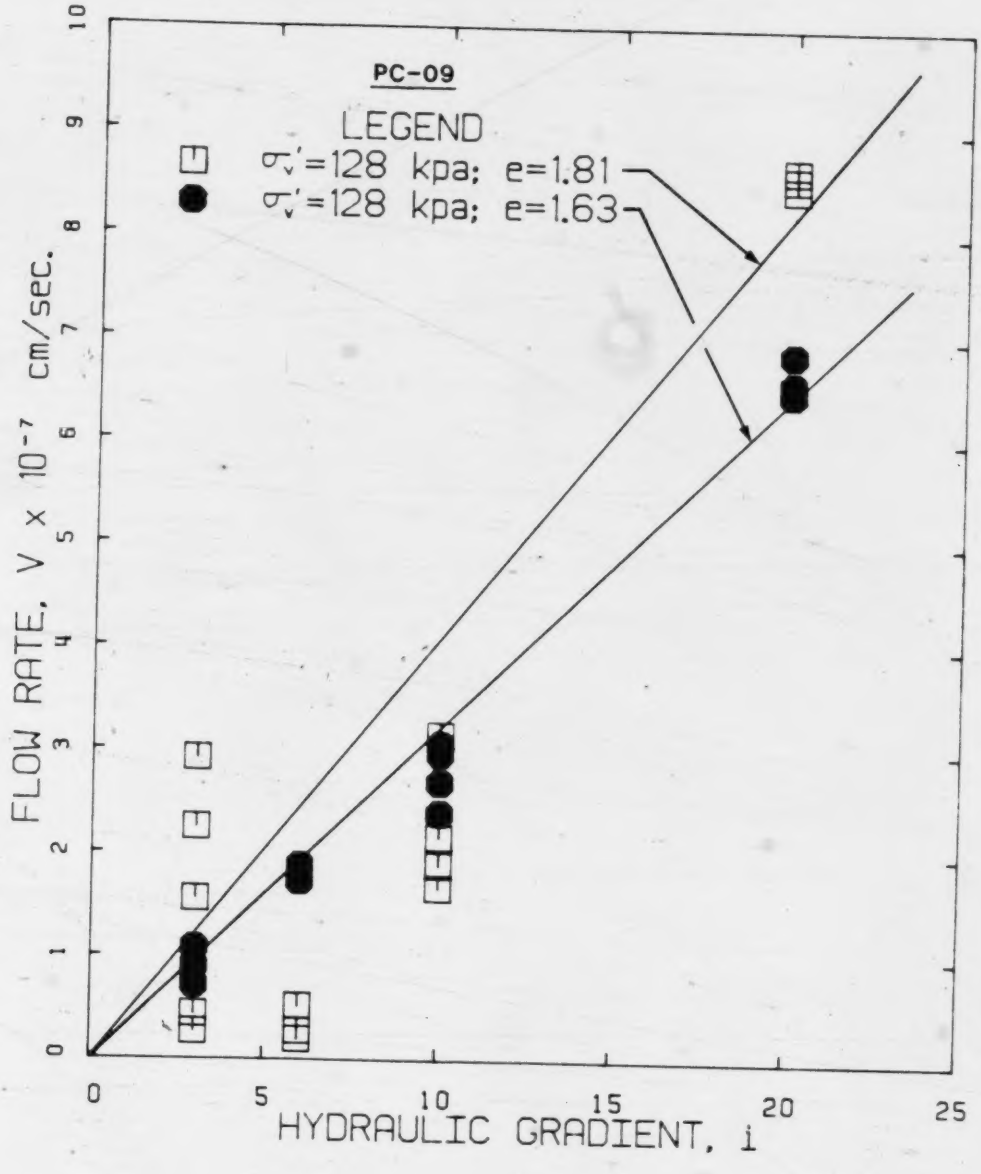

Figure 5.1 Flow velocity data from PC-09 versus hydraulic gradient showing the validity of the assumption of laminar flow.

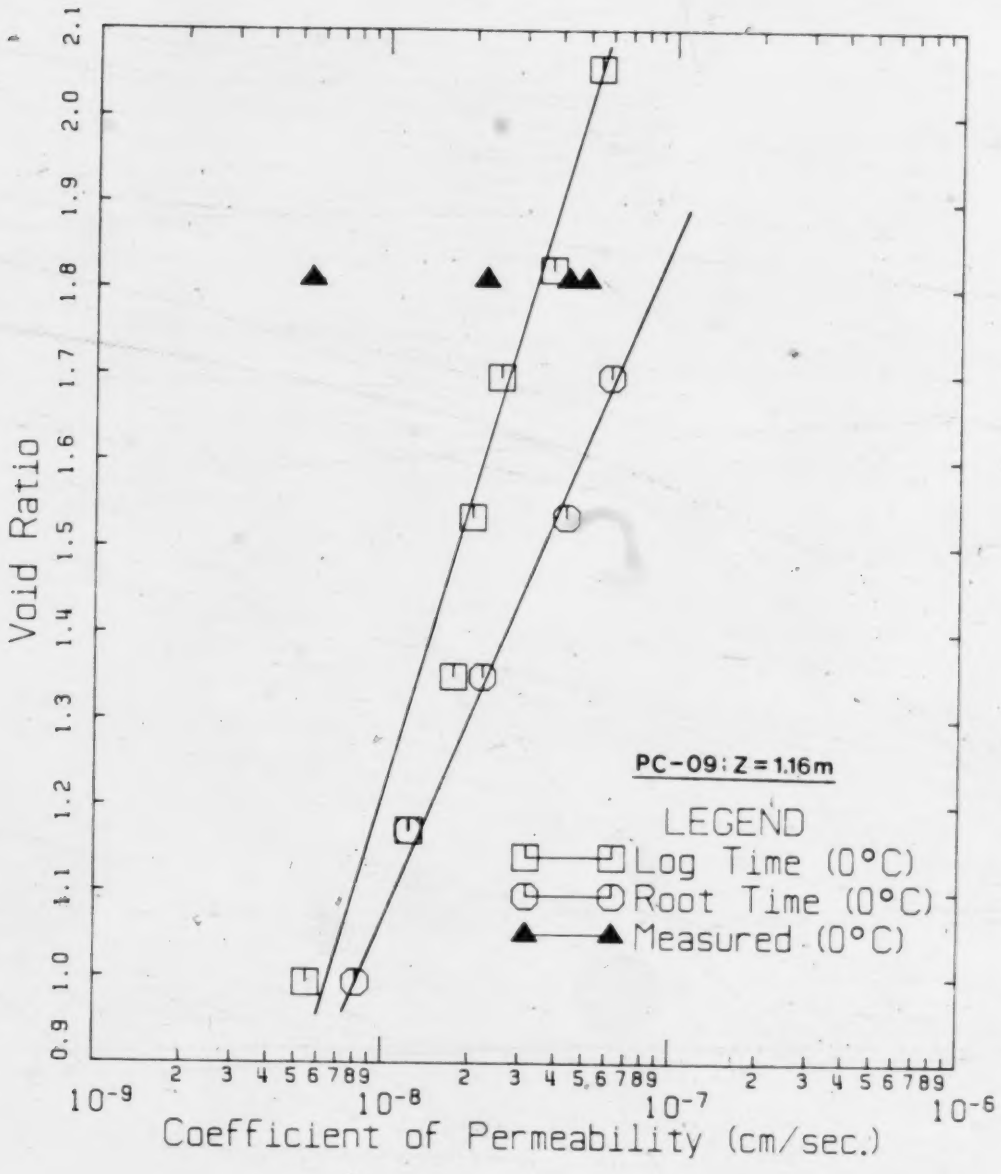

Figure 5.2 Measured and predicted values of the coefficient of permeability versus void ratio for PC-09; Z=1.16 m.

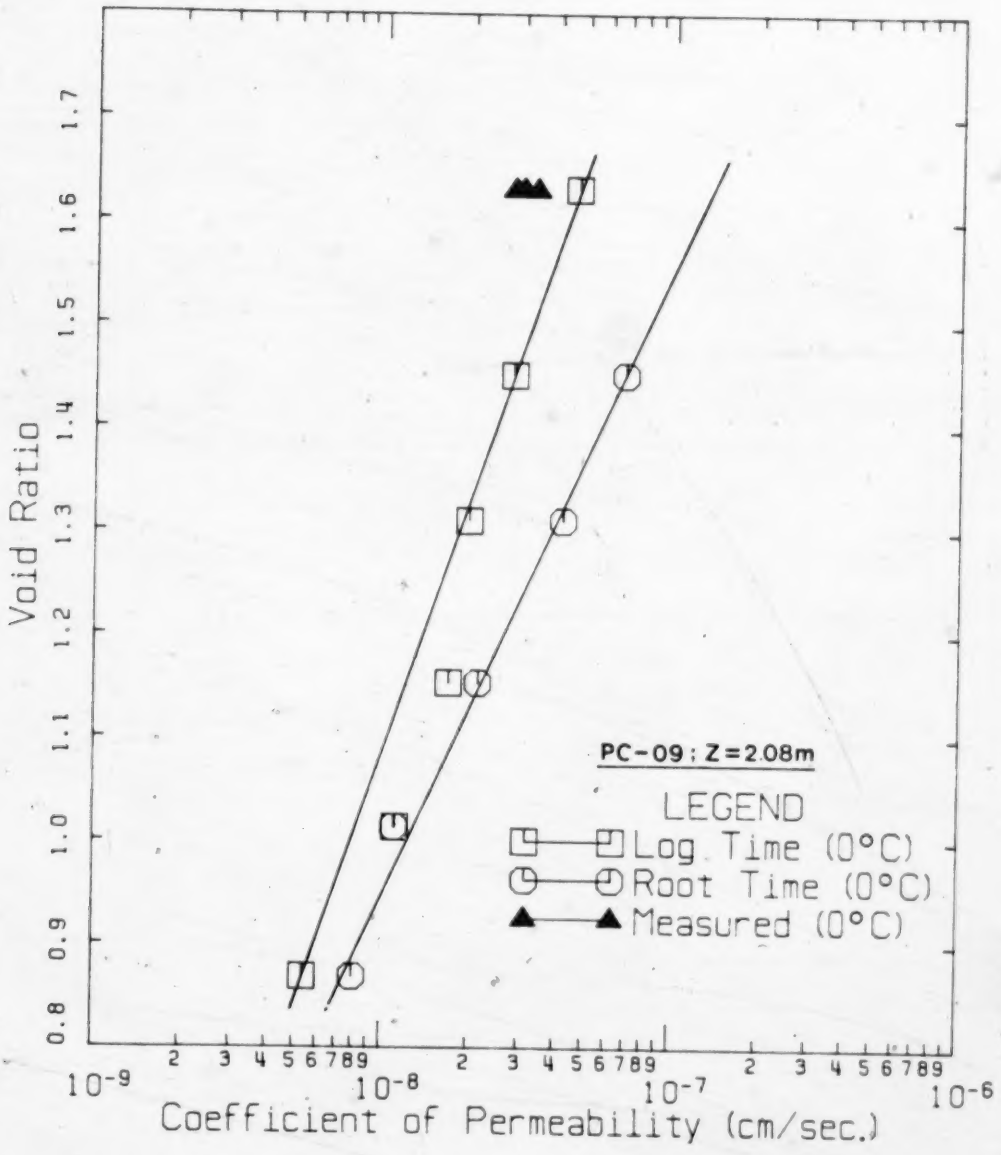

Figure 5.3 Measured and predicted values of the coefficient of permeability versus void ratio for PC-09; Z=2.08 m.

5.3 Transgressive Silts and Clays in the Beaufort Sea

Two samples from BH 20+00, from burial depths of 4.85 and 13.74 m were tested for permeability. Both samples were organic-rich silts containing between 10 and 15 percent clay-sized particles by weight.

One permeability test was performed on the shallower sample at a vertical consolidation stress of 1024 kpa, thus creating a state of normal consolidation. Two tests were performed on the deeper sample at stress levels of 128 and 1024 kpa in order to determine the slope of the void ratio versus coefficient of permeability relationship. The void ratio was equal to 0.75 at the 1024 kpa stress level for the shallow sample.

Figure 5.4 shows the flow veloc versus hydraulic gradient data for all three tests. Again, the assumption of laminar flow was validated, as is evident from the linear correlation. Figure 5.5 reveals that the measured values of permeability were somewhat lower than the values predicted by the methods of log and root time. Figure 5.6 illustrates very clearly the similarity in the slopes of the measured and predicted permeability versus void ratio relationships, which gives credence to the view that a linear correlation exists between log permeability and void ratio.

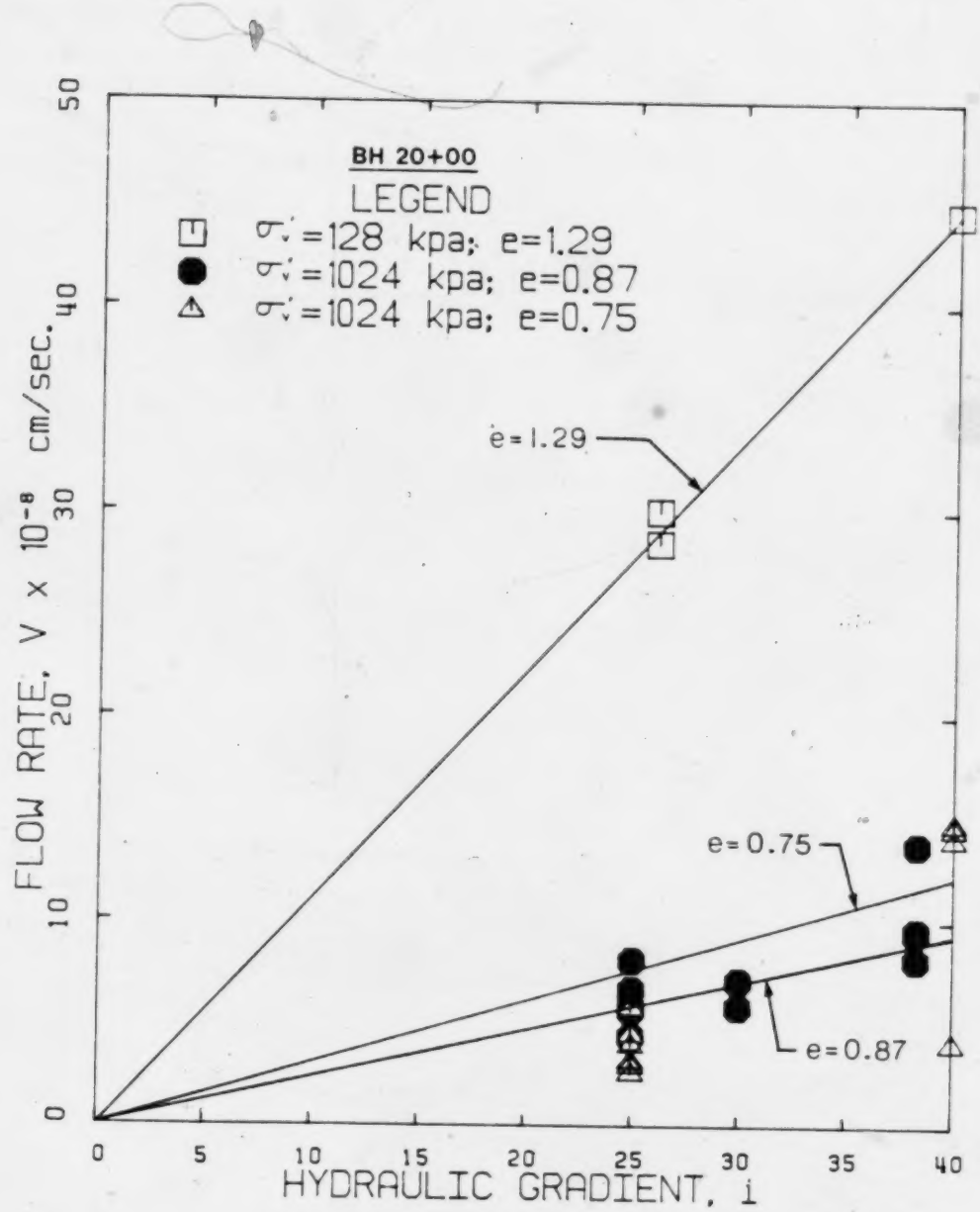

Figure 5.4 Flow velocity data from BH 20+00 verifying the assumption of laminar flow during the permeability test.

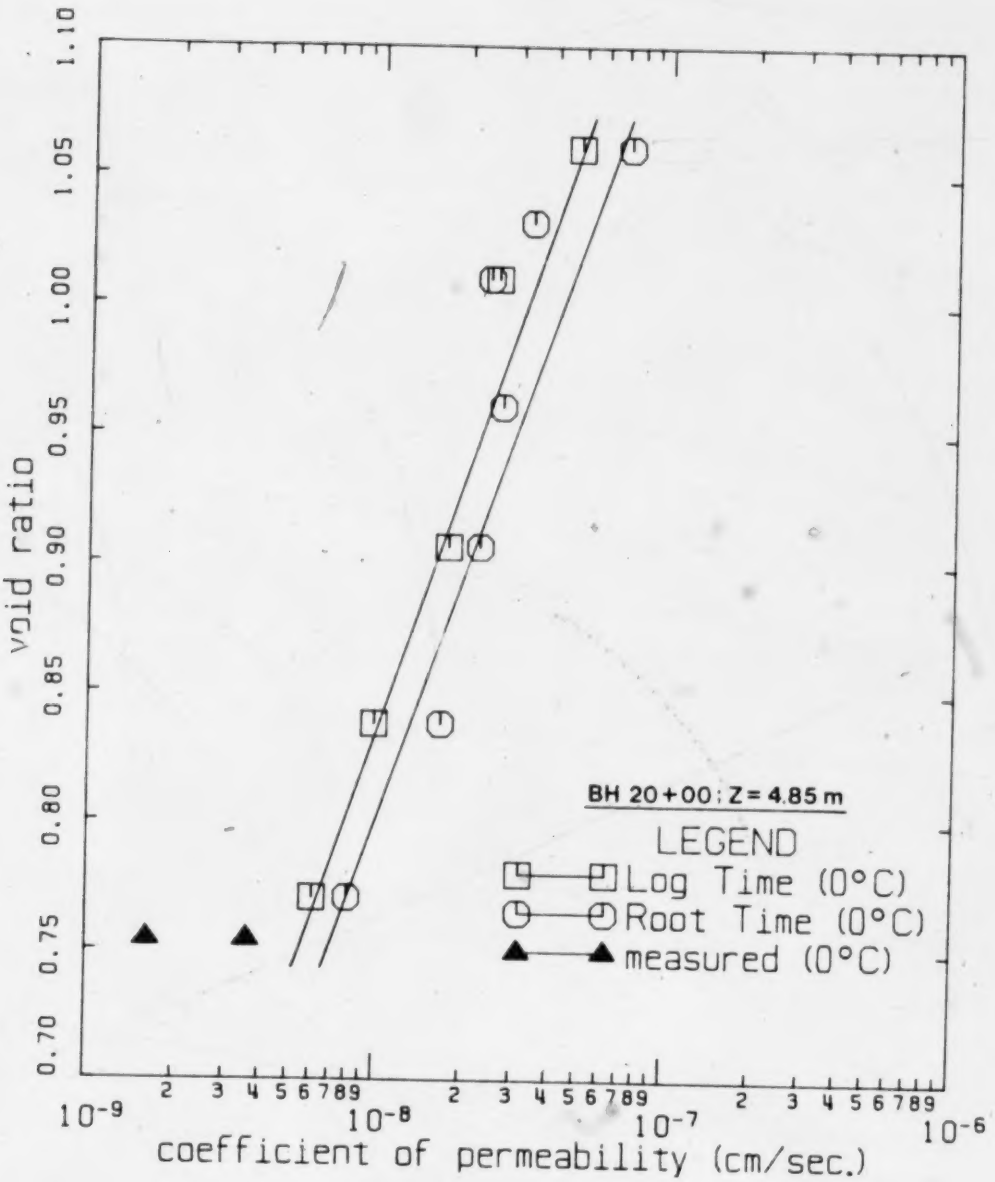

Figure 5.5 Measured and predicted values of the coefficient of permeability versus void ratio for BH 20+00; Z=4.85 m.

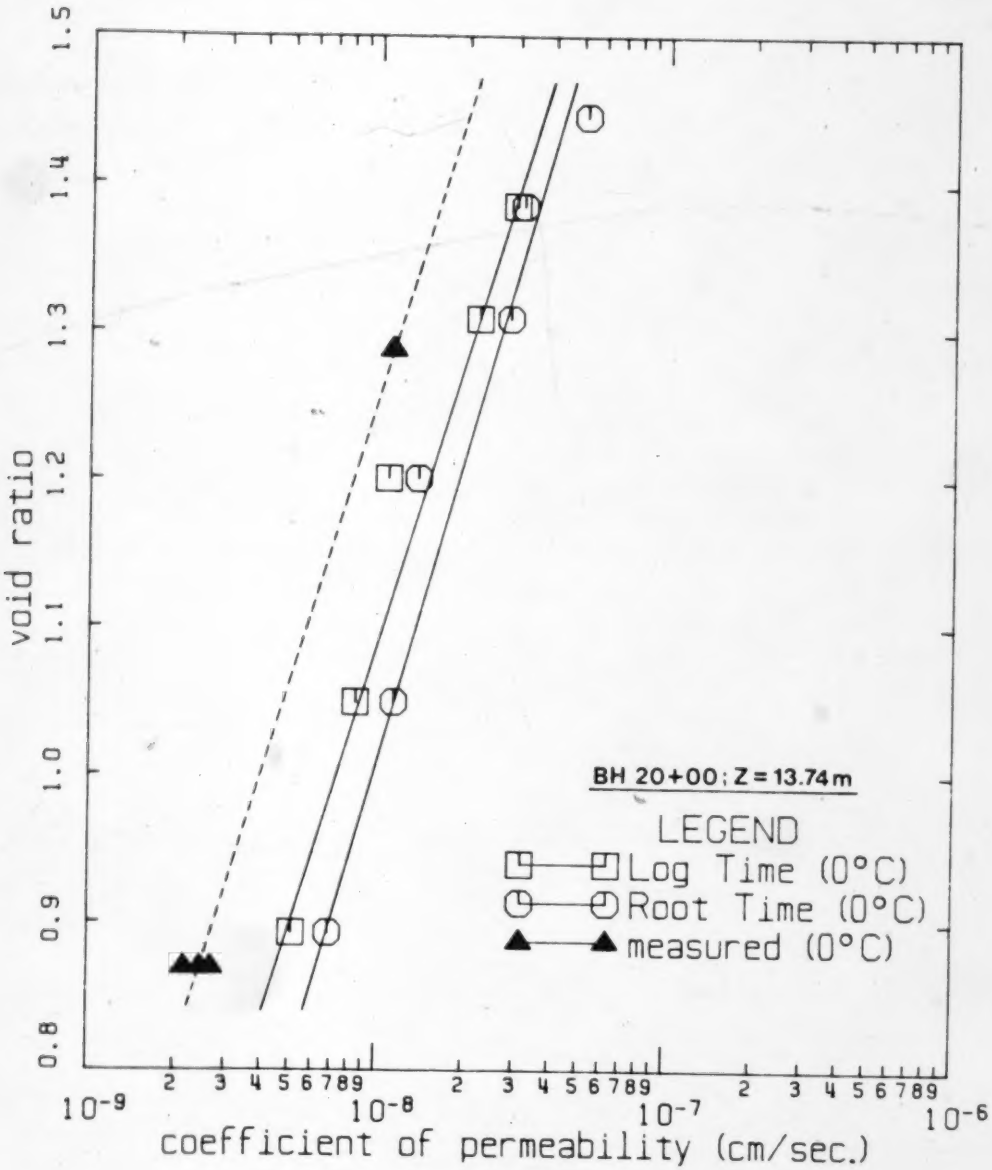

Figure 5.6 Measured and predicted values of the coefficient of permeability versus void ratio for BH 20+00; Z=13.74 m.

5.4 Comparisons with Other Sediments

It has been found in this study that a linear relationship exists between void ratio and log permeability. Measured values of the coefficient of permeability fall somewhat below values predicted by the time-compression plotting methods of logarithm of time and square root of time, with the highest permeabilities arising from the root time method.

It may be likely that in situ permeabilities may differ from these measured values by as much as an order of magnitude. In the case of clays, field values would probably be lower than the values measured in PC-09, due to the effects of preferential flow up around the ring wall in the consolidation cell. Highly laminated sediments in the Beaufort Sea could also have lower field permabilities than in the lab as a result of ice-bonding between the coarser particles. Field permeabilities would be substantially different from the values measured on the BH 20+00 samples when the soils in situ are similar in lithology but contain significant amounts of gas. The samples from BH 20+00 are thought to represent the upper limit of permeabilities for the silts in the Beaufort Sea, the silts being slightly more permeable than the clays existing immediately at the mudline. Where the silts are interbedded with clays, one should expect all of the head loss to occur across the clay beds.

Silva et al (1981) has produced a chart showing the measured values of permeability for a number of deep-sea sediment types, classified according to their mineralogy. The data collected in this study has been added to Silva's plot (Figure 5.7) and compares very well with the region for illitic clays.

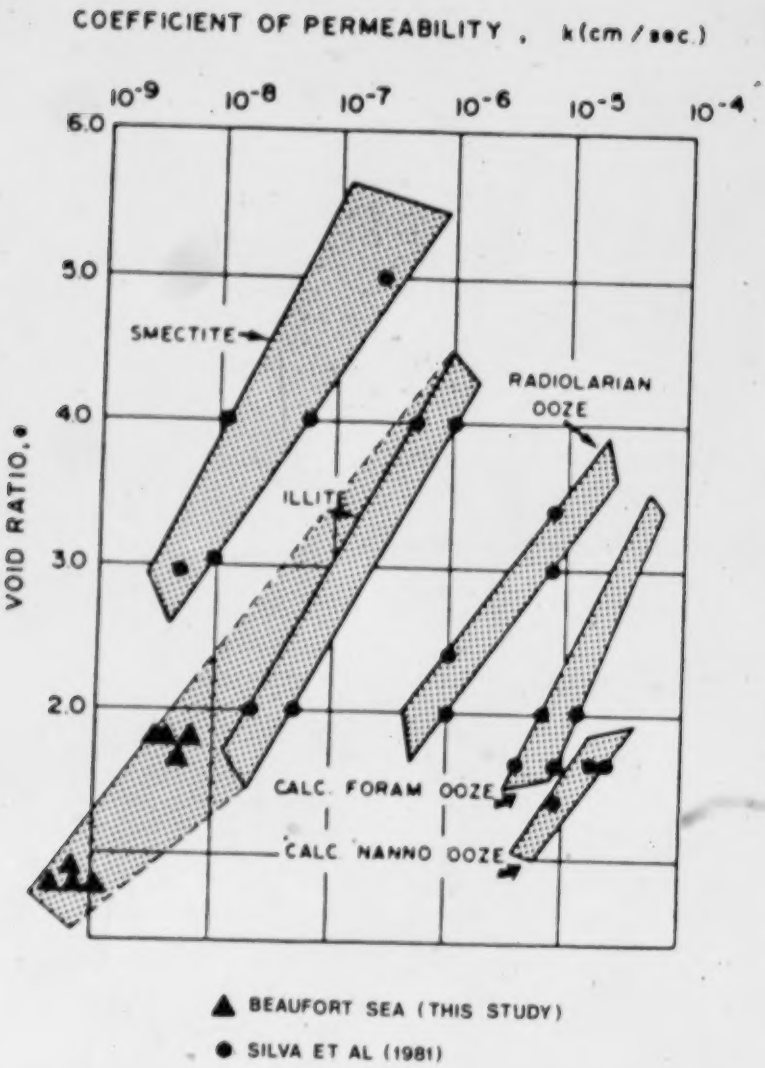

Figure 5.7 Void ratio vs. coefficient of permeability plots showing range of measurements made to date for, five marine sediment types (mod. Silva et al, 1981).

5.5 Comparison with Terrestrial Soils

Lambe and Whitman (1969) have produced a chart summarizing the coefficient of permeability versus void ratio measurements made for a number of terrestrial soils. The data from this study is shown on their plot in Figure 5.8. Two divisions are apparent in the Beaufort Sea data, one for the recent surficial clays and a second for the transgressive silts and silty clays.

It is noteworthy that both soils plot at the lower end of the measureable scale of permeability, and over short periods of time are considered to be practically impermeable. However, given that the permeabilities are so low does not rule out the potential for large amounts of settlement, especially in the hi hly compressible soft clays at the seabed. These materials constitute a source of concern wherever they exist in an area of offshore artificial island construction, since in addition to being very compressible and prone to excessive settlement, they are in many cases very weak.

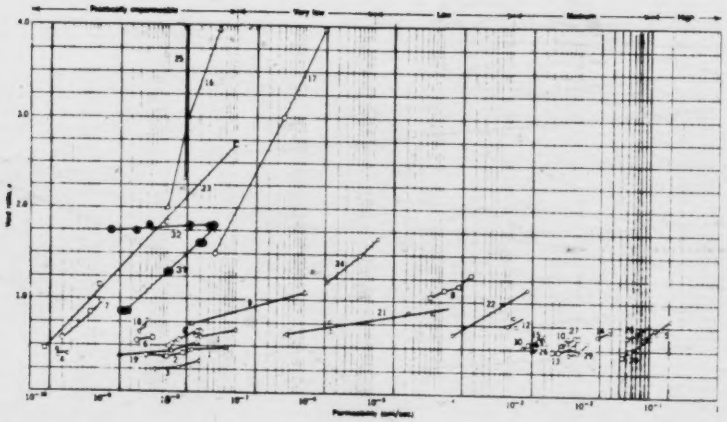

Soil Identification Code

1 Compacted caliche
2 Compacted caliche
3 Silty sand
4 Sandy clay
5 Beach sand
6 Compacted Boston blue clay
7 Vicksburg buckshot clay
8 Sandy clay
9 Silt—Boston
10 Ottawa sand
11 Sand—Gaspee Point
12 Sand—Franklin Falls
13 Sand—Scituate
14 Sand—Plum Island
15 Sand—Fort Peck
16 Silt—Boston
17 Silt—Boston
18 Loess
19 Lean clay
20 Sand—Union Falls
21 Silt—North Carolina
22 Sand from dike
23 Sodium—Boston blue clay
24 Calcium kaolinite
25 Sodium montmorillonite
26-30 Sand (dam filter)
31 Silty clay—Beaufort Sea
32 Clay—Beaufort Sea

Figure 5.8 Comparison of permeabilities for various soil types (mod. Lambe and Whitman, 1969).

6.0 Strength of Surficial Sediments

6.1 Synopsis

The Beaufort Sea is characterized in many cases by a well defined break in lithology at the position of the most recent unconformity. The eastern reaches of the continental shelf possess a very thin veneer of soft clayey sediments (2 to 4 m thick) which directly overlie the pre-unconformity sands and silts. The mantle of soft surficial sediments thickens considerably into the relic buried valleys (Niglik Channels, Kugmallit Channel, and the Ikit Trough). Much of this clayey sediment has been extensively reworked by the grounding of large ice features, especially within the 10 and 50 m isobath. Many relic scours have be n observed on seismic records (O'Connor, 1982a). One should expect low shear strengths within this unit on a widespread basis, owing to the disturbance caused by impinging ice features.

The underlying sands are very dense and well-sorted, resulting in the fact that no ice keels penetrate very far below the unconformity. This major change in soil type consistently denotes the upper limit of the well-bonded permafrost table, with the overlying fine-grained sediments being largely unfrozen because of their high pore water salinity as well as their colloidal activity.

To the west, the change from the well-stratified marine unit to the pre-unconformity strata is less pronounced, especially in the Mackenzie Trough and over the Kringalik

Plateau. The surficial sediments are more silty in this region as a result of their proximity to the sediment source. The pre-unconformity strata are predominantly silts and silty sands with intervals of softer marine clays and silty clays. The pre-unconformity strata are only marginally ice-bonded over the Kringalik Plateau (O'Connor, 1982b) and the sediments in the Mackenzie Trough are completely unfrozen beyond the 15 m isobath.

Sharp variations in the undrained shear strength occur in the pre-unconformity interbedded silts and clays, which correspond to changes in soil type and pore water salinity.

6.2 Recent Clayey Sediments (Unit A)

A modest amount of overconsolidation has been observed within the upper 10 m of recent marine sediments in the Beaufort Sea. This feature is thought to arise from the effects of ageing and is magnified by the manner in which OCR is calculated. AOC is least pronounced within the Mackenzie Trough, an area possessing a very high sedimentation rate and therefore younger sediments than at similar depths in other regions.

Two piston cores were made available by the Geological Survey of Canada for consolidated-undrained triaxial testing in this study (PC-02 and PC-03). These cores were taken in 50 m of water along the boundary between the Kringalik Plateau and the Mackenzie Trough. The consistency was very soft with undrained shear stengths averaging 5 kpa over the sampled depth of 2 m. No structure was visible, suggesting a random orientation of clay particles similar to that existing at the time of deposition. The water contents fell between 45 and 70 percent, generally exceeding the liquid limit. These sediments are very similar to the silty clays found in the Kugmallit Channel (PC-09). The plasticity was in the order of 30 percent.

Table 6.1 summarizes the results of the triaxial testing program. One sample was consolidated isotropically to its estimated in situ effective lateral stress (6.1 kpa), assuming that the effective vertical stress was equal to 12 kpa and the coefficient of earth pressure at rest was 0.5.

Table 6.1 Results of isotropic triaxial compression tests performed on piston core samples PC-02 and PC-03.

TEST	CIUC	CIUC	CIUC	CIUC
HOLE	PC-02	PC-03	PC-03	PC-02
DEPTH (m)	1.78	2.31	1.07	0.75
w_N (%)	45.4	70.0	68.5	61.3
γ (kN/m)	17.31	16.04	15.25	16.10
σ_c (kpa)	6.1	25.0	75.0	150.0
$\left(\frac{\sigma_1-\sigma_3}{2}\right)_f$ (kpa)	8.2	18.5	2.0	54.3
$\left(\frac{\sigma_1+\sigma_3}{2}\right)_f$ (kpa)	9.8	31.5	40.7	108.9
u_f (kpa)	308.6	311.7	336.2	394.5
ε_f (%)	0.59	2.72	1.38	8.99
A_f	0.53	0.31	0.70	0.79

The other three samples were consolidated isotropically to stresses of 25, 75, and 150 kpa before being sheared.

In all cases, the B-parameter was equal to unity following consolidation. A back pressure of 300 kpa was used to restore the hydrostatic pressure within the sample to its in situ condition. The samples were sheared undrained after consolidation. The sample reconsolidated to 6.1 kpa was significantly stiffer than the other samples and had a much lower water content. Therefore, emphasis is placed on the data from the other three samples. The stress-strain curves for all four tests are shown in Figure 6.1.

Pore pressures generated during undrained shear were always positive, resulting in a curved stress path and strain-softening behaviour (Figure 6.2). The sample consolidated to 75 kpa was somewhat stronger than the other two samples having similar water contents (consolidation pressures of 25 and 150 kpa). This difference in maximum strength may be due to minor geologic differences between samples, such as grain size. A modified Mohr failure envelope was drawn through the points denoting failure on the p'-q plot, based on a loss of strength evident in the stress paths. This envelope was then drawn in the form of a Mohr envelope with the Mohr circles at failure plotted for each test in Figure 6.3. The effective angle of shearing resistance proved to be 27.5 degrees and the failure envelope had an effective cohesion intercept of 4.5 kpa. The existence of a cohesion intercept supports the idea that

these surficial clays are actually overconsolidated.

These results illustate the difficulty one has in measuring shear strengths on such weak material. The problems of loading ram friction in the triaxial cell during shear were known to constitute a source of error and future tests on this material should be performed using an internal load cell rather than an external one.

The value of the A-parameter at failure verified that the samples reconsolidated to 6.1 and 25 kpa were still somewhat overconsolidated. An A value of 0.53 was observed at failure in the 6.1 kpa sample corresponding to an OCR of about 1.6 (Bishop and Henkel, 1962). This means that the preconsolidation pressure would be about 40 kpa, which is reasonable for this depth compared to data from PC-09 keeping in mind that the sediments at that depth in PC-09 are somewhat older and therefore stiffer (P_c = 38.5 kpa at 2.08 m bsb. in PC-09). The sample reconsolidated to 25 kpa behaved in a similar manner, but strain-softened after yield. Apparently the flocculated structure of the clay matrix was disrupted to the point where no further dilation could occur. This loss in strength occurred at an average effective normal stress of about 32 kpa. The A value at failure was 0.31, corresponding to an OCR of about 2 (Bishop and Henkel, 1962). Thus the preconsolidation pressure would have been in the order of 64 kpa, which is slightly high but still reasonable. The effective overburden pressure for this sample is only 13.7 kpa, which would result in an even

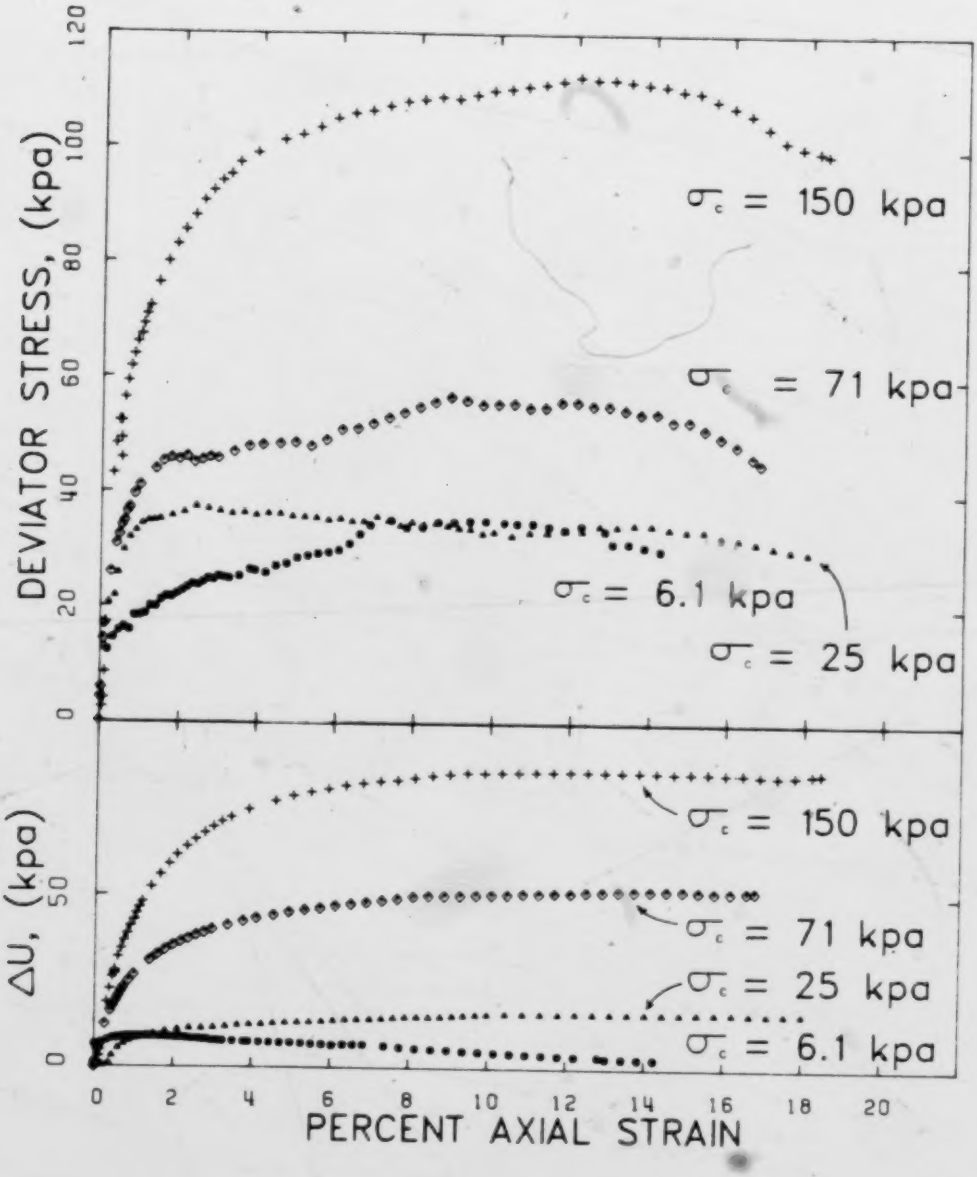

Figure 6.1 Stress-strain curves for the triaxial tests of soft recent marine clays (PC-02 and PC-03).

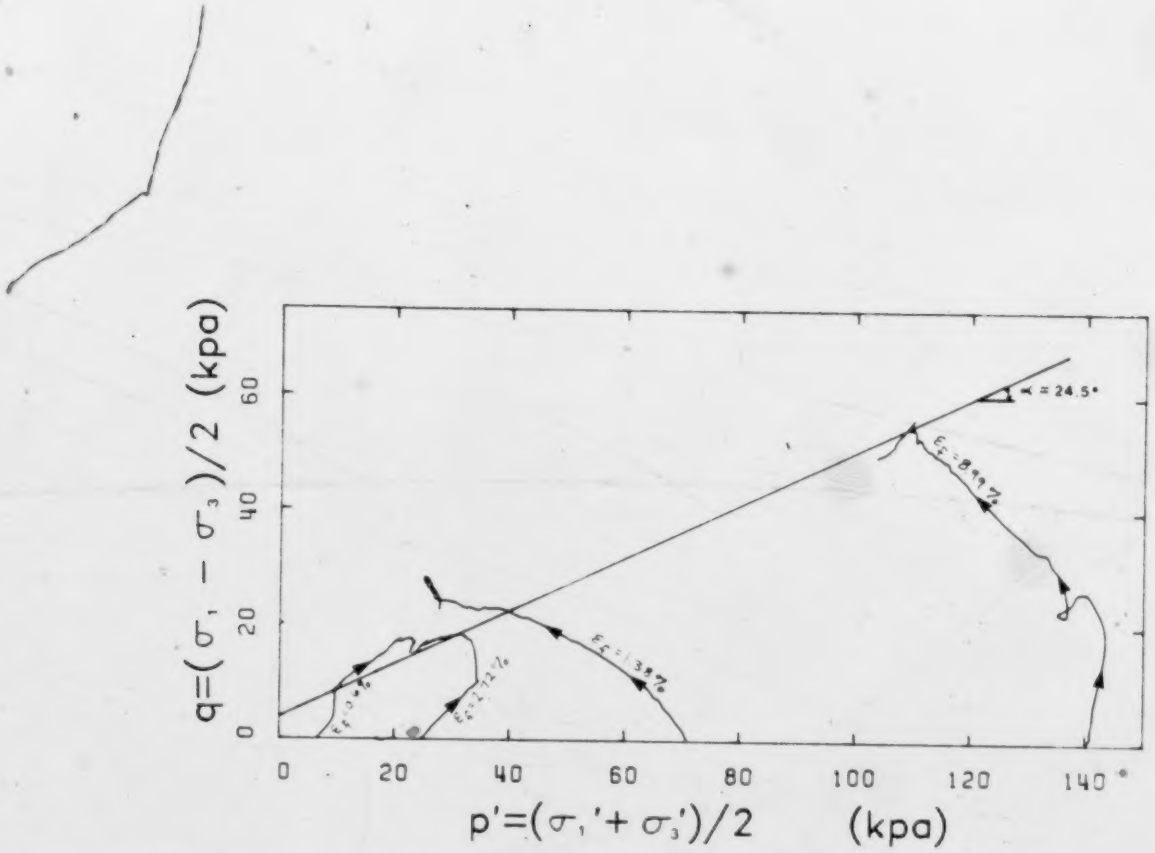

Figure 6.2 Modified Mohr plot showing the effective stress paths followed during undrained shear for the tests shown in Figure 6.1.

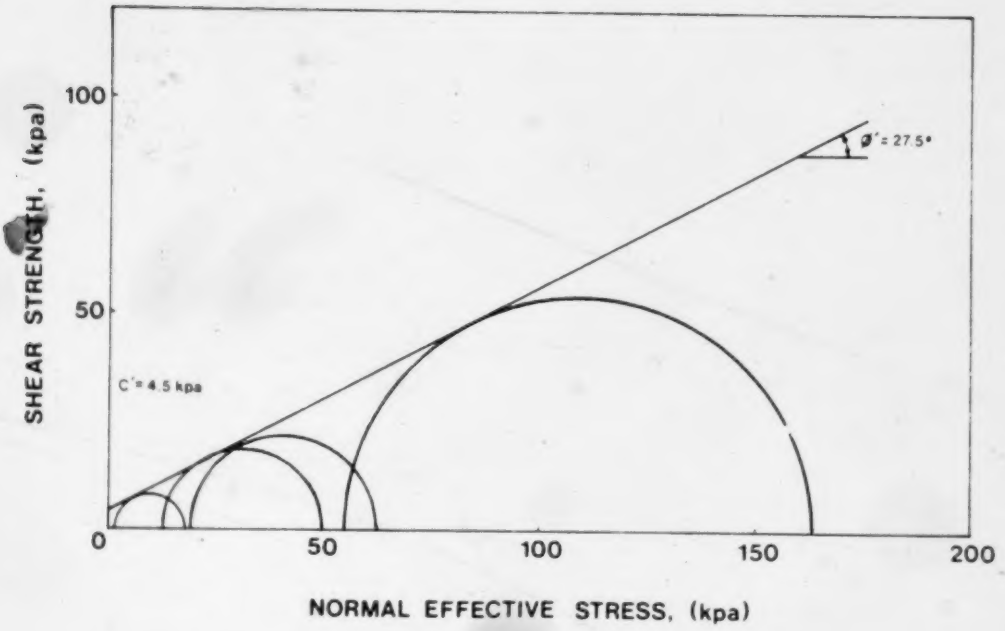

Figure 6.3 Mohr failure envelope for the tests in Figures 6.1 and 6.2.

higher OCR.

The other two samples were consolidated well beyond their in situ preconsolidation pressures and were therefore truly normally consolidated. This was reflected in the stress paths during undrained shear (Figure 6.2). The A values at failure were 0.7 and 0.79 for the samples consolidated to 75 and 150 kpa respectively, which corresponds to an OCR of about 1 (Bishop and Henkel, 1962).

6.3 Transgressive Silty Sediments (unit B)

A well-stratified silt and clay unit commonly underlies the veener of recent soft marine sediments and terminates abruptly at the unconformity. In some areas this transgressive sequence is equivalent to the pre-unconformity strata. The depositional environment would in those cases be substantially different than the simple reworking of older outwash deposits during transgression. It would then be synomous with a pro-deltaic environment (e.g. the Mackenzie Trough and relic channels found to the east), where frequent changes in the location of deposition occurs as the delta front shifts from place to place and marine deposition takes over for awhile.

The study area near Puller and Hooper Islands was sampled during the 1984 GSC Spring Drilling Program. The depositional environment is complex and the stratigraphy includes a sequence of unit B from 3 to 14 m bsb. in BH 20+00, below which lie the pre-unconformity sands. Several shelby tubes from this transgressive silt unit were sent to the Geotechnical Laboratory at the National Research Council in Ottawa, and the author is indebted to Dr. J-M. Konrad for making available his data for this study. One shelby came from BH 20+00, a borehole for which the author has tested consolidation samples and has compiled a summary profile.

Consolidation tests have shown the silt unit to be slightly overconsolidated down as far as the unconformity. This unit has highly variable shear strengths, depending on

whether the index property testing intersected a clay lamination or not. Table 6.2 summarizes the results of the static triaxial compression testing program. Konrad (1985) also performed a number of cyclic triaxial tests which are not used in this study.

Three isotropically consolidated and one anisotropically consolidated tests were run on silt samples by Konrad (1985). The stress-strain curves are reproduced in Figures 6.4 and 6.5. The undrained compression (CIUC) test performed on the sample consolidated isotropically to 65 kpa showed that negative pore pressures were developed during shear beginning at an axial strain of 4 percent. All tests resulted in S-shaped stress paths (Figure 6.6) and dilatant, strain-hardening behaviour during undrained shear.

The degree of strain hardening was greatest for the sample consolidated to 65 kpa, as can be seen in Figure 6.6. All stress paths rode up the failure envelope during shear and reached a point where the existing structure in the soil was obliterated, after which the soil lost strength.

The A values at failure revealed that the soil behaved in an elastic manner. The occurrence of significant strain hardening raises a serious question in the case of these silts. What should one select as the minimum anticipated design strength based on the triaxial testing program? It may be unsafe to rely on triaxial tests to provide minimum shear strengths at a given consolidation pressure, since conditions below a wide gravity structure or along a failure

Table 6.2 Summary of static triaxial compression tests conducted on Beaufort Sea silts (mod. Konrad, 1985).

TEST	CIUC	CIUC	CAUC	CIUC
HOLE	BH 20+00	BH 10+00	BH 7+60	BH 10+00
DEPTH (m)	7.6	16.0	18.8	16.3
σ_1 (kpa)	65	130	227	258.4
σ_3 (kpa)	65	130	150	258.4
$\frac{(\sigma_1-\sigma_3)}{2}$ (kpa)	50	72	108	150
$\frac{(\sigma_1'\ \sigma_3')}{2}$ (kpa)	91.5	130	200	271.4
u_f (kpa)	21	72	58	137
ε_f(%)	1.7	5.2	4.8	7.0
A_f	0.21	0.50	0.27	0.46

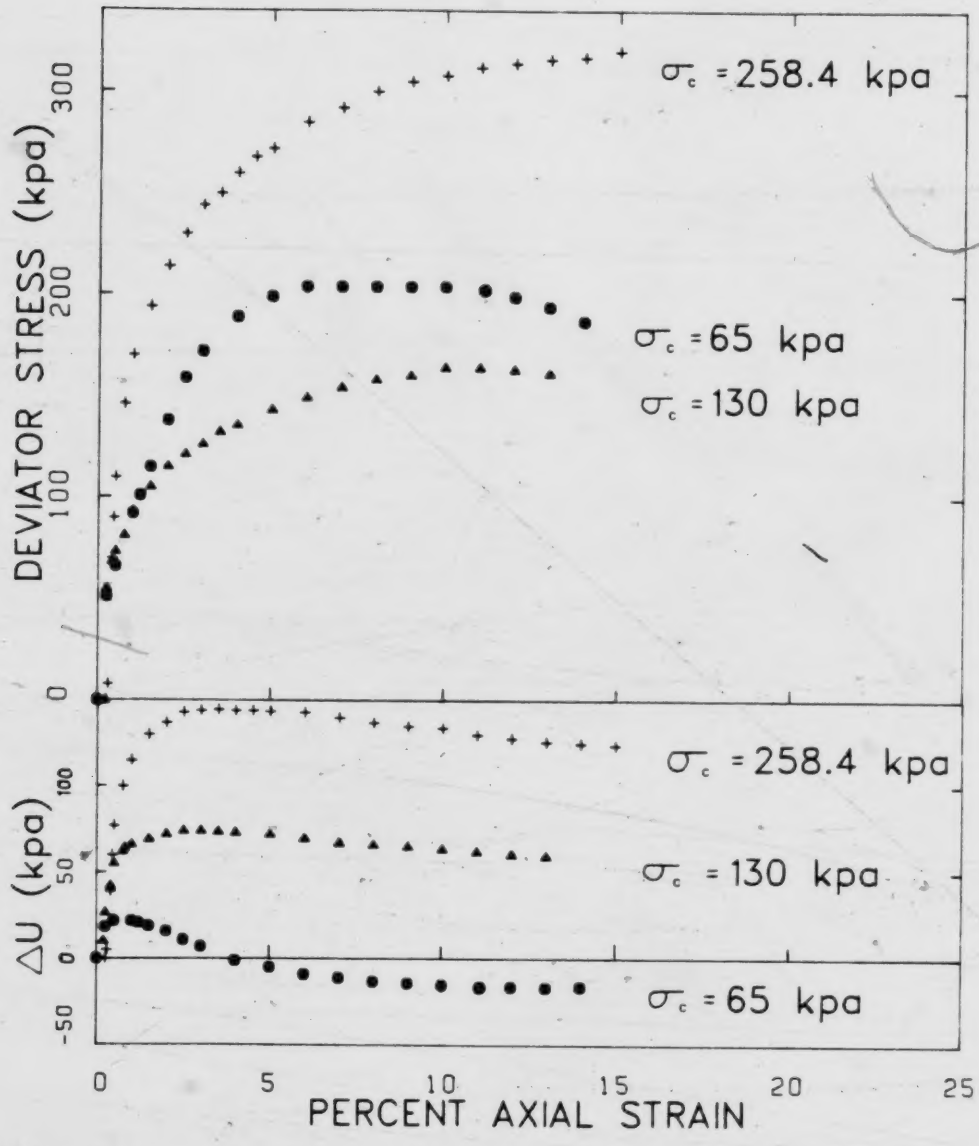

Figure 6.4 Stress-strain curves for isotropically consolidated triaxial compression tests on Beaufort Sea silt (mod. Konrad, 1985).

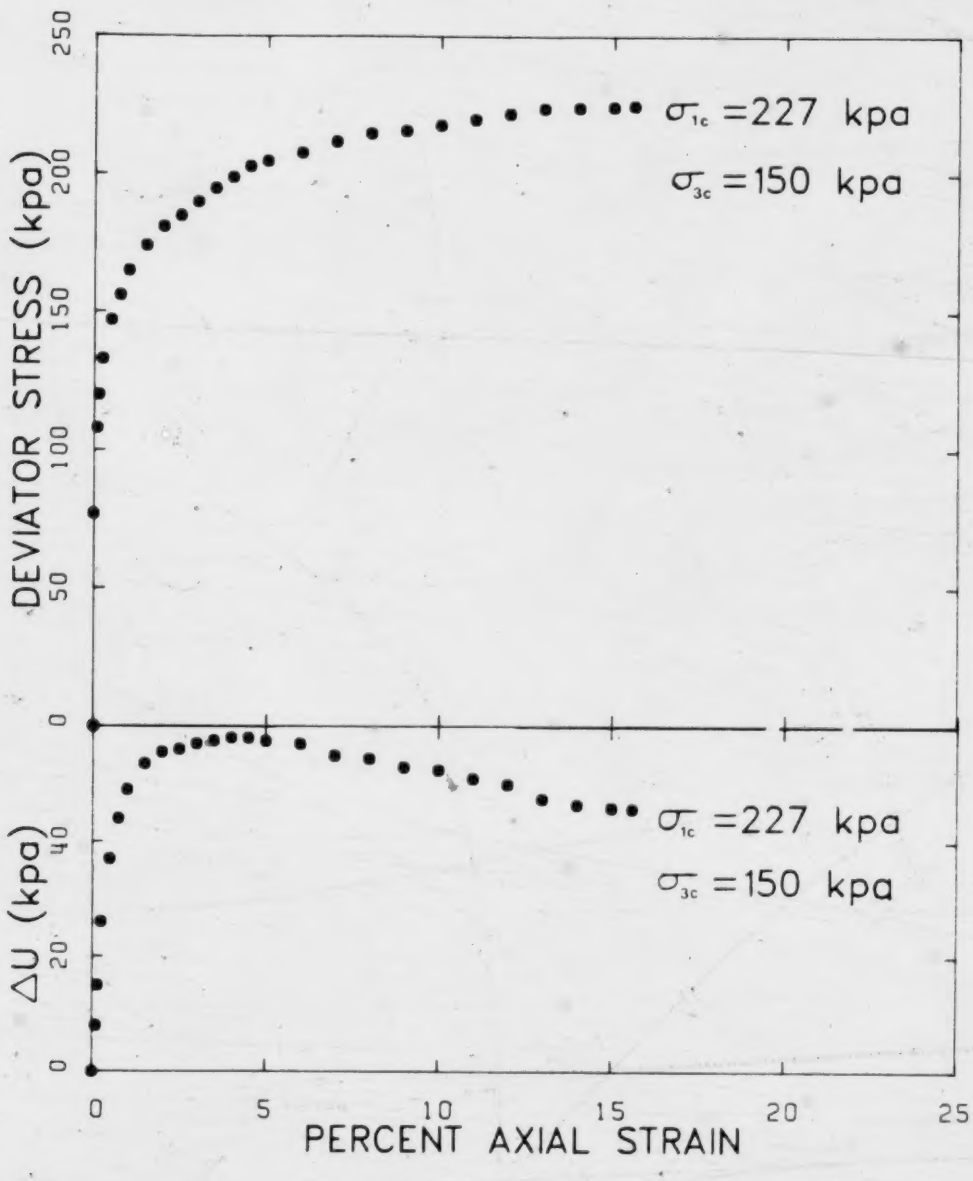

Figure 6.5 Stress-strain curves for an anisotropically consolidated triaxial compression test on Beaufort Sea silt (mod. Konrad, 1985).

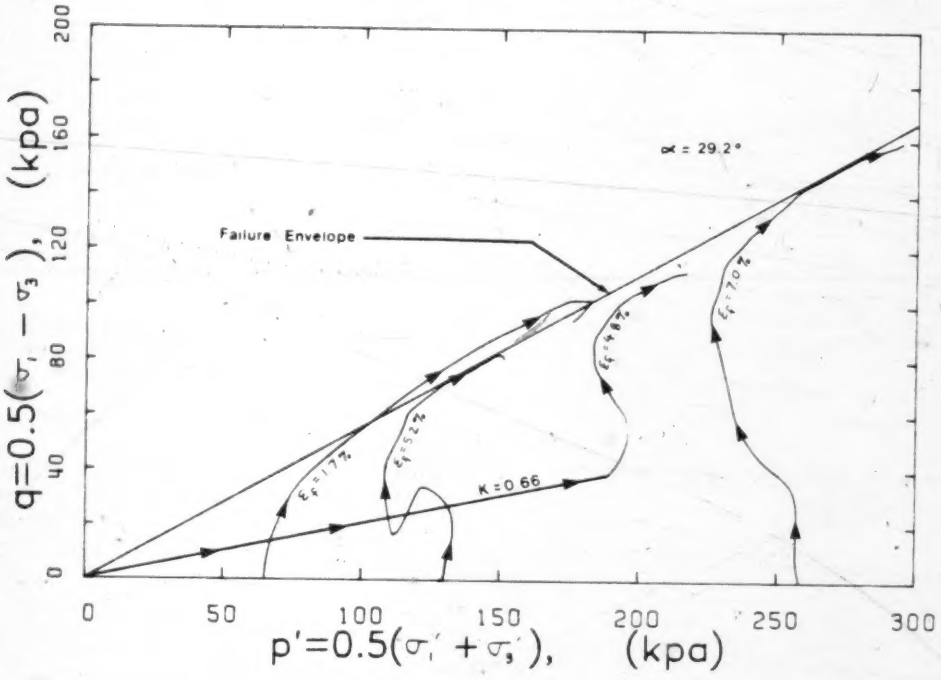

Figure 6.6 Effective stress paths for the triaxial tests in Figure 6.4 and 6.5 (mod. Konrad, 1985).

surface include different stress paths which lead to reductions in shear strength beyond the triaxial compression results, for example, direct simple shear (Ladd et al, 1985).

Should one denote failure as occurring in a triaxial specimen of dilatant silt when the stress path first touches the critical state line, or should one take failure as occurring at the point where strain-hardening ceases and the soil begins to strain-soften? Clearly, the failure strength depends upon the amount of strain involved. For this study, failure was assumed to have occurred at the point where the effective stress path first reaches the failure envelope.

Figure 6.7 shows the Mohr envelope for the tests conducted by Konrad (1985), resulting in an effective angle of shearing resistance of 34 degrees and a cohesion intercept equal to zero. This indicates that the silts are normally to perhaps slightly overconsolidated. Unfortunately, silts are quite susceptible to disturbance during sampling, which may be reflected in the lack of a small amount of cohesion in the triaxial samples.

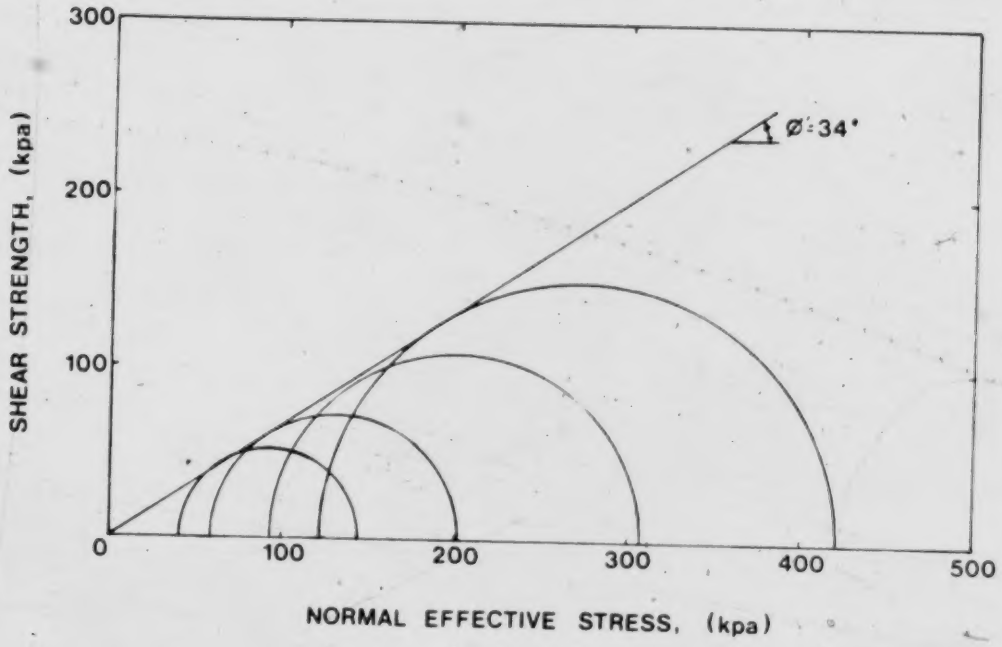

Figure 6.7 Failure envelope for triaxial compression tests performed on Beaufort Sea silt (mod. Konrad, 1985).

Conclusions

This study has been undertaken to determine the state of consolidation within the surficial sediments covering the continental shelf in the Canadian Beaufort Sea. Testing was also conducted to determine the permeability characteristics of these sediments. An apparatus was developed and constructed in order to perform this specialized testing.

Samples were supplied by the Geological Survey of Canada, taken during several field programs conducted in the Beaufort Sea over the past three years. Strength properties were determined from representative samples taken in both surficial units A and B. Recommendations for further study will be presented later in this section.

6.1 General

This study began with a review of the surficial geology in the Beaufort Sea which later facilitated the identification of different soil types and was used as a basis for relating the geotechnical behaviour to the geologic history. It became evident that one-dimensional consolidation testing provided useful information on stress history, once the significance of the phenomenon of apparent overconsolidation was understood.

6.2 Consolidation Testing

The occurrence of apparent overconsolidation was shown to be related to the age of the sediments through the rate of sedimentation, as well as the depth below seabed. The effect of sampling and handling disturbance is to decrease the accuracy with which the preconsolidation pressure is determined. More data on rates of sedimentation and sediment age is needed before comparisons can be made with confidence between areas having different depositional environments.

Clayey sediments existing at very shallow burial depths were shown to have unusually high values of OCR, more so than underlying silts. This is attributed to the small stresses existing within the uppermost unit (A) and is a direct result of a finite cohesion intercept at the mudline. It became obvious that specialized sampling and testing procedures are required for these very soft clays in order to minimize sample disturbance.

Because a certain amount of cohesion is created between clay particles existing at the mudline during deposition, and possibly later through ageing, the very nature of the equation for calculating OCR becomes asymptotically unstable near the mudline. It is doubtful whether enough sensitivity remains in the present definition of OCR within this zone of 6 to 10 meters below seabed, and a redefinition of the stress history interpretation is needed to make use of consolidation data. A more useful parameter for evaluating relative amounts of overconsolidation is the difference

between the preconsolidation and the effective overburden pressure. This could then be divided by the existing effective overburden pressure to yield a better measure of overconsolidation. Using this technique, it should be possible to differentiate between overconsolidation caused by ageing and/or cyclic loading within the apparently overconsolidated zone, and overconsolidation existing at unconformities that have been exposed to significant overconsolidation by subaerial exposure and dessication along with thaw consolidation.

The technique of strain energy has been used to determine values of preconsolidation and overburden pressure for comparison with average values obtained by the more conventional Casagrande construction. The results from the strain energy method fell well within the sensitivity of the Casagrande technique. The swelling and compressive behaviour of the surficial soft marine clays was dominated by the predominance of illite.

The behaviour of the recent marine sediments in the Beaufort Sea is shown to be completely consistent with the behaviour of other apparently or quasi-overconsolidated marine sediments found in the deep sea.

6.3 Permeability Testing

The surficial marine clays have been shown to possess extremely low coefficients of permeability. Comparisons have been made between values predicted from time-compression

oedometer data and measured values using the modified Anteus apparatus.

Agreement was consistently found between values calculated based on both the square root of time and the logarithm of time methods of plotting the compression data, which gave slightly higher values of permeability than measured.

A distinction was made between measured permeabilities in the surficial clays and the transgressive interbedded silts and clays found in the Beaufort Sea. The clayey sediments possessed high proportions of illite, and measured permeabilities corresponded closely to measurements made on aged clays from the deep-sea (Silva et al, 1981).

A linear relationship was noted between log permeability and void ratio, which is consistent with data reported by Silva et al (1981).

6.4 Shear Strength Testing

Data was obtained from isotropically consolidated triaxial compression tests which showed that the soft surficial clays possess a measureable effective cohesion, indicating that they are slightly overconsolidated. The effective angle of shearing resistance was equal to 27.5 degrees for this elasto-plastic material (1 to 2 m bsb.), indicating that the standard piston corer used was effective in obtaining undisturbed samples in these very soft sediments.

No cohesion was detected from triaxial tests on silt samples from below the soft surficial clays, which agreed with normally consolidated behaviour observed in consolidation tests on the same material at similar depth. The angle of shearing resistance was somewhat higher, being 34 degrees for the silt. The silts behaved in a highly dilatant manner during undrained shear and strain-hardened significantly after reaching the failure envelope before ultimate failure.

6.5 Recommendations for further study

More back pressure consolidation testing is required on a site-specific basis to determine a better understanding of the relationship between the amount of overconsolidation caused by sub-aerial erosion and dessication and the amount of overconsolidation created through deposition and ageing. Future sampling should be undertaken in areas of anticipated post-depositional modification, for example in the Mackenzie Trough between the 30 and the 50 meter water depth, and also on the outer continental shelf at the level of the minor unconformity created during the stillstand or recent recession in sea level proposed by Hill et al (1985).

The interpretation of stress history based on oedometer data generally does not support the existence of unusually high in situ lateral stresses. However, the area around Sauvrak does appear to be anomalous based on the profile of vertical preconsolidation pressure as compared to the rest

of the Beaufort Sea. High lateral stresses occurring in situ need to be investigated, particularly within surficial clayey sediments. High lateral stresses occurring within competent silt units may in fact result in some strain hardening during the application of an additional shearing force. However, the stresses set up during ice loading can serve to rotate the major principal stress, subsequently decreasing the average shearing resistance along a failure surface, leading to strain hardening at first followed by progressive failure. This would be more likely to be initiated within the weakest, least dilatant soil layer, which herein comprises unit A.

The effective stress path followed during unloading of beaufort Sea soils appears to fal through the in situ yiel surface, resulting in the fact that disturbance is largely unavoidable for these soils. This effect is caused by the narrow, almost bullet-shaped curvature of the yield surface and is most pronounced in silts. (Jefferies, pers. comm., 1985). The highly dilatant nature of these silts almost certainly results in a loss of sample quality during sampling. It is thought that the technique of strain energy is able to recover lost sample quality and can accurately predict effective overburden and preconsolidation pressures in samples taken both in the vertical and the horizontal direction (Jefferies, pers. comm., 1985).

This may be true, but the author is skeptical since disturbance during sampling tends to reorient the soil

structure which means that the in situ stress path cannot be recreated and the soil must behave differently during reloading. Highly structured soils like these silts would thus appear disturbed in any test and the memory of the yield strength achieved in situ would be degraded. This conclusion is verified by results of a constant-rate-of-strain consolidation test conducted on an undisturbed sample from Ukalerk and analyzed by the author and Ms. K. Moran.

The constant-rate-of-strain test applies a changing load continously to the sample, avoiding the effects of load-increment ratio, secondary consolidation during the test; thus resulting in an instantaneous compression curve. The same degree of disturbance in this test was observed as in standard oedometer tests on similar material, even after application of the technique of strain energy.

It is finally proposed that stress-controlled triaxial tests be performed to determine the shape and location of the yield surface for both the soft marine clays and the highly stratified, dilatant transgressive silts in the Beaufort Sea. Knowledge of the value of the coefficient of earth pressure at rest (K_o) is essential to the recreation of the in situ stress state in triaxial samples and is required for accurate determinations of the actual shearing resistance of the foundation soils. This would neccesitate the stress-controlled triaxial programme containing at least one or two K_o tests.

References

ASTM. 1984. Symposium on Laboratory and In-Situ Determination of Strength of Marine Soils. American Society for Testing and Materials, Jan.

Bishop, A.W. and Henkel, D.J. 1962. The Measurement of Soil Properties in the Triaxial Test. 2nd. ed., Edward Arnold Ltd., London.

Bjerrum, L. 1967. Engineering Geology of Norwegian Normally-Consolidated Marine Clays as Related to Settlements of Buildings. Geotechnique, Vol. 17, pp. 81-118.

Black, D.K. and Lee, K.L. 1973. Saturated Laboratory Samples by Back Pressure. Journal of the Soil Mechanics and Foundation Division, ASCE, Vol. 99, No. SM1, pp.75-93.

Blasco, S.M. and O'Connor, M.J. 1982. The Relationship Between Surficial Geology and the Ice Scouring in the Southern Beaufort Sea. Presented at the NRC Workshop on Ice Scour, Montebello, Quebec.

Brown, R.J.E. and Kupsch, W.O. 1974. Permafrost Terminology. ACGR/NRC Technical Memoramdum No. 111, 62 p.

Bryant, W.R., Cernock, P. and Morelock, J. 1967. Shear Strength and Consolidation Characteristics of Marine Sediments from the Western Gulf of Mexico. in: Marine Geotechnique, ed. A.F. Richards, Univ. of Illinois Press, Urbana, pp. 41-62.

Bryant, W.R., Deflache, A.P. and Trabant, P.K. 1974. Consolidation of Clays and Carbonates in Deep-Sea Sediments. in: Physical and Mechanical Properties, ed. A.L. Inderbitzen, Plenum Press, New York, pp. 209-244.

Burmister, D.M. 1951. The Application of Controlled Test Methods in Consolidation Testing. Symposium on Consolidation Testing of Soils, American Society for Testing and Materials, STP 126, pp. 83-97.

Callender, G.W., Jr. 1973. Compressibility Characteristics of Submarine Sediments and Settlement Estimation for Ocean Structures. Ph.D. thesis, Georgia Inst. of Tech., June.

Carchedi, D.R. 1979. Apparent Overconsolidation and Intrinsic Strength of Deep Sea Sediments. M.Sc. thesis, Univ. of Rhode Island, 163 p.

Casagrande, A. 1936. The Determination of the Pre-Consolidation Load and its Practical Significance. Proc. First International Conference on Soil Mechanics and Foundation Engineering, Vol. 3, pp. 60-64.

Crooks, J.H.A. and Graham, J. 1976. Geotechnical Properties of the Belfast Estuarine Deposits. Geotechnique, Vol. 26, No. 2, pp. 293-315.

De Josselin de Jong, G. 1968. Consolidation Models Consisting of an Assembly of Viscous Elements of a Cavity Channel Network. Geotechnique, Vol. 18, pp. 195-228.

Demars, K.R. 1975. Strength and Stress-Strain Behaviour of Deep Ocean Carbonate Soils. Ph.D. thesis, Univ. of Rhode Island.

Hamilton, E.L. 1964. Consolidation Characteristics and Related Properties of Sediments from Experimental Mohole (Guadalupe Site). Journal of Geophysical Research, Vol. 69, No. 20, pp. 4257-4269.

Hawkins, A.B. 1984. Submarine Slope Failures. in: Seabed Mechanics, ed. B. Denness, Graham and Trotham, London, pp. 51-64.

Hill, P.R., Mudie, P.J., Moran, K. and Blasco, S.M. 1985. A Sea Level Curve for the Canadian Beaufort Shelf. Canadian Journal of Earth Sciences, (IN PRESS).

Hivon, E. 1983. Stress History in the Beaufort Sea: An Initial Study. Unpublished Report to the Geological Survey of Canada, August.

Hunt, R.E. 1984. Geotechnical Engineering Investigation Manual, McGraw-Hill, 983 p.

Jakobson, B. 1953. Origin Cohesion of Clay. Proc. of the Third International Conference on Soil Mechanics and Foundation Engineering, Zurich, Vol. 1, pp.35-37.

Jefferies, M.G., Ruffell, J.P., Crooks, J.H.A. and Hughes, J.M.O. 1984. Some Aspects of the Behaviour of Beaufort Sea Clays. Symposium on Laboratory and In Situ Determination of the Strength of Marine Soils, American Society for Testing and Materials, Jan.

Kenney, T.C. 1964. Sea Level Movements and the Geologic Histories of the Post-Glacial Soils at Boston, Nicolet, Ottawa and Oslo. Geotechnique, Vol. 14, pp. 203-230.

Konrad, J-M. 1985. Undrained Cyclic Behaviour of Beaufort Sea Silt. ASCE Specialty Conference, Arctic '85, San Francisco, March 25-27, pp. 830-837.

Koppula, S.D. and Morgenstern, N.R. 1982. On the Consolidation of Sedimenting Clays. Canadian Geotechnical Journal, Vol. 19, No. 3, pp. 260-268.

Ladd, C.C., Weaver, J.S., Germaine, J.T. and Sauls, D.P. 1985. Strength-Deformation Properties of Arctic Silt. ASCE Specialty Conference, Arctic '85, San Francisco, March 25-27, pp. 820-829.

Lambe, T.W. and Whitman, R.V. 1969. Soil Mechanics. John Wiley and Sons, New York, 553 p.

Lowe, J. and Johnson, T.C. 1960. Use of Back Pressure to Increase Degree of Saturation of Triaxial Test Specimens. ASCE Research Conference on Shear Strength of Cohesive Soils, Boulder, Col., pp. 819-836.

Lowe, J., , Zaccheo, P.F. and Feldman, H.S. 1964. Consolidation Testing with Back Pressure. Journal of the Soil Mechanics and Foundation Division, ASCE, Vol. 90, No. SM5, pp. 69-86.

Mackay, J.R. 1958. Glacier Ice-Thrust Features of the Yukon

Coast. Geological Bulletin No. 13, pp. 5-21.

Martin, G.R., Lam, I. and Tsai, C. 1980. Pore Pressure Dissipation During Offshore Cyclic Loading, Journal of the Geotechnical Engineering Division, ASCE, Vol. 106, No. GT9, pp. 981-996.

McClelland, B. 1967. Progress of Consolidation in Delta Front and Prodelta Clays of the Mississippi River. in: Marine Geotechnique, ed. A.F. Richards, Univ. of Illinois Press, Urbana, pp. 22-40.

Mesri, G. 1973. Coefficient of Secondary Compression. Journal of the Soil Mechanics and Foundation Division, ASCE, Vol. 99, No. SM1, pp. 123-137.

Mesri, G. and Godlewski, P.M. 1977. Time-and-Stress-Compressibilty Interrelationship. Journal of the Geotechnical Engineering Division, ASCE, Vol. 103, No. GT5, pp. 417-430.

Mitchell, J.K. 1969. Temperatur Effects on the Engineering Properties and Behaviour of Soils. Highway Research Board Pub. No. 103, Proc. of the International Conference on Temperature Effects on Engineering Properties of Soils.

Moran, K. 1982. Cruise Report: CCGS Nahidik, August through September, Beaufort Sea Group, Atlantic Geoscience Centre.

Moran, K., Hill, P.R. and Harmes, B. 1984. Beaufort Sea Spring Program: Preliminary Data Report, Atlantic Geoscience Centre Internal Report.

Nacci, V.A., Kelly, W.E., Wang, M.C. and Demars, K.R. 1974. Strength and Stress-Strain Characteristics of Deep-Sea Sediments. in: Deep Sea Sediments: Physical and Mechanical Properties, ed. A.L. Inderbitzen, Plenum Press, New York, pp. 129-150.

Nacci, V.A., Wang, M.C. and Demars, K.R. 1975. Engineering Behaviour of Calcerous Soils. Civil Engineering in the Oceans , Vol. 1, pp. 380-400.

Noorany, I. 1984. Phase Relationships in Marine Soils. Journal of the Geotechnical Engineering Division, ASCE, Vol. 110, No. 4, pp. 539-543.

Noorany, I. and Gizienski, S.F. 1970. Engineering Properties of Submarine Soils; A State-of-the Art Review. Journal of the Soil Mechanics and Foundation Engineering Division, ASCE, Vol. 96, No. SM5, pp. 1735-1762.

O'Connor, M.J. 1977. Gas Seeps, Permafrost and Acoustic Voids in the Southern Beaufort Sea. Symposium of Permafrost Geophysics, Saskatoon, Sask.

O'Connor, M.J. and Associates. 1980. Development of a Proposed Model to Account for the Surficial Geology of the Southern Beaufort Sea. Report to the Geological Survey of Canada, 2 vols., Open File Report 954.

O'Connor, M.J. and Associates. 1982a. An Evaluation of the Regional Surficial Geology of the Southern Beaufort Sea. Report to the Geological Survey of Canada, March, 187 p.

O'Connor, M.J. and Associates. 1982b. A Review of the Distibution and Occurrence of Shallow Acoustic Permafrost in the Southern Beaufort Sea. Report to the Geological Survey of Canada, March, 114 p.

O'Connor, M.J. and Associates. 1984. Surficial Geology of Mackenzie Trough. Report to the Geological Survey of Canada, March.

Olson, L.O. and Ewart, T.E. 1982. In Situ Heat Transfer Experiments. Subseabed Disposal Program, Annual Report, Vol. 2, Part 1.

Parry, R.H.G. and Wroth, C.P. 1981. Shear Stress-Strain Properties of Soft Clay. in: Soft Clay Engineering, ed. E.W. Brand and R.P. Brenner, Elsevier Scientific Publishing Co., Amsterdam, pp. 309-364.

Poley, D. 1982. Detailed Study of Submerged Pingo-Like Features in the Canadian Beaufort Sea. B.Sc. thesis, Dalhousie Univ., Halifax, August.

Quinlan, G. and Beaumont, C. 1981. A Comparison of Observed and Theoretical Postglacial Relative Sea Level in Atlantic Canada. Canadian Journal of Earth Sciences, Vol. 18, No.7, pp. 1146-1163.

Richards, A.F. 1976. Marine Geotechnics of the Oslofjorden Region. in: Laurits Bjerrum Memorial Volume, ed. N. Janbu, F. Jorsted and B. Kjoernsli, Norwegian Geotechnical Institute, Oslo, pp. 41-63.

Richards, A.F. 1984. Modelling and Consolidation of Marine Soils. in: Seabed Mechanics, ed. B. Denness, Graham and Trotham, London, pp. 3-8.

Richards, A.F. and Hamilton, E.L. 1967. Investigations of Deep Sea Sediment Cores, ; Consolidation. Proc. of the International Research Conference on Marine Geotechnology, Univ. of Illinois Press, Urbana, pp. 93-117.

Richards, A.F. and Parks, J.M. 1976. Marine Geotechnology: Average Sediment Properties, Selected Literature and Review of Consolidation, Stability, and Bioturbation-geotechnical Interactions in the Benthic Boundary Layer. in: The Benthic Boundary Layer, ed. I.N. McCave, Plenum Press, New York, pp. 159-181.

Roscoe, K.H., Schofield, A.N. and Wroth, C.P. 1958. On the Yielding of Soils. Geotechnique, Vol. 8, pp. 22-52.

Rosholt, J.N., Emiliani, C., Geiss, J., Koczy, F.F. and Wangersky, P.J. 1961. Absolute Dating of Deep-Sea Cores by the Pa^{231}/Th^{230} Method. Journal of Geology, Vol. 69, pp. 162-185.

Schmertmann, J.H. 1955. The Undisturbed Consolidation of Clay. Trans. ASCE, Vol. 120, pp. 1201-1233.

Schofield, A.N. and Wroth, C.P. 1968. Critical State Soil Mechanics. McGraw-Hill, London, 310 p.

Shearer, J.M. 1972. Geological Structure of the Mackenzie Canyon Area of the Beaufort Sea. Report of Activites, Part A, Geological Survey of Canada, Paper 72-1A, pp. 179-180.

Shepard, F.B. 1973. Submarine Geology. Harper and Row, New York, pp. 20-21.

Silva, A.J. 1978. Geotechnical Aspects of Sea Disposal of Radioactive Wastes, Research Progress Report: Annual Workshop of the Seabed Disposal Program, Nov. 16-18, Boulder, Col.

Silva, A.J. 1979. Geotechnical Properties of Deep Sea Clays - A Brief Discussion. First Canadian Conference on Marine Geotechnical Engineering, Calgary, pp. 262-269.

Silva, A.J. and Jordan, S.A. 1984. Consolidation Properties and Stress History of Some Deep Sea Sediments. in: Seabed Mechanics, ed. B. Denness, Graham and Trotham, London, pp.25-39.

Silva, A.J., Hollister, C.D., Laine, E.P. and Beverly, B. 1976. Geotechnical Properties of Deep Sea Sediments: Bermuda Rise. in: Marine Geotechnology, Vol. 1, No. 3, Crane, Russak and Co., pp. 195-232.

Silva, A.J., Hetherman, J.R. and Calnan, D.I. 1981. Low-Gradient Permeability Testing of Fine-Grained Marine Sediments. Permeability and Groundwater Contaminant Transport, American Society for Testing and Materials, STP 746, pp. 121-136.

Skempton, A.W. 1954.The Structure of Inorganic Soil (discussion). Proc. ASCE, Vol. 80, separate 478, pp. 19-22.

Skempton, A.W. 1960. Effective Stress in Soils, Concrete and Rocks. Conference on Pore Pressure and Suction in Soils, London, pp. 4-16.

Skempton, A.W. 1970. The Consolidation of Clays by Gravitational Compaction. Quarterly Journal of the Geological Society of London, Vol. 125, pp. 373-411.

Skempton, A.W. and Northey, R.D. 1953. The Sensitivity of Clays. Geotechnique, Vol. 3, pp. 30-53.

Tavenas, F., Des Rosiers, J-P., Leroueil, S., La Rochelle, P. and Roy, M. 1979. The Use of Strain Energy as a Yield and Creep Criterion for Lightly Overconsolidated Clays. Geotechnique, Vol. 29, No. 3, pp. 285-303.

Terzaghi, K. 1941. Undisturbed Clay Samples and Undisturbed Clays. Journal of the Boston Society of Civil Engineers., Vol. 28, pp. 211-231.

Wroth, C.P. 1979. Correlations of Some Engineering Properties of Soils. Second International Conference on Behaviour of Offshore Structures, Imperial College, London, Aug. 28-31, pp. 121-132.

Yorath, C.J. 1973. Geology of Beaufort-Mackenzie Basin and Eastern Part of Northern Interior Plains. in: Arctic Geology, ed. M.C. Ritcher, American Association of Petroleum Geologists, Memoir 19, pp.41-47.

Youssef, M.S., El Ramli, A.H. and El Demery, M. 1965. Relationships Between Shear Strength, Consolidation, Liquid Limit, and Plastic Limit for Remoulded Clays. Proc. Sixth International Conference on Soil Mechanics and Foundation Engineering, Montreal, Vol. 1, pp. 126-129.

Appendix A

Operating Manual for Modified Consolidometer/Permeameter

A.1 Operating Procedure

A.1.1 Consolidation

A.1.1.1 Saturation and Back Pressuring

1. Control panel is not pressurized; all valves off.
2. Open valves 9 and 10 on Back Pressure Reservoir.
3. Turn valve 8 to CONS.
4. Deair water in the deaireator; after deairing open valve 2 (deairaetor vent), deairaetor drain, and valve 1 (supply to system).
5. System has previously been deaired by running water through all lines until no air bubbles remain; deair line to bottom porous stone by opening valve 3, then closing.
6. Place boiled bottom porous stone in receptacle. Cover with a damp filter paper. Put aside for the momemt.
7. Push the soil sample from the thin-walled sampling ring into the teflon-lined consolidation ring using the spacer block previously used to trim the sample to its required height of 0.75 in. Weigh the sample along with the consolidation ring. Push the bottom receptacle with the bottom porous stone into the base of the consolidation ring until it lies flush.
8. Insert the consolidation ring into the hole in the base of the cell. Add a moist filter paper to the

top of the sample in the ring. Add the top porous block to the consolidation ring. Assemble the rest of the cell (add the lucite window to the cell; insert the loading cap into the hole beneath the loading platen.

9. Fill the cell with water almost to the top of the lucite wall by opening the supply valve on the top of the valve tree along with valve 5. Note that valves 4 and 6 must be closed. When the cell is full, close the supply valve but leave 5 open. Ensure that valve 19 on the top of the loading dome is closed to avoid accidentally loading the sample. It is necessary that the loading platen be fully retracted into the loading dome or there will not enough clearance between the sample and the loading cap. To push the platen into the dome, open valve 19 on the dome and valve F on the control panel. The load regulator must be set at minimum with no pressure in the system. The retraction of the loading platen is assisted by raising the entire dome above the height of the load reservoir and pushing with your fingers. Close valve 19 when the platen is fully retracted into the dome. Attach the loading dome to the base, engaging the bayonet locks.

10. The cell is now firmly anchored to the base. Close valve 3 and open valves 4 and 7. Check that valve 8

is in the CONS position for back pressuring. The sliding load reservoir should be at the zero mark during back pressuring.

11. The permeability system should be back pressured along with the sample at this point. This is accomplished by opening 15, setting 13 and 14 to the DOWN or UP position, closing 16, and opening 11 and 12. Check that the water level in both the back pressure and the permeability reservoirs is at the halfway mark. If it isn't, water must now be added to the back pressure reservoir by opening valve E on the control panel with the back pressure regulator set at minimum, and opening the water supply valve on the top of the valve tree until the water is at the appropriate level. Close the supply valve. To add water to the permeability reservoir, open the supply valve, valves 3 and 7, turn valve 8 to PERM, open 11 and 12 on the permeability reservoir, and valve G on the control panel until enough water has entered. Close the supply valve, valve 3 and turn 8 back to CONS. Actually, it makes no difference whether valve 3 is left open from here on, provided that the test is to be run with double drainage.
12. To back pressure the system, turn on the air supply and set the wall regulator to 150 psi. All regulators on the control panel should be set to minimum. Open valves H and I on the control panel

and close F and G. Open valve A. Only the back pressure regulator will be used so that the entire system receives equal pressure during back pressuring; as well as load increments up to 32 kpa (which will be delivered by the sliding load reservoir). Increase the back pressure regulator output in stages of 25 kpa until the required back pressure has been achieved. Allow sufficient time between increases for the pressure to be equalized.

13. Install the dial gauge to the top of the loading dome. After back pressuring, open valve 19 allowing the loading platen to fall and make contact with the sample. Note the final reading on the dial gauge at the end of back pressuring. This can be used to calculate a change in height during saturation based on a reference dial reading of 4567 div. for System A and 388 div. for System B; measured at the point of contact with an aluminum disk exactly 0.75 inches in height. It is important that one keeps track of which dial gauge holder goes with which cell.
14. It is possible using this apparatus to measure the swelling pressure by moving the sliding load reservoir up the rod in order to prevent any swell of the sample from occurring. The same back pressure is applied to both sides of the loading platen by the back pressure regulator; the swelling pressure can be calculated from the height of the sliding

load reservoir above the zero mark using the low range calibration charts (Figures A.2 and A.4). Of course, valve 19 must be open for application of the swelling pressure.

15. At the end of back pressuring, close valve 19. You may now begin the consolidation test.

A.1.1.2 Consolidation

1. Stress increments up to 32 kpa are supplied by the sliding load reservoir, and increments up to 1280 kpa are delivered with the load pressure regulator set to the desired load increment plus the back pressure; with the sliding load reservoir now set at the zero mark.
2. The dial gauge should now be removed from the cell entirely, along with its holder arm. Swing the DCDT into position over the stem in the loading dome and take a zero reading. Remember that this zero reading corresponds to the new height after saturation (as previously determined) and must be used in the calculation of the initial void ratio. This void ratio will not necessarilly be equal to the in situ void ratio as determined from the index properties.
3. With valve 19 closed, set the sliding load reservoir to the height corresponding to the desired stress increment (Table A.1). Simultaneously open valve 19, applying the stress increment, and begin data

aquisition at appropriate time intervals. It is suggested that the data aquisition system be operated manually for the first hour, after which it can be set to record data automatically. Valve 19 should be closed at the end of 100 percent primary compression, as determined from a plot of the square root of time versus change in height of the sample. Secondary compression data may be aquired later on in the test after the sample reaches the normally consolidated state.

4. For stress levels beyond 32 kpa, the sliding load reservoir must be set to zero and the load pressure applied with the load regulator. At this point, close valves H and I on the control panel. (Note that one must apply a pressure with the load regulator that includes the back pressure.) An option exists with this apparatus to perform either falling or constant head permeability tests with flow in either direction through the sample, at the end of each load increment.

A.1.2 Permeability

A.1.2.1 Constant Head Test

1. During the constant head test, the hydraulic gradient is varied across the sample by increasing the pressure differential. Hydraulic gradients up to

20 can be achieved by moving the permeability reservoir up or down with respect to the level of water in the back pressure reservoir; up for upward flow and down for downward flow through the sample. For higher gradients, the permeability reservoir is set even with the level of water in the back pressure reservoir, and a pressure differential is supplied by the permeability regulator as determined from:

$$\text{Perm. Press.} = \text{Back Press.} + i * H * 0.001 * \gamma_{sw} \quad \text{A.1}$$

where i is the hydraulic gradient, H is the present height of the sample, and γ_{sw} is the unit weight of the pore fluid.

2. To perform a permeability test between stress increments, one must make sure valve 7 is open, turn valve 8 to PERM, and close valve 15. Set both 13 and 14 to either UP or DOWN.
3. Set the permeability regulator to the back pressure and the permeability reservoir up or down to deliver the required hydraulic gradient. Begin taking readings of elapsed time and change in the level of water in the burette. After consistent values of rates of flow are established, change the gradient

and take a new set of flow readings. A linear relationship between the flow velocity and the hydraulic gradient is proof of verification of the existence of laminar flow and the test may be terminated.

4. The coefficient of permeability is given by Darcy's Law for laminar flow as being:

$$k = \frac{\nu_t * Q * L}{\nu_f * t * h * A} \qquad A.2$$

5. At the end of the permeability test, turn valve a back to CONS and apply the next stress increment.

A.1.2.2 Falling Head Test

1. No falling head tests were conducted in this study. Application of the procedure is not as straightforward as with the constant head test and is rarely used.

Calibration of modified Anteus back pessured consolidometers:

	SYSTEM "A"			SYSTEM "B"		
σ_v' (kpa)	HT. OIL RES. (cm)	B.P. + L.P. (kpa)	L.P. REG. (mV)	HT. OIL RES. (cm)	B.P. + L.P. (kpa)	L.P. REG. (mV)
2	9.8	--	--	8.0	--	--
4	18.8	--	--	17.1	--	--
5	23.4	--	--	21.7	--	--
8	37.0	--	--	35.4	--	--
10	46.0	--	--	44.6	--	--
16	73.2	--	--	72.1	--	--
20	91.3	--	--	90.4	--	--
32	145.7	--	--	145.4	--	--
40	--	263.020	-2.366	--	262.541	11.412
64	--	274.098	-2.476	--	273.576	11.935
80	--	281.483	-2.550	--	280.933	12.283
128	--	303.638	-2.770	--	303.003	13.328
160	--	318.407	-2.916	--	317.716	14.025
256	--	362.717	-3.356	--	361.856	16.115
320	--	392.256	-3.650	--	391.283	17.508
512	--	473.245	-4.454	--	479.562	21.688
640	--	524.125	-4.960	--	532.537	24.196
1024	--	676.765	-6.476	--	687.173	31.518
1280	--	778.525	-7.487	--	790.265	36.400

NOTE: Maximum load capacity of bellofram is 1000 lbs.

B.P. .....Back pressure = 250 kpa
L.P. .....Load pressure = variable
L.P. REG. .....Load pressure regulator output (Ch. 33)
HT. OIL RES. ....Height of sliding lo.. pressure reservoir above datum

Table A.1 Calibration chart showing load pressure settings for Systems A and B.

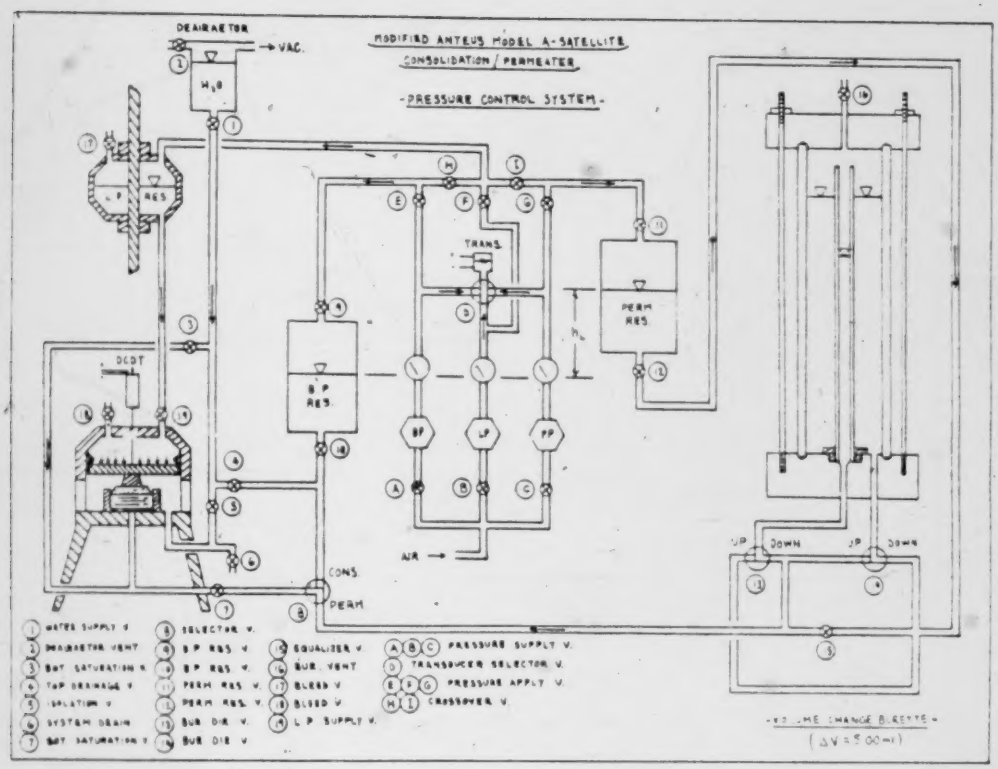

Figure A.1 Schematic of Modified Anteus Back Pressured Consolidometer/Permeameter

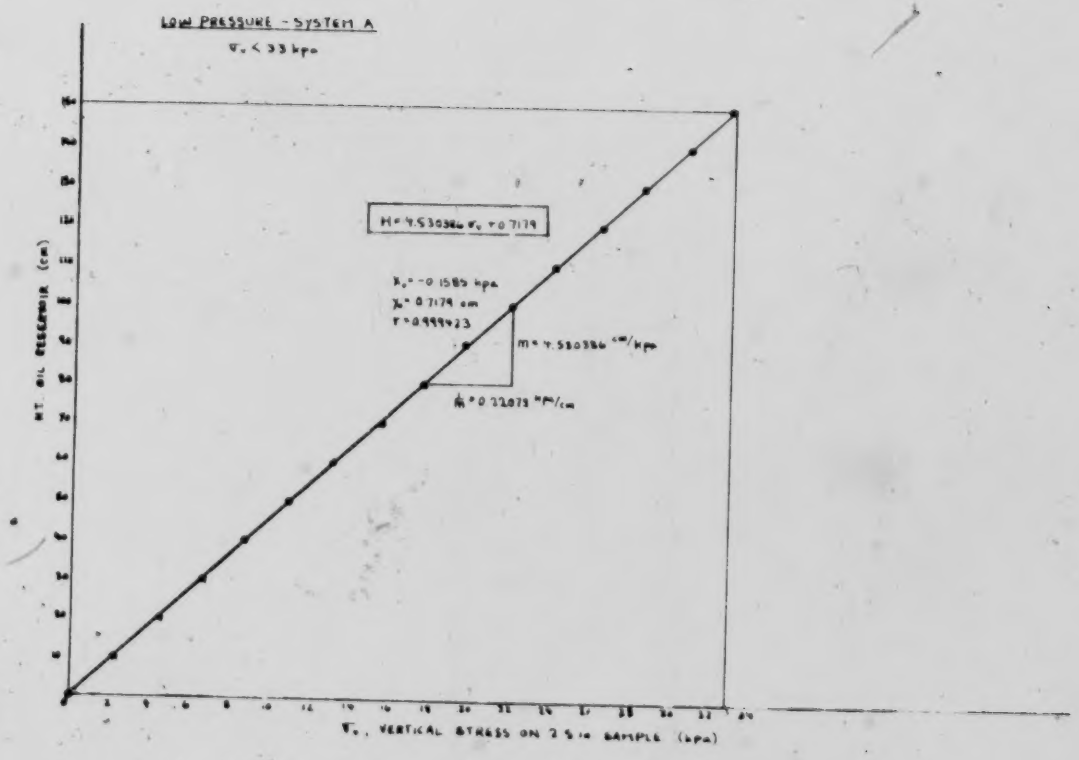

Figure A.2 Calibration of loading system of System A (low range).

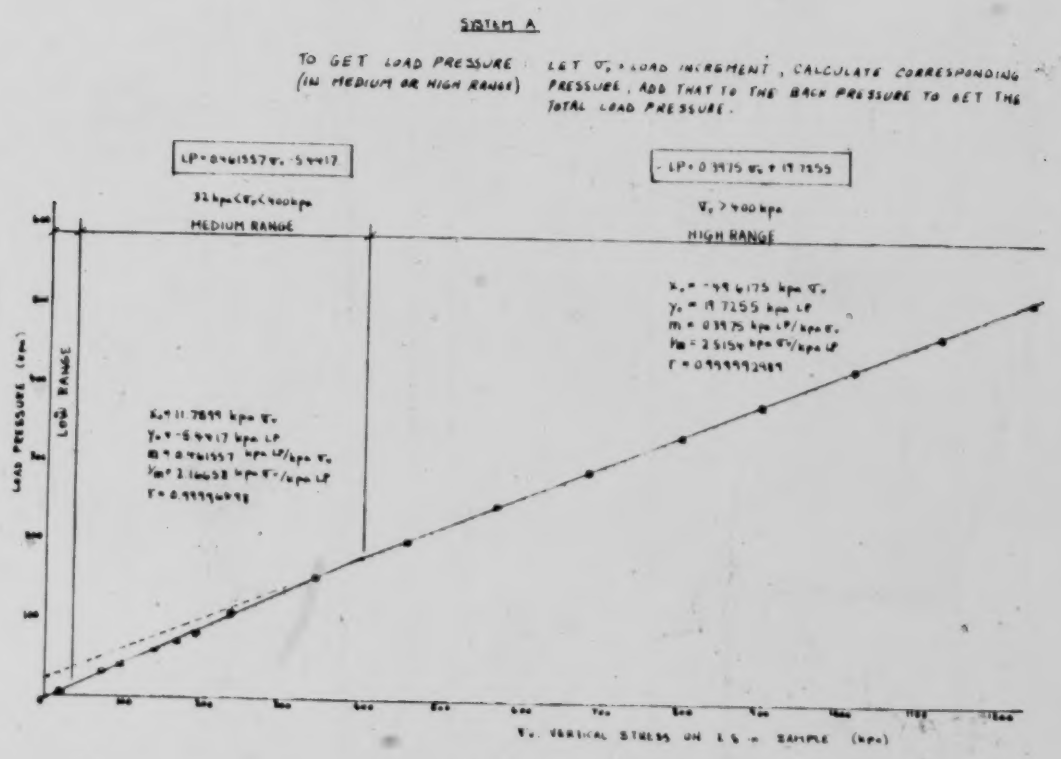

Figure A.3 Calibration of loading system of System A (high range).

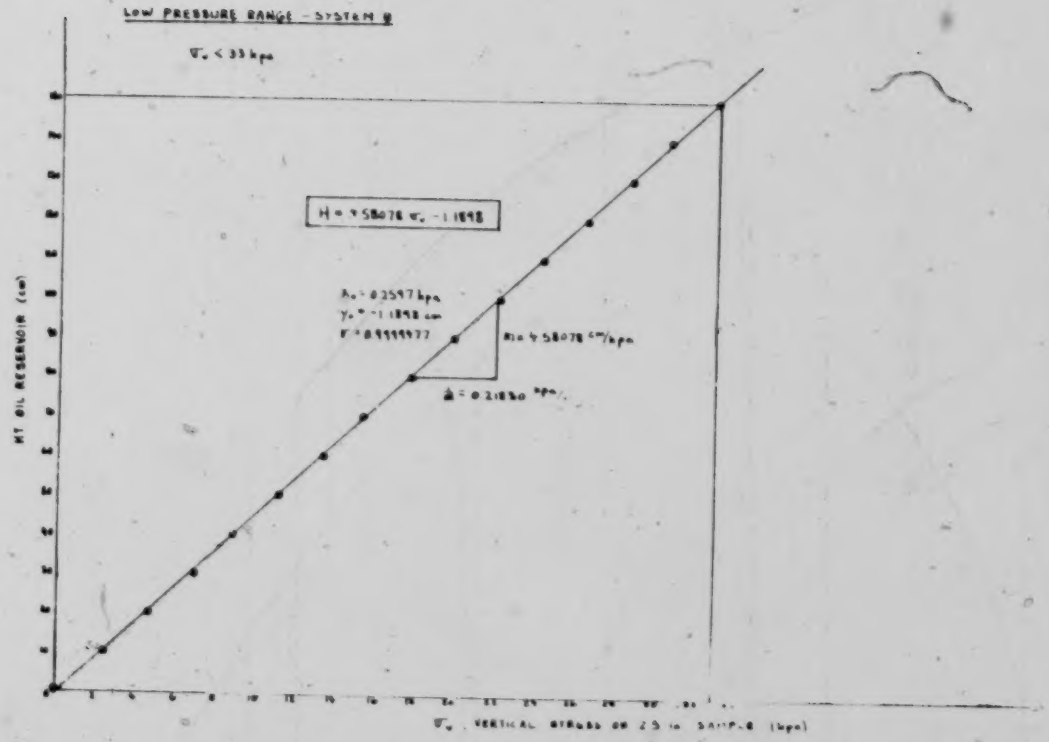

Figure A.4 Calibration of loading system of System B (low range).

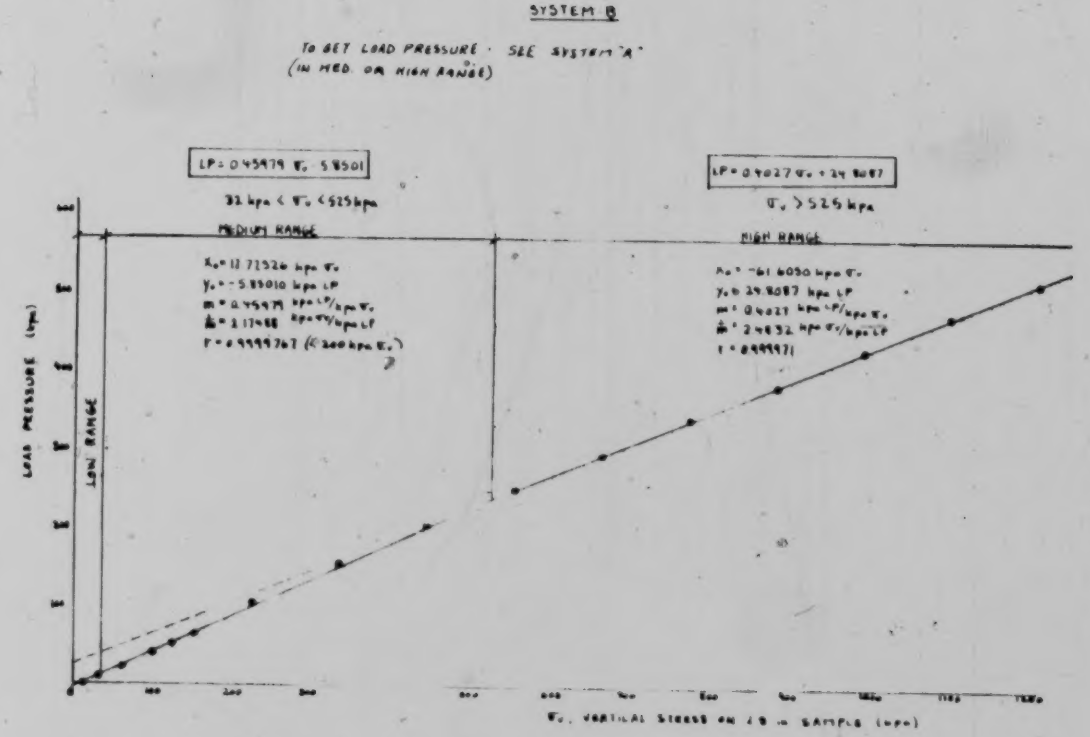

Figure A.5 Calibration of loading system of System B (high range).

Appendix B

Borehole Logs for all Sites

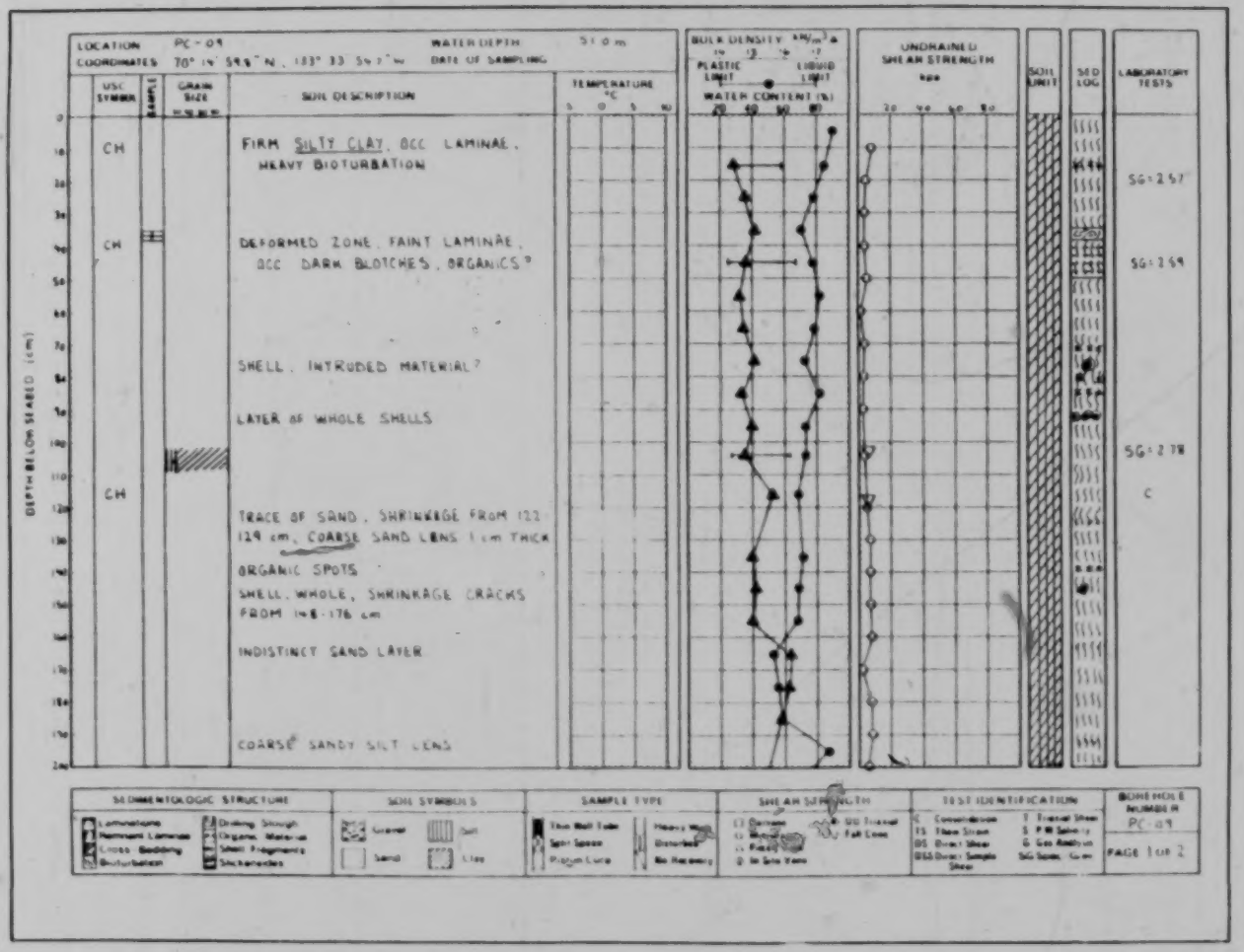

Figure B.1 Borehole log for PC-09 (1 of 2).

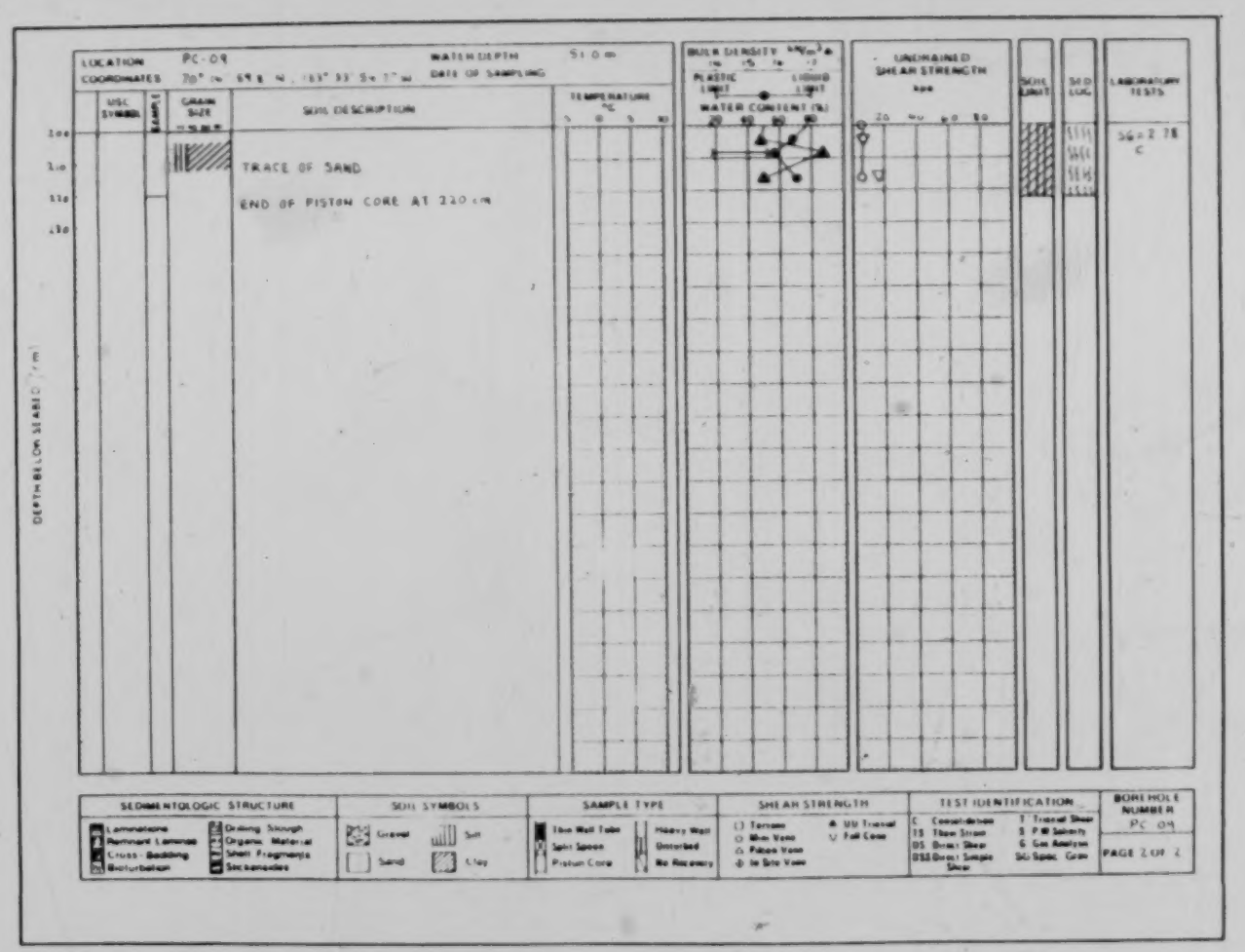

Figure B.2 Borehole log for PC-09 (2 of 2).

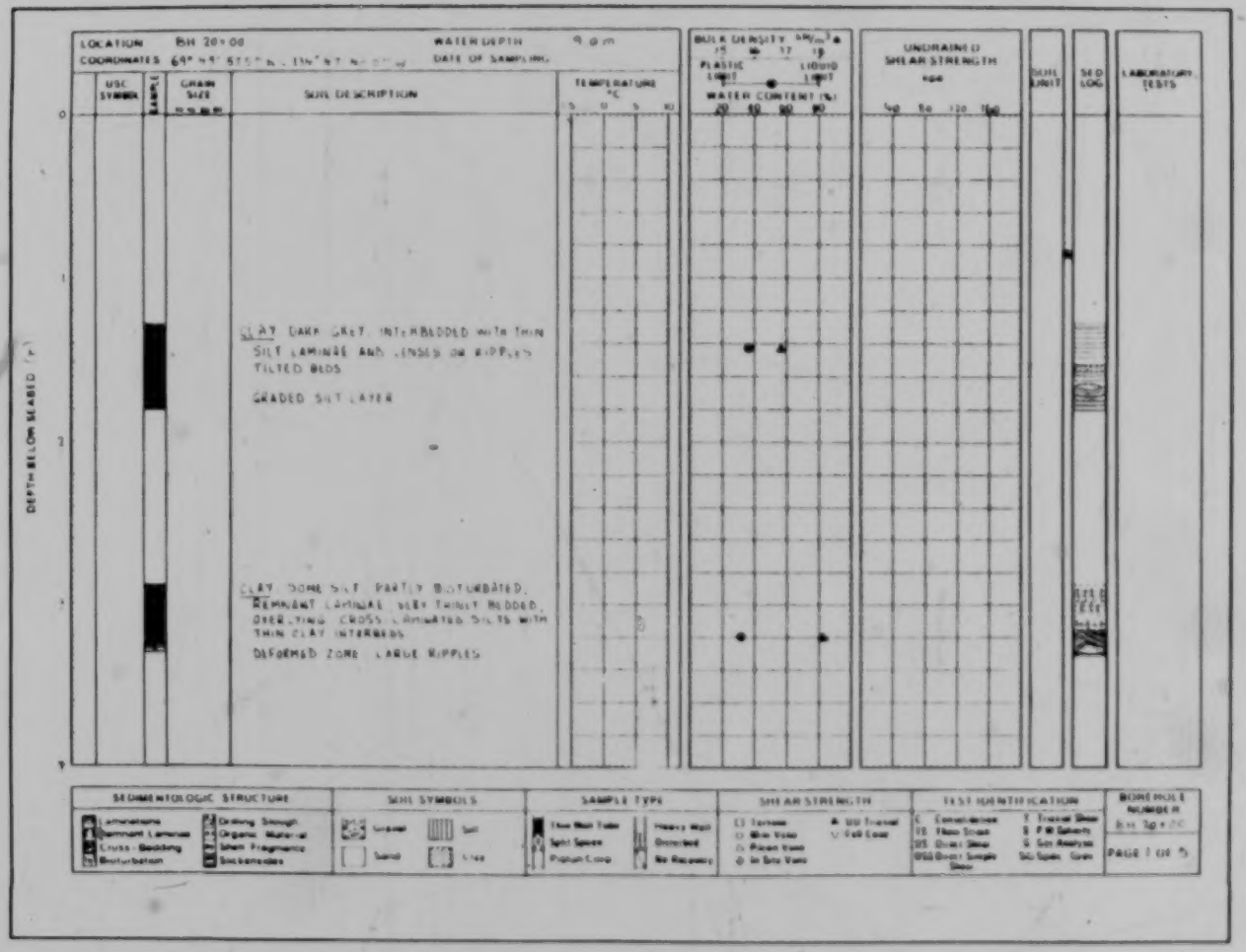

Figure B.3 Borehole log for BH 20+00 (1 of 5).

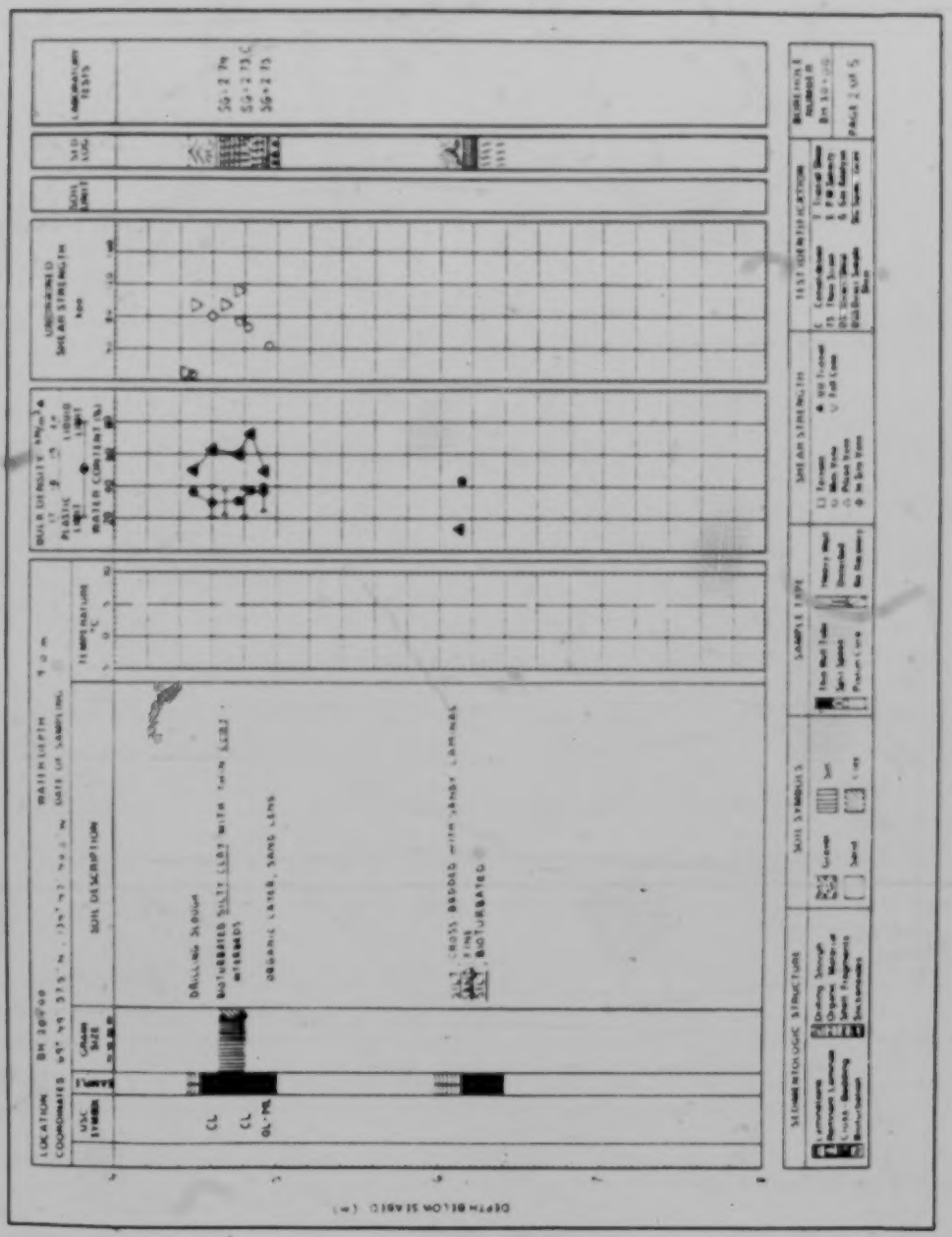

Figure B.4 Borehole log for BH 20+00 (2 of 5).

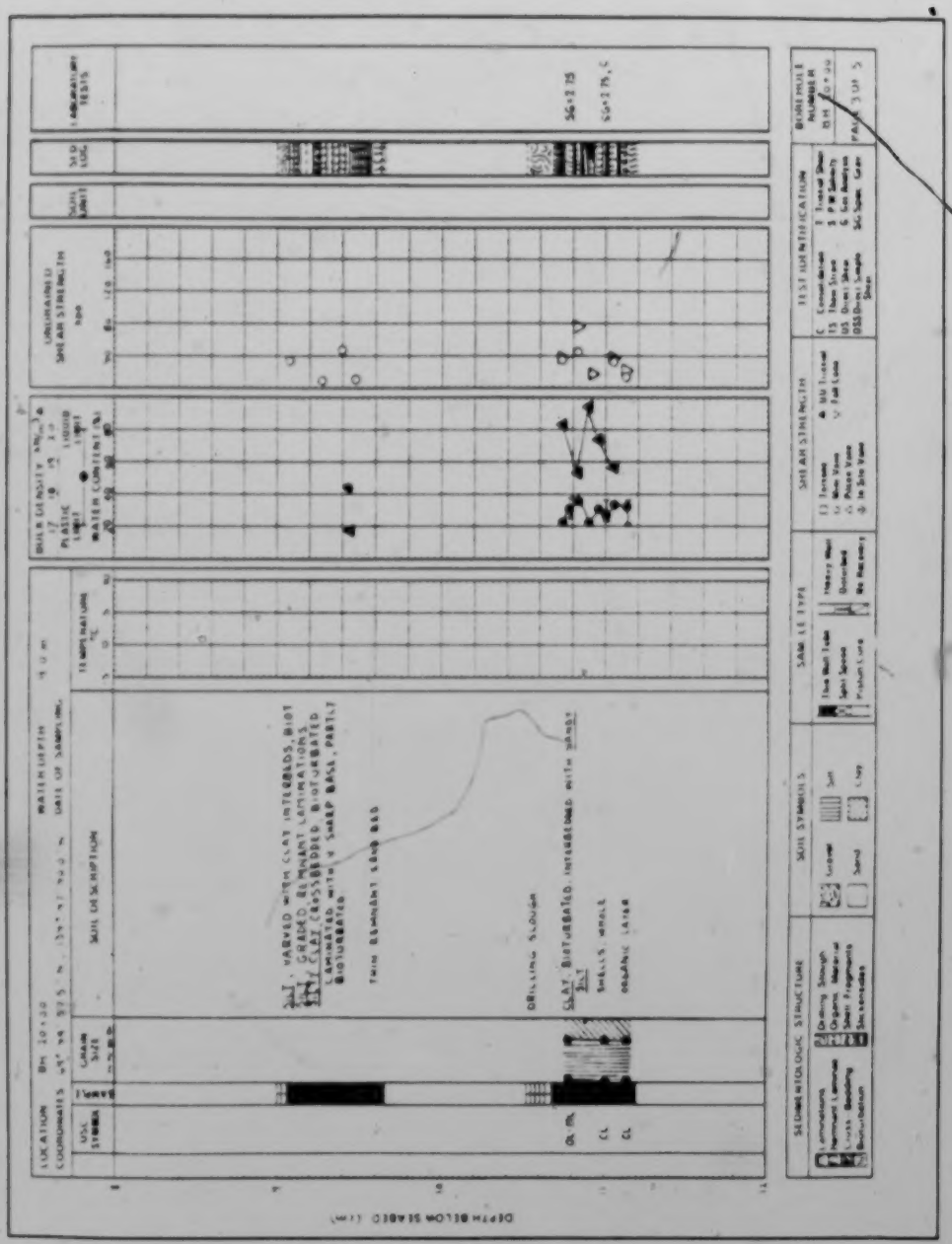

Figure B.5 Borehole log for BH 20+00 (3 of 5).

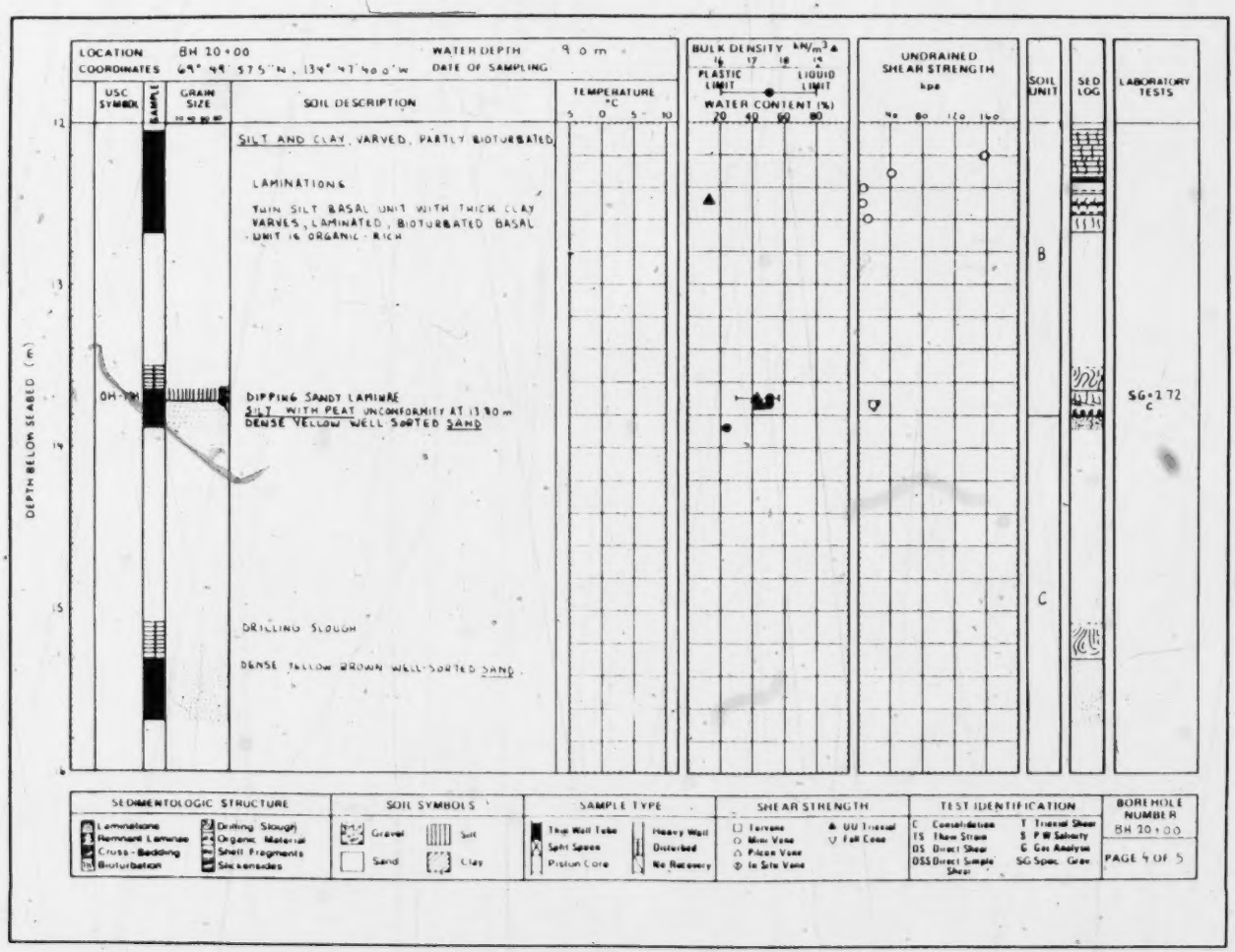

Figure B.6 Borehole log for BH 20+00 (4 of 5).

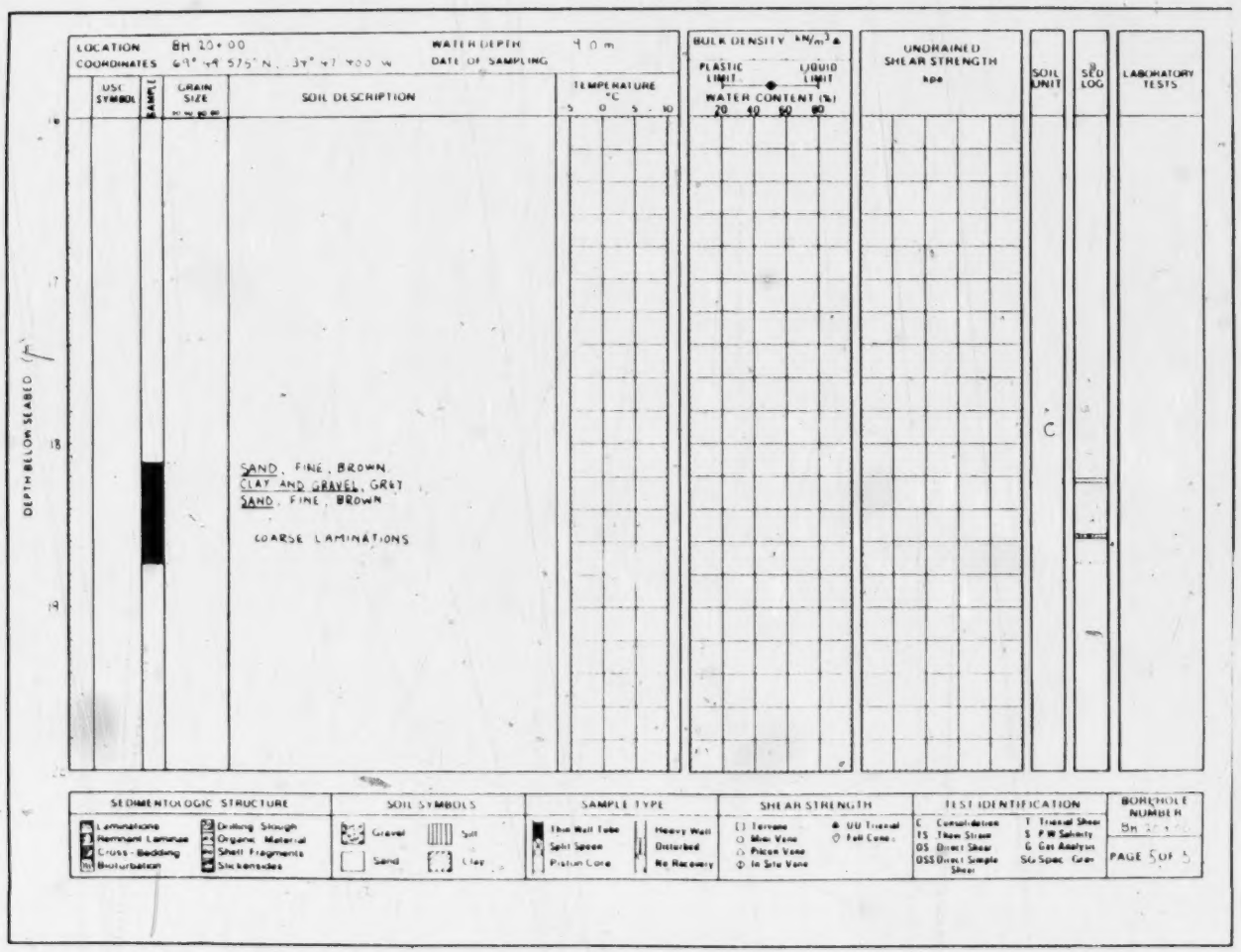

Figure B.7 Borehole log for BH 20+00 (5 of 5).

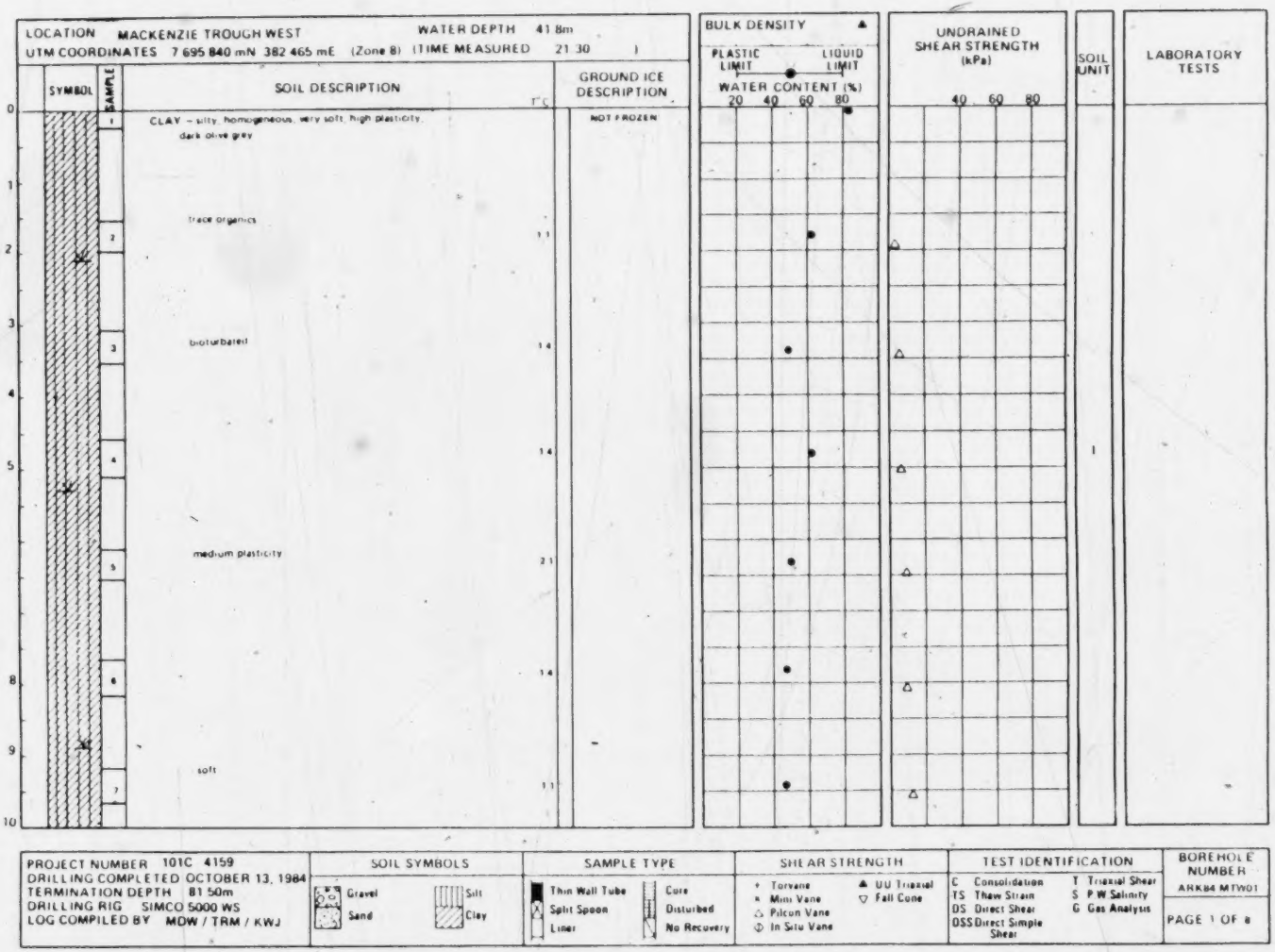

Figure B.8 Borehole log for BH MTWS1 (1 of 8).

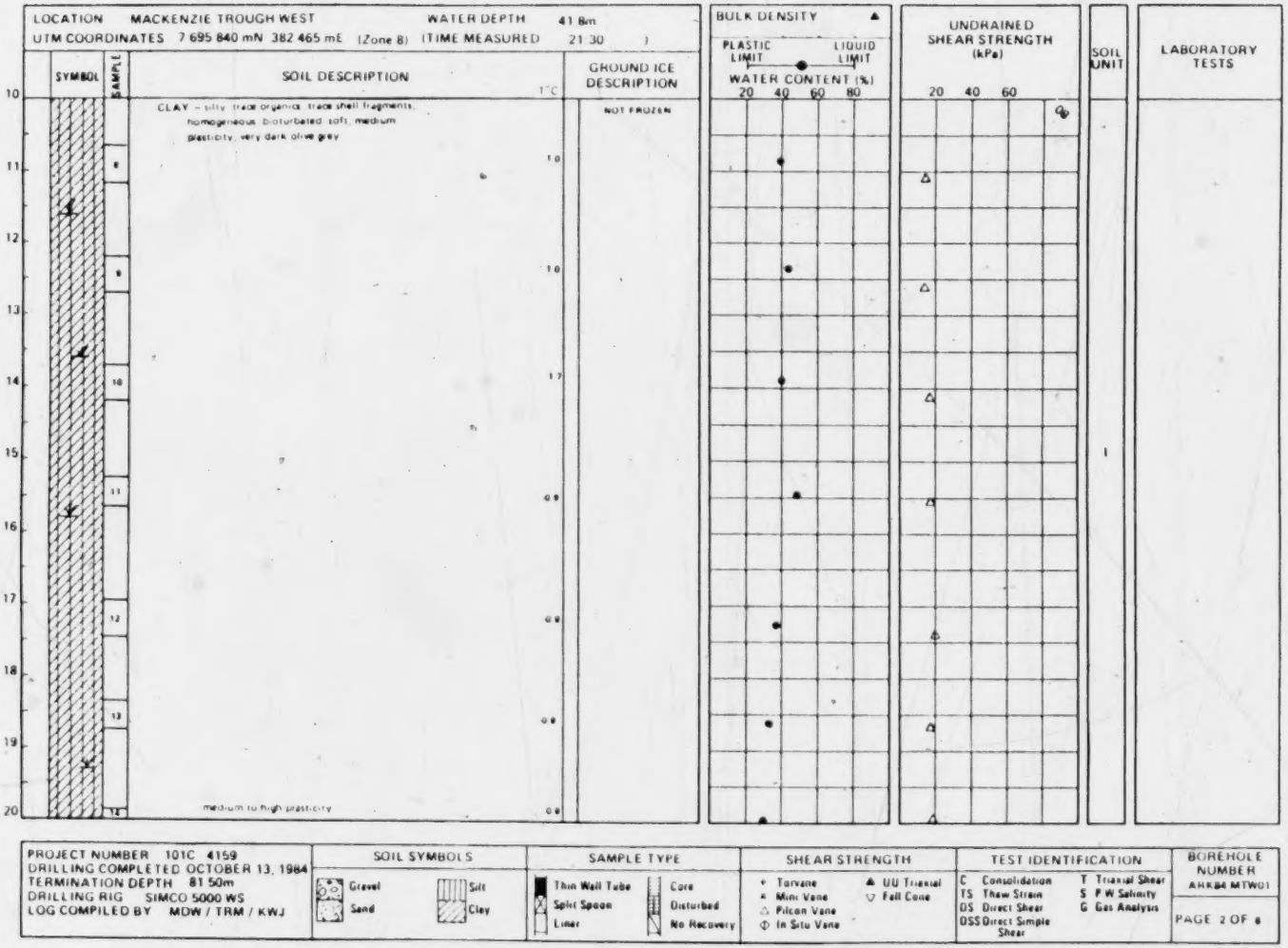

Figure B.9 Borehole log for BH MTWS1 (2 of 8).

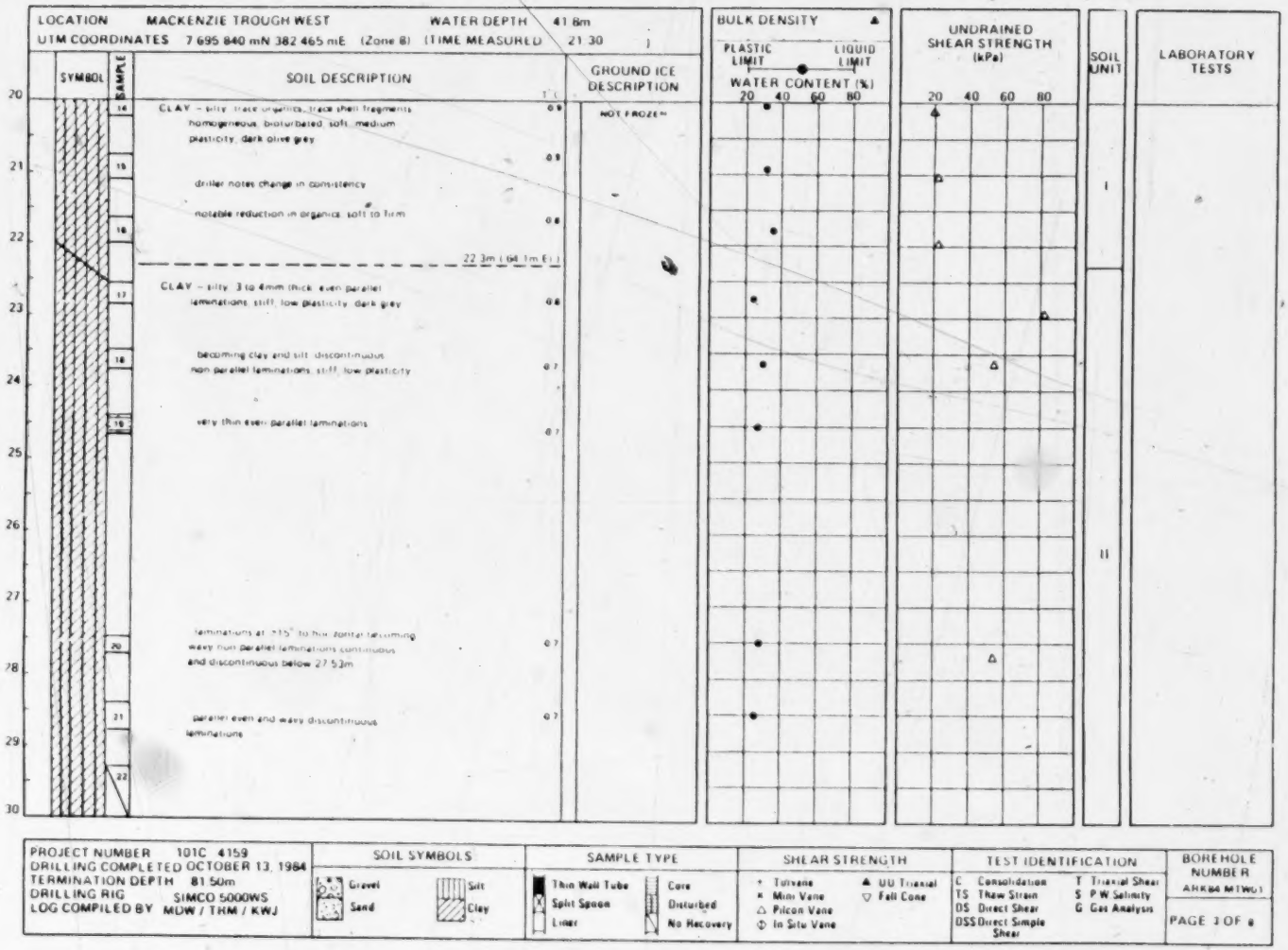

Figure B.10 Borehole log for BH MTWS1 (3 of 8).

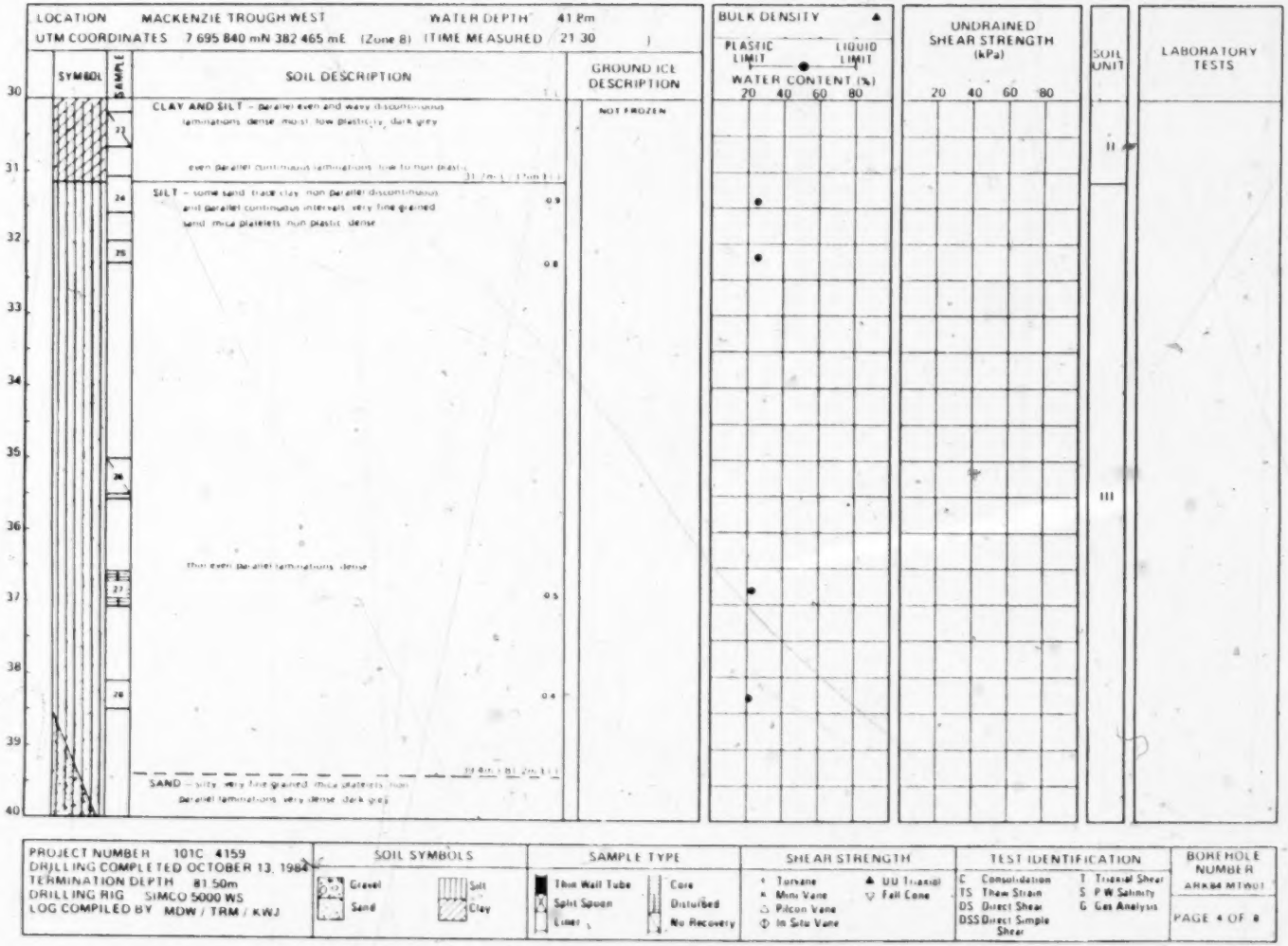

Figure B.11 Borehole log for BH MTWS1 (4 of 8).

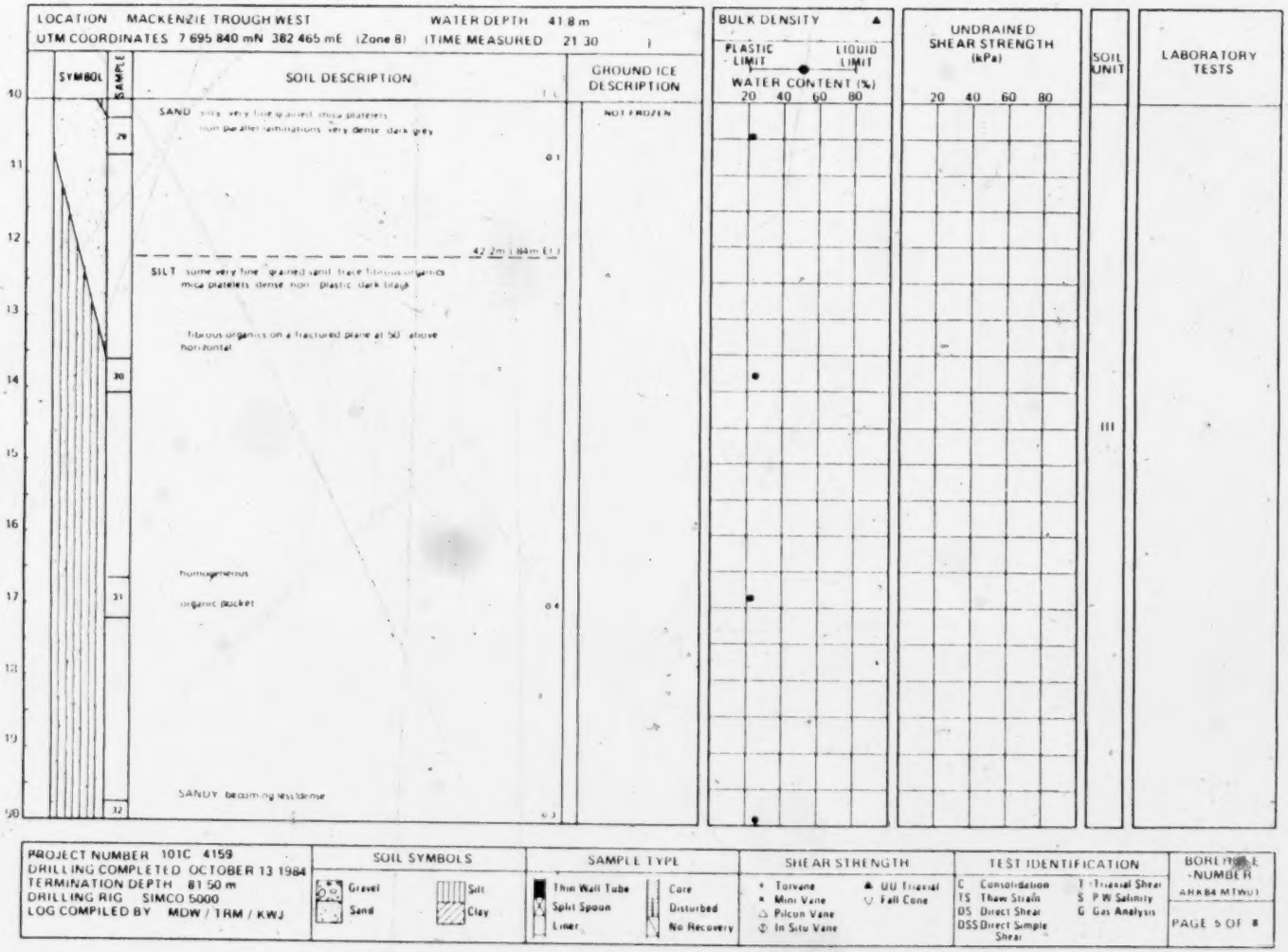

Figure B.12 Borehole log for BH MTWS1 (5 of 8).

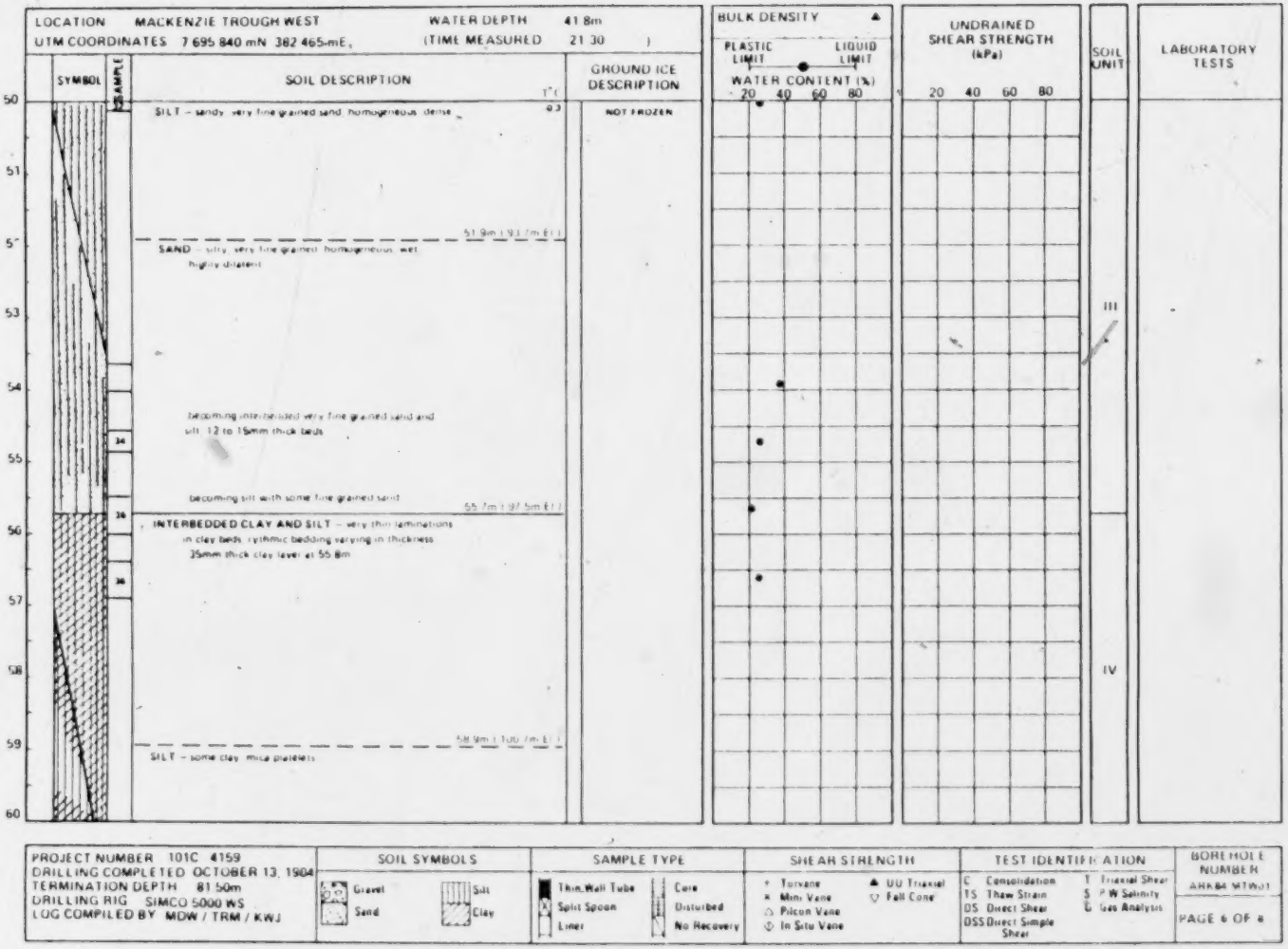

Figure B.13 Borehole log for BH MTWS1 (6 of 8).

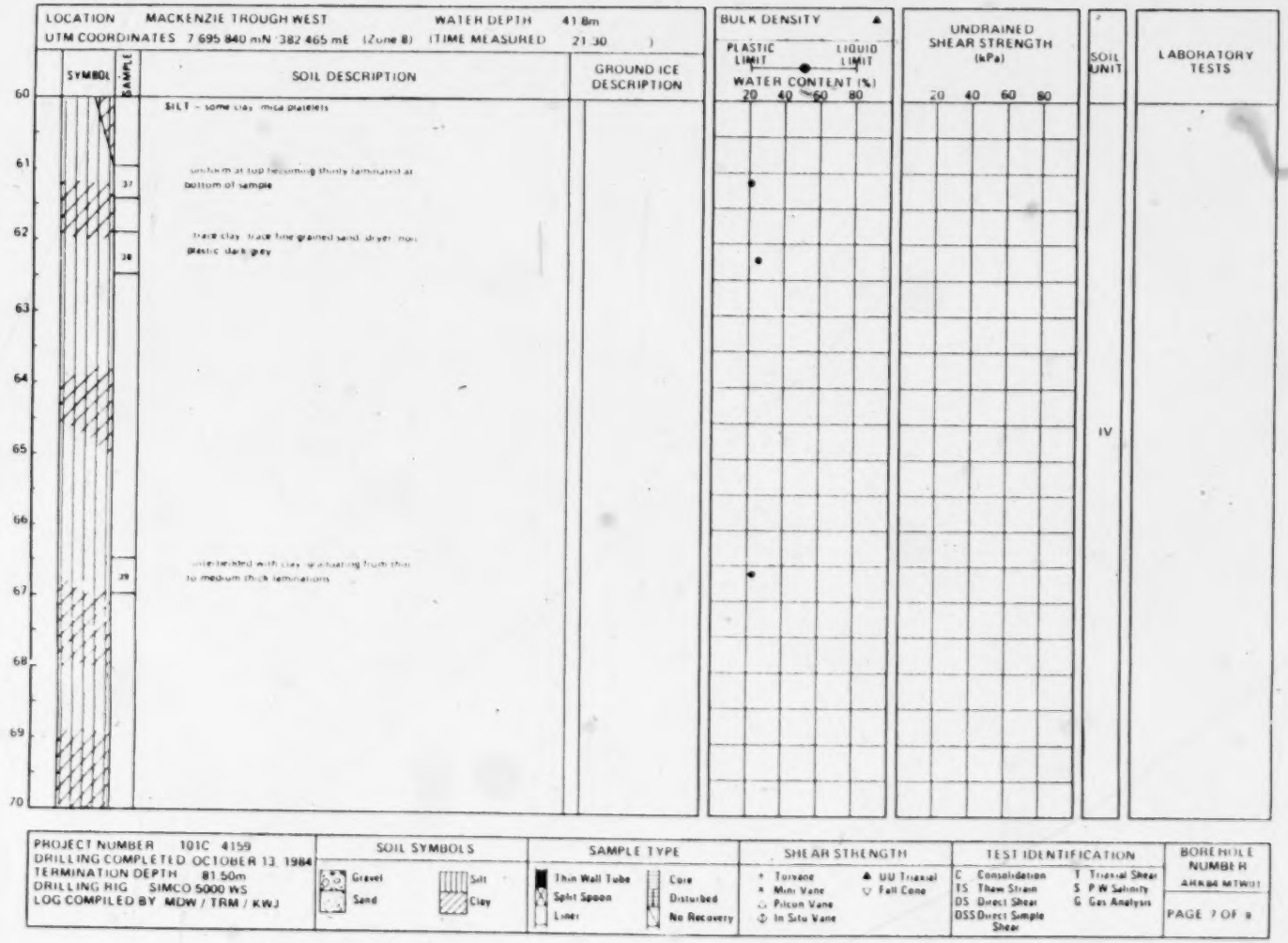

Figure B.14 Borehole log for BH MTWS1 (7 of 8).

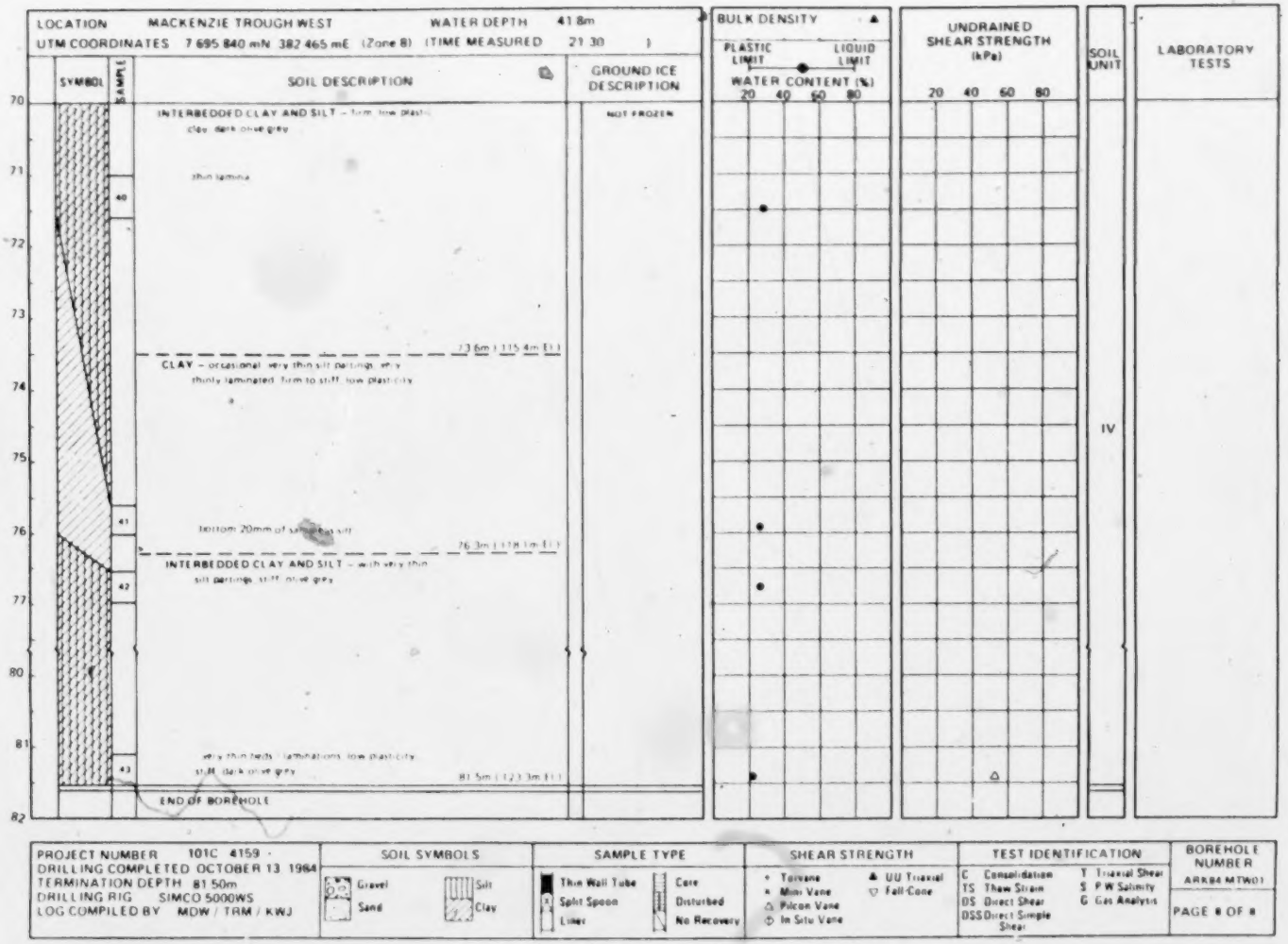

Figure B.15 Borehole log for BH MTWS1 (8 of 8).

Appendix C

Index Property Data Sheets for PC-09

Table C.1 Index property data for PC-09 (1 of 2).

BH NO PC-09

DEPTH BSB (cm)	w_n (%)	w_p (%)	w_L (%)	PI (%)	LI	γ (kN/m³)	G_s	PERCENT			C_u (kPa)		S_t	e_o	$k_{f.o's}$ (m/sec)	$\frac{C_u}{P_o}$	USC CLASS	ACTIVITY
								SAND	SILT	CLAY	VANE	CONE						
5	90.1					NA								2.505				
10		28.7	58.5	29.8	2.012		2.78 2.57				93					29.1	CH	
15	87.2	"	"	"	1.963	14.36	"							2.424				
20		"	"	"	1.825		"				66					7.3		
25	79.0	"	"	"	1.688	14.76	"							2.196				
30											56					9.8		
35	69.6					15.13								1.935				
40		26.3	67.2	40.9	1.145		2.78 2.59				59					3.0	CH	
45	76.7	"	"	"	1.232	14.77	"							2.132				
50		"	"	"	1.291		"				70					3.0		
55	81.5	"	"	"	1.350	14.64	"							2.266				
60											22					0.80		
65	78.8					14.68								2.191				
70											51					1.71		
75	71.6					15.12								1.990				
80											45					1.18		
85	81.7					14.59								2.263				
90											32					0.70		
95	72.9					14.95								2.027				
104	72.8	27.8	62.9	35.1	1.282	14.71	2.78				51 / 4.9	9.2	2.0	2.024		10.6		
116	66.1					15.39		0	12	78				2.1229	3.0×10^{-8}		CH	0.45
120											8.6 / 2.0	9.2	4.3			1.34		
130											8.6					1.31		
135	71.3					14.98								1.982				
140											8.1					1.17		
145	69.4					15.10								1.929				

Table C.2 Index property data for PC-09 (2 of 2).

BH NO PC-09

DEPTH BSB (cm)	w_n (%)	w_p (%)	w_l (%)	PI (%)	LI	γ (kN/m³)	G_s	PERCENT SAND	PERCENT SILT	PERCENT CLAY	C_u (kPa) VANE	C_u (kPa) CONE	S_t	e_o	$k_{c.o}$ (cm/s)	$\frac{C_u}{P'_o}$	USC CLASS	ACTIVITY
150											7.9	-				1.06		
155	69.4					15.09								1.929				
160											9.0					1.01		
165	51.4					16.21								1.429				
170											1.9					~		
175	53.5					16.12								1.487				
180								-			8.3					0.78		
185	57.5					15.90								1.598				
190											9.1					0.84		
195	87.0					NA								2.419				
200											6.8					0.63		
204	67.0	18.8	46.6	27.8	1.734	15.38	2.78				9.0 / 5.2	4.9	1.7	1.863		0.83		
208	57.3					17.35		13.2	16.5	70.2				1.7058			SILTY CLAY CL-CH	0.40
216	66.1					15.46					6.9 / 6.5	15.5	1.2	1.837		0.59		

Appendix D

Index Property Data Sheets for BH 20+00

BH NO BH 20+00

Table D.1 Index property data for BH 20+00 (1 of 2).

DEPTH BSB (m)	w_n (%)	w_p (%)	w_L (%)	PI (%)	LI (%)	γ (kN/m^3)	G_s	PERCENT SAND	PERCENT SILT	PERCENT CLAY	C_u (kPa) VANE	C_u (kPa) CONE	S_t	e_o	P_o' (kPa)	C_c	USC CLASS
1.43	36.7					16.78								1.0203	9.57		
1.98		28.2	51.7	23.5							21.4						
1.65											26.2						
3.00											21.0						
3.16											105.7						
3.19											74.8						
3.20	32.2	25.6	40.1	14.5	0.455	18.08								0.8823	25.6		
4.44												10.1					
4.48	35.8					18.48					79/43		2.0	0.9809	37.6		
4.50												95.1					
4.56																	
4.60	29.7	21.5	39.8	18.3	0.448	19.22					100/29.2		3.3	0.8138	42.0		CL
4.64																	
4.68		22.7	38.5	15.8	0.544		2.74	0		23		95.1					CL
4.76	31.3					19.02					73.1/13.3	109.8	4.0	0.8560	42.5		
4.80		20.8	39.0	17.2	0.610		2.73	0	85	15							CL
4.82											66.3/35.7		1.9				
4.85	37.61					19.60								1.0267	46.1	0.223	
4.88												109.8					
4.92	36.8	26.2	41.3	15.1	0.702	18.44	2.73							1.0096	41.1		OL-MH
4.95											44.3/13.7		3.2				
~~5.00~~ 5.15	43.6	31.8	51.0	19.2		18.64								1.1903	40.3		
9.18											32.6						
9.27											10.9						
9.40											47.9						
9.45	44.3	27.7	37.6	9.9	1.677	16.86								1.2138	64.0		

Table D.2 Index property data for BH 20+00 (2 of 2).

BH NO BH 20+00

DEPTH BSB (m)	w_n (%)	w_p (%)	w_L (%)	PI (%)	LI (%)	$\bar{\gamma}$ (kN/m³)	G_s	PERCENT SAND	PERCENT SILT	PERCENT CLAY	C_u (kPa) YANE	C_u (kPa) CONE	S_t	e_o	P_c' (kPa)	C_c	USC CLASS
9.48											8.1						
10.74	22.41					20.19					36.7 / 9.3	39.2	3.7	0.6763	108.5		OL-ML
10.78	31.25	25.8	37.9	12.1	0.450		2.75	6	62	32				0.8594			
10.83	34.38					18.61					44.3 / 14.3	76.5	3.1	0.9454	92.3		
10.90	22.38					20.63								0.6154	114.9		P
10.93											23.5 / 8.4	23.5	2.8				
10.95	31.32					19.65								0.9613	104.7	0.15	CL
11.01	27.04	23.1	36.3	13.2	0.298		2.75	2	64	34				0.7436			
11.06	32.78					18.83					32.4 / 9.0	39.2	3.6	0.9014	96.7		
11.14	32.00	20.9	35.5	14.6	0.760			2	60	38	22.9 / 7.3	27.5	3.0	0.8800			CL
12.20											157.1						
12.31		24.0	36.5	12.5							41.7						
12.41											7.1						
12.48	43.90					15.58								1.1941	68.5		
12.50											8.1						
12.59											19.0						
13.66								0	89	11							
13.71	49.10	30.0	54.1	24.1	0.378	17.09	2.72							1.3355	96.0		OH-MH
13.74	50.20					17.32					19.6 / 12.0	20.6	1.6	1.3654	99.3	0.523	
13.88	23.90							88	12	0				0.6501			

Appendix E

Index Property Data Sheets for BH MTWS1

Table E.1 Index property data for BH MTWS1 (1 of 7).

SUMMARY OF TEST RESULTS

Sample Number	Sample Type	Depth (m) (Sample Position)	Modified Unified Soil Classification	Ground Ice Description (%)	Temp (°C)	Moisture Content (%)	Fraction Moisture Content (%)	Bulk Density (kPa)	ATTERBERG LIMITS: Liquid Limit (%)	ATTERBERG LIMITS: Plastic Limit (%)	GRAIN SIZE DISTRIBUTION: Clay (%)	Silt (%)	Sand (%)	Gravel (%)	D_{50} (μm)	SHEAR STRENGTH: Test	Shear Strength (kPa)	Failure Strain (%)	Consistency	CONSOLIDATION CHARACTERISTICS: P_o	P_c	C_c	TEST RESULTS FROM SEPARATED SAMPLE
1A	B	0.00 - 0.20		NF		83																	S=10ppt
2A	T	1.52 - 1.95		NF		82		1.66								MV	8.4		V.Soft	10.7			
2B	B	1.52 - 1.95		NF	-1.1	62										PV	4		V.Soft				S=12ppt
2B'	NS	1.90 - 1.95		NF		81		1.45															
3A	T	3.05 - 3.50		NF		69																	
3B	B	3.05 - 3.50		NF	-1.4	49										PV	6		V.Soft				S=25ppt
3B'	NS	3.45 - 3.50		NF		69		1.54															
4A	T	4.57 - 5.08		NF		71		1.73								MV	8.4		V.Soft	39.1			
4B	B	4.57 - 5.08		NF	-1.4	62										PV	7		V.Soft				S=25ppt
4B'	NS	5.03 - 5.08		NF		64		1.50															
5A	T	6.10 - 6.50		NF		69		1.70												41.4			
5B	B	6.10 - 6.50		NF	-2.1	51										PV	8.5		V.Soft				S=15ppt
5B'	NS	6.45 - 6.48		NF		61		1.49															
6A	T	7.62 - 8.12		NF		71		1.71								MV	4.4		V.Soft	52.5			
6B	B	7.62 - 8.12		NF	-1.4	48										PV	9		V.Soft				S=15ppt
6B'	NS	8.04 - 8.07		NF		66		1.50															
7A	T	9.14 - 9.61		NF																			
7B	B	9.14 - 9.61		NF	-1.1	46										PV	12		V.Soft				S=21ppt
7B'	NS	9.49 - 9.52		NF		59		1.56															

LEGEND AND NOTES

B Bag Sample
L Log Sample
L Liner Sample
P Piston Sample
NR No Recovery
NS No Sample Remaining

F Frozen Core
PM Permeator Sample
T Sample Stored in Tube
W Waxed Sample
RC Radiocarbon sample

MV Minivane
FS Fall Cone
TV Torvane
PV Pilcon Vane
HV Hamata Vane

UU Unconsolidated Undrained Triaxial
UUp UU Triaxial with Pore Pressure Measurements
CU Consolidated Undrained Triaxial
CUp CU Triaxial with Pore Pressure Measurements
CD Consolidated Drained Triaxial

M Organic Content
S Salinity
TS Thaw Strain
SG Specific Gravity

1984 OFFSHORE GEOTECHNICAL PROGRAM
MACKENZIE TROUGH WEST

NOTE: Bulk densities and corresponding water contents, minivane shear strengths and salinity data provided by GSC

Project Number 1010.4159

Reviewed By _____ P.Eng

Page 1 of 6

Table E.2 Index property data for BH MTWS1 (2 of 7).

SUMMARY OF TEST RESULTS

MTWS1 Sample Number	Type	Depth (m)	Modified Unified Soil Classification	Geological Description	Temp (°C)	Moisture Content (%)	Fraction Gravel (%)	Bulk Density (kg/m³)	ATTERBERG LIMITS: Liquid Limit (%)	ATTERBERG LIMITS: Plastic Limit (%)	GRAIN SIZE DISTRIBUTION: Clay (%)	Silt (%)	Sand (%)	Gravel (%)	D_{50} (mm)	SHEAR STRENGTH: Test	Shear Strength (kPa)	Failure Strain (%)	Consistency	CONSOLIDATION CHARACTERISTICS: P_o	P_c	C_c	TEST RESULTS TABULATED ON PAGE #
8A	T	10.67 - 11.17		NF		56		1.85								MV	14		Soft	87.9			
8B	B	10.67 - 11.17		NF	-1.0	39										PV	14		Soft				S-12ppt
8B'	NS	11.07 - 11.10		NF		47		1.60															
9A	T	12.19 - 12.69		NF		55										MV	12		V. Soft				
9B	B	12.19 - 12.69		NF	-1.0	44										PV	14.5		Soft				S-20ppt
9B'	NS	12.58 - 12.60		NF		52		1.61															
10A	T	13.72 - 14.18		NF		59		1.80												105 5			
10B	B	13.72 - 14.18		NF	-1.7	40										PV	16		Soft				S-16ppt
10B'	NS	14.02 - 14.05		NF		50		1.57															
11A	T	15.24 - 15.60		NF																			
11B	B	15.24 - 15.60		NF	-0.9	49										PV	18		Soft				S-13ppt
11B'	NS	15.54 - 15.56		NF		48		1.58															
12A	T	16.92 - 17.42		NF		53		1.84								MV	13		Soft	136 5			
12B	B	16.92 - 17.42		NF	-0.9	38										PV	14		Soft				S-14ppt
12B'	NS	17.38 - 17.40		NF		52		1.57															
13A	T	18.29 - 18.69		NF																			
13B	B	18.29 - 18.69		NF	-0.9	34										PV	19		Soft				S-19ppt
13B'	NS	18.66 - 18.68		NF		47		1.63															
14A	T	19.81 - 20.22		NF		53		1.83								MV	19		Soft	157.2			
14B	B	19.81 - 20.22		NF	-0.9	31										PV	20		Soft				S-9ppt
14B'	NS	20.12 - 20.14		NF																			

LEGEND AND NOTES

B Bag sample	L Liner Core	MV Minivane	UU Unconsolidated Undrained Triaxial	O Organic Content			
G Grab Sample	BP Piezocone Sample	PL Pocketvane	UUp UU Triaxial with Pore Pressure Measurements	S Salinity			
L Liner Sample	T Sample stored in Tube	PV Torvane	CU Consolidated Undrained Triaxial	TS Fiber Strain			
P Piston Sample	W Waxed Sample	Pen Penetrometer	CUp CU Triaxial with Pore Pressure Measurements	Mc Specific Gravity			
NR No Recovery	RL Relocation sample	Mv Remolding Vane	CAU Consolidated Drained Triaxial				
NS No sample Remaining							

1984 OFFSHORE GEOTECHNICAL PROGRAM
MACKENZIE TROUGH WEST

NOTE: Bulk densities and corresponding water contents, minivane shear strengths and salinity data provided by GSC

Project Number 1014-9159 Reviewed By: Page 2 of 4

Table E.3 Index property data for BH MTWS1 (3 of 7).

SUMMARY OF TEST RESULTS

MTWS1 Sample Number	Sample Type	Depth (m) *Sample Photographed	Modified Unified Soil Classification	Ground Ice Description (%)	Temp (°C)	Moisture Content (%)	Fraction Retained (%)	Bulk Density (Mg/m³)	ATTERBERG LIMITS Liquid Limit (%)	ATTERBERG LIMITS Plastic Limit (%)	GRAIN SIZE DISTRIBUTION Clay (%)	Silt (%)	Sand (%)	Gravel (%)	D_{50} (μm)	SHEAR STRENGTH Test	Shear Strength (kPa)	Failure Strain (%)	Consistency	CONSOLIDATION CHARACTERISTICS P_o	P_c	C_c	TEST RESULTS TABULATED SEPARATELY
15A	T	20.73 - 21.09		NF		60										MV	17.6		Soft				
15B	B	20.73 - 21.09		NF	-0.9	31										PV	22		Soft				S=15ppt
15B'	WS	20.98 - 21.09		NF		52		1.65															
16A	T	21.64 - 21.99		NF																			
16B	B	21.64 - 21.99		NF	-0.8	35										PV	22		Soft				S=20ppt
16B'	WS	21.88 - 21.90		NF		51		1.61															
17A	T	22.56 - 22.85		NF		26																	
17B	B	22.56 - 22.85		NF	-0.6	24										PV	82		Stiff				S=20ppt
17B'	WS	22.80 - 22.82		NF		24		1.91															
18A	T	23.47 - 24.37		NF																			
18B	B	23.47 - 24.37		NF	-0.7	29																	S=20ppt
18B'	WS	23.70 - 23.73		NF		26		1.84															
19A	B	24.38 - 24.66		NF	-0.7	27																	S=18ppt
19A'	WS	24.59 - 24.61		NF		25		1.84															
20A	B	27.43 - 27.66		NF	-0.7	28										PV	52		Stiff				
20A'	WS	27.66 - 27.68		NF		24		1.87															
21A	T	28.35 - 28.73		NF		30		2.09												196.9			
21B	B	28.35 - 28.73		NF	-0.7	27										PV	44		Firm				
21B'	WS	28.70 - 28.72		NF		25		1.85															
22	NR	29.26																					
23	NR	30.18																					

LEGEND AND NOTES

B	Bag Sample	C	Frozen Core	MV	Minivane	UU	Unconsolidated Undrained Triaxial	O	Organic Content		
G	Gas Sample	PW	Porewater Sample	PC	Pat Core	UUP	UU Triaxial with Pore Pressure Measurements	S	Salinity		
L	Liner Sample	T	Sample Stored in Tube	TV	Torvane	CU	Consolidated Undrained Triaxial	TS	Thaw Strain		
P	Piston Sample	W	Waxed Sample	PV	Pitcher Vane	CUP	CU Triaxial with Pore Pressure Measurements	SG	Specific Gravity		
NR	No Recovery	RS	Radioactive Sample	HV	Hermite Vane	CD	Consolidated Drained Triaxial				
WS	No Sample Remaining										

1984 OFFSHORE GEOTECHNICAL PROGRAM
MACKENZIE TROUGH WEST

NOTE: Bulk densities and corresponding water contents, minivane shear strengths and salinity data provided by G.S.C.

Project Number 1UIE-8159 Reviewed By _____ P.Eng Page ___ of ___

Table E.4 Index property data for BH MTWS1 (4 of 7).

SUMMARY OF TEST RESULTS

MTWS1 Sample Number	Sample Type	Depth (m) *Sample Photographed	Modified Unified Soil Classification	Grain Size Description (%)	Temp (°C)	Moisture Content (%)	Frozen Moisture Content (%)	Bulk Density (kg/m³)	ATTERBERG LIMITS Liquid Limit (%)	Plastic Limit (%)	GRAIN SIZE DISTRIBUTION Clay (%)	Silt (%)	Sand (%)	Gravel (%)	D_{50} (μm)	SHEAR STRENGTH Test	Shear Strength (kPa)	Failure Strain (%)	Consistency	CONSOLIDATION CHARACTERISTICS P_o	P_c	C_c	TEST RESULTS TABULATED SEPARATELY
24A	B	31.09 - 31.61		NF	-0.9	26																	S=15ppt
24A'	NS	31.58 - 31.61		NF		25		1.81															
25A	T	32.00 - 32.31		NF	-0.8	27		2.12												393			S=26ppt
25A'	NS	32.28 - 32.31		NF		28		1.89															
26	NR	35.05		NF																			
27A	T	36.58 - 37.07		NF		25		2.14												401.2			
27B	B	36.58 - 37.07		NF	-0.5	24																	
27B	NS	37.04 - 37.07		NF		22		1.99															
28A	T	38.10 - 38.50		NF		26		2.16												429.7			
28B	B	38.10 - 38.50		NF	-0.4	21																	
28B'	NS	38.40 - 38.45		NF		16		1.99															
29A	T	40.23 - 40.73		NF		22		2.20												469.3			
29B	B	40.23 - 40.73		NF	-0.1	21																	
29B'	NS	40.60 - 40.65		NF		20		1.88															
30A	B	43.59 - 44.04		NF		24																	S=31ppt
30A'	NS	43.90 - 43.95		NF		39		2.28															
31A	T	46.63 - 47.18		NF		24		2.18												529.9			
31B	B	46.63 - 47.18		NF	-0.4	22																	
31B'	NS	47.00 - 47.05		NF		19		1.97															

LEGEND AND NOTES

B Bag Sample; C Frozen Core; MV Minivane; UU Unconsolidated Undrained Triaxial; O Organic Content
G Gas Sample; PW Porewater Sample; PC Pat Core; UUp UU Triaxial with Pore Pressure Measurements; S Salinity
L Liner Sample; T Sample Stored in Tube; TV Torvane; CU Consolidated Undrained Triaxial; TS Thaw Strain
P Piston Sample; W Waxed Sample; PV Piston Vane; CUp CU Triaxial with Pore Pressure Measurements; SG Specific Gravity
NR No Recovery; RC Rediscarbon sample; RV Remote Vane; CD Consolidated Drained Triaxial
NS No Sample Remaining

1984 OFFSHORE GEOTECHNICAL PROGRAM
MACKENZIE TROUGH WEST

NOTE Bulk densities and corresponding water contents, minivane shear strengths and salinity data provided by GSC

Project Number 101C-4159 Reviewed By _____ P Eng Page 4 of 6

Table E.5 Index property data for BH MTWS1 (5 of 7).

SUMMARY OF TEST RESULTS

MTWS1 Sample Number	Sample Type	Depth (m) (Sample Photographs)	Modified Unified Soil Classification	Ground Ice Description (%)	Temp (°C)	Moisture Content (%)	Fraction Moisture Content	Bulk Density (Mg/m³)	ATTERBERG LIMITS Liquid Limit (%)	ATTERBERG LIMITS Plastic Limit (%)	GRAIN SIZE DISTRIBUTION Clay (%)	Silt (%)	Sand (%)	Gravel (%)	D_{50} (mm)	SHEAR STRENGTH Test	Shear Strength (kPa)	Failure Strain (%)	Consistency	CONSOLIDATION CHARACTERISTICS P_o	P_c	C_c	TEST RESULTS TABULATED SEPARATELY?
J2A	T	49.68 - 50.13		NF		25		2.16												553 ?			
J2B	BS	49.68 - 50.13		NF	-0.3	26																	S=32ppt
J2B'	NS	50.00 - 50.05		NF		21		1.92															
J3A	B	53.64 - 54.00		NF		38																	
J4A	T	54.56 - 54.86		NF		26		2.12												585 ?			
J4B	B	54.56 - 54.86		NF		26																	
J4B'	NS	54.70 - 54.75		NF		21		1.86															
J5A	B	55.47 - 56.00		NF		27																	
J5A'	NS	55.6		NF		19		2.11															
J5B	B	55.47 - 56.00		NF		21																	
J5B'	NS	55.9		NF		18		2.18															
J6A	T	56.39 - 56.90		NF		30										HV	20.6		Soft				
J6B	B	56.39 - 56.90		NF		28																	
J6B'	NS	56.80		NF		29		1.90															
J7A	B	60.96 - 61.41		NF		21																	S=30ppt
J7A'	NS	61.20		NF		16		1.99															
J8A	T	61.87 - 62.47		NF		22		2.20												713 ?			
J8B	B	61.87 - 62.47		NF		20																	
J8B'	NS	62.3		NF		21		1.92															

LEGEND AND NOTES

B Bag Sample; G Gas Sample; L Liner Sample; P Piston Sample; NR No Recovery; NS No Sample Remaining; C Pocket Core; PR Pocketer Sample; T Sample Stored in Tube; W Waxed Sample; RC Recirculation Sample; Mv Minivane; PL Pat Core; Tv Torvane; PV Piston Vane; RV Remote Vane; UU Unconsolidated Undrained Triaxial; UUp UU Triaxial with Pore Pressure Measurements; CU Consolidated Undrained Triaxial; CUp CU Triaxial with Pore Pressure Measurements; CD Consolidated Drained Triaxial; OC Organic Content; S Salinity; TS Thaw Strain; Gs Specific Gravity

1984 OFFSHORE GEOTECHNICAL PROGRAM
MACKENZIE TROUGH WEST

Note: Bulk densities and corresponding water contents, minivane shear strengths and salinity data provided by GSC

Project Number 1011 4159 Reviewed By P Eng Page 5 of 6

Table E.6 Index property data for BH MTWS1 (6 of 7).

SUMMARY OF TEST RESULTS

MTWS1 Sample Number	Sample Type	Depth (m)	Modified Unified Soil Classification	Geological Description	Penetrometer (kPa)	Moisture Content (%)	Bulk Density (Mg/m³)	Atterberg Limits: Liquid Limit (%)	Atterberg Limits: Plastic Limit (%)	Grain Size Distribution: Clay (%)	Silt (%)	Sand (%)	Gravel (%)	D_{50} (μm)	Shear Strength: Test	Shear Strength (kPa)	Failure Strain (%)	Consistency	Consolidation Characteristics: P_o	P_c	C_c	Test Results Included in Separate Report
39A	T	66.45 - 66.95		NF		32		2.15							MV	191.5		Hard	733.2			
39B	BS	66.45 - 66.95		NF		24																S-3upp
39B'	NS	66.9		NF		28		1.92														
40A	T	71.02 - 71.60		NF		33																
40B	B	71.02 - 71.60		NF		29																
40B'	NS	71.4		NF		26		1.83														
41A	BS	75.59 - 76.00		NF		26																
41A'	NS	75.80		NF		26		2.13														
42A	TS	76.50 - 76.95		NF		27									MV	64		Stiff				
42B	B	76.50 - 76.95		NF		28																
42B'	NS	76.90		NF		22		1.93														
43A	T	81.08 - 81.50		NF		22		2.24											965.3			
43B	B	81.08 - 81.50		NF		24									PV	54		Stiff				
43B'	NS	81.4		NF		22		1.99														

LEGEND AND NOTES

B Bag Sample	C Frozen Core	MV Minivane	UU Unconsolidated Undrained Triaxial	O Organic Content			
G Jar Sample	PW Porewater Sample	FS Fall Cone	UUp UU Triaxial with Pore Pressure Measurements	S Salinity			
J Liner Sample	T Sample Stored in Tube	TV Torvane	CU Consolidated Undrained Triaxial	TS Thaw Strain			
P Piston Sample	R Rhizon Sample	PX Pilcon Vane	CUp CU Triaxial with Pore Pressure Measurements	WC Water Content			
NR No Recovery	RS Redrive Barrel Sample	HV Hanson Vane	CD Consolidated Drained Triaxial				
NS No Sample Remaining							

1984 OFFSHORE GEOTECHNICAL PROGRAM
MACKENZIE TROUGH WEST

NOTE: Bulk densities and corresponding water contents, minivane shear strengths and salinity data provided by GSC

Project Number 1215-9152 Reviewed By PEng Page 6 of 6

Table E.7 Index property data for BH MTWS1 (7 of 7).

BH NO MTWS1

DEPTH BSB (m)	w_n (%)	w_p (%)	w_L (%)	PI (%)	LI (%)	I (kN/m³)	G_s	PERCENT			C_u (kPa)		S_t	e_o	P_o' (kPa)	C_c	USC CLASS
								SAND	SILT	CLAY	VANE	CONE					
6.13	65.54													1.8296			
6.16	65.78					16.04								1.8353	36.6	0.57	
6.19	65.97					16.04					67/24	7.1	2.8	1.8406	36.8		
6.20		27.7	65.2	37.5	1.020		2.79										CH
6.26	68.65													1.9153			
9.29	63.03					16.19					9.0/4.7	12.3	1.9	1.7585	56.6		
9.37		30.8	65.4	34.6	0.700			6	7	87							CH
9.39	55.04					16.75					11.8/4.1	20.6	2.9	1.5356	62.5		

Appendix F

Vertical Oedometer Data and Strain Energy Plots for Gulf Sauvrak

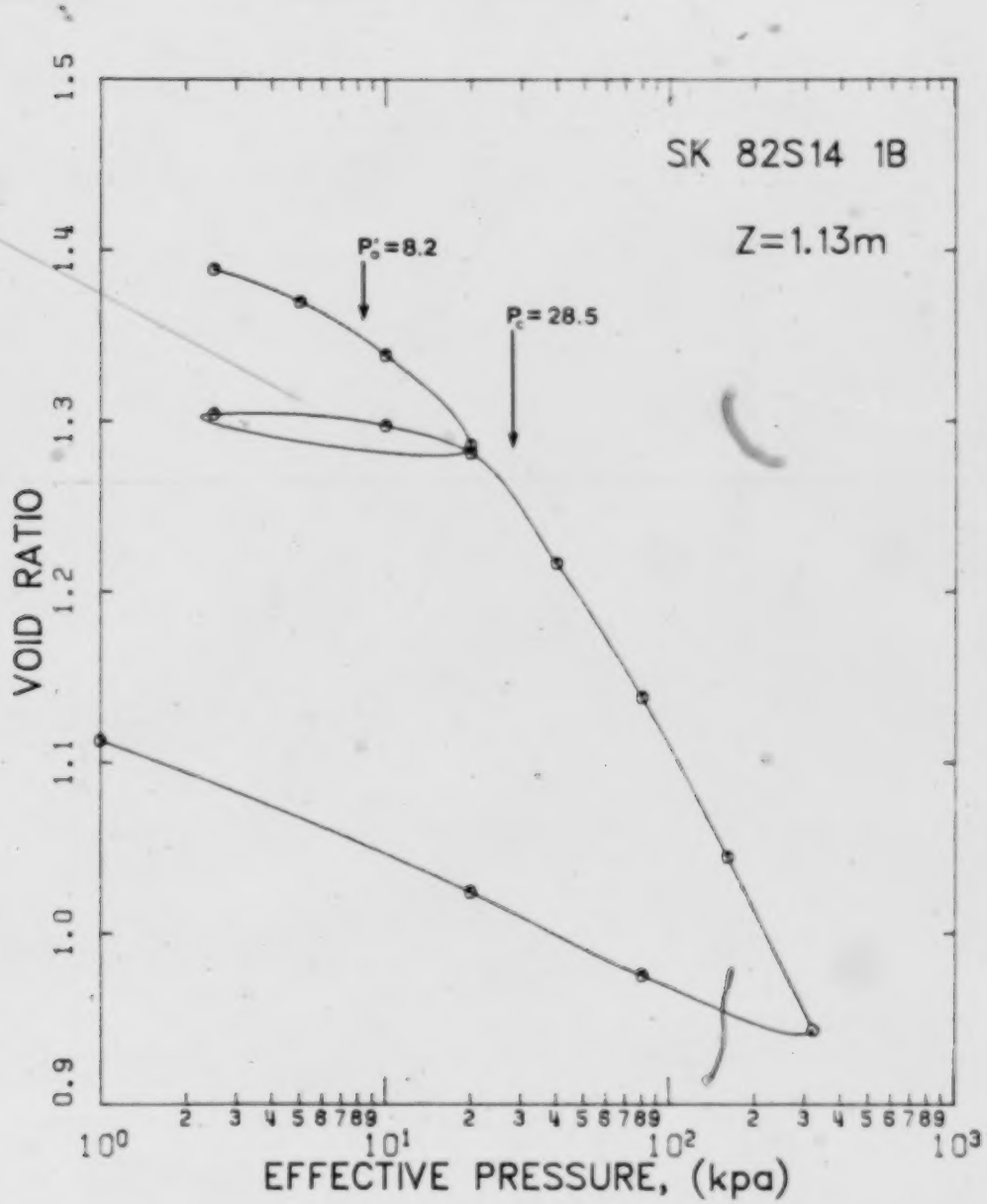

Figure F.1 Void ratio versus log effective vertical stress for BH SK 82S14; Z=1.13 m bsb. (Jefferies, pers. comm., 1985).

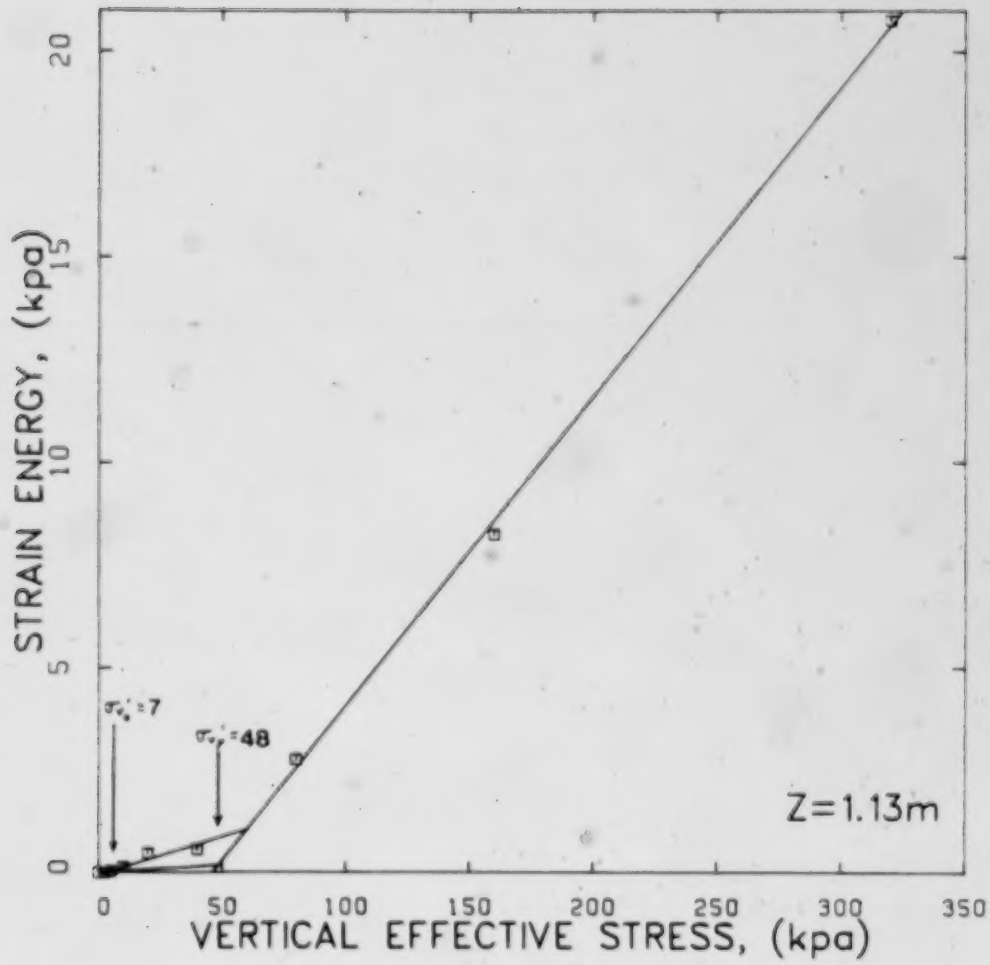

Figure F.2 Strain energy versus effective vertical stress for BH SK 82S14; Z=1.13 m bsb.

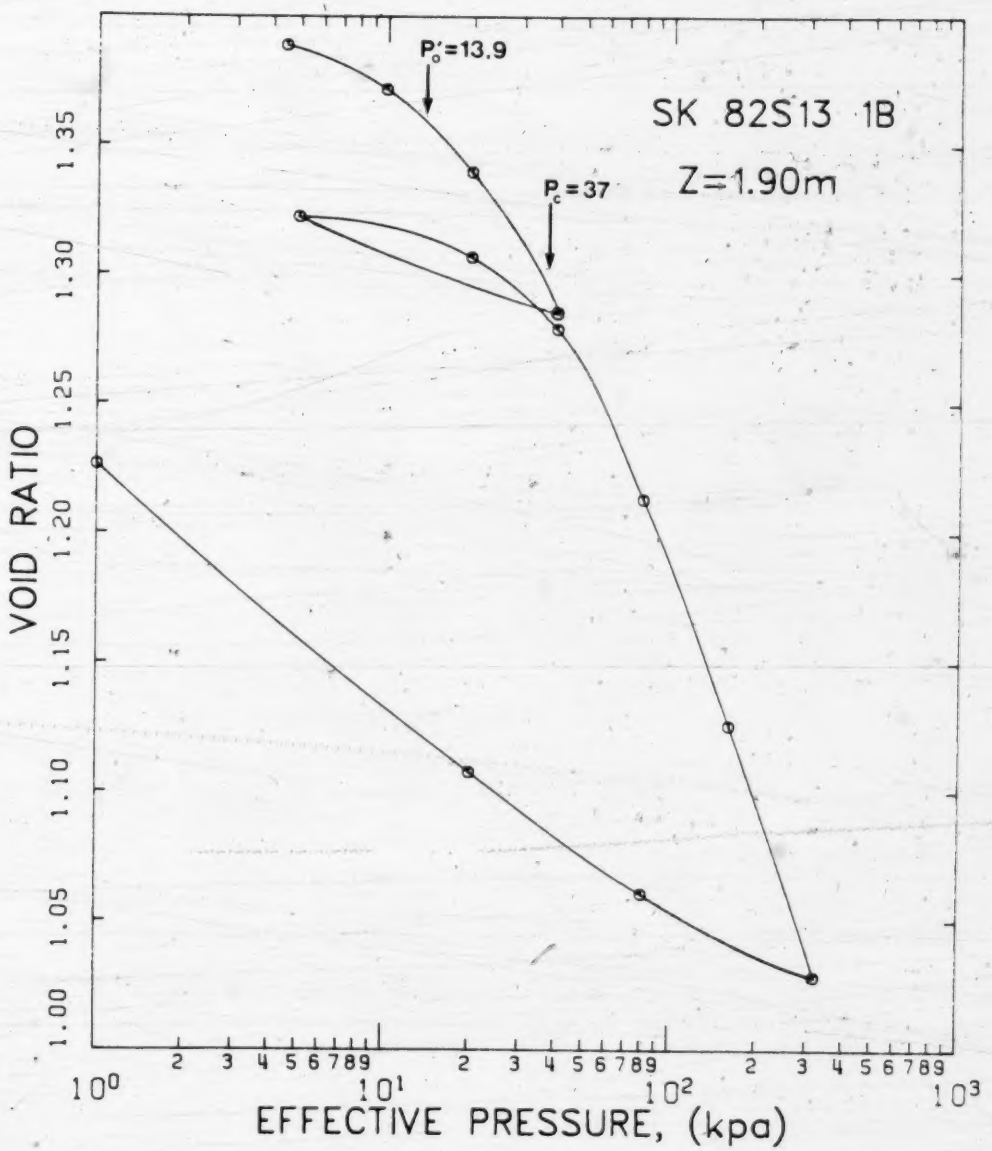

Figure F.3 Void ratio versus log effective vertical stress for BH SK 82S13 1B; Z=1.90 m bsb. (Jefferies, pers. comm., 1985).

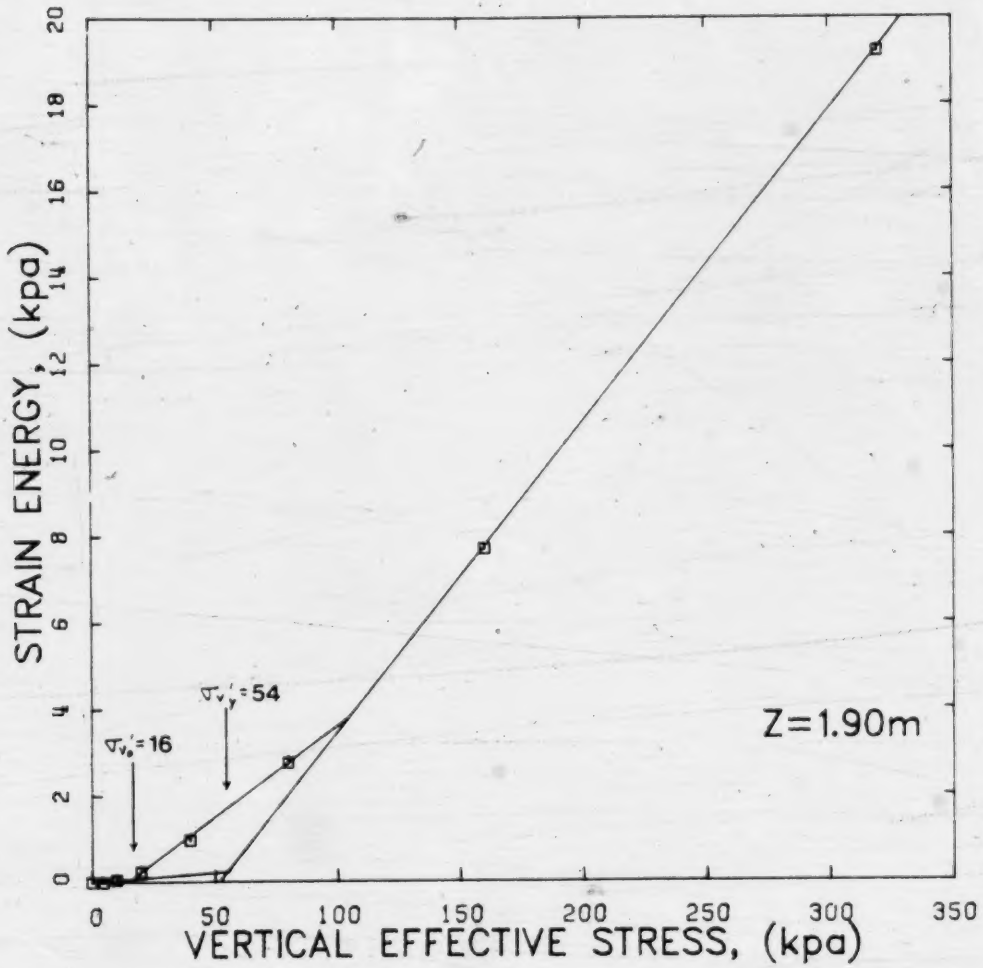

Figure F.4 Strain energy versus effective vertical stress for BH SK 82S13 1B; Z=1.90 m bsb.

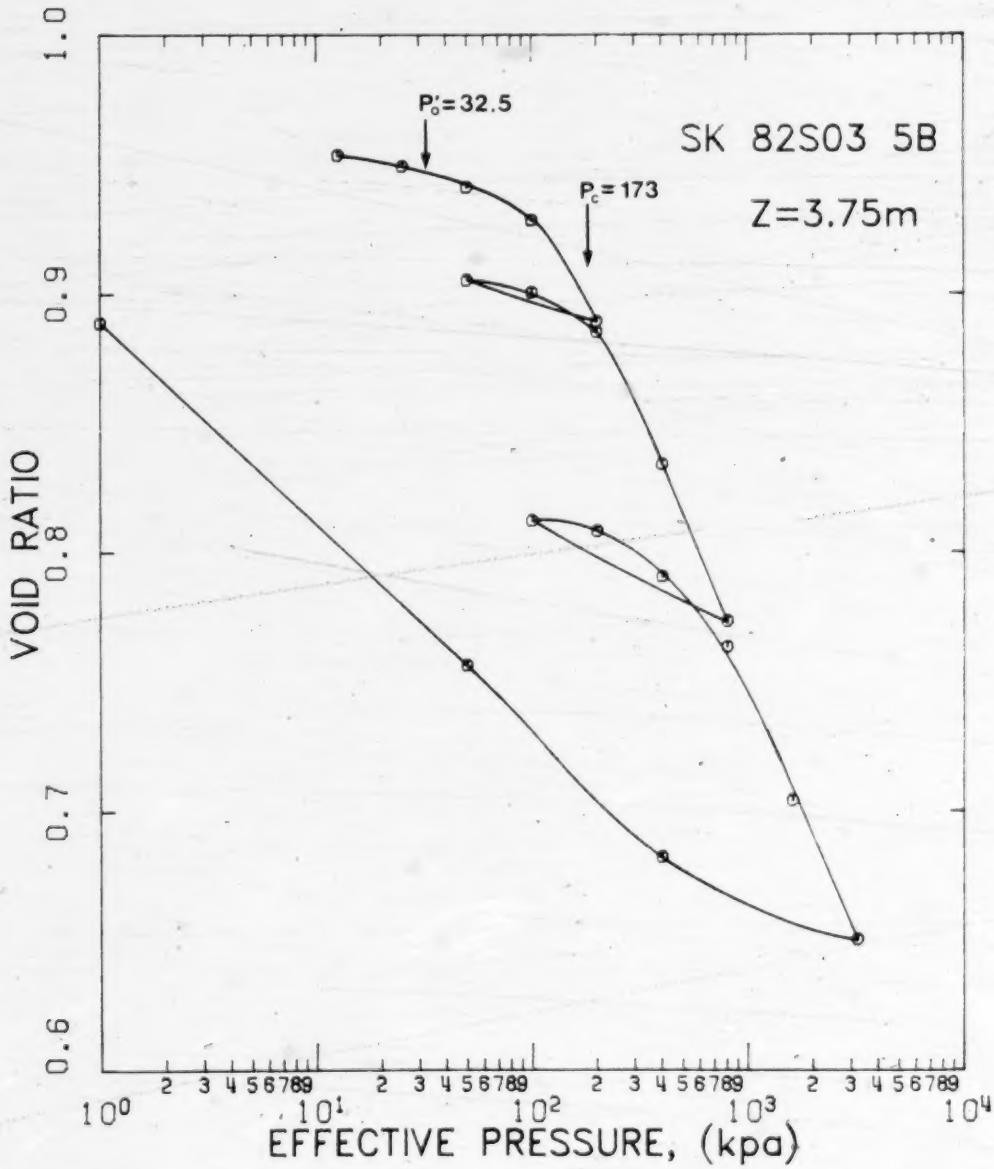

Figure F.5 Void ratio versus log effective vertical stress for BH SK 82S03 5B; Z=3.75 m bsb. (Jefferies, pers. comm., 1985).

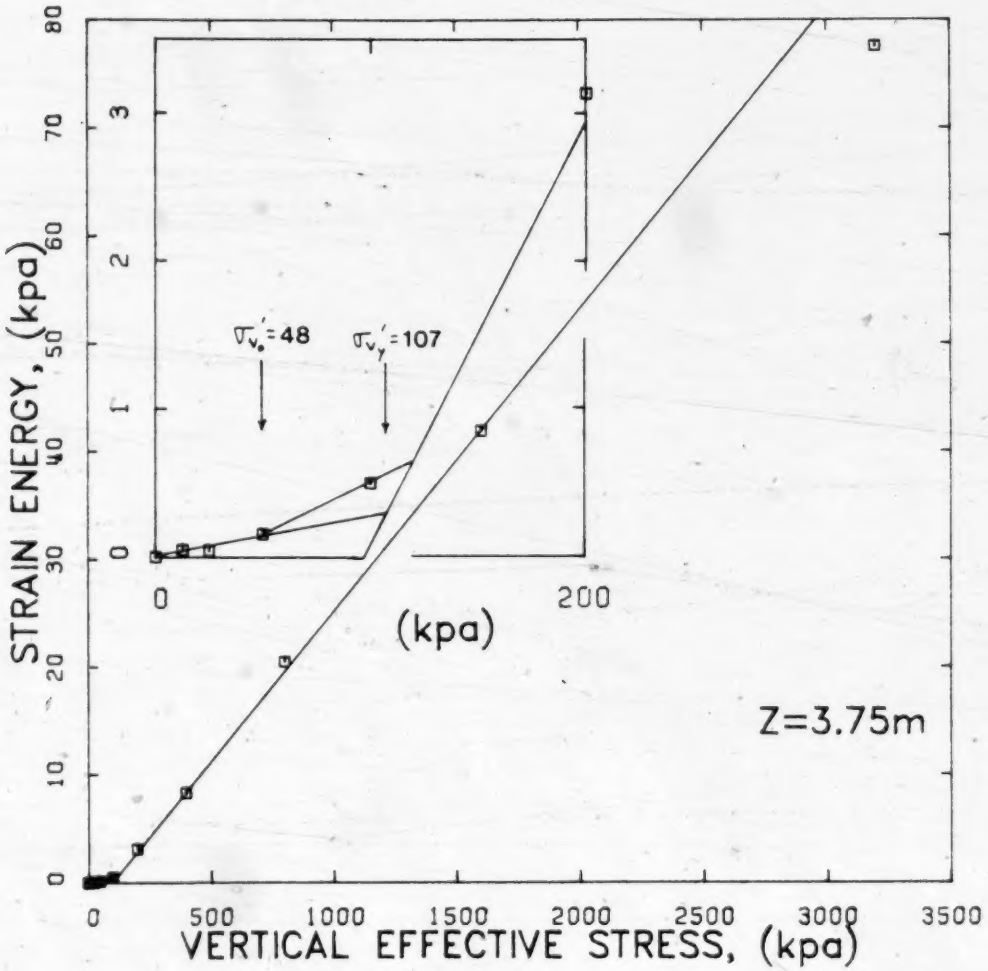

Figure F.6 Strain energy versus effective vertical stress for BH SK 82S03 5B; Z=3.75 m bsb.

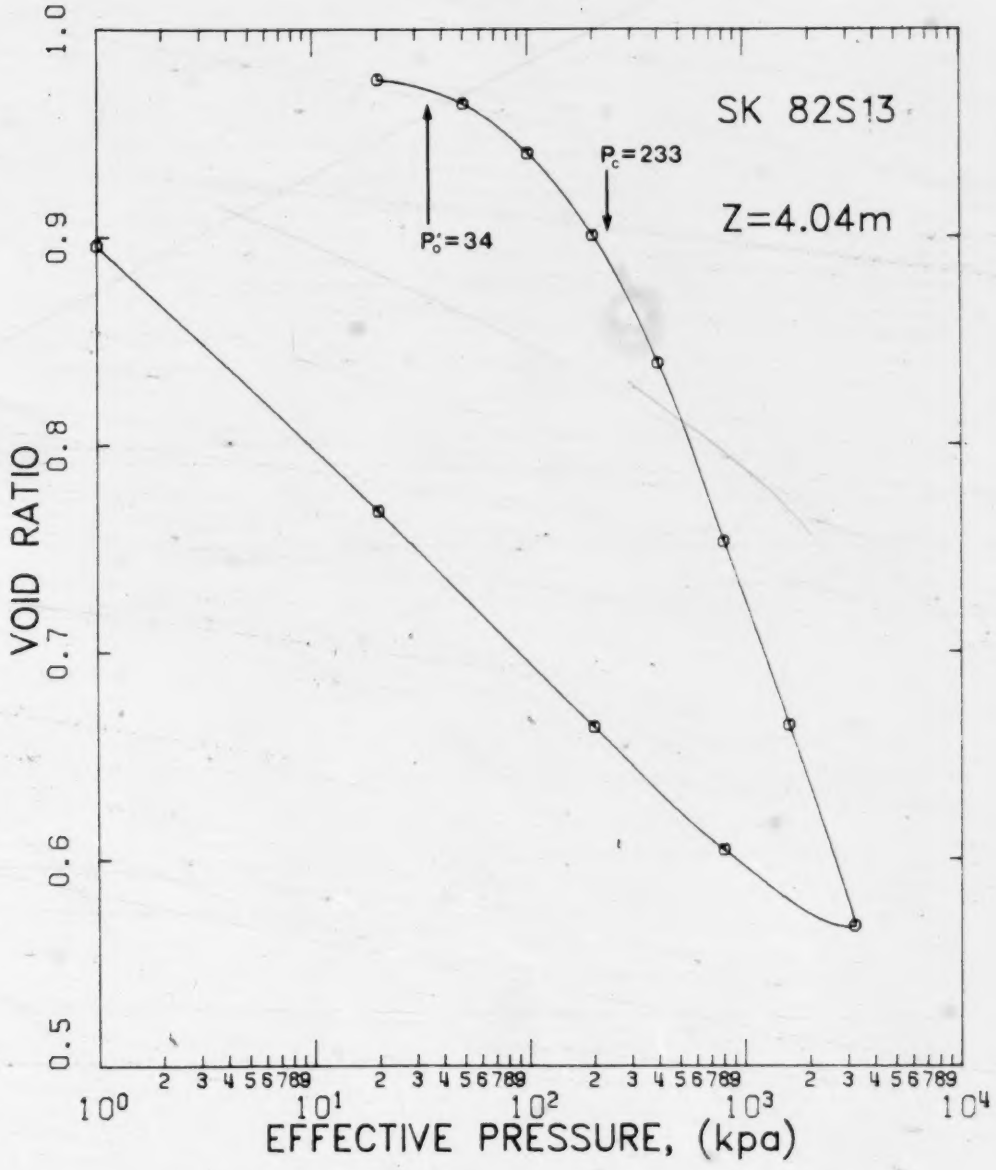

Figure F.7 Void ratio versus log effective vertical stress for BH SK 82S13; Z=4.04 m bsb. (Jefferies, pers. comm., 1985).

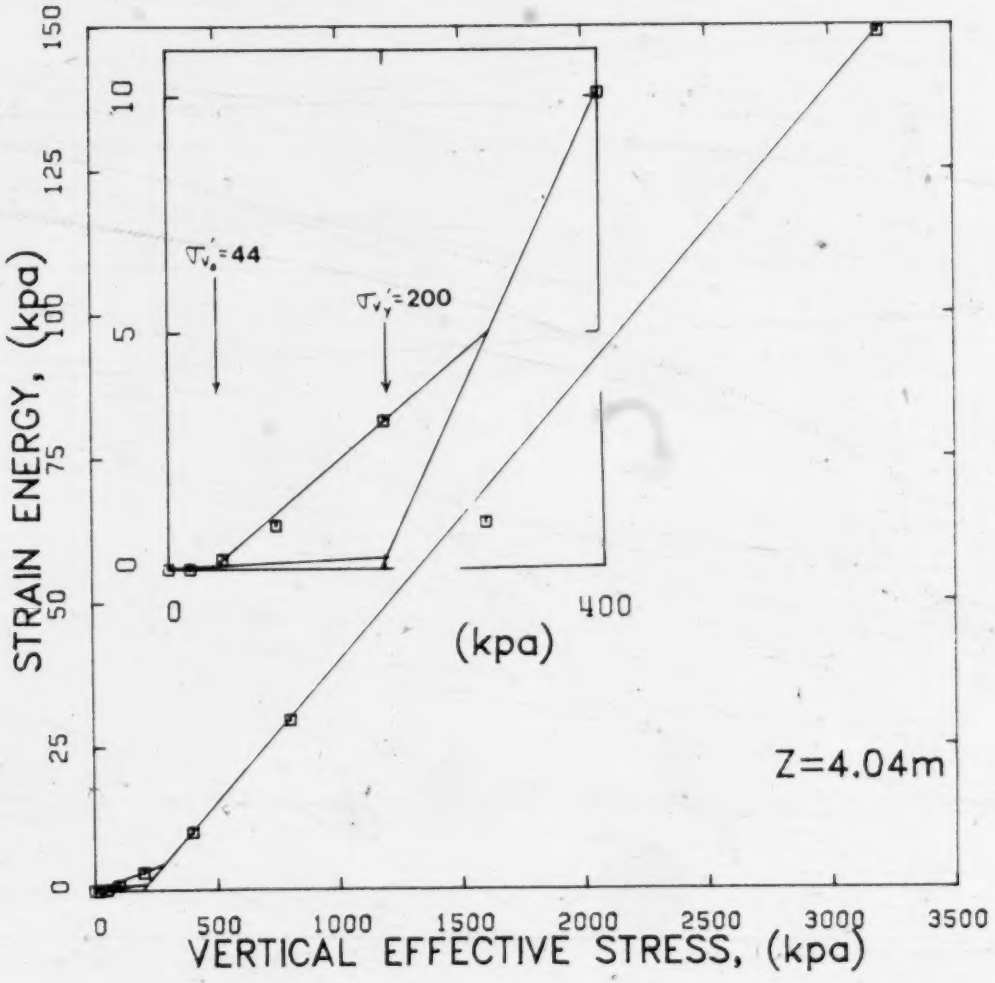

Figure F.8 Strain energy versus effective vertical stress for BH SK 82S13; Z=4.04 m bsb.

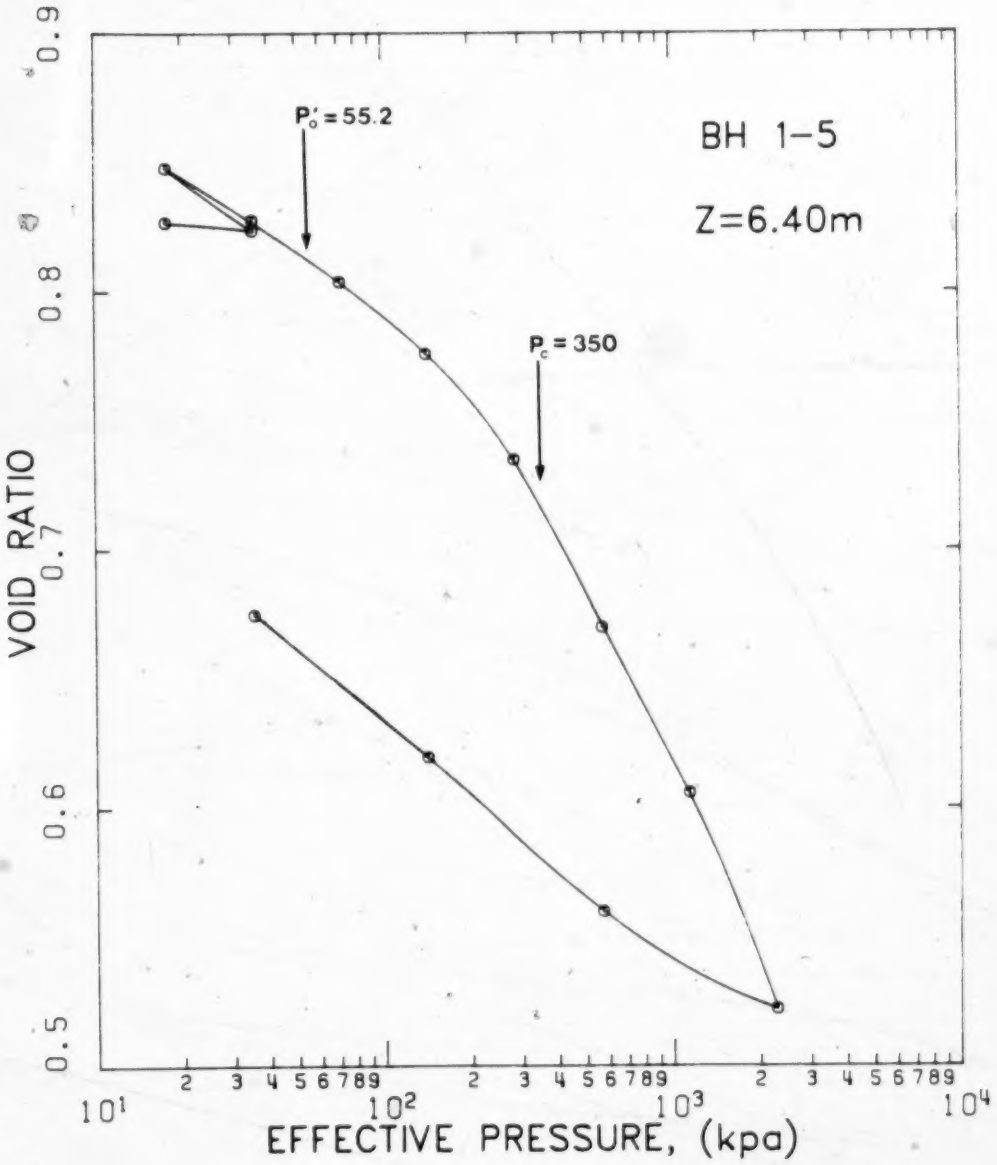

Figure F.9 Void ratio versus log effective vertical stress for BH 1-5; Z=6.40 m bsb. (Jefferies, pers. comm., 1985).

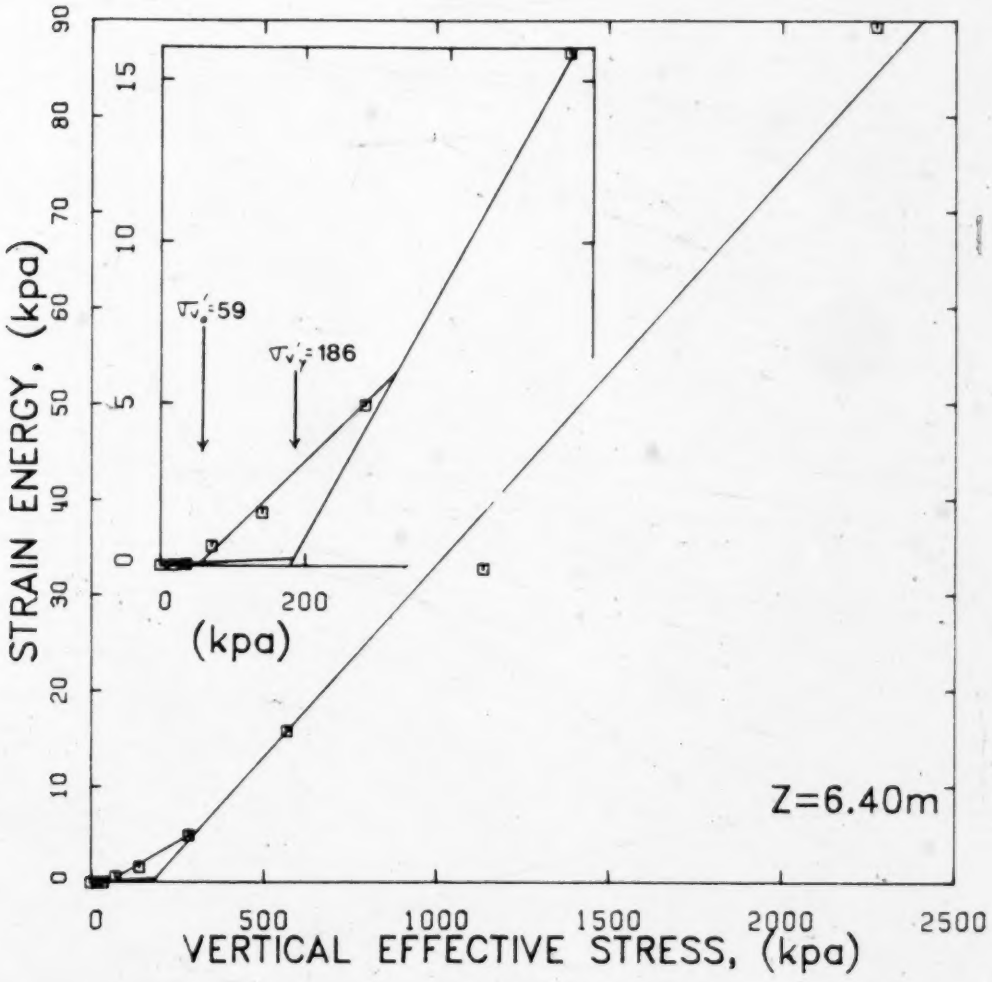

Figure F.10 Strain energy versus effective vertical stress for BH 1-5; Z=6.40 m bsb.

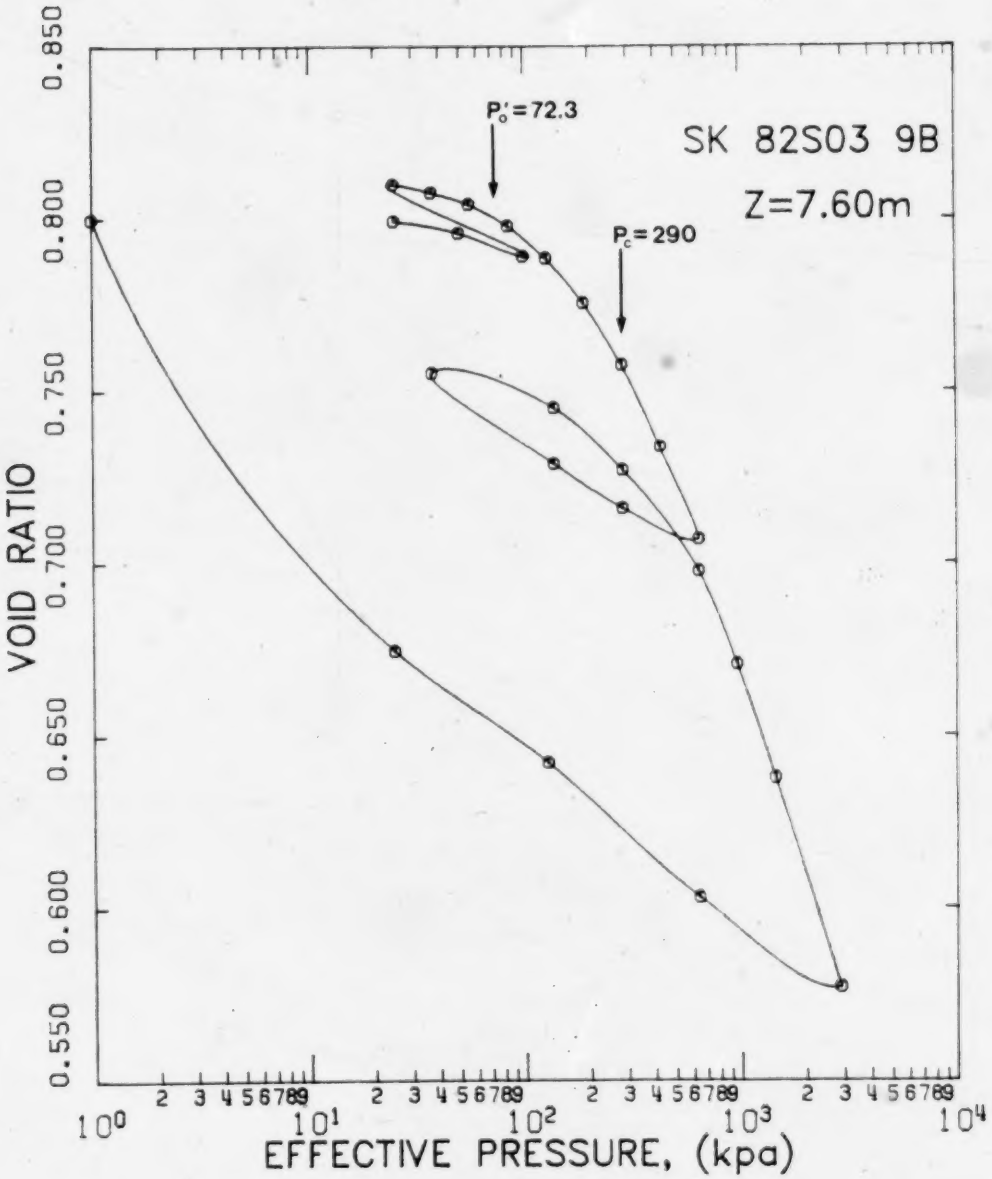

Figure F.11 Void ratio versus log effective vertical stress for BH SK 82S03 9B; Z=7.60 m bsb. (Jefferies, pers. comm., 1985).

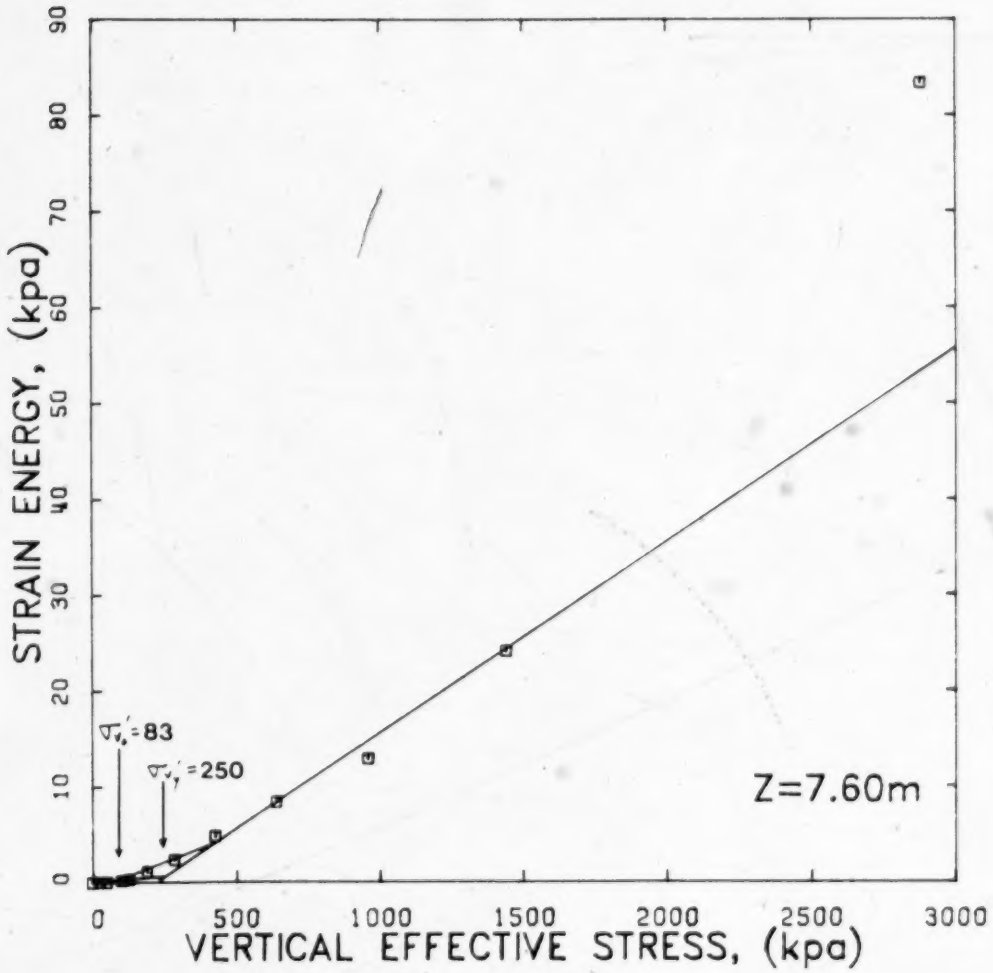

Figure F.12 Strain energy versus effective vertical stress for BH SK 82S03 9B; Z=7.60 m bsb.

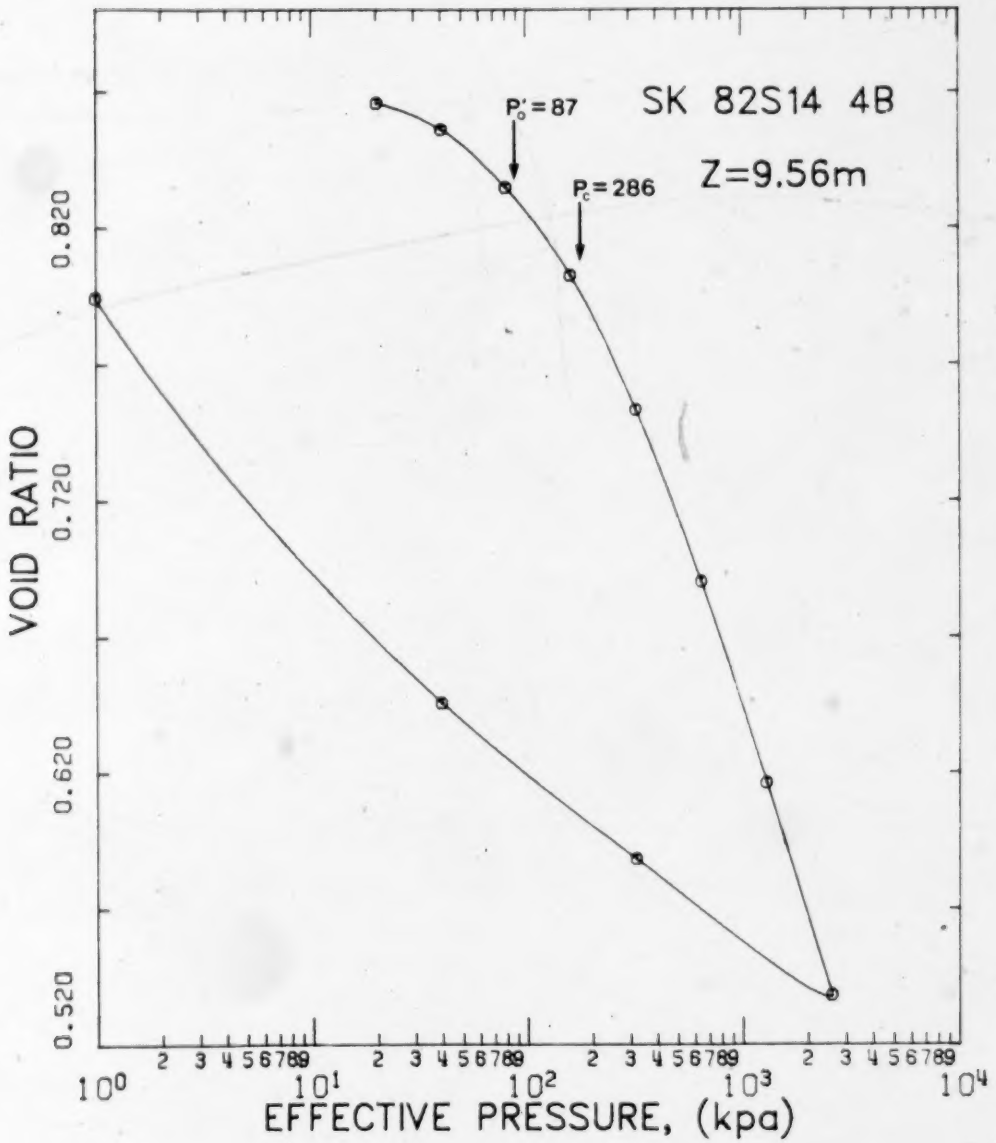

Figure F.13 Void ratio versus log effective vertical stress for BH SK 82S14 4B; Z=9.56 m bsb. (Jefferies, pers. comm., 1985).

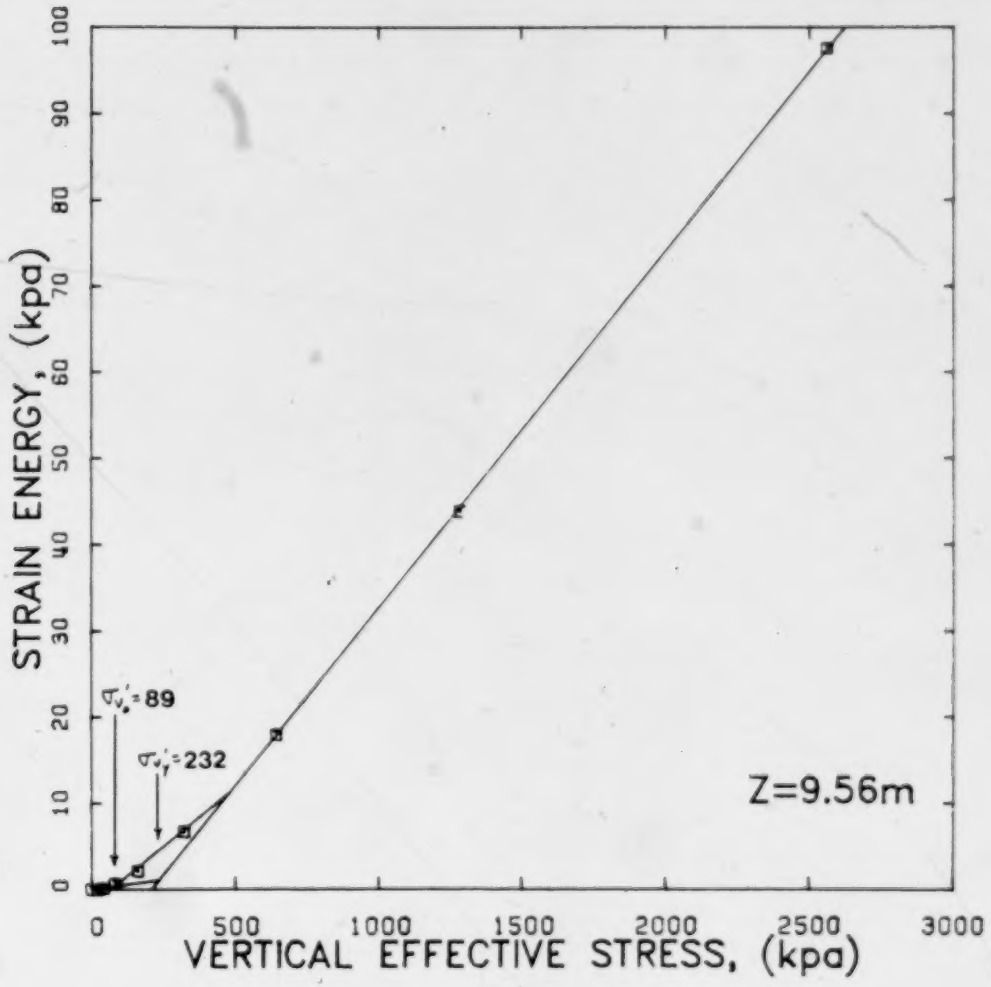

Figure F.14 Strain energy versus effective vertical stress for BH SK 82S14 4B; Z=9.56 m bsb.

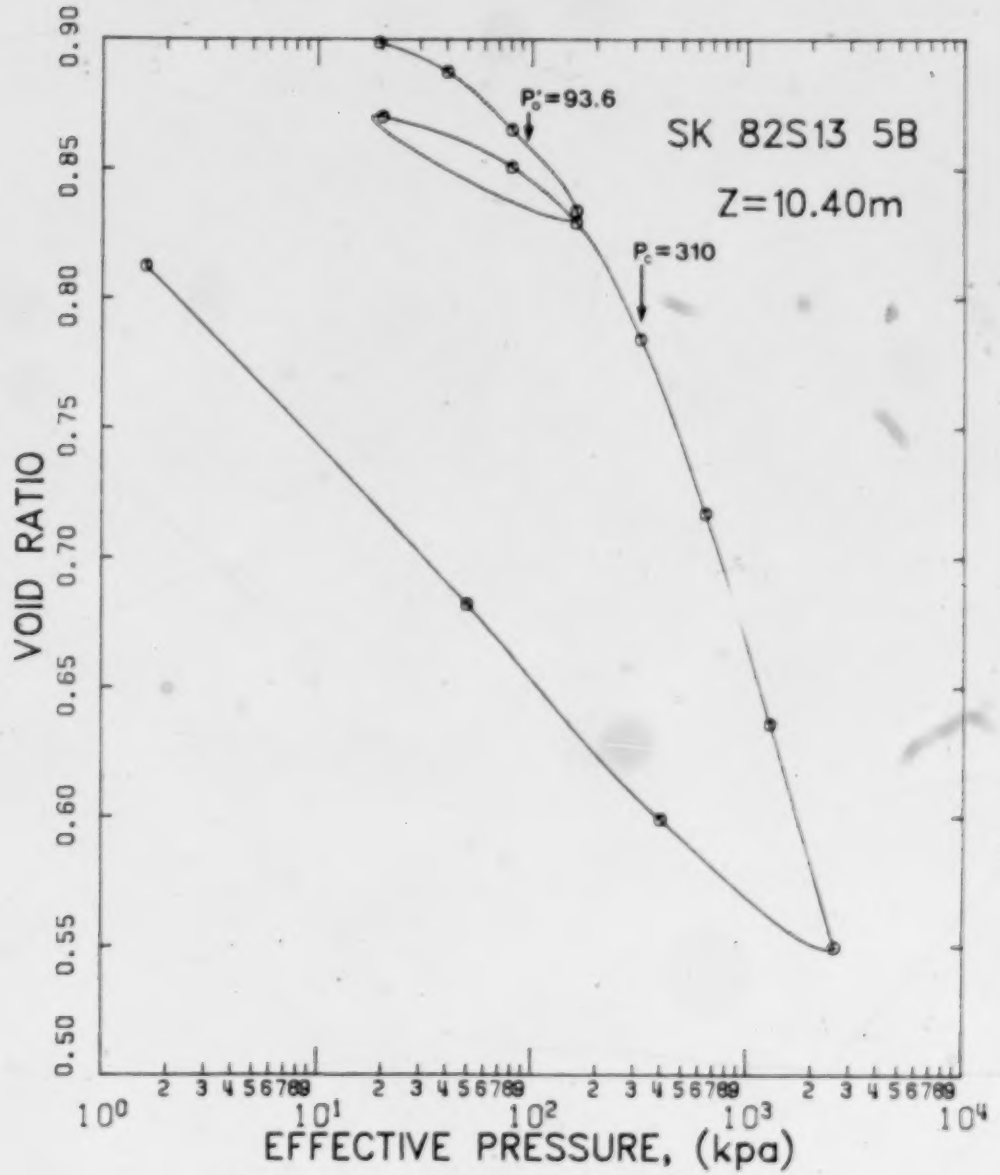

Figure F.15 Void ratio versus log effective vertical stress for BH SK 82S13 5B; Z=10.40 m bsb. (Jefferies, pers. comm., 1985).

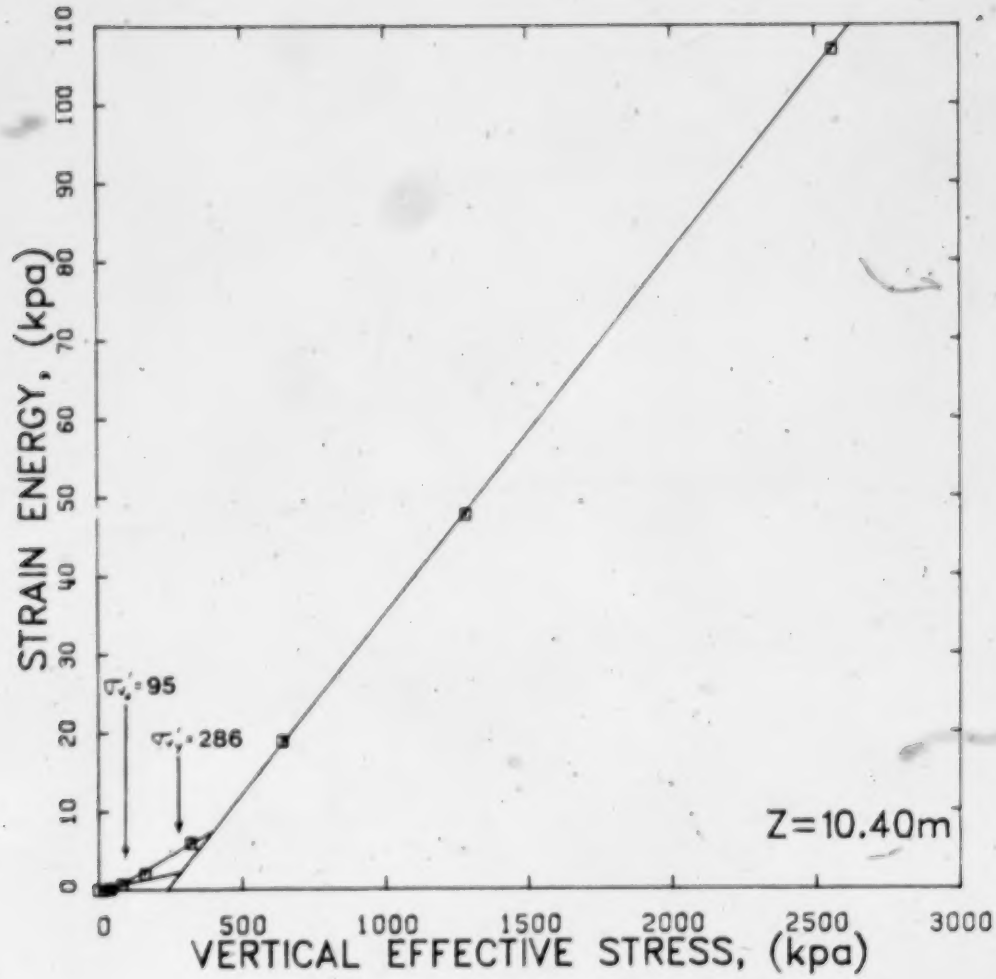

Figure F.16 Strain energy versus effective vertical stress for BH SK 82S13 5B; Z=10.40 m bsb.

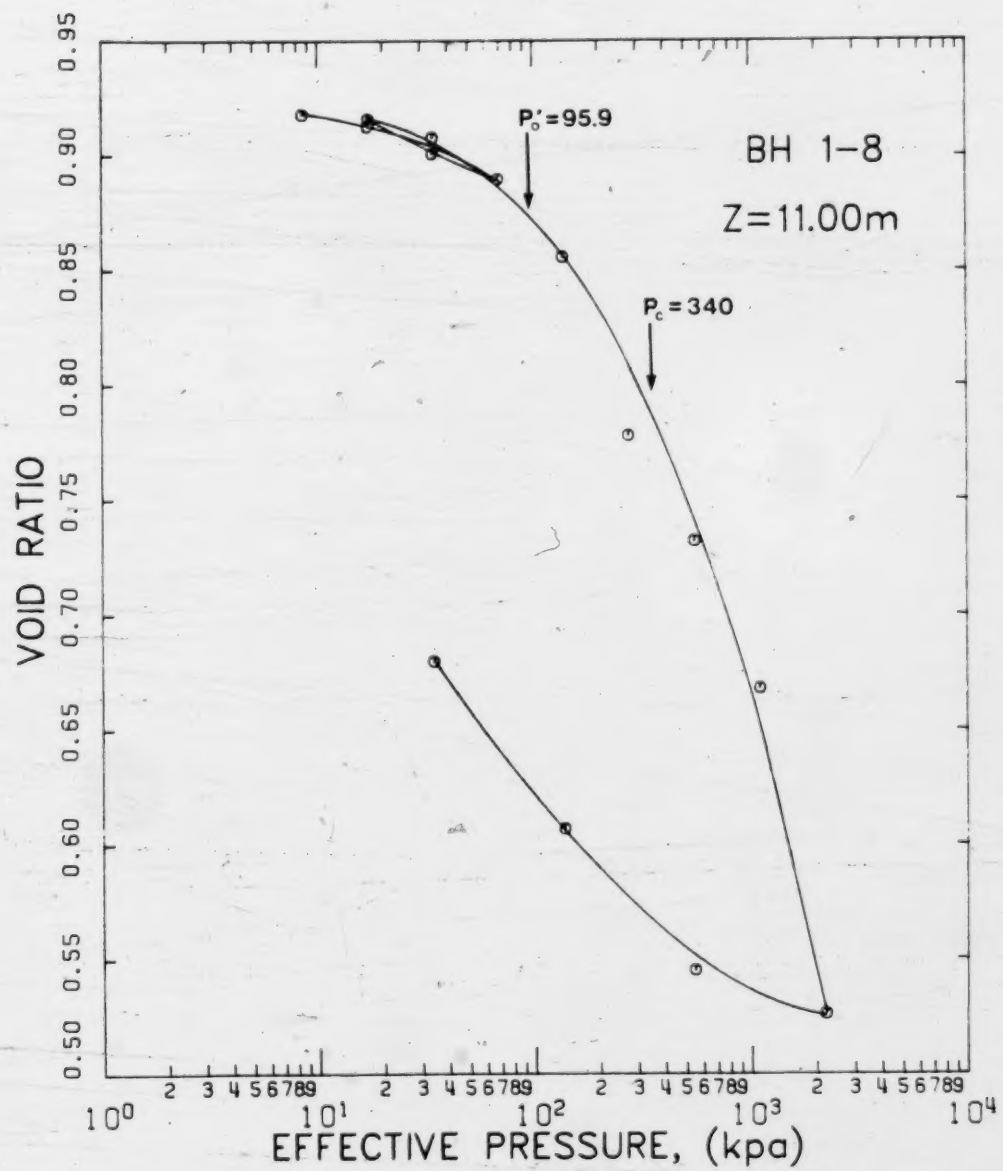

Figure F.17 Void ratio versus log effective vertical stress for BH 1-8; Z=11.00 m bsb. (Jefferies, pers. comm., 1985).

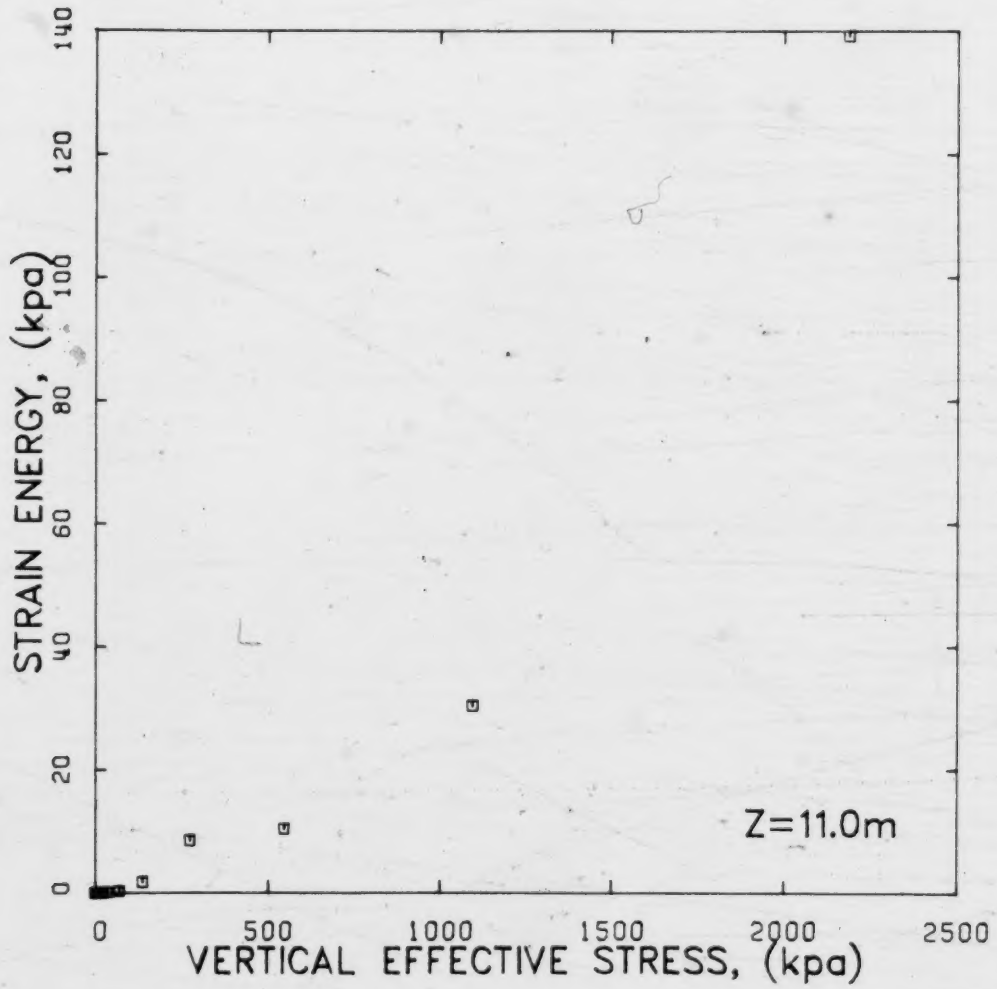

Figure F.18 Strain energy versus effective vertical stress for BH 1-8; Z=11.00 m bsb.

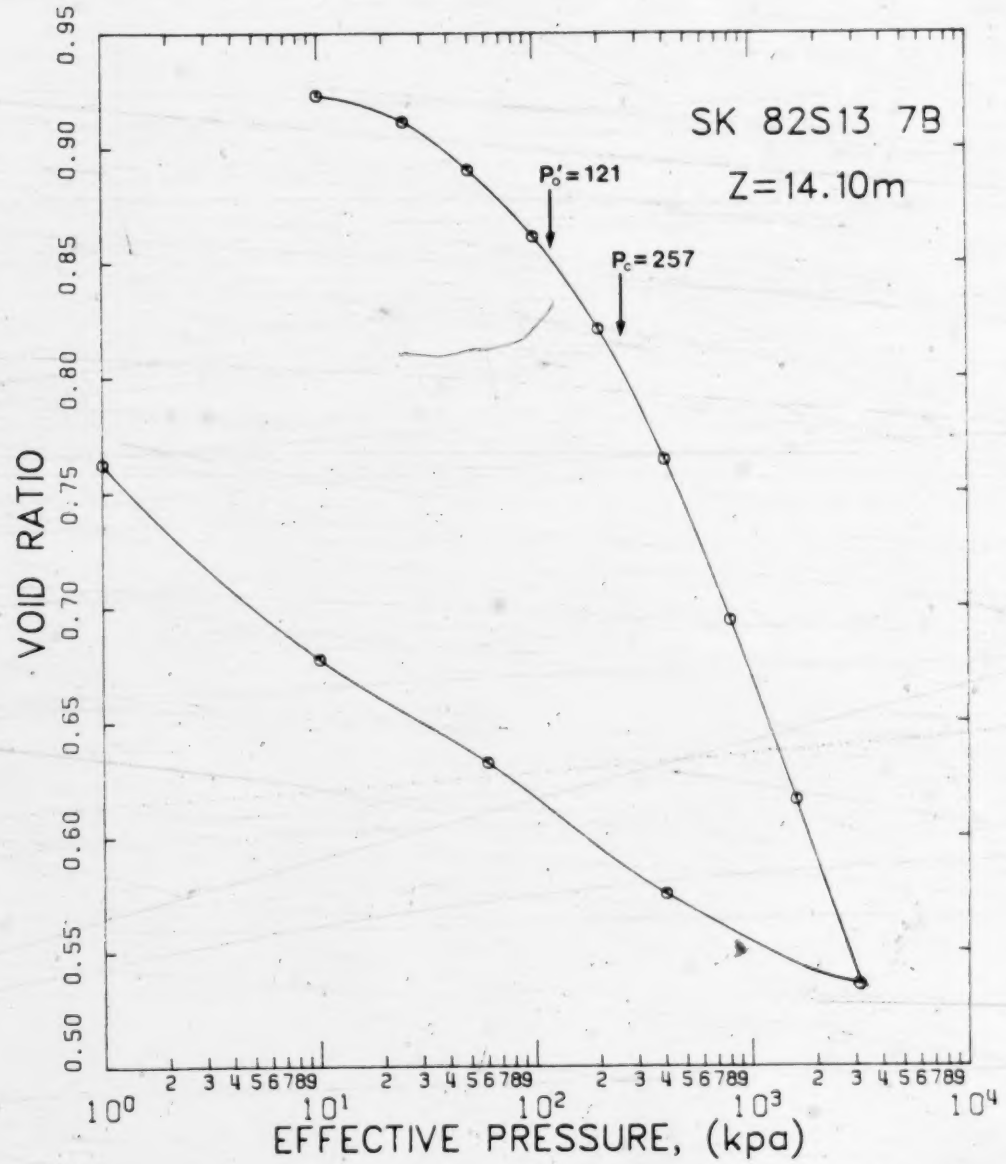

Figure F.19 Void ratio versus log effective vertical stress for BH SK 82S13 7B; Z=14.10 m bsb. (Jefferies, pers. comm., 1985).

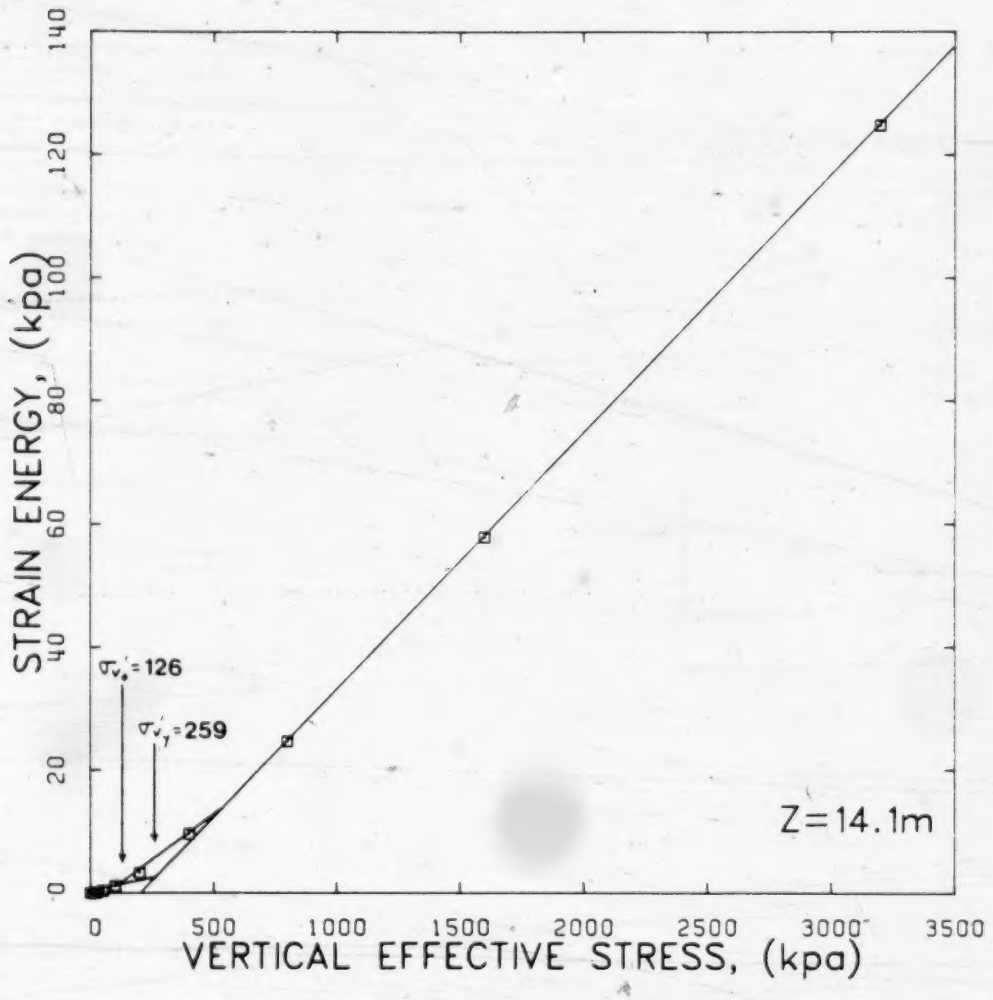

Figure F.20 Strain energy versus effective vertical stress for BH-SK 82S13 7B; Z=14.10 m bsb.

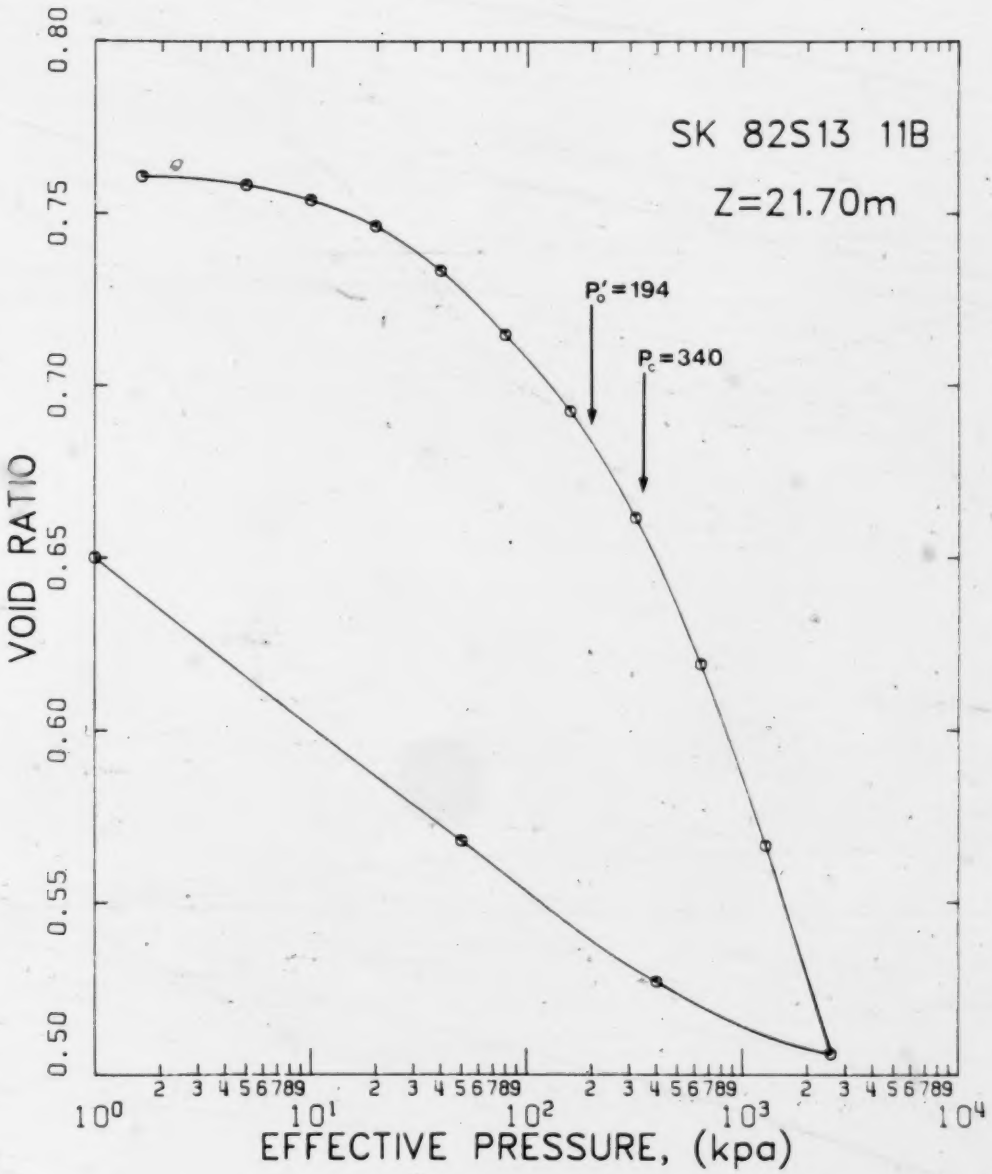

Figure F.21 Void ratio versus log effective vertical stress for BH SK 82S13 11B; Z=21.70 m bsb. (Jefferies, pers. comm., 1985).

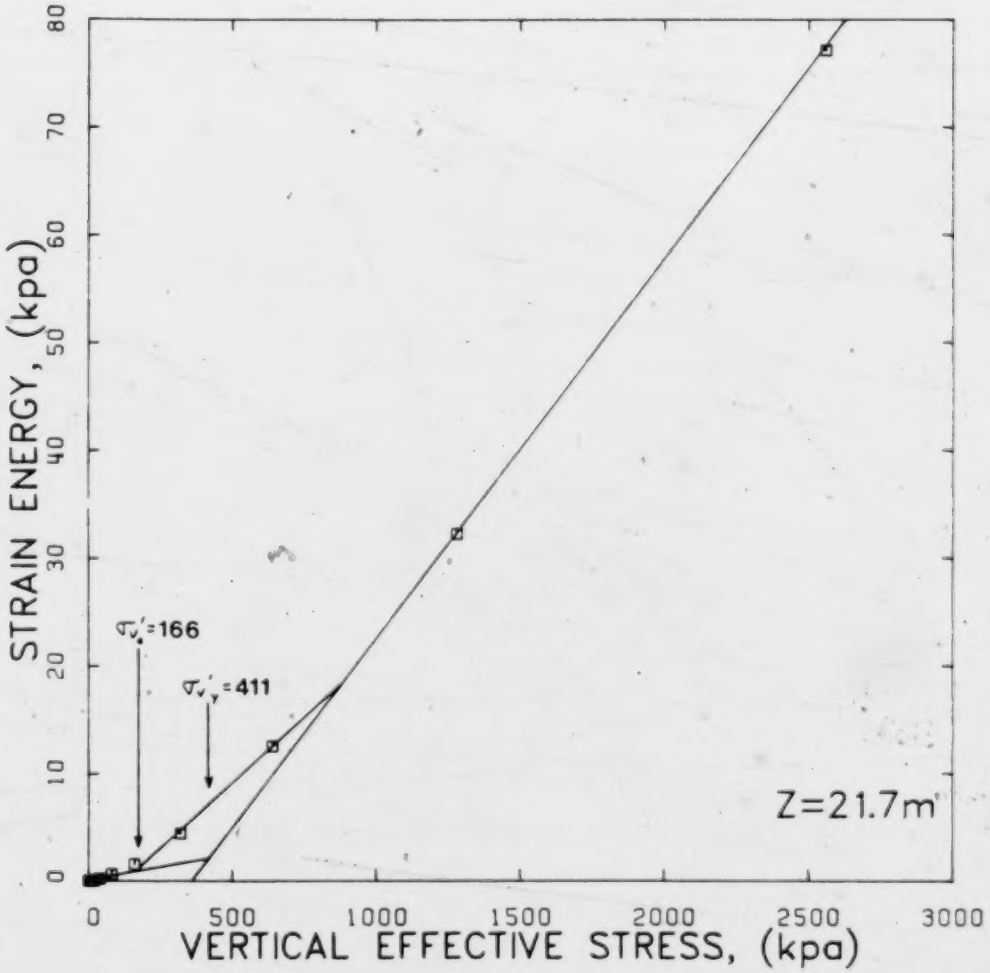

Figure F.22 Strain energy versus effective vertical stress for BH SK 82S13 11B; Z=21.70 m bsb.

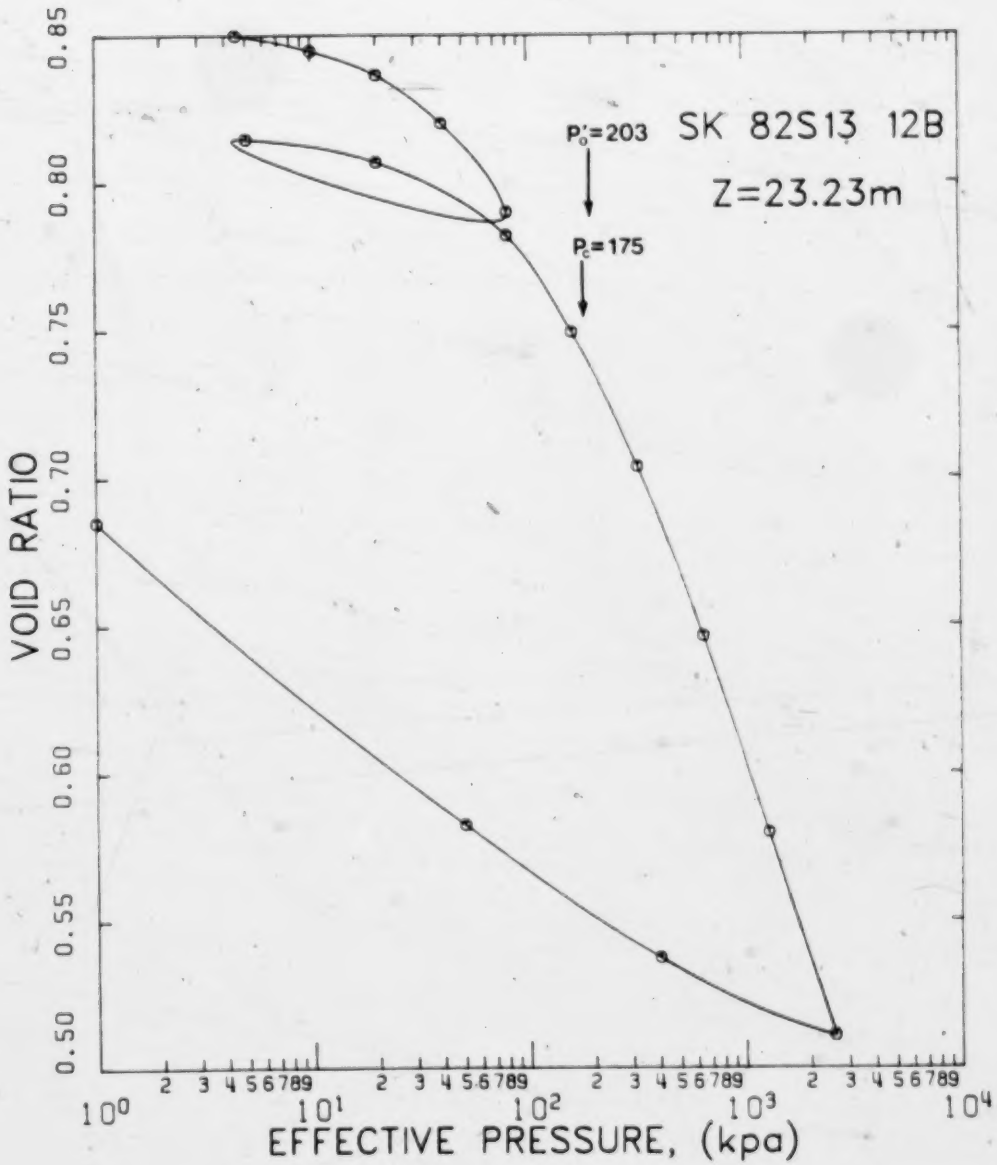

Figure F.23 Void ratio versus log effective vertical stress for BH SK 82S13 12B; Z=23.23 m bsb. (Jefferies, pers. comm., 1985).

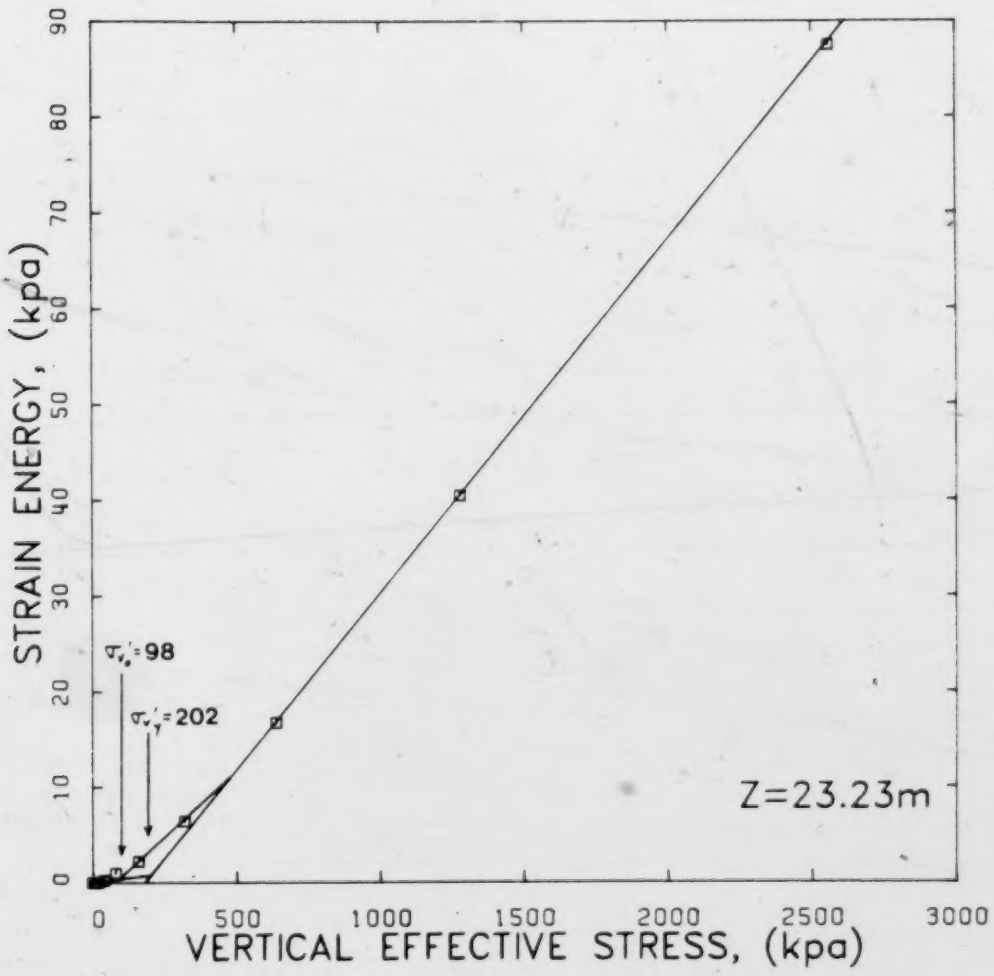

Figure F.24 Strain energy versus effective vertical stress for BH SK 82S13 12B; Z=23.23 m bsb.

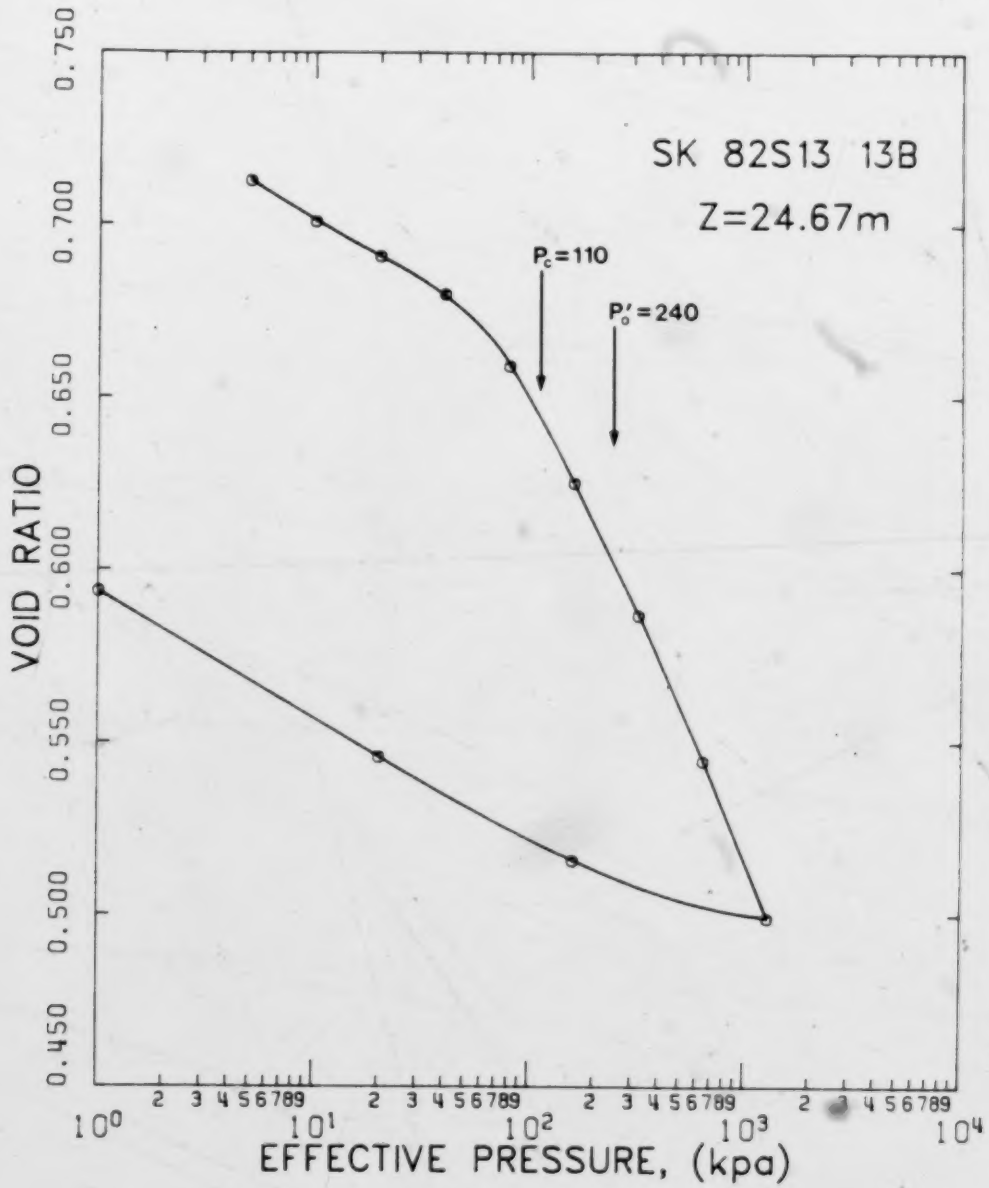

Figure F.25 Void ratio versus log effective vertical stress for BH SK 82S13 13B; Z=24.67 m bsb. (Jefferies, pers. comm., 1985).

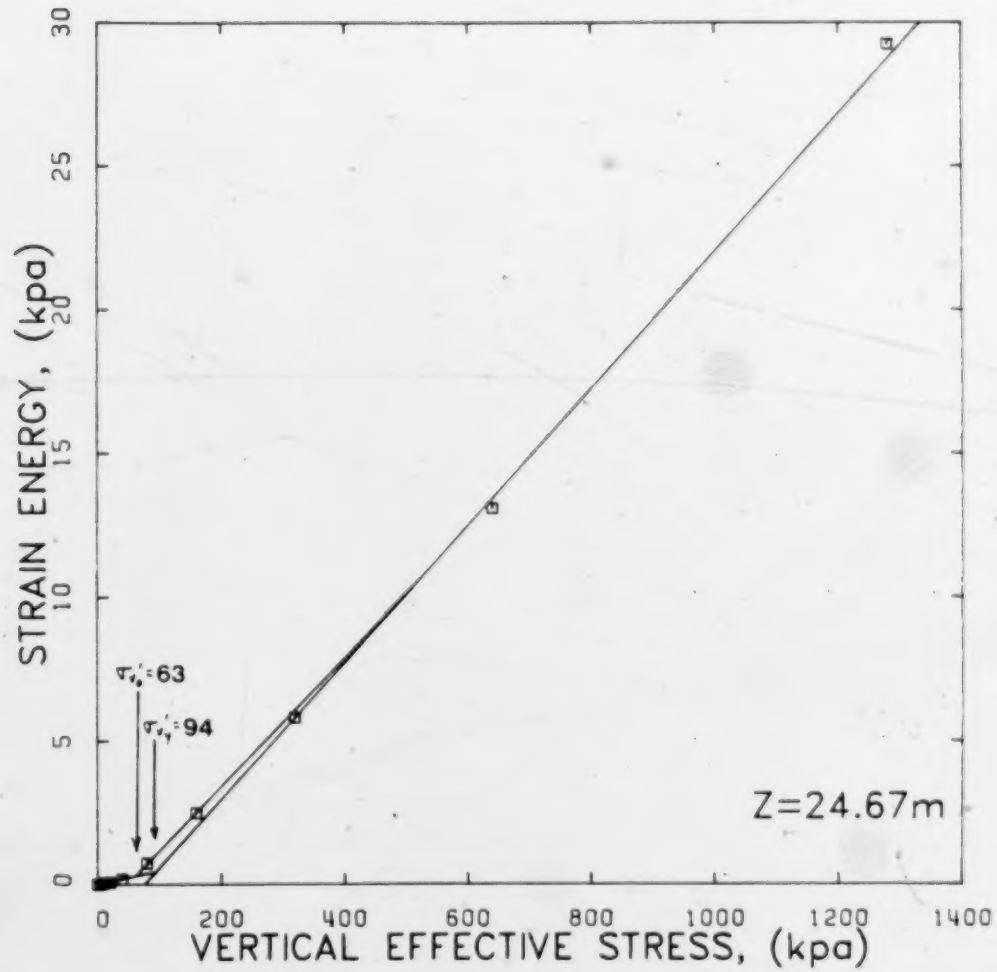

Figure F.26 Strain energy versus effective vertical stress for BH SK 82S13 13B; Z=24.67 m bsb.

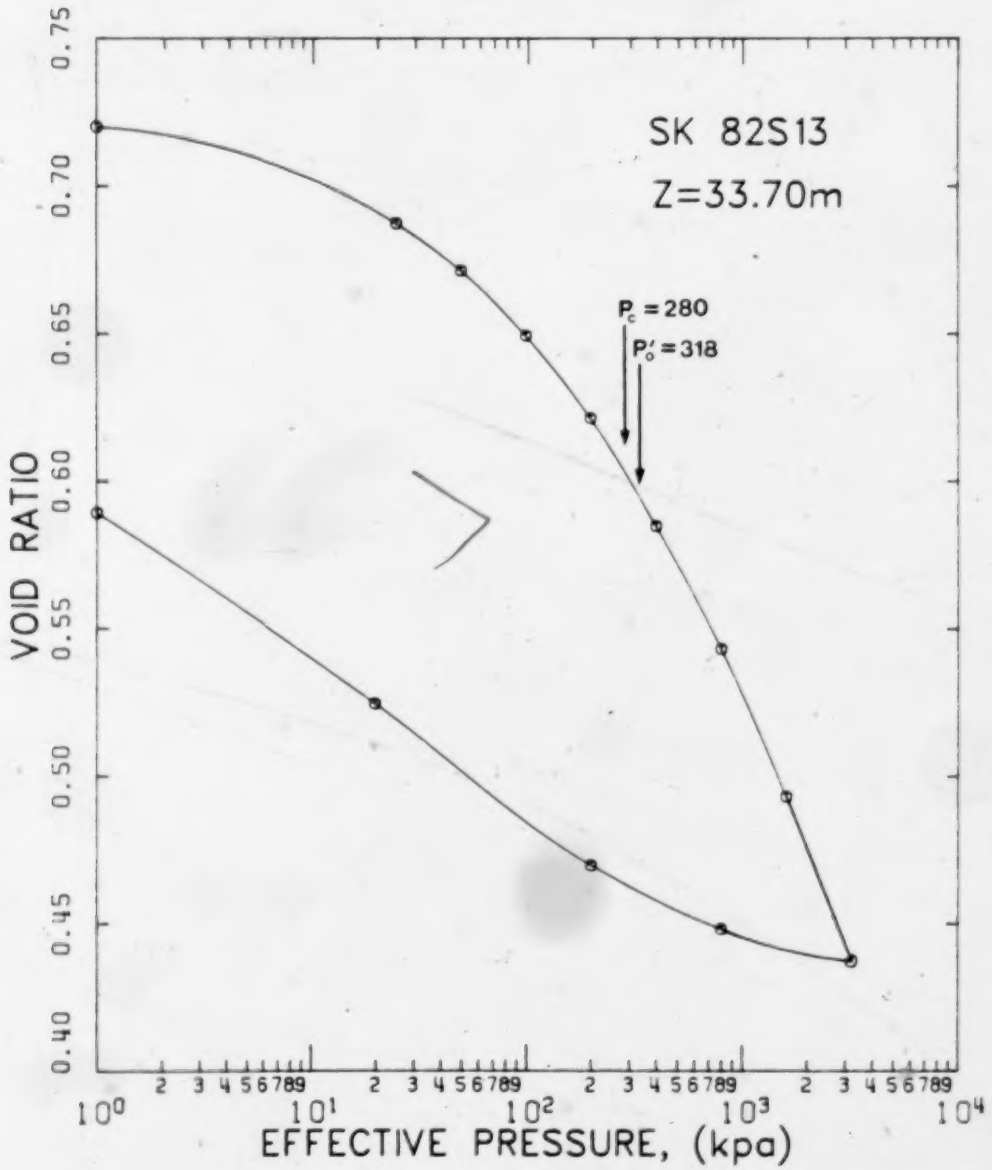

Figure F.27 Void ratio versus log effective vertical stress for BH SK 82S13; Z=33.70 m bsb. (Jefferies, pers. comm., 1985).

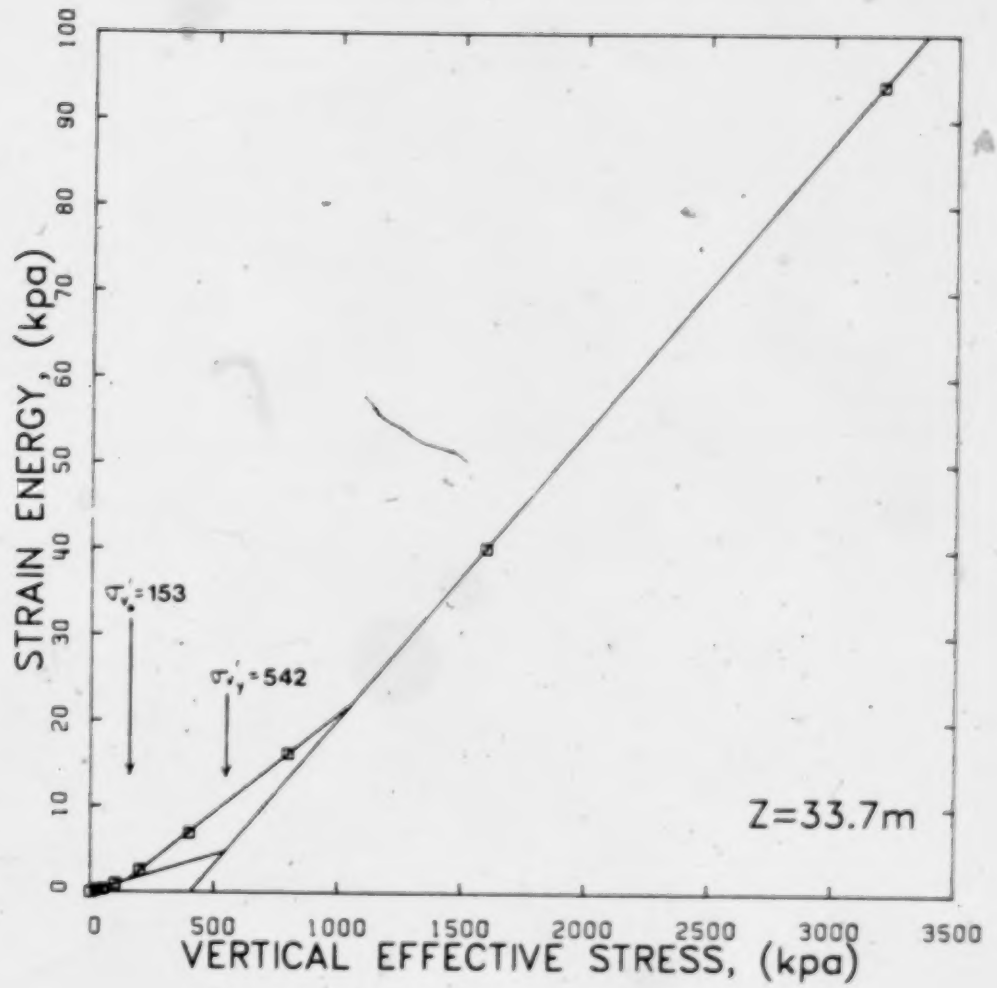

Figure F.28 Strain energy versus effective vertical stress for BH SK 82S13; Z=33.70 m bsb.

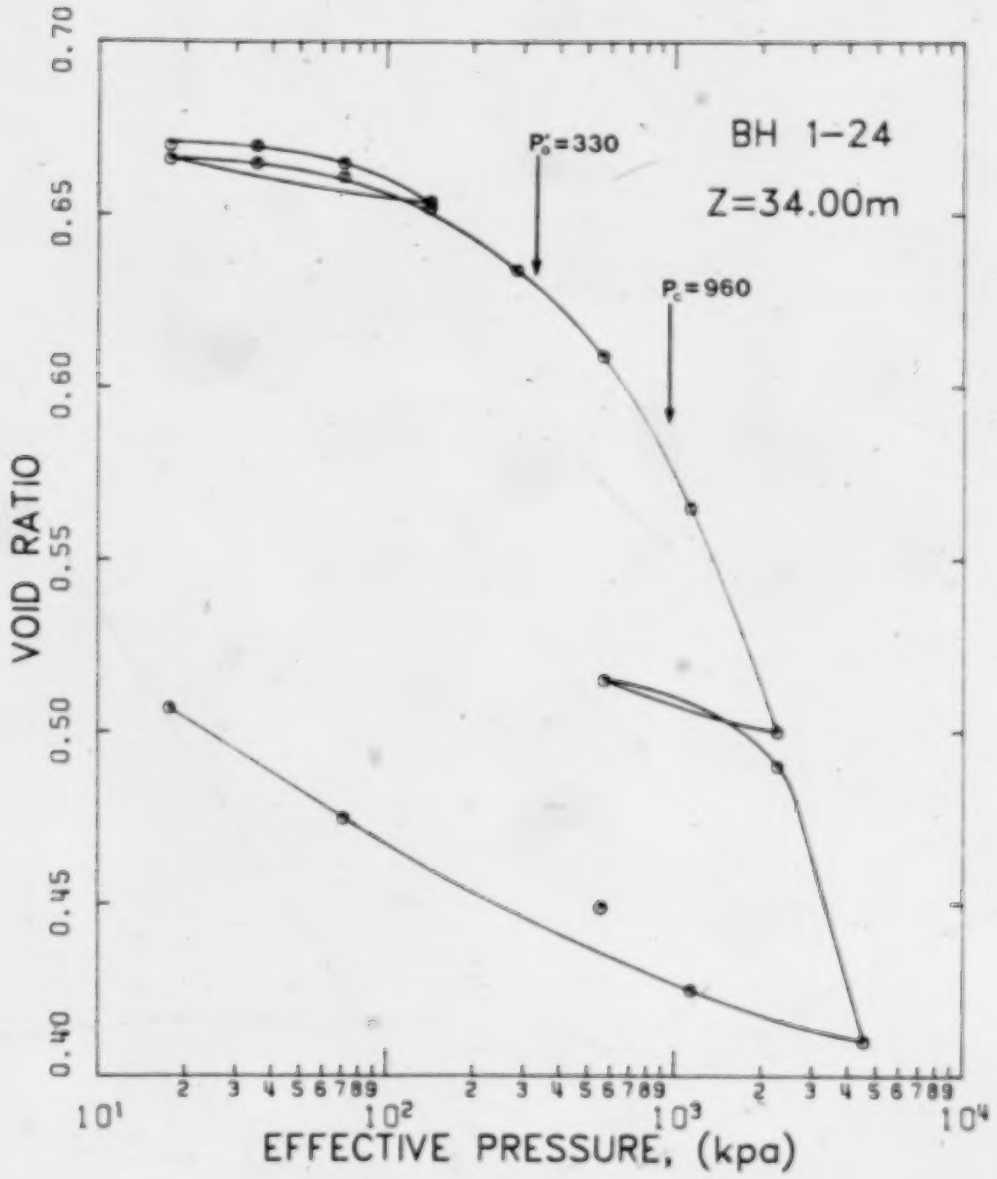

Figure F.29 Void ratio versus log effective vertical stress for BH 1-24; Z=34.00 m bsb. (Jefferies, pers. comm., 1985).

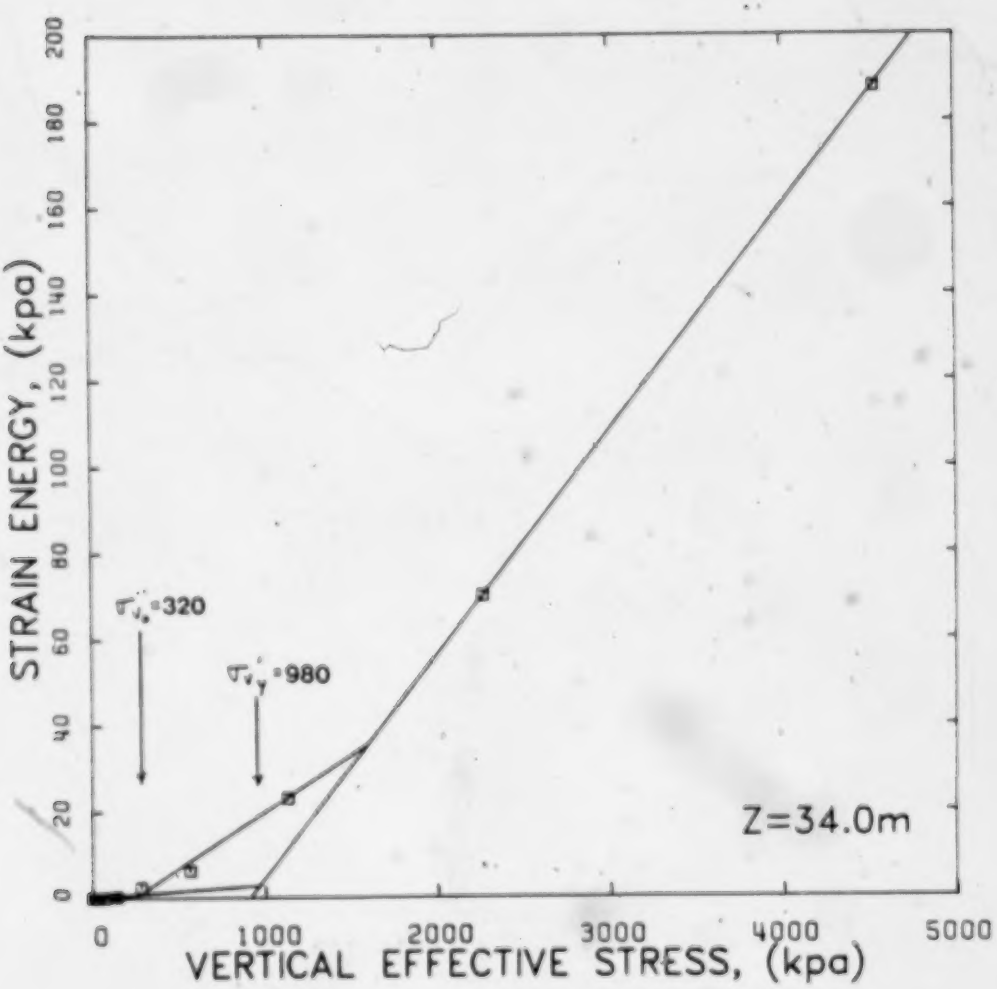

Figure F.30 Strain energy versus effective vertical stress for BH 1-2; Z=34.00 m bsb.

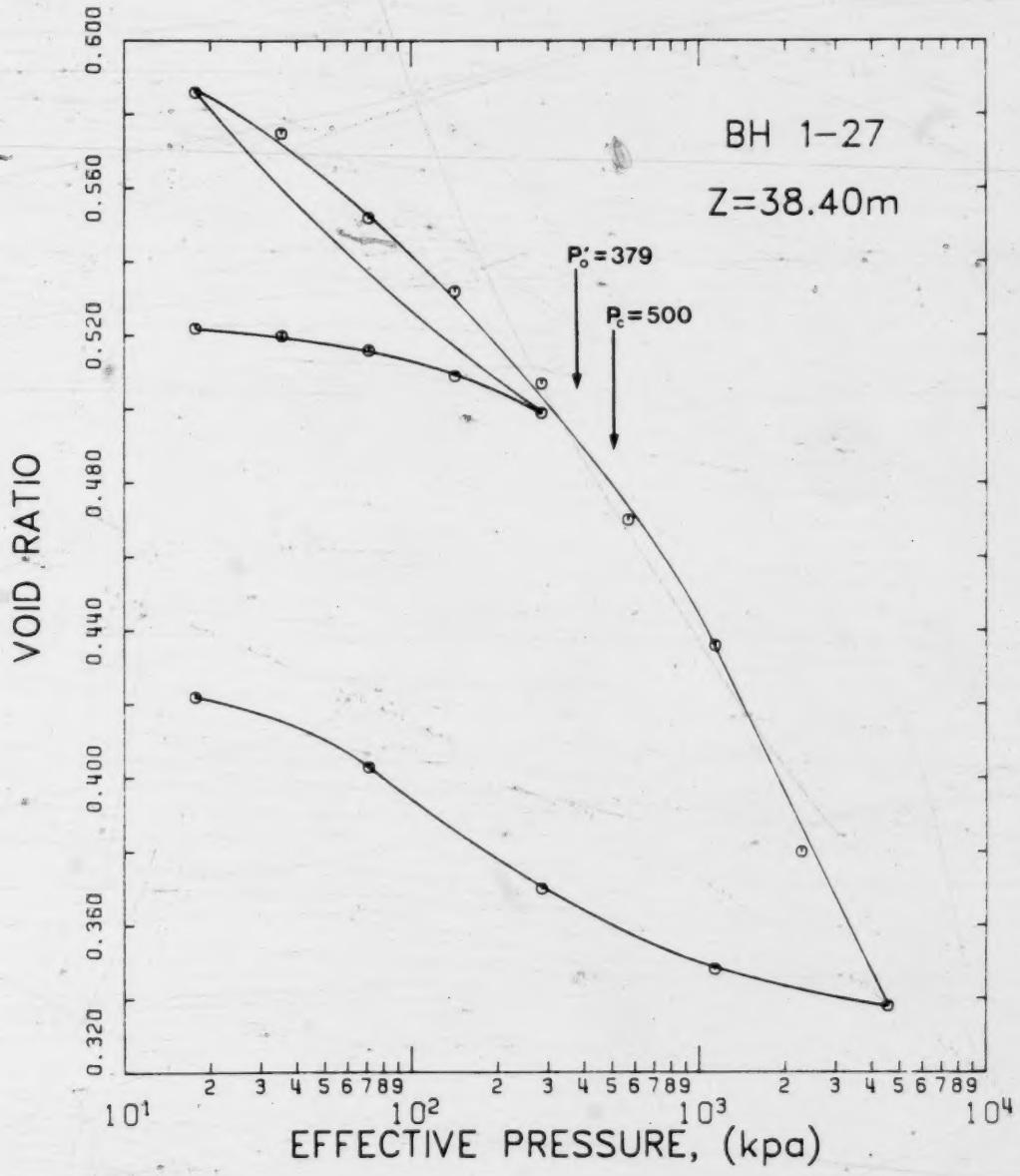

Figure F.31 Void ratio versus log effective vertical stress for BH 1-27; Z=38.40 m bsb. (Jefferies, pers. comm., 1985).

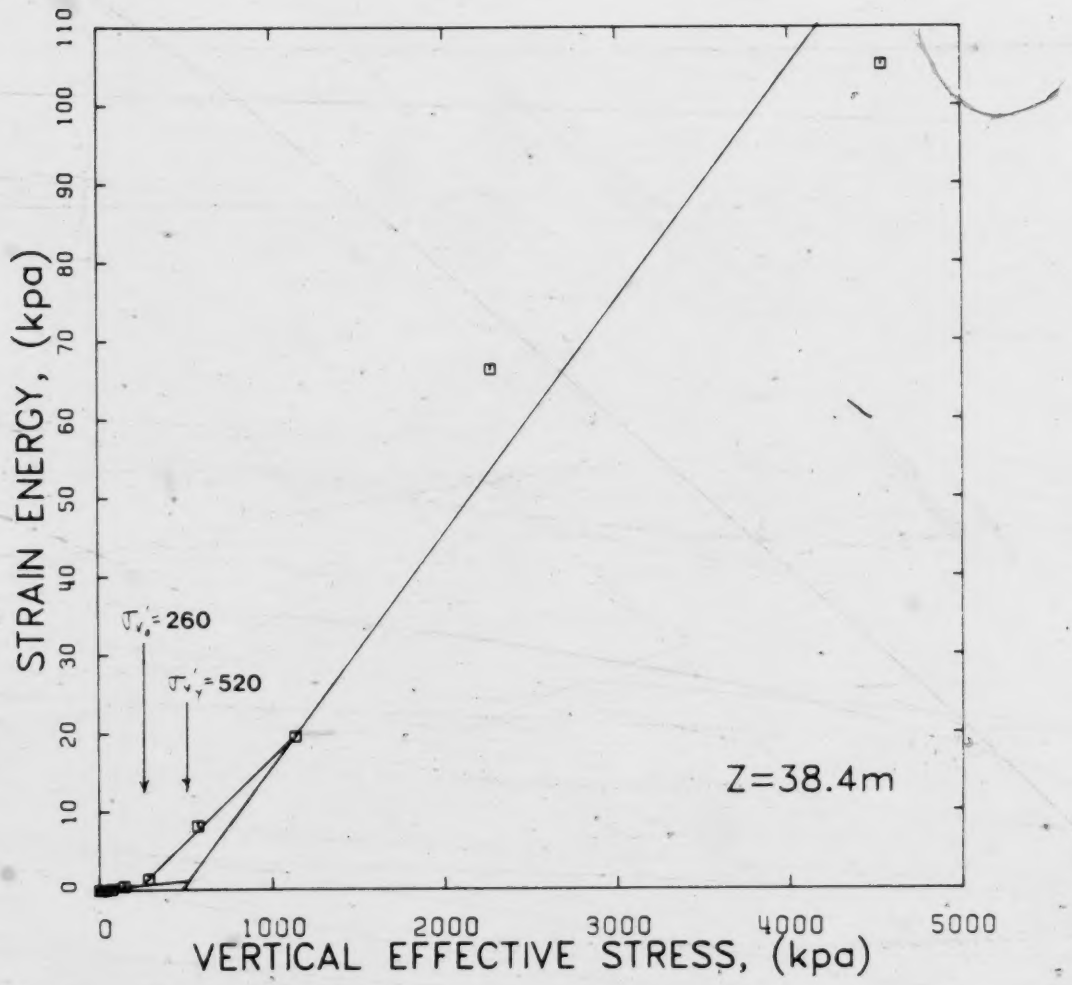

Figure F.32 Strain energy versus effective vertical stress for BH 1-2; Z=38.40 m bsb.

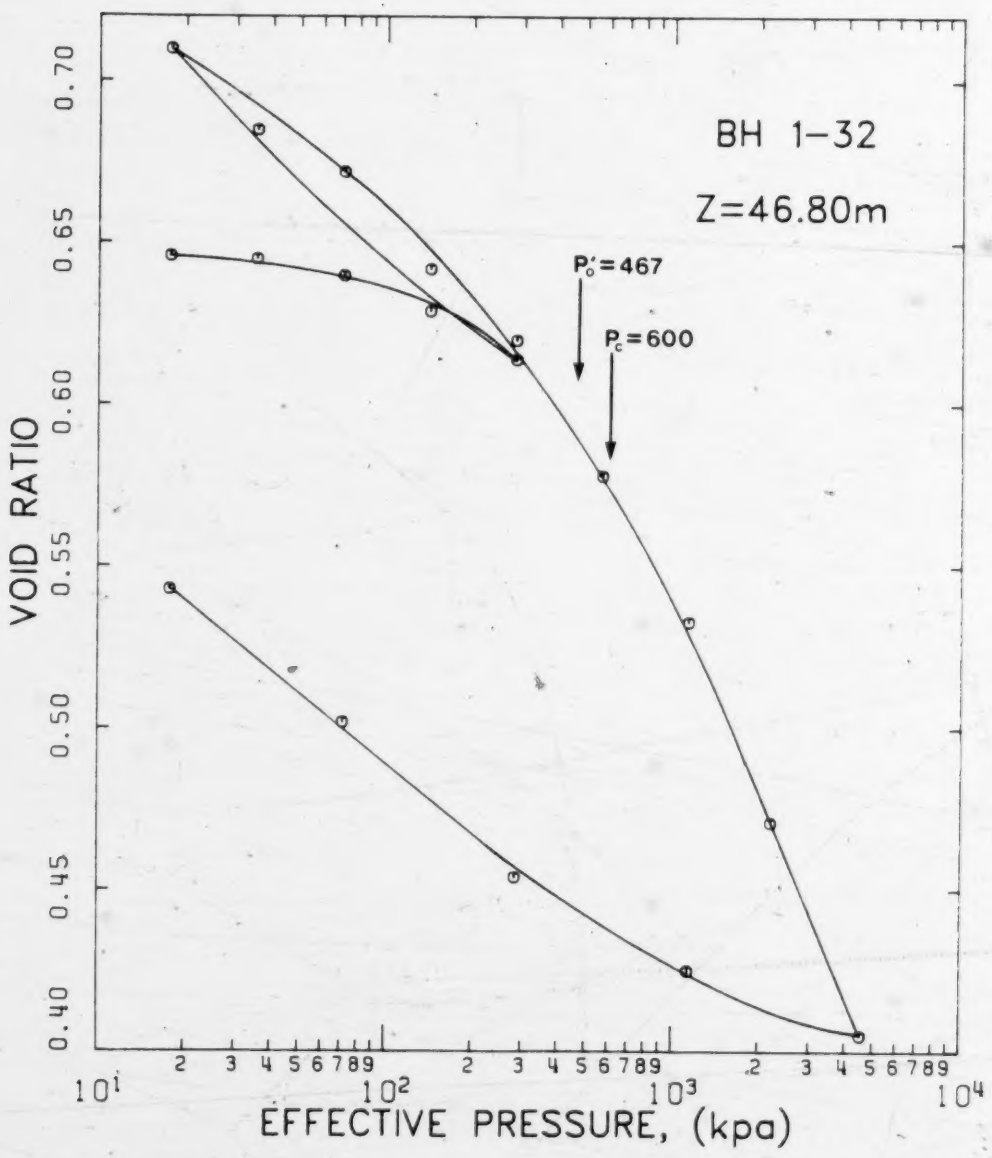

Figure F.33 Void ratio versus log effective vertical stress for BH 1-32; Z=46.80 m bsb. (Jefferies, pers. comm., 1985).

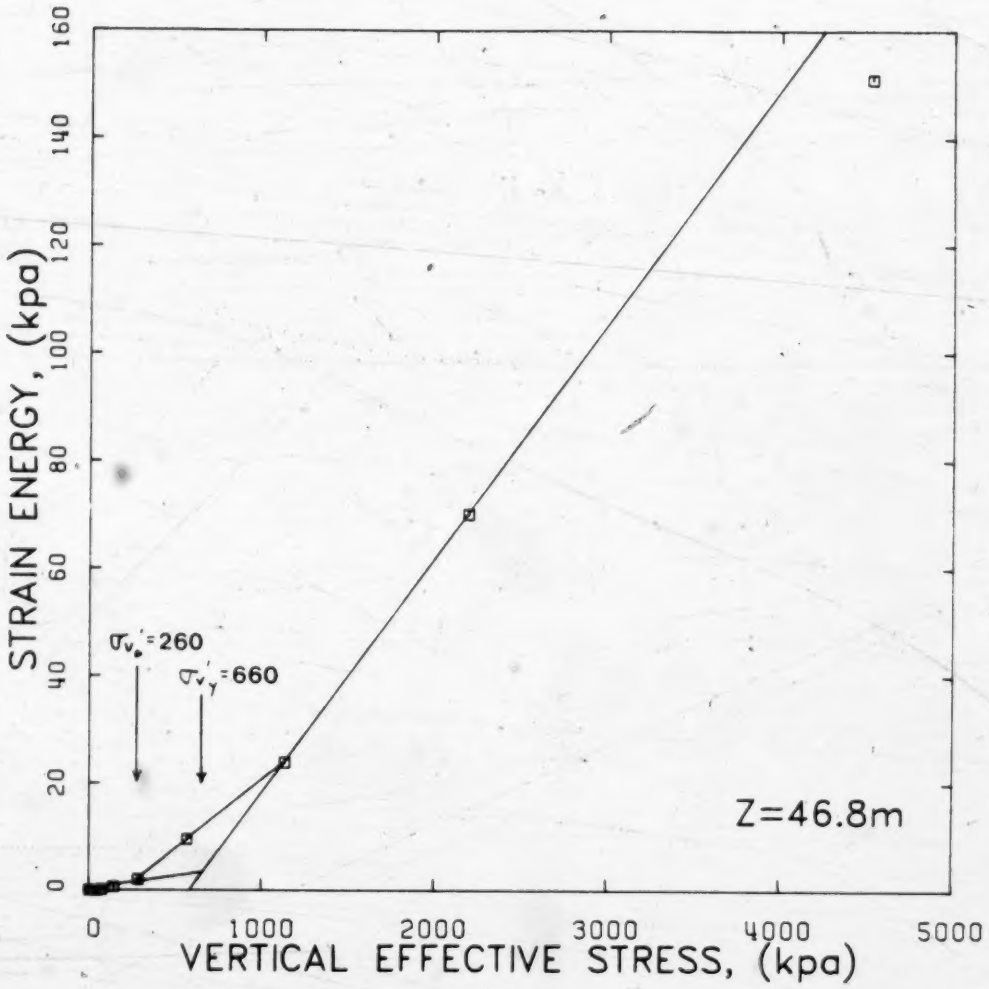

Figure F.34 Strain energy versus effective vertical stress for BH 1-32; Z=46.80 m bsb.

Appendix G

Results of Consolidation Testing

Table G.1 Consolidation summary for PC-09, back pressure = 250 kpa.

Consolidation data for PC-09 Z=1.16m bsb.

PC-09		Z = 1.16m		ROOT TIME		LOG TIME	
σ_v' (kpa)	HT. (mm)	e	m_v (m^2/kN)	C_v (cm/s^2)	k (cm/s)	C_v (cm/s^2)	k (cm/s)
0	19.2989	2.1229	--	--	--	--	--
4.7	19.2255	2.1109	8.245e-4	2.644e-4	1.13e-8	7.613e-4	3.25e-8
6.7	19.1240	2.0942	2.581e-3	2.132e-4	2.85e-8	2.524e-4	3.38e-8
10.9	18.8920	2.0562	2.959e-3	3.144e-4	4.82e-8	3.563e-4	5.47e-8
19.2	18.4350	1.9813	2.949e-3	3.325e-4	5.08e-8	1.483e-4	2.27e-8
46.4	17.4660	1.8224	1.959e-3	5.358e-4	5.44e-8	3.723e-4	3.78e-8
81.8	16.7000	1.6969	1.256e-3	9.344e-4	6.08e-8	3.854e-4	2.51e-8
152.6	15.7060	1.5339	8.536e-4	9.649e-4	4.27e-8	4.571e-4	2.02e-8
294.1	14.5800	1.3493	5.148e-4	8.276e-4	2.21e-8	6.542e-4	1.75e-8
561.6	13.4850	1.1698	2.856e-4	8.315e-4	1.23e-8	8.375e-4	1.24e-8
1073.6	12.4040	0.9926	1.595e-4	9.864e-4	8.16e-9	6.653e-5	5.50e-9
561.6	12.3100	0.9772	BACK PRESSURE = 250 kpa				
294.1	12.4812	1.0053					
0	14.5488	1.3442					

Consolidation data for PC-09 Z=2.08m bsb.

PC-09		Z = 2.08m		ROOT TIME		LOG TIME	
σ_v' (kpa)	HT. (mm)	e	m_v (m^2/kN)	C_v (cm/s^2)	k (cm/s)	C_v (cm/s^2)	k (cm/s)
0	19.8145	1.7058	--	--	--	--	--
2.9	19.8029	1.7042	2.018e-4	2.797e-4	2.93e-9	8.052e-4	8.42e-9
3.8	19.7720	1.7000	1.849e-3	2.263e-4	2.17e-8	--	--
5.4	19.7135	1.6920	1.807e-3	3.369e-4	3.16e-8	--	--
8.7	19.5424	1.6686	2.852e-3	3.618e-4	5.35e-8	1.613e-4	2.38e-8
15.3	19.2676	1.6311	2.126e-3	6.054e-4	6.67e-8	4.207e-4	4.64e-8
68.6	17.9480	1.4509	1.285e-3	1.028e-3	6.85e-8	4.240e-4	2.82e-8
143.7	16.9200	1.3105	7.627e-4	1.063e-3	4.20e-8	5.034e-4	1.99e-8
293.9	15.7660	1.1530	4.538e-4	9.128e-4	2.15e-8	7.216e-4	1.70e-8
573.6	14.7430	1.0133	2.319e-4	9.239e-4	1.11e-8	9.306e-4	1.12e-8
1085.6	13.6800	0.8681	1.408e-4	1.101e-3	8.04e-9	7.426e-4	5.42e-9
573.6	13.5907	0.8559	BACK PRESSURE = 250 kpa				
293.9	13.7687	0.8802					
0	15.6999	1.1439					

Table G.2 Consolidation summary for BH 20+00, back pressure = 250 kpa.

Consolidation data for BH 20+00 Z=4.85m bsb.

BH 20+00		Z = 4.85m		ROOT TIME		LOG TIME	
σ_v (kpa)	HT. (mm)	e	m_v (m^2/kN)	C_v ($cm/s^{\frac{1}{2}}$)	k (cm/s)	C_v ($cm/s^{\frac{1}{2}}$)	k (cm/s)
0	21.0160	1.0968	--	--	--	--	--
2	21.0088	1.0961	1.669e-4	--	--	--	--
4	20.9450	1.0897	1.527e-3	3.174e-4	2.50e-8	5.474e-4	4.31e-8
8	20.8548	1.0807	1.077e-3	6.194e-4	3.44e-8	5.996e-4	3.33e-8
16	20.6566	1.0609	1.189e-3	1.183e-3	7.24e-8	7.919e-4	4.85e-8
32	20.3668	1.0320	8.764e-4	7.373e-4	3.33e-8	5.020e-4	2.27e-8
2	20.7315	1.0684					
4	20.7086	1.0661					
8	20.6690	1.0622					
16	20.5280	1.0481					
32	20.3620	1.0315					
64	20.1468	1.0101	3.368e-4	1.375e-3	2.38e-8	1.363e-3	2.36e-8
128	19.6516	0.9606	3.848e-4	1.342e-3	2.66e-8	1.281e-3	2.54e-8
256	19.1078	0.9064	2.160e-4	2.027e-3	2.25e-8	1.573e-3	1.75e-8
512	18.4216	0.8379	1.403e-4	2.309e-3	1.67e-8	1.358e-3	9.82e-8
1024	17.7460	0.7705	7.162e-5	2.176e-3	8.03e-9	1.652e-3	6.09e-9
256	17.7440	0.7703	BACK PRESSURE = 250 kpa				
32	18.3456	0.8303					
2	19.2281	0.9184					

Consolidation data for BH 20+00 Z=10.95m bsb.

BH 20+00		Z = 10.95m		ROOT TIME		LOG TIME	
σ_v (kpa)	HT. (mm)	e	m_v (m^2/kN)	C_v ($cm/s^{\frac{1}{2}}$)	k (cm/s)	C_v ($cm/s^{\frac{1}{2}}$)	k (cm/s)
0	19.8526	0.9193	--	--	--	--	--
2	19.8114	0.9153	--	7.92e-4	--	8.50e-4	--
4	19.7723	0.9115	--	2.13e-3	--	1.89e-3	--
8	19.6200	0.8968	--	1.68e-3	--	7.80e-4	--
16	19.3632	0.8720	--	2.55e-3	--	2.87e-4	--
32	19.3118	0.8496	--	3.36e-3	--	3.03e-3	--
64	18.8819	0.8255	--	3.52e-3	--	2.56e-3	--
128	18.6092	0.7991	--	6.32e-3	--	4.90e-3	--
256	18.2482	0.7642	--	7.62e-3	--	5.96e-3	--
512	17.7792	0.7189	--	7.66e-3	--	3.73e-3	--
1024	17.3260	0.6750	--	6.60e-3	--	4.57e-3	--
256	17.3504	0.6774	BACK PRESSURE = 250 kpa				
32	17.7511	0.7161					
2	18.2729	0.7666					

Consolidation data for BH 20+00 Z=13.74m bsb.

BH 20+00		Z = 13.74m		ROOT TIME		LOG TIME	
σ'_v (kpa)	HT. (mm)	e	m_v (m^2/kN)	C_v ($cm/s^{\frac{1}{2}}$)	k (cm/s)	C_v (cm/s^2)	k (cm/s)
0	19.4310	1.4753	--	--	--	--	--
2	19.4195	1.4738	3.030e-4	--	--	2.24e-4	3.52e-9
4	19.3980	1.4711	5.463e-4	1.09e-3	3.09e-8	4.62e-4	1.31e-8
8	19.3653	1.4669	4.249e-4	1.48e-3	3.26e-8	1.08e-3	2.38e-8
16	19.2000	1.4459	1.064e-3	9.37e-3	5.17e-8	9.01e-4	4.97e-8
32	19.0675	1.4290	4.318e-4	8.60e-4	1.92e-8	6.76e-4	1.51e-8
2	19.9124	1.5366					
4	19.8100	1.5236					
8	19.5754	1.4937					
16	19.2692	1.4547					
32	18.9736	1.4170					
64	18.7240	1.3852	5.635e-4	1.07e-3	3.13e-8	1.01e-3	2.95e-8
128	18.1230	1.3087	5.011e-4	1.09e-3	2.83e-8	8.51e-4	2.21e-8
256	17.2760	1.2008	3.651e-4	7.26e-3	1.37e-8	5.70e-4	1.08e-8
512	16.0860	1.0492	2.691e-4	8.14e-3	1.14e-8	6.02e-4	8.40e-9
1024	14.8580	0.8928	1.491e-4	8.83e-3	6.83e-9	6.61e-4	5.11e-9
256	15.2706	0.9453	BACK PRESSURE = 250 kpa				
32	16.0925	1.0500					
2	17.0204	1.1682					

Table G.3 Consolidation summary for BH MTWS1, back pressure = 250 kpa.

Consolidation data for BH MTWS1 Z=6.16m bsb.

BH MTWS1		Z = 6.16m		ROOT TIME		LOG TIME	
σ_v' (kpa)	HT. (mm)	e	m_v (m^2/kN)	C_v (cm/s^2)	k (cm/s)	C_v (cm/s^2)	k (cm/s)
0	20.0330	2.0968	--	--	--	--	--
2	19.9116	2.0780	--	--	--	--	--
4	19.7600	2.0546	--	3.88e-4	--	2.95e-4	--
8	19.4843	2.0120	--	3.26e-4	--	3.56e-4	--
16	19.0000	1.9371	--	4.45e-4	--	3.13e-4	--
32	18.5439	1.4891	--	5.15e-4	--	5.55e-4	--
64	17.7962	1.7510	--	4.29e-4	--	3.81e-4	--
128	16.7371	1.5873	--	7.14e-4	--	5.55e-4	--
256	15.6403	1.4178	--	9.55e-4	--	6.53e-4	--
512	14.6514	1.2649	--	1.08e-3	--	8.23e-4	--
1024	13.7162	1.1203	--	1.12e-3	--	8.35e-4	--
256	13.7880	1.1314	BACK PRESSURE = 250 Kpa				
32	14.6524	1.2651					
2	15.6639	1.4214					

Appendix H

Results of Constant Head Permeability Testing

Table H.1 Permeability data for PC-09, Z = 1.16 m bsb.

DATA SHEET No 4 — CONSTANT HEAD PERMEABILITY TEST

NOTE: PERMEABILITY IS MEASURED DURING AN ODOMETER TEST IN THE VERTICAL DIRECTION

INITIAL SAMPLE DIMENSIONS — SAMPLE No 1.16 m — BOREHOLE PC-09

DIAMETER	D = 6.35 cm	AREA	A = 31.6693 cm²	
HEIGHT	H = 1.905 cm	VOLUME	V = 60.3398 cm³	
WT WET SOIL	M = 99.93 g	UNIT WT	γ = 1.59 mg/m³	
VOID RATIO	e₀ = 1.139	TEMP	T = 15°C	
		VIS RATIO	$\frac{\mu_T}{\mu_{20°C}}$ = 0.9137	

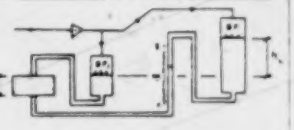

PERMEABILITY DATA

LOAD INCREMENT (kPa)	VOID RATIO	HT SAM L (cm)	TEST No	i (= h₁/L)	h₁ (cm)	t (sec)	h₀ (ml)	h_f (ml)	Q = h₀ − h_f (cm³)	k_T (cm/sec)	k_20°C (cm/sec)
50.0	1.123	1.739	1	3	5.23	3600	2.47	0.55	2.045	5.05 × 10⁻⁶	5.31 × 10⁻⁶
			2	"	"	3600	2.515	0.58	0.265	4.89 × 10⁻⁶	4.29 × 10⁻⁶
			3	"	"	3600	2.58	0.63	2.050	7.41 × 10⁻⁶	7.79 × 10⁻⁶
			4	"	"	14.400	0.63	0.675	0.045	2.37 × 10⁻⁶	1.97 × 10⁻⁶
			5	"	"	60.300	0.675	0.78	0.105	1.10 × 10⁻⁶	0.97 × 10⁻⁶
									Avg:	3.68 × 10⁻⁶	3.91 × 10⁻⁶
			1	6	10.43	1800	2.78	0.90	0.067	1.60 × 10⁻⁶	1.68 × 10⁻⁶
			2	"	"	5760	0.80	0.867	0.007	0.98 × 10⁻⁶	1.39 × 10⁻⁶
			3	"	"	17.040	2.827	2.99	0.133	1.59 × 10⁻⁶	1.81 × 10⁻⁶
									Avg:	1.39 × 10⁻⁶	1.53 × 10⁻⁶
			1	9	17.35	1200	2.901	2.997	2.056	1.71 × 10⁻⁶	1.81 × 10⁻⁶
			2	"	"	3600	2.997	1.039	2.037	1.15 × 10⁻⁶	1.47 × 10⁻⁶
			3	"	"	1800	1.039	1.085	2.021	2.68 × 10⁻⁶	1.89 × 10⁻⁶
			4	"	"	1200	1.085	1.090	2.026	4.19 × 10⁻⁶	3.19 × 10⁻⁶
									Avg:	2.33 × 10⁻⁶	2.33 × 10⁻⁶
[illegible]	[illegible]	[illegible]		20	34.78	300	1.87	1.921	0.049	5.20 × 10⁻⁶	4.23 × 10⁻⁶
BP = 350 kPa (1.331 m)			2	"	"	1800	1.331	1.387	0.056	3.33 × 10⁻⁶	2.78 × 10⁻⁶
PP = 250 kPa (1.331 m)			3	"	"	900	1.327	1.375	2.048	5.03 × 10⁻⁶	4.32 × 10⁻⁶
									Avg:	3.33 × 10⁻⁶	3.78 × 10⁻⁶

Table H.2 Permeability data for PC-09, Z = 2.08 m bsb.

DATA SHEET No 4 — CONSTANT HEAD PERMEABILITY TEST

NOTE PERMEABILITY IS MEASURED DURING AN OEDOMETER TEST IN THE VERTICAL DIRECTION

INITIAL SAMPLE DIMENSIONS — SAMPLE NO 2.08 m — BOREHOLE PC-09

DIAMETER	D= 6.79 cm	AREA	A = 36.267 cm²	
HEIGHT	H= 1.965 cm	VOLUME	V = 71.278 cm³	
WT WET SOIL	M= 156.71 g	UNIT WT	γ = 1.35 ... g/cm³	
VOID RATIO	e_o = 1.7058	TEMP	T = 19.5°C	
		VIS RATIO	$\frac{\mu_T}{\mu_{T_s}}$ = 0.5.32	

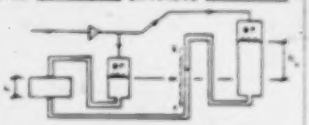

PERMEABILITY DATA

LOAD INCREMENT (kPa)	VOID RATIO	WT SAM L (cm)	TEST NO	$i = \frac{h_o}{L}$	h_o (cm)	T (DEG)	h_o (cm)	h_f (cm)	$Q = h_o - h_f$ (cm³)	k_T (cm_{sec})	$k_{20°C}$ (cm_{sec})
19.3	1.7309	1.936	1	3	5.78	19.50	0.926	0.504	0.040	5.80×10^{-5}	5.00×10^{-5}
			2			19.50	0.510	0.493	0.073	7.00×10^{-5}	6.39×10^{-5}
			3			19.50	2.493	1.048	0.117	7.00×10^{-5}	6.50×10^{-5}
									avg =	6.83×10^{-5}	7.99×10^{-5}
			1	6	11.56	19.50	1.063	1.130	0.067	6.45×10^{-5}	5.90×10^{-5}
			2			19.50	1.130	1.197	0.067	6.43×10^{-5}	5.87×10^{-5}
			3			19.50	1.197	1.255	0.058	5.61×10^{-5}	5.13×10^{-5}
									avg =	6.16×10^{-5}	5.63×10^{-5}
			1	10	19.26	19.50	1.038	1.107	0.077	5.79×10^{-5}	5.29×10^{-5}
			2			19.50	1.107	1.190	0.083	6.45×10^{-5}	5.89×10^{-5}
			3			19.50	1.190	1.273	0.083	6.23×10^{-5}	5.69×10^{-5}
			4			19.50	1.273	1.357	0.084	6.34×10^{-5}	5.79×10^{-5}
									avg =	6.21×10^{-5}	5.67×10^{-5}
38.3 kPa	1.6.2	1.956	1	10	19.51	19.50	2.165	2.338	0.173	8.70×10^{-5}	7.95×10^{-5}
0.997 cm	PP: 1.317		2			19.50	2.338	2.510	0.172	8.61×10^{-5}	7.86×10^{-5}
0.1351 - 20	1.305	1.779	3			19.50	2.510	2.678	0.168	8.40×10^{-5}	7.67×10^{-5}
									avg =	8.57×10^{-5}	7.83×10^{-5}

Table H.3 Permeability data for BH 20+00, Z = 4.85 m bsb.

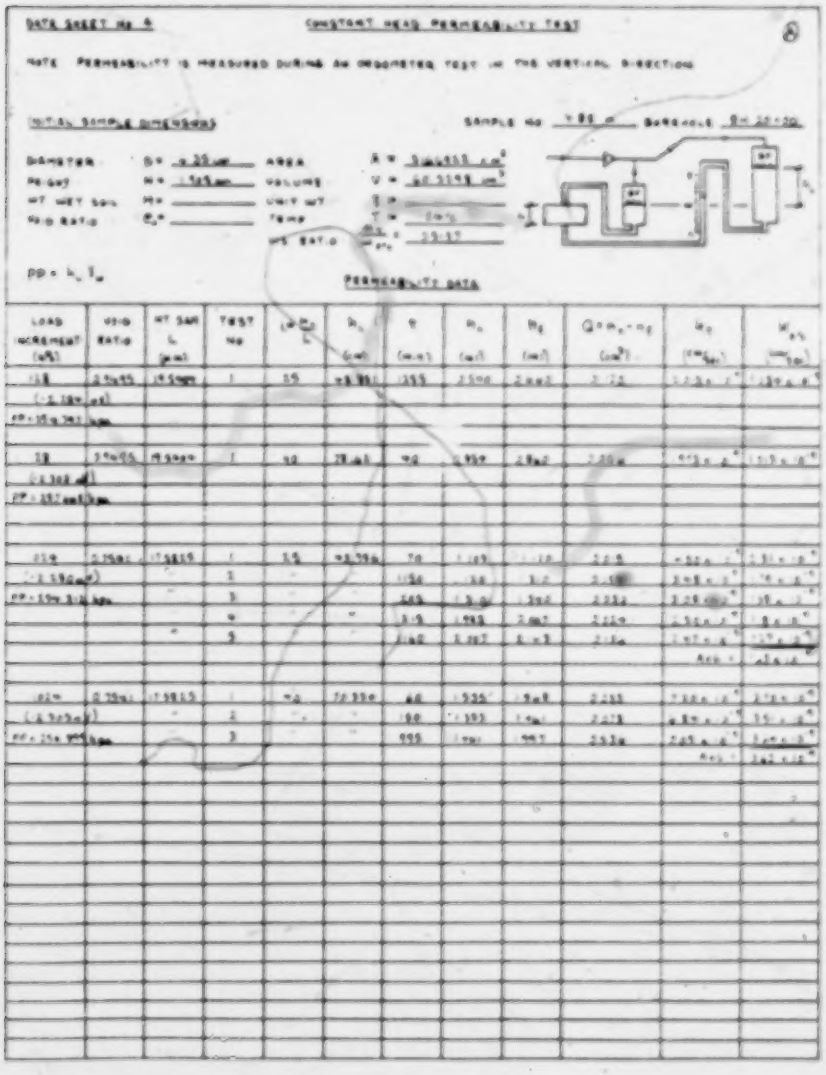

DATA SHEET No. 4 — CONSTANT HEAD PERMEABILITY TEST — 8

NOTE: PERMEABILITY IS MEASURED DURING AN UNDISTURBED TEST IN THE VERTICAL DIRECTION

INITIAL SAMPLE DIMENSIONS — SAMPLE No. Y 85 m — BOREHOLE B= 20+00

DIAMETER D = 0.10 m — AREA A = 7.854 x 10⁻³ m²
HEIGHT H = 0.125 m — VOLUME V = 98.175 x 10⁻⁶ m³
INIT. WET SOIL m = ——— — UNIT WT. γ = ———
VOID RATIO e₀ = ——— — TEMP T = 10°C
γs = 26.5 kN/m³

pp = h_w I_w

PERMEABILITY DATA

LOAD INCREMENT (kPa)	VOID RATIO	INIT SAM L (mm)	TEST No	Δe/e₀ L	h_w (cm)	t (min)	h_o (cm)	h_f (cm)	Q = a_c·dh/dt (cm³)	k_T (cm/sec)	k_20 (cm/sec)
25	2.745	124.5	1	25	24.8	355	2.500	2.442	2.72	1.13 x 10⁻⁶	1.30 x 10⁻⁶
(+ 150 kPa)											
pp = 150 kPa											
25	2.705	119.0	1	25	24.8	70	2.550	2.492	2.28	4.73 x 10⁻⁶	5.43 x 10⁻⁶
(+ 300 kPa)											
pp = 300 kPa											
219	2.750	119.5	1	25	24.8	70	2.503	2.45	2.5	4.32 x 10⁻⁶	4.91 x 10⁻⁶
(+ 150 kPa)			2			150	2.54	2.5	2.58	2.08 x 10⁻⁶	2.4 x 10⁻⁶
pp = 150 kPa			3			245	2.50	2.50	2.232	2.29 x 10⁻⁶	2.6 x 10⁻⁶
			4			3.5	2.493	2.467	2.229	1.34 x 10⁻⁶	1.5 x 10⁻⁶
			5			2.60	2.487	2.43	2.24	1.07 x 10⁻⁶	1.2 x 10⁻⁶
										Avg.	2.4 x 10⁻⁶
450	2.730	119.5	1	25	24.8	60	2.535	2.48	2.251	2.32 x 10⁻⁶	2.7 x 10⁻⁶
(+ 300 kPa)			2			150	2.503	2.464	2.213	1.89 x 10⁻⁶	2.2 x 10⁻⁶
pp = 300 kPa			3			255	2.491	2.457	2.213	1.65 x 10⁻⁶	1.9 x 10⁻⁶
										Avg.	2.27 x 10⁻⁶

Table H.4 Permeability data for BH 20+00, Z = 13.74 m bsb.

DATA SHEET No. 6 — CONSTANT HEAD PERMEABILITY TEST

NOTE: PERMEABILITY IS MEASURED DURING AN ODOMETER TEST IN THE VERTICAL DIRECTION

INITIAL SAMPLE DIMENSIONS

SAMPLE NO. [illegible] BOREHOLE BH 20+00

DIAMETER	D = 6.35 cm	AREA	A = [illegible] cm²		
HEIGHT	H = 1.905 cm	VOLUME	V = 60.3109 cm³		
WT WET SOIL	Mo = _____	UNIT WT	γ = _____		
MC/D RATIO	$\frac{H_o}{D_{FC}}$ = _____	TEMP	T = 24°C		
		VIS RATIO	$\frac{\mu_T}{\mu_{FC}}$ = 0.937		

PERMEABILITY DATA

LOAD INCREMENT (kPa)	VOID RATIO	WT SAT SOIL (g/cm³)	TEST No.	$i = \frac{h_c}{L}$	h_c (cm)	t (min)	h_c (cm)	h_f (cm)	$Q = h_c - h_f$ (cm³)	k_c (cm/sec)	k_{FC} (cm/sec)
138	1.877	1.795	1	19.1	36.83	45	0.693	0.703	2.050	1.139 x 10⁻⁶	1.215 x 10⁻⁶
(0.035 cm²)			2			1155	0.703	1.031	1.319	2.93 x 10⁻⁶	3.14 x 10⁻⁶
PP = 137 kPa										Avg	2.14 x 10⁻⁶
138	1.877	1.795	1	24	45.833	960		2.793	1.040	1.45 x 10⁻⁶	1.55 x 10⁻⁶
(0.03 cm²)										Avg	1.55 x 10⁻⁶
PP = 137 kPa											
690	1.847	1.913	1	95	36.83	70	0.83	2.87	0.26	4.33 x 10⁻⁶	4.64 x 10⁻⁶
(0.035 cm²)			2			1130	0.87	1.05	2.218	0.92 x 10⁻⁶	1.04 x 10⁻⁶
PP = 137 kPa			3			245	1.05	1.32	2.233	3.42 x 10⁻⁶	3.75 x 10⁻⁶
			4			168	1.28	1.57	2.23	4.49 x 10⁻⁶	4.82 x 10⁻⁶
			5			999	1.70	1.93	2.167	5.10 x 10⁻⁶	5.47 x 10⁻⁶
										Avg	4.74 x 10⁻⁶
1314	1.847	1.913	1	95	36.83	3.5	0.83	3.07	2.67	1.72 x 10⁻⁶	1.85 x 10⁻⁶
(0.035 cm²)			2			1140	1.07	1.31	2.215	0.4 x 10⁻⁶	3.57 x 10⁻⁶
PP = 137 + 3.5 kPa										Avg	3.71 x 10⁻⁶
2628	1.847	1.913	1	182	36.83	15	0.833	2.87	2.67	7.38 x 10⁻⁶	7.93 x 10⁻⁶
(0.035 cm²)			2			1320	0.846	1.05	2.196	0.38 x 10⁻⁶	0.41 x 10⁻⁶
PP = 137 + 137 kPa			3			60	1.032	1.29	2.27	0.7 x 10⁻⁶	0.76 x 10⁻⁶
			4			34	1.067	1.32	2.2	0.81 x 10⁻⁶	0.87 x 10⁻⁶
										Avg	0.69 x 10⁻⁶